12-2014

Experimental Evidence for Colloid-Facilitated Transport of Plutonium

Hilary Emerson
Clemson University, hilaryp@clemson.edu

EXPERIMENTAL EVIDENCE FOR COLLOID-FACILITATED TRANSPORT OF PLUTONIUM

A Dissertation
Presented to
the Graduate School of
Clemson University

In Partial Fulfillment
of the Requirements for the Degree
Doctor of Philosophy
Environmental Engineering and Science

---

by
Hilary Palmer Emerson
December 2014

Accepted by:
Brian A. Powell, Committee Chair
O. Thompson Mefford
Fred J. Molz
Lindsay Shuller-Nickles

ABSTRACT

Colloid-facilitated transport of the actinides has been observed previously in the field on the kilometer scale. The objective of this work is to investigate the mechanisms of colloid-facilitated transport with controlled settings and conditions. The experimental work in this dissertation investigates transport of a ternary complex with iron oxide colloids, organic ligands and actinides in the presence of quartz or a natural sandy soil as well as simplified systems building up to the ternary complexes. The first three papers investigate the following: (1) unsaturated transport of iron oxide colloids in a natural sandy soil lysimeter with and without natural organic matter, (2) sorption and reduction of plutonium on iron oxide colloids through batch sorption and ATR FT-IR experiments, and (3) the reversibility of sorption in ternary systems with variable ligands and salts, a natural sandy soil and plutonium. The fourth and final paper brings together the concepts investigated in the first three papers to demonstrate colloid-facilitated transport of the actinides on iron oxide colloids and fulvic acid through quartz or natural sandy soil in laboratory scale column experiments. The ATR FT-IR experiments observed surface-mediated reduction in real time and measured peaks for Pu(VI) and Pu(V) sorbed to hematite for the first time at ~916 and 836 cm^{-1}, respectively. Batch experiments with Pu showed that sorption is strong at near-neutral pH and desorption is minimal even in the presence of different ligands. However, the lability of sorbed Pu complexes may be changing with time. This body of work has shown that colloidal transport of iron oxides and associated contaminants is minimal under unsaturated conditions and in the presence of natural, clay-sized soil coatings. While organic ligands significantly increased

transport of iron oxide colloids and associated contaminants in the saturated quartz sand systems, the increase in transport was not significant in the presence of natural soils with clay-sized coatings. The following complexes are listed in order of mobility in quartz: fulvic acid – actinide > iron oxide colloid – fulvic acid – actinide > dissolved actinide > precipitated actinide ~ iron oxide colloid – actinide.

DEDICATION

I would like to dedicate this manuscript to my family and friends who have always supported me in all of my endeavors. A special thank you to my mom for her endless encouragement. To my dad for instilling a love for learning very early in life. He first inspired me to to explore science through our annual science fair projects. To my aunts and uncles for always being there for me growing up. To my husband for always believing in me, for managing the rest of our lives as I finished this manuscript, and for making sure that I had plenty of food to eat through the final months of this process. To all of my friends who will finally get to hear about something other than this dissertation. Finally, to Dr. Powell for all of his help and inspiration throughout my time here at Clemson.

TABLE OF CONTENTS

TABLE OF CONTENTS (Continued)

Page

TABLE OF CONTENTS (Continued)

Page

TABLE OF CONTENTS (Continued)

LIST OF FIGURES

Page

LIST OF FIGURES (Continued)

Page

Page

Page

LIST OF FIGURES (Continued)

Page

LIST OF TABLES

LIST OF TABLES (Continued)

Page

LIST OF TABLES (Continued)

Page

CHAPTER ONE INTRODUCTION

Introduction

Plutonium exists due mostly to anthropogenic sources with only two of the nineteen possible isotopes contributing a small amount of naturally produced plutonium due to cosmic interactions (^{244}Pu) and neutron absorption in concentrated uranium ores (forming ^{239}Pu) (Kauffman, 2007). Plutonium currently exists in the environment due to accidental releases, improper disposal and testing of nuclear weapons. Examples of these releases for the U.S. are shown in Table 1 below. Runde and Neu give a comprehensive review of the documented releases of plutonium and other actinides worldwide (Runde and Neu, 2010). The fate of plutonium released to the environment is an important area of study because all of its isotopes are radioactive and have high heavy metal toxicity. While these previously contaminated areas are remediated, the stockpiles of plutonium wastes are still increasing yearly by about 70-75 metric tons (Albright and Kramer, 2004; Ewing et al., 2010). It is very important that the transport capabilities of plutonium in the environment are understood, especially with plans for its long term disposal underground in deep geologic repositories.

Table 1.1: Plutonium inventories at various sites in the United States

Site	Release Conditions	Activity	Reference
Nevada Test Site	Subsurface weapons testing	2775 kg (3.1×10^{16} Bq)	(Bowen et al., 2001)
Savannah River Site, GA	Streams, seepage basins, atmosphere	16.4 Ci (6.07×10^{11} Bq)	(Carlton et al., 1992)
Los Alamos, NM	Unlined seepage basins	3.7×10^{11} Bq	(Nyhan et al., 1985)
Hanford, WA	Liquid waste	11,800 Ci (4.37×10^{14} Bq)	(Cantrell, 2009; Felmy et al., 2010)

The following work provides background and data for the examination of environmental transport of plutonium by colloids. Colloids are particles <1000 nm, with a high surface area and a terminal gravitational settling velocity of $<10^{-2}$ cm/sec (Stumm, 1977). In addition, colloids are generally classified as intrinsic or associative/pseudo colloids. Intrinsic colloids are composed of actinides as oxides or hydroxides (Utsunomiya et al., 2009), but will not be a major process in the geochemical environment in the context of a nuclear disposal site (Moulin and Ouzounian, 1992). Associative colloids are defined as colloids formed as a result of adsorption of trace amounts of actinides onto impurities or other foreign materials (Silva and Nitsche, 1995). While colloid-facilitated transport of contaminants is not a new concept, the mechanisms of colloid-facilitated transport of the actinides are still not well understood and better predictive models are needed (Honeyman, 1999; Kersting, 2013; McCarthy and Zachara, 1989; Ryan and Elimelech, 1996; Zanker and Hennig, 2014). This work will be used to better understand previous field studies that have attributed enhanced transport of plutonium to its association with natural colloids or pseudo colloids (Buesseler et al., 2009; Kaplan et al., 1994; Kersting et al., 1999; McCarthy and Zachara, 1989; Novikov et al., 2011; Novikov et al., 2009; Novikov et al., 2006; Penrose et al., 1990; Santschi et al., 2002) and suggests that colloid-facilitated transport could occur as pseudo colloids in both the near and far field (Novikov et al., 2006; Smith and Degueldre, 1993; Zanker and Hennig, 2014). It is important to note that in the scenario for deep geologic waste disposal, colloid transport could be due to pseudo colloids formed from environmental particles or degradation of the waste form, package or backfill materials (Avogadro and

Marsily, 1984). Iron oxide colloids will be the major focus of this work because of previously field studies suggesting association of plutonium with iron oxide colloids (Novikov et al., 2011; Novikov et al., 2009; Novikov et al., 2006). Further, hematite colloids will be used as a model for laboratory-scale transport experiments because they are the expected end product in Fe(III) oxides (Schwertmann, 1991) and because they may form due to the degradation of waste packages of deep geologic waste repositories. The data will be used to modify risk assessment models for the future disposal of high level waste in deep geological waste repositories. Previously, Contardi and team concluded that the population's total effective dose from the radionuclides stored at the proposed Yucca Mountain nuclear waste repository could increase by as much as 60-fold after 10,000 years if colloid-mediated transport is included in the fate and transport models (Contardi et al., 2001). Their transport model accounts for enhanced colloidal transport due to irreversible formation of actinide colloids. However, work by Mills *et al*. reported that the increase in aqueous contaminant concentration and the decrease in travel time in the presence of colloids were not remarkable even on the order of thousands of years (Mills et al., 1991). In addition, colloidal release of ^{239}Pu may be the second largest dose contributor after 70,000 years based on performance assessment models (Lu et al., 2003). The currently proposed work is necessary to fully understand the mechanisms of colloid-facilitated transport of plutonium and quell discrepancies in current models for colloid-facilitated transport.

Background

Previous researchers (Honeyman, 1999; McCarthy and Zachara, 1989; Ryan and Elimelech, 1996) summarize the important conditions for colloid and colloid-facilitated transport of radionuclides as described below:

1. Colloids must exist in appreciable concentration
2. Colloids must be mobile and stable in the environment of interest
3. Colloids must be able to sorb radionuclides
4. Colloids and the associated radionuclides must be transported through the aquifer

While satisfaction of these four conditions may appear simple, environmental systems are complex and changing. These conditions for enhanced transport of contaminants by colloids will be discussed individually with respect to colloid-facilitated transport specifically for actinides associated with iron oxide colloids.

Colloid concentrations in groundwater systems

The existence of colloids in the natural environment is well documented and briefly reviewed by Hochella *et al*. (Hochella et al., 2008). Colloids are defined as particles having a diameter from a few nanometers to 1 micrometer and may form and persist in environments where nucleation rates are high and growth rates are slow. Generally, field studies have shown that colloid concentrations decrease as ionic strength concentrations increase (Degueldre et al., 2000). However, the oceans are an exception where it is expected that a significant fraction of the 'dissolved' (<0.4 μm) iron is actually composed of 2-5 nm nanoparticles coated with organic compounds as described in a review by Hochella *et al*. (Hochella et al., 2008). Colloid concentrations in

subsurface systems can be significant and have been measured between $10^{7.5}$ and 10^{17} particles/L (Degueldre et al., 1989; Degueldre et al., 1996; Degueldre et al., 2000; Kim, 1991; Kim, 1994; Kim et al., 1994; Novikov et al., 2006; Sen et al., 2002; Zanker and Hennig, 2014) or 0.1 to 260 mg/L concentrations (Buddemeier and Hunt, 1988; Degueldre et al., 1996; Kersting, 2013; McCarthy and Degueldre, 1993; Moulin and Ouzounian, 1992; Roberts et al., 2004; Vilks et al., 1988) in previous works. In addition, researchers have noted that colloids are present at some concentration in all groundwaters (Degueldre et al., 1996; McCarthy and Degueldre, 1993). Buddemeier and Hunt (1988) specifically noted that colloid concentrations were increased near detonation cavities at the Nevada Nuclear Security Site with concentrations near 55 mg/L. Colloids may be present in environmental systems as inorganic minerals or organic ligands. In granitic systems the dominant colloids identified are phyllosilicates and silica colloids. However, the Underground laboratory within a granitic formation in Canada identified clay, iron oxide with organic, and carbonate minerals within the colloidal size fraction (Degueldre et al., 1996). The French granitic site identified mostly silica and organic colloids.

However, concerns have been raised as to the sampling practices for measurement of colloids (Degueldre et al., 1996; McCarthy and Zachara, 1989). There are possible experimental artifacts due to sampling procedure including: flow rate disturbances mobilizing colloids from solid surfaces, subsurface fractures exposing mobile colloids, and instantaneous changes in oxidation/reduction conditions causing precipitation of colloids. The most important aspect during sampling being the flow rate as a high flow rate can produce inflated estimations of mobile colloid fractions. In addition, laboratory

practices have made comparison of measurements difficult due to differences in characterization technique (Choppin, 2007; Degueldre et al., 1996; Hassellov et al., 2008). Most importantly the characterization of different size fractions of particles by different techniques including filtration, centrifugation, and particle size analyzers are extremely variable. For example, Choppin notes that the fraction of Pu(IV) measured in the dissolved phase is dependent on filter type and size (Choppin, 2007). There is a possibility for measurement of unstable colloids, precipitated colloids, artificially-generated colloids, and stable and mobile colloids. Each of these must be considered with the measurement of colloids from subsurface groundwater samples. Throughout the work presented below, multiple techniques will be utilized for each experimental setup described to allow for better comparison.

Stability of colloids in groundwater systems

It is expected that the colloidal fraction will be representative of minerals in the bulk of the subsurface; however, some minerals may be more mobile or stable in suspension than others. A colloid suspension that is stable will be less likely to aggregate and/or sorb to bulk mineral surfaces. The primary generation process for colloidal particles is due to physical fragmentation of the bulk minerals in contact with groundwater (Degueldre et al., 1996). Previous work has shown that a secondary mechanism for release of colloids is strongly controlled by the chemical composition of the pore water and that their persistence in suspension can be described by a nonexponential decay (in most cases a power law) which allows for a small fraction of mobilized colloids to remain in suspension for long periods of time where transport is not

significantly reduced by reattachment or deposition (Degueldre et al., 1996; Grolimund et al., 2001a; Grolimund and Borkovec, 2001, 2005; Grolimund et al., 2001b). In addition, infiltration waters that are dilute solutions composed of monovalent ions, especially sodium, are most effective for mobilization and release of colloids (Gamerdinger and Kaplan, 2001; Grolimund et al., 2001a; Grolimund and Borkovec, 2001, 2005; Grolimund and Borkovec, 2006; Grolimund et al., 2001b; Roy and Dzombak, 1996; Ryan and Elimelech, 1996) and higher concentrations of strong flocculants like Fe^{+3} and Al^{+3} can lead to decreased colloid concentrations. However, mobilization and release mechanisms will not be the focus of this work. The focus of this work will be the transport of colloids after they have been mobilized or stabilized.

Throughout this manuscript stability will refer to the likelihood of particles to remain suspended in solution with the assumption that a particle with greater stability will exhibit a greater mobility in the environment. In addition to a particle's stability in suspension, a mineral's thermodynamic stability could affect results. Hematite nanoparticles are the focus of this work as they are the most thermodynamically stable iron oxide mineral which can be formed through different conditions from dissolved iron, ferrihydrite or goethite (Navrotsky et al., 2008; Schwertmann, 1991). While a smaller particle size (greater surface area) can lead to a more positive Gibb's free energy decreased surface hydration leading to changes in thermodynamic stability, this is not the focus of this work. The nanoparticles will be monitored over time for overall changes in size, stability and dissolution but changes are not expected to be significant over the timescale of this work. This concept will be important in this work as a primary objective

is the investigation of the transport ability of colloids. In addition, other iron oxides and some clay minerals will be discussed as some systems in these experiments will include other naturally occurring minerals.

The stability of colloids can be theoretically estimated by DLVO theory as described by Derjaguin and Landau (1941) and Verwey and Overbeek (1948) previously (Derjaguin and Landau, 1941; Verwey et al., 1948). It defines the stability of a particle in suspension as the sum of the repulsive (Van der Waals) and attractive (electrostatic) forces. Van der Waals forces are long range forces (generally greater than 10 nm), follow an inverse power law with respect to distance, and will be largely insensitive to pH and electrolyte fluctuations. These forces are attractive for similar particles in suspension. Electrostatic forces are considered to be short range forces that are repulsive for similar particles and increase exponentially with respect to distance. In addition, these forces are greatly affected by changes in pH and electrolyte concentration. DLVO theory does neglect some other forces for simplicity including steric or osmotic forces and structural or hydration forces. Steric interactions; however, will be important under environmentally relevant conditions and may allow particles to reach greater stability through the presence of various organic ligands (with variable pH and electrolyte solution as these are generally repulsive like electrostatic interactions). Macromolecules (like NOM with hydrophobic components to anchor to the particles and hydrophilic, stabilizing moieties) can be used to sterically stabilize colloids.

Stability can be determined theoretically by DLVO theory or experimentally by estimation of the stability constant (W) which is the inverse of the collision efficiency

(α). Elimelech and Ryan note that theoretical DLVO predictions are not as reliable in environmental systems due to soil surface heterogeneities, roughness and poor characterization of surface properties (Elimelech and Ryan, 2002). Stability constants (W) can be determined experimentally by the following equation (Berg, 2010), through measurement of the changes in particle size with time.

$$W = \frac{dr/dt_{fast}}{dr/dt} = \frac{k_{fast}}{k}$$

where W= stability constant

dr/dt= average rate of change of hydrodynamic particle radius with time

dr/dt fast= average rate of change of radius during initial fast aggregation/coagulation

Zeta potential measurements of nanoparticles or colloids in suspension can also give a better understanding of a particle's stability. Measurements within the range of +20 to -20 mV are generally considered to be unstable in suspension because this is the threshold for the energy of *kT* (where k=Boltzmann constant and T=absolute temperature) (Berg, 2010). The potential energy of particles is generally less than a few *kT* due to the effects of Brownian motion; therefore, this is a fair assumption for nanoparticle and colloid stability in suspensions (Elimelech et al., 1995). In environmental systems there are four major mechanisms that can lead to the deposition of colloids and associated contaminants: straining, Brownian motion, interception and sedimentation (Elimelech et al., 1995). The ratio of L_s/L_d (equations below) represents the relative influence of Brownian motion versus settling/sedimentation with L_s

representing the Stoke's settling time for a particle and L_d defined as the Brownian motion length scale [as summarized in (Zvikelsky and Weisbrod, 2006)]. The impact of Brownian motion can also be estimated by Fick's second law and is generally important for particles with a diameter less than 1 μm. Straining will only be important in porous media systems where the ratio of the particle diameter to the grain diameter is greater than 0.2.

$$L_s = \left(\frac{1}{18\mu}\right)(\rho_p - \rho_f) g {d_p}^2 \tau$$

$$L_d = \sqrt{2D\tau}$$

where $D = \frac{kT}{3\mu\pi d_p}$

D= Stokes-Einstein diffusion coefficient
T=water temperature
k= Boltzmann constant
d_p= particle diameter
ρ_p= particle density
ρ_f= fluid density
τ= time
g= gravity
μ= fluid viscosity

The size of the colloids may also be important in determining the stability of colloids in the subsurface. However, work by Guzman *et al*. reported that aggregated titania nanoparticles over a range of pH values can still be mobile (Dunphy Guzman et al., 2006). There is currently a paradox when considering the ideal size of the colloid for stability and transport conditions. In terms of mechanical interactions with the soil and lift forces near the surface's turbulent boundary layer, the smallest colloid is expected to be the most mobile. However, Sen and Khilar have proposed that any ratio of colloid

size to pore size will result in some losses due to size exclusion, multiparticle blocking, and/or surface deposition (Kanti Sen and Khilar, 2006). In terms of equilibrium forces of a suspension excluding velocity, a smaller nanoparticle may or may not be more stable. In addition, as the particles are made smaller, thermal energies play a greater role while inertial and gravitational forces become negligible. This lesser affect by gravity as size decreases may result in a decrease in the likelihood of settling of nanoparticles or colloids. However, if the vapor pressure increases as the particle size decreases as described by the Kelvin effect, particles are more likely to be trapped in soil pores and solubility may increase.

Some studies have noted an increase in the reactivity of nanoparticles as their size decreases leading to a decrease in their stability in solution. In a review by Hochella, it was suggested that the surface area-normalized variations begin with nanoparticles smaller than a few tens of nanometers (Hochella et al., 2008). An increase in reactivity was reported by He *et al*. with hematite nanoparticles of 12, 32, and 65 nm with lower electrostatic repulsion and critical coagulation and greater aggregation rates for the smallest nanoparticles (He et al., 2008). Other researchers also noted changes in reactions with dissolved metals as particle size decreases. For example, an increase in adsorption affinity as particle size decreased was reported for copper sorption to hematite (Madden et al., 2006) and oxidation and reduction reactions were significantly increased for aqueous Mn^{2+} oxidation by hematite nanoparticles and hydroquinone-driven reductive dissolution of goethite nanoparticles as compared to bulk-sized minerals (Anschutz and Penn, 2005; Hochella et al., 2008). The increased reactivity as particle size decreases

could lead to increased growth rates and settling from suspension or sorption to larger particles and settling. Schrick *et al.* proposed an optimum particle size of 400-500 nm and notes that the calculations are almost independent of soil grain sizes and that the smaller particles are dominated by diffusion processes (Schrick et al., 2004). Zviskelsy and Weisbrod found an optimum particle size of approximately 200 nm for transport through chalk fractures but noted several other studies that found an optimal particle size dependence between 360 and 500 nm for transport (Zvikelsky and Weisbrod, 2006).

Studies often consider a particle's surface area (which is generally correlated with particle size) for prediction of sorption capacity; however, a recent study found that these measurements are not adequate for predicting the sorption capacity of particles because other changes can occur at interfaces including alteration of the ordering of water molecules and counterion layers (Gilbert et al., 2009; Navrotsky et al., 2008). These authors found that environmental changes such as variations in pH, ionic strength and water content can greatly affect sorption of contaminants to colloids but concluded with drying exhibiting the greatest effect. Ostwald ripening is another factor to be considered. This process occurs because larger particles are more energetically favorable than smaller particles which can lead to particle growth and deposition from solution. The working hypothesis for this work is that the colloid with the greatest potential for transport may not be the smallest particle size but will be most stable in suspension; therefore, particles will be monitored over time for settling and dissolution by filtration and centrifugation as well as aqueous particle size, zeta potential, and total iron measurements.

The stability of colloids in the environment is not fully understood; however, there is evidence that the presence of organics could increase their stability and decrease sorption in groundwater systems. Because the points of zero charge (PZC) for many iron oxides are near-neutral to basic pH with reported hematite values ranging from 7-9.3 (Kosmulski, 2002, 2011), iron oxides are expected to have a slightly positive charge or zeta potential for the neutral pH of most groundwater systems. Groundwater systems with a slightly basic pH would be the most unlikely system for transport of iron oxide colloids because the particles would be least stable near the PZC. This was shown previously with titania nanoparticles where transport was observed across the pH range even in suspensions with visible settling with the exception of pH values near the PZC where complete settling occurred (Dunphy Guzman et al., 2006). Also, because most subsurface sediments have an overall negative charge at neutral pH, iron oxide colloids are expected to be attracted to the subsurface sediments based on the system pH (Kosmulski, 2002, 2011; McCarthy and Zachara, 1989). Therefore, the stability of iron oxide colloids in environmental systems is expected to be low (Vilks et al., 1998; Zanker and Hennig, 2014). However, Moulin *et al*. reported that an increase in pH led to a decrease in colloid retention (Moulin et al., 1996).

There are conditions that can lead to a reversal of the colloid surface charge (like the presence of organic ligands) and heterogeneities in the subsurface sediments may alter colloid-surface attraction (Ryan and Elimelech, 1996). For example, Degueldre *et al.* showed a correlation between organic content and natural colloid mobility (Degueldre et al., 2000). The presence of stabilizing organic ligands will be crucial for colloid-

facilitated transport on iron oxide colloids as it can reverse the charge (Zanker and Hennig, 2014). Several studies have investigated the ability of natural organic matter (NOM) to stabilize iron oxide nanoparticles (Baalousha, 2009; Baalousha et al., 2008; Dunnivant, 1992; Gu et al., 1995; Kretzschmar and Sticher, 1997; Schafer et al., 2003; Schrick et al., 2004) and to sorb to iron oxides in the environment (McKnight et al., 1992a; McKnight et al., 1992b; Seijo et al., 2009). The sorption of humic substances to inorganic colloids is increased at acidic pH and decreases as pH increases (Banik et al., 2007; Murphy et al., 1999; Reiller et al., 2002).Another study demonstrated increased stability of natural colloids in the presence of natural organic matter by isolation of mobile colloids from saprolite cores followed by column studies with isolated colloids with and without a NaOCl pretreatment to remove organics (Kretzschmar, 1995). Previous work in natural systems have reported a varying range of organic matter from 0.2 to 50 mg C/L for surface waters like rivers and lakes and 0.1 to 19.5 mg C/L for groundwater systems with the exception of shallow groundwater systems with surface water recharge which can be greater (Choppin and Allard, 1985; Short et al., 1988; Thurman, 1986; Vilks et al., 1997). Dissolved organic carbon has even been measured at 150 - 200 mg C/L in interstitial clay water in Belgium (Moulin and Ouzounian, 1992; Moulin et al., 1996; Reiller et al., 2002). In addition, impacted area such as the Nevada test site have measured dissolved organic carbon in the range of 0.3-21 mgC/L (Zhao et al., 2011).

Brownian dynamics simulations by Seijo *et al*. include colloid architecture, physicochemical properties and solution properties to show that at low ionic strength

fulvic acid adsorption to hematite and biocolloids colloids is controlled by electrostatic interactions and fulvic acid interactions with colloids can be considered instantaneous as compared to coagulation processes (Seijo et al., 2009). While these simulations were run at a high fulvic acid concentration (2 g/L), they also estimate critical coagulation at an ionic strength of 0.3 mol/L and present images of fulvic acid adsorption to hematite at variable ionic strengths showing adsorption of coagulated chains of fulvic acid at higher ionic strength. Further, Righetto *et al*. showed that the charge (zeta potential) of colloids could be reversed with 25 mg/L but not 5 mg/L of humic acid in suspensions of 200 mg/L of alumina in 0.1 M $NaClO_4$ (Righetto et al., 1991).

While previous studies have demonstrated increased stability of colloids in the presence of NOM through reversal of the electrostatic charge, the complexity and variability of NOM leaves multiple functional groups to explain the enhanced stability with a great likelihood that the stability is enhanced by a combination of groups. While the identification of these functional groups is not the focus of this study, it is important to review proposed theories for comparison with the organic ligands in our experiments. Previous work hypothesized that the negative surface charge is likely due to the carboxylic and phenolic groups within humic acid (Murphy et al., 1999; Righetto et al., 1991). Fulvic acids are soluble under acidic pH and represent the lower molecular weight fraction of humic substances which are the major natural organic carbon content of soils and natural waters. Fulvic acids can represent a large fraction of the dissolved organic carbon in natural waters [15-80%] (Leenheer and Huffman, 1976). Fulvic acids high in carboxylate (Marley et al., 1993) or hydrophilic acids (like many amino acids)

(Dunnivant, 1992) may be the most mobile. However, McKnight showed that aromatic moieties, carboxylic acid and amino acid groups may be preferentially removed along the flow path in a creek due to ligand exchange mechanisms with suspended oxides (>450 nm by filtration) and that fulvic acids sorbed to suspended oxides were more aromatic [35%] (McKnight et al., 1992a). In addition, Roberts *et al.* did not measure any nitrogen above detection limits in colloid samples concentrated from groundwater from Rocky Flats where plutonium has been shown to be associated with colloids of primarily crystalline organic content (Roberts et al., 2004). Therefore, amines may not be contributing significantly to transport in the Rocky Flats system.

Because NOM has many different functional groups, each may be contributing to the stabilizing effect, charge reversal and sorption of NOM coatings on colloids. Some of the major components include: carboxyl groups, phosphates, amino acids, and aromatic functional groups. Steric stabilization can occur based on the presence of both hydrophilic and hydrophobic fractions of NOM as nanoparticle steric stabilization theory requires that an effective macromolecule has both anchor groups and stabilizing moieties meaning that they commonly include both hydrophilic (stabilizing) and hydrophobic (anchoring) groups (Berg, 2010). Because a stabilizing and an anchoring group are required for sufficient steric stabilization, it is hypothesized that a combination of the aforementioned functional groups and components will aide in the sorption and stabilization process. The smaller fulvic and organic acid fractions will be the focus of this work because they are expected to be the most mobile (Dunnivant, 1992; Marley et al., 1993; Moulin et al., 1996), have been shown to be present in groundwater systems

(Leenheer and Huffman, 1976; Mladenov et al., 2010), and sorb strongly to iron oxide minerals (McKnight et al., 1992a; McKnight et al., 1992b). Work by Mercier *et al*. has shown that trace metals have a greater affinity for the smaller fraction (<15 nm) of humic substances with an association with 31% of trace metal fraction (Mercier et al., 2001). The major theories for sorption of NOM to minerals are (1) complexation or ligand exchange, (2) cation or hydrogen bond bridging, and/or (3) entropy drive physical adsorption or hydrophobic repulsion (Murphy et al., 1999; Reiller et al., 2002).

Previous work also supports other mechanisms (besides NOM) for the stabilization of colloids. For example, while the body of work on stability of colloids in the presence of changing ionic strength has shown that divalent (and polyvalent in general) salts have a greater destabilizing effect than monovalent salts (Lu et al., 2003), some studies have noted a reversal for calcium in the presence of iron oxide colloids. For example, Kretzschmar and Sticher recorded breakthrough of hematite colloids prior to the tracer in the presence of dissolved calcium and sandy soils due to the exclusion of positively charged colloids from small pores (Kretzschmar and Sticher, 1997). Another study noted an increase in mobility in the presence of dissolved calcium specific to goethite (Seaman et al., 1995).

Colloids may also be stabilized based on their greater affinity for complexation with other dissolved complexes. Degueldre *et al*. reported that fluorites may contribute to colloid leaching and mobility because of their ability to form strong complexes (Degueldre et al., 2000). It is possible that other common groundwater constituents like carbonates and phosphates may similarly contribute to stability. When considering the

different mechanisms that may be contributing to the mobility and stability of colloids, the systems will be well-characterized. Each mechanism will be investigated separately as proposed with (1) characterization of colloid interactions with soils, (2) plutonium interactions with colloids, (3) NOM interactions with colloids, and (4) plutonium interactions with soils before adding all of the components together into transport experiments. Systems with different electrolytes will be investigated, including NaCl because it has been proposed that chlorides interact specifically with iron oxides (Kosmulski, 2002), calcium salts for the aforementioned properties and $NaClO_4$ because the perchlorate ion is generally non- reactive.

Sorption of actinides to colloidal-sized minerals

Due to the strong sorption of the actinides to inorganic minerals and their low solubility (Choppin, 2006, 2007; Knopp et al., 1999; Neck et al., 2007; Neck and Kim, 2001), it is generally expected that transport of the actinides will be minimal. However, if the actinides sorb to mobile colloids, their mobility could be significantly increased (Kersting, 2013; McCarthy and Zachara, 1989; Zanker and Hennig, 2014). Further, the focus of this work will be tetravalent plutonium as it has the greatest sorption affinity and lowest solubility as discussed below. In addition, deep groundwaters are expected to exhibit reducing conditions that would lead to the tetravalent oxidation state of the actinides being dominant (Degueldre et al., 1996; Kim and Grambow, 1999). In addition, Pu(IV) is generally expected to be the dominant oxidation state of plutonium in natural systems (Choppin, 2007). However, Th is the most commonly used tetravalent analog. Although it has no f electrons and has a slightly larger ionic radii, it is a common stable

oxidation state analog for tetravalent actinides especially plutonium (Choppin, 1999, 2007; Krauskopf, 1984; Neck and Kim, 2001). It does exhibit slightly weaker sorption as compared to Pu.

Plutonium will be discussed in depth here due to its complex redox chemistry. Plutonium has been shown to sorb very strongly to bulk iron oxides (Hixon et al., 2010; Hixon and Powell, 2014; Powell et al., 2011; Powell et al., 2004, 2005) and to hematite nanoparticles (Lu et al., 1998; Lu et al., 2003; Romanchuk et al., 2011). Evidence published by Powell *et al*. supports incorporation of plutonium intrinsic nanoparticles into goethite based on a distortion of the plutonium colloid crystal structure wherein the goethite surface facilitates an epitaxial distortion of the PuO_2(s) nanocolloid which forms a very strong plutonium-iron oxide complex and Schmidt *et al*. used EXAFS to show that muscovite can adsorb 40 times more Pu as NPs than that expected for the Pu^{4+} ion (Powell et al., 2011; Schmidt et al., 2012). In addition, Lu *et al.* demonstrated low reversibility of sorption based on desorption experiments of up to 293 days with less than 1% of the plutonium desorbed (Lu et al., 1998; Lu et al., 2003). Begg *et al*. was able to achieve significant desorption of Pu from goethite in the presence of 5-500 μM H_2O_2 (greater than 30% over 21 days at pH 4 and 6) and some desorption from montmorillonite and silica (Begg et al., 2014). H_2O_2 can form photolytically in oceans and natural waters (Choppin, 2007). Pu sorbs much more strongly to minerals containing Fe and Mn as opposed to those that do not in the presence of H_2O_2 (Begg et al., 2013). However, Banik *et al*. reported that Pu desorption was partially irreversible with only 1-10% desorption (Banik et al., 2007). Furthermore sorption and desorption kinetics of the contaminant to

the colloid have been shown to effect to transport by Turner *et al*. with cesium and strontium on illite colloids and Tinnacher *et al*. reported that desorption kinetics for neptunium sorption to goethite colloids was significantly less than the adsorption parameter (Tinnacher et al., 2011; Turner et al., 2006). Strong sorption of plutonium to iron oxide mineral phases is required for colloidal transport on iron oxide colloids; however, it is important to remember that there will certainly be competing sorption sites on the bulk soils and rock. This competition is commonly neglected in laboratory column experiments with quartz sand; however, much stronger sorption sites will be present in environmentally relevant, heterogeneous soils. There will be a combination of sorption of plutonium to bulk minerals and to mobile colloidal material. However, if sorption is irreversible, colloids could control the transport of a fraction of actinides through groundwater systems (Moulin and Ouzounian, 1992). Several studies have noted that the reversibility of actinide sorption decreases with time (Kaplan et al., 2004; Missana et al., 2004; Tinnacher et al., 2011; Vilks and Baik, 2001).

Tinnacher *et al.* defines the following terms that could describe changes in (de)sorption kinetics (Tinnacher et al., 2011) with visual representation in Figure 1.1 below.

1. Aging- one or more surface chemical processes that follows the initial sorption reaction and causes changes in contaminant surface speciation over time (interpreted by an increase in K_d with time)
2. Hysteresis- a thermodynamic property, which is indicated by different sorption affinities depending on the net direction of surface reactions (often used as an

equivalent to some degree of irreversible desorption behavior, implies a non-equilibrium transfer of contaminants between solution and mineral surfaces)

3. Irreversible sorption- one specific case of hysteresis, where a fraction of contaminant remains adsorbed after complete desorption equilibration with a solute-free solution

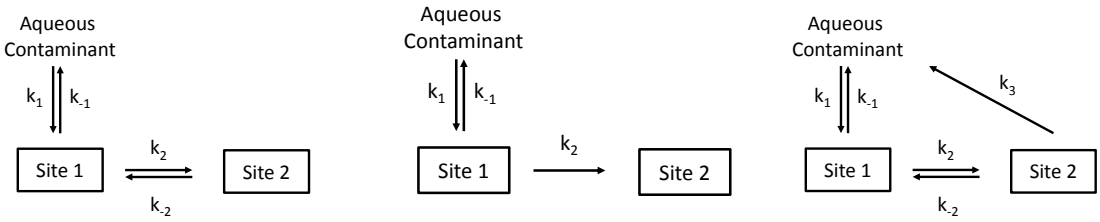

Figure 1.1: Conceptual description of two site model sorption behavior exhibiting reversible (left), irreversible (middle), and hysteretic (right) sorption processes. Note: The sites represented in the figure do not necessarily represent a movement of the contaminant to another surface site. They could represent changes of the contaminant (i.e. loss of hydrating waters) or of the surface (i.e. relaxation of the surface).

It is hypothesized that plutonium sorbs to the surface through surface complexation (i.e. covalent bonding with the mineral surface) followed by reduction (Keeney-Kennicutt and Morse, 1985). The affinity of plutonium oxidation states for sorption increases with effective charge. In addition, the different oxidation states for plutonium follow similar electrochemical potentials as shown below allowing for the presence of multiple oxidation states simultaneously. Previous laboratory studies have shown reduction and sorption of plutonium to non-reducing mineral surfaces (Powell et al., 2006; Powell et al., 2004, 2005; Romanchuk et al., 2011; Sanchez et al., 1985; Shaughnessy et al., 2003).

This is an important concept in this work because hematite is considered a non-reducing mineral as it is an Fe^{+3} compound.

$$+4\ [Pu(IV)] > +3.3\ [Pu(VI)O_2] > +3\ [Pu(III)] > +2.3\ [Pu(V)O_2]$$

(Silva and Nitsche, 1995)

Table 1.2: Electrochemical potentials for redox couples (mV) of plutonium

Couple	Acidic (Lemire et al., 2001)	Neutral (Allard et al., 1980)	Basic (Abuzwida et al., 1991)
Pu(IV)/Pu(III)	+0.982	-0.39	-0.96
Pu(V)/Pu(IV)	+1.17	+0.70	-0.67
Pu(VI)/Pu(V)	+0.913	+0.60	+0.12
Pu(VI)/Pu(IV)	+1.043	+0.65	+0.34
Pu(V)/Pu(III)	-	1.076	-
Pu(VII)/Pu(IV)	-	-	+0.85

The mechanisms of sorption and reduction are not completely understood and there are several hypotheses proposed to describe surface mediated reduction Pu(V) and frequently observed strong sorption of Pu(IV). These hypotheses are summarized below from previous researchers (Powell et al., 2005; Romanchuk et al., 2013)

1. Thermodynamic favorability of Pu(IV) hydroxide complexes
2. Self-reduction via radiolysis byproducts
3. Presence of trace reductants such as Mn(II) and Fe(II) on the surface
4. Electron shuttling from semiconductor materials
5. Plutonium disproportionation

It is important to understand these mechanisms for reduction and sorption of plutonium because the sorption affinities, and thus subsurface migration, are profoundly dependent

on which oxidation state is present. The plutonium-hematite batch sorption studies described in section 5 will investigate some of the hypotheses above describing theories for surface mediated sorption and reduction including electron shuttling from semiconductor materials and presence of trace reductants. It is important to note that self-reduction via radiolysis products (Hixon et al., 2013; McCubbin et al., 2002; Romanchuk et al., 2011) has been ruled out and disproportionation is unlikely at low, environmental concentrations. In addition, it has been proposed that there would be adequate Fe(II) to promote reduction of plutonium(V) in hematite (Romanchuk et al., 2011) as well as montmorillonite (Begg et al., 2013).

The conditions under which the colloids were generated and the actinides entered the environment may also contribute to mobility and stability in subsurface environments. Choppin and Allard (1985) and Buffle (1988) previously emphasized the importance of iron oxide and organic colloids as cation scavengers and field studies confirm this with the actinide elements (Buffle et al., 1998; Choppin and Allard, 1985). For example, Duff *et al*. reported that plutonium sorbed to Yucca Mountain tuff could not be associated with iron oxides in tuff materials due to passivation of iron oxide surfaces by coatings of silica, carbonate minerals or organic matter (Duff et al., 1999). Another study by Schafer *et al*. generated iron oxide colloids in the presence of americium that transported americium more quickly than those exposed to americium after synthesis likely because the americium was incorporated into the colloids (Schafer et al., 2003). In another study by Vilks and Baik increased transport of a small fraction of americium (8.2%) in the presence of natural colloids and an irreversibility of sorption was reported (Vilks and

Baik, 2001). While the conditions under which the colloids and complexes are formed may be important for transport, it may not be especially important for plutonium in the presence of iron oxide colloids due to its strong affinity/sorption and hysteresis as discussed above.

Furthermore, sorption of actinides to organic matter has been previously investigated (Artinger et al., 2003; Marley et al., 1993; McCarthy et al., 1998a; McCarthy et al., 1998b; Novikov et al., 2011; Righetto et al., 1991; Santschi et al., 2002; Silva and Nitsche, 1995; Zhao et al., 2011). Work at the Rocky Flats site by Santschi *et al*. has shown that plutonium is commonly associated with organic macromolecules in the environment (Santschi et al., 2002). In addition, experiments by Litaor and Ibrahim with sequential extractions of plutonium from Rocky Flats soils resulted in 70-90% of the plutonium being associated with organics and sesquioxide (minerals with three oxygen atoms and two of another element) minerals (Litaor and Ibrahim, 1996). Further work by Litaor *et al*. on mobilization experiments in Rocky Flats reported plutonium and americium transported fractions of 1-3.3% to greater depths and possibly to groundwater and 0.3-6.8% associated with the colloidal size fraction (Litaor et al., 1998). McCarthy *et al*. reported re-mobilization of actinides by natural organic matter in waste disposal trenches (McCarthy et al., 1998a; McCarthy et al., 1998b). Previous work reported actinide transport in surface water high in dissolved organic carbon (> 60 ppm) that was primarily fulvic acid (81-98%) (Marley et al., 1993) and strongly associated with organic macromolecules with a pH_{iep} of 3.1 and molecular weight of 10-15 kDa (Santschi et al., 2002). Batch sorption experiments with groundwater and tuff samples from the Nevada

test site by Zhao *et al*. estimate Kd's of 1.3 to 13 times higher for samples with dissolved organic matter removed (Zhao et al., 2011). In addition, Xie *et al*. has completed colloid-facilitated transport experiments of Pu with natural colloids at variable colloid concentration (0-2000 mg/L), ionic strength (0.01-0.96 mol/L NaCl) and flow rate (0.472-4.56 mL/min) (Xie et al., 2013; Xie et al., 2014c). The optimum colloid concentration was 375 mg/L with greater than 50% of Pu within the mobile fraction (Xie et al., 2013). As ionic strength increased, transport decreased and zeta potential became more positive (Xie et al., 2014c). With respect to flow rate, their results show that transport increases with increasing pH and hydrodynamic shear forces play a role (Xie et al., 2014c).

Silva and Nitsche report that the affinity of plutonium for humic acids is 100 times greater than that for carbonate species showing a very strong affinity of plutonium for organic matter (Silva and Nitsche, 1995). Reiller *et al*. show that thorium complexation by humic acid can be significant down to 1 mg/L at neutral to alkaline pH based on complexation constants and noted that it may decrease sorption to goethite and hematite iron oxides at concentrations down to 10 mg/L or a ratio of humic sites to iron oxide sites of 2.8 (Reiller et al., 2002, 2003). Zimmerman *et al*. estimated that Pu-humic acid complexation constants were three orders of magnitude greater than those for Th (Zimmerman et al., 2014). Previous work has shown humic substances can reduce Pu and that Pu(IV) will be the dominant oxidation state in the presence of humic substances (Blinova et al., 2007; Marquardt et al., 2004; Shcherbina et al., 2007). In addition, fulvic acids reportedly have greater reduction capacity of Pu than humic acids (Blinova et al.,

2007). Np has also been reported to reduce in the presence of humic substances (Artinger et al., 2003). It has been hypothesized that actinides may be complexed by the carboxylate, carbonyl, ether, alcohol, phenol and amine functional groups. However, Choppin and Allard report that fatty acids, amino acids, and phenolic compounds will not be important complexants below 10 mg C/L (Choppin and Allard, 1985). It will be important to carefully consider the conditions of the experiments discussed below as it is clear that the mechanism of Pu association with colloids (i.e. co-precipitation vs. sorption) and the influence of complexing ligands can alter actinide behavior.

In addition to field experiments demonstrating the strong association of plutonium with organic matter or inorganic minerals, laboratory experiments have begun on the more complex ternary systems. Previous studies have considered batch sorption of actinides in ternary systems with inorganic mineral and citrate (Tanaka et al., 2009), mineral and phosphate, and mineral and humic substances (Banik et al., 2007; Murphy et al., 1999; Reiller et al., 2002, 2003; Xie et al., 2014a, b; Zimmerman et al., 2014). In the presence of humic substances, actinide sorption to minerals is generally increased at low pH and decreased at high pH with respect to binary actinide-mineral systems (Banik et al., 2007; Murphy et al., 1999; Reiller et al., 2002, 2003; Righetto et al., 1991; Zimmerman et al., 2014). Zimmerman *et al*. presented the first ternary surface complexation model for Pu-gibbsite-humic acid (Zimmerman et al., 2014). However, researchers have yet to investigate transport in actinide-ternary systems in laboratory scale experiments.

Evidence for colloid-facilitated transport

There is strong evidence for enhanced colloidal transport of plutonium documented in field studies (Buesseler et al., 2009; Dai et al., 2002; Kaplan et al., 1994; Kersting et al., 1999; Novikov et al., 2011; Novikov et al., 2009; Novikov et al., 2006; Penrose et al., 1990; Santschi et al., 2002). In addition, recent in situ studies by Geckeis *et al*. have shown that colloidal transport will be especially important for the strongly sorbing tri- and tetravalent actinides (Geckeis et al., 2004). It is important to note that the environmental systems considered above are sites with high concentrations of Pu disposed in the subsurface with an extremely small fraction exhibiting colloid facilitated transport. Measured concentrations of plutonium at these sites is 10^{-12} to 10^{-18} M (Buesseler et al., 2009; Dai et al., 2002; Kaplan et al., 1994; Kersting et al., 1999; Novikov et al., 2011; Novikov et al., 2009; Novikov et al., 2006; Penrose et al., 1990; Santschi et al., 2002). Colloid facilitated transport of actinides may be due to iron oxides (Novikov et al., 2011; Novikov et al., 2009; Novikov et al., 2006; Penrose et al., 1990; Short et al., 1988), clay minerals (Kersting et al., 1999), natural organic matter or microbial constituents (Santschi et al., 2002), or possibly nucleation of intrinsic plutonium colloids (McCarthy and Zachara, 1989). Sen and Khilar compiled a review of studies documenting colloid-facilitated transport of metals and identified mobile colloids including iron oxide, iron sulfide, quartz, feldspar, muscovite, lepidocrite, illite, smectite, bentonite and zeolite (Kanti Sen and Khilar, 2006). Short *et al*. reported a strong association of thorium with iron and silica colloids in the Alligator Rivers Region of Australia (Short et al., 1988). Novikov *et al*. reported a strong association of uranium

with amorphous iron hydroxide and hematite colloids in the Mayak region with an atomic ratio of U:Fe of 0.0004 but could not definitively prove association of plutonium with iron oxide colloids due to a much lower molar concentration of plutonium (Novikov et al., 2006). In addition, recent reviews discussing field and laboratory work on colloid facilitated transport of actinides (Zanker and Hennig, 2014) and specifically plutonium (Kersting, 2013) confirm the necessity of understanding colloid facilitated transport of plutonium.

For colloid-facilitated transport to be significant either a large fraction must be mobilized or a small fraction of a large amount of contaminant released must be mobilized within the subsurface as compared to the limit allowed to be present in the groundwater. Previous work has shown that colloid-facilitated transport will be greatest when dissolved organic carbon or inorganic colloid levels are high, aquifers are porous or highly fractured, flow rates are high, and ionic strength is low. Because iron oxide colloids are ubiquitous in the environment and have been suggested as a mechanism for colloidal transport of plutonium by field measurements and subsequent laboratory characterization of the mobile colloid phase (Novikov et al., 2006), iron oxide colloids will be the focus of this investigation of colloid-facilitated transport of plutonium. In addition, an organic ligand will be used to stabilize complexes as previous work by Litaor *et al*. to mobilize plutonium and americium from the soil surface by simulated rain events resulted in 70-90% of the plutonium being associated with organics and sesquioxide minerals (Litaor et al., 1998). In addition, Zanker and Hennig highlight the mechanisms

of stabilization of iron oxide colloids by organic matter to be an important knowledge gap for colloid facilitated transport of actinides by iron oxides (Zanker and Hennig, 2014).

Summary of major knowledge gaps and needs in colloid-facilitated transport of actinides (Kersting, 2013; Moulin and Ouzounian, 1992; Zanker and Hennig, 2014):

Note: knowledge gaps directly addressed in this work are in italics

1. *Develop studies at more representative conditions*
2. *Studies on the kinetic aspects of pseudocolloid formation*
3. Better models describing cation-colloid systems
4. Colloid concentration effect on sorption properties
5. *Reversibility of sorption reactions*
6. *Further investigation of ternary systems with inorganic and organic colloids*

Objectives

The working hypothesis of this research is that colloidal transport of plutonium may be due to strong sorption of plutonium to an iron oxide mineral surface followed by coating and stabilization of that mineral with a naturally-occurring organic ligand. Based on this hypothesis, the overall objective for the proposed dissertation research is to investigate the mechanisms for colloid-facilitated transport of plutonium on iron oxide colloids under environmental conditions with a focus on the conditions for stability and transport. Previous field studies have attributed enhanced mobility of plutonium to colloid-facilitated transport (Buesseler et al., 2009; Dai et al., 2002; Kaplan et al., 1994; Kersting et al., 1999; Novikov et al., 2011; Novikov et al., 2009; Novikov et al., 2006; Penrose et

al., 1990; Santschi et al., 2002). Because of the low concentrations in field locations, the types of colloids present are difficult to quantify. Kersting *et al*. has implicated clay colloids but could not directly show association of plutonium with natural clay colloids only that plutonium was within the colloidal size fraction and clay colloids were present (Kersting et al., 1999).

Specific objectives and prospective publications are organized following the paper by Ryan and Elimelech that outlines the major conditions for colloid facilitated transport of contaminants as discussed previously (Ryan and Elimelech, 1996). These objectives aim to develop a better understanding of the mechanisms behind colloid-facilitate transport of plutonium.

1. Investigate the transport and sorption of iron oxide nanoparticles in the presence of ligands and natural sediments
2. Understand the sorption of plutonium to iron oxide nanoparticles and the stability of these complexes
3. Examine the sorption of plutonium to natural sediments with a focus on the reversibility of sorbed complexes following aging
4. Demonstrate colloid-facilitated transport of plutonium on iron oxide colloids stabilized with organic ligands on a laboratory scale

Table 3 below connects each objective with the planned experimental work, expected results, and the paper that the work will be associated with.

The first paper demonstrates the transport of iron oxide nanoparticles in the presence and absence of Suwanee River Fulvic Acid (SRFA) under unsaturated

conditions with a sandy soil from the Savannah River Site through the use of a novel, field-scale lysimeter setup. These experiments as well as batch sorption and transport experiments in the fourth paper will be used to prove that organic ligands are capable of stabilizing iron oxide-plutonium complexes in environmental systems leading to enhanced transport. The second paper will investigate the sorption and reduction of plutonium on hematite nanoparticles through batch sorption experiments and FTIR measurements of plutonium and its analogs. These experiments will show that plutonium sorbs very strongly to iron oxide nanoparticles and demonstrate reduction of oxidized plutonium following sorption. The third paper will be evidence for the irreversibility and aging effects of plutonium sorption over time on environmental sediments. These aging effects observed on heterogeneous soils are expected to be similar for sorption to the hematite nanoparticles. The final paper will incorporate concepts from the previous papers through a laboratory-scale transport study of hematite nanoparticle – plutonium – SRFA complexes through laboratory columns packed with quartz or natural sand. This work will provide the laboratory data to confirm field studies suggesting colloid-facilitated transport of plutonium.

Table 1.3: Summary of objectives with respect to the experimental work, results, and potential publications

Objective	Experiment	Results	Paper Title
Investigate the transport and uptake of iron oxide nanoparticles in the presence of organic ligands and natural sediments (1)	▪ Field lysimeter experiments with bare magnetite and SR-NOM coated magnetite under unsaturated conditions in SRS sediments ▪ Characterization of lysimeter source materials by TEM and SEM	▪ Qualitative understanding of interactions of iron oxide NP's with environmental sediments ▪ Determination of environmentally relevant ligands with greatest stabilization capacity	"Characterization of physical transformations of iron oxide and silver nanoparticles from an intermediate scale field transport study"
Understand the sorption of plutonium to iron oxide nanoparticles and investigate the reduction mechanisms for plutonium (2)	▪ Batch sorption of plutonium to hematite NP's at variable pH and hematite Fe(II) content ▪ Batch sorption of plutonium to hematite NP's at variable light intensity ▪ ATR-FTIR demonstration of reduction of plutonium in the presence of hematite	▪ Quantitative understanding of sorption kinetics of plutonium to hematite NP's ▪ Refinement of theories for reduction mechanisms of plutonium ▪ Characterization of expected reduction and sorption by observing changes in axial oxygen of Pu by ATR-FTIR	"Observations of surface-mediated reduction of Pu(VI) to Pu(IV) on hematite nanoparticles by ATR FT-IR"
Examine the sorption of plutonium to natural sediments with a focus on the reversibility of sorbed complexes following aging (3)	▪ Batch desorption experiments with a variety of ligands using SRS sediments exposed to plutonium 30 years ago ▪ Batch selective extraction experiments with multiple plutonium isotopes ▪ Electron microprobe and TEM microscopy of aged SRS sediments (ongoing)	▪ Demonstration of the irreversibility of sorbed complexes with aging ▪ Show common minerals that plutonium associates with in natural sediments	"Examining the effects of aging on Pu (de)sorption from 32-year-old Pu contaminated sediments using multiple Pu isotopes"
Demonstrate colloid-facilitated transport of tetravalent actinides on hematite colloids on a laboratory scale (4)	▪ Stability and particle size measurements of hematite NP's in the presence of SRFA at variable pH ▪ Batch sorption of Th to hematite and quartz ▪ Column transport studies with tetravalent actinides on hematite colloids coated with fulvic acid through columns	▪ Culmination of previous objectives' work with a demonstration of colloid-facilitated transport on the laboratory scale with a transport model to validate field transport data	"Experimental evidence for colloid-facilitated transport of tetravalent actinides on hematite colloids in the presence of Suwanee River fulvic acid"

References

1. 2000. Total system performance assessment for the site recommendation, in: Contractor, U.S.D.o.E.b.Y.M.P.M.a.O. (Ed.).

2. Abuzwida, M.A., Maslennikov, A.G., Peretrukhim, V.F., 1991. Voltamperometric determination of uranium and plutonium in alkaline solutions. Journal of Radioanalytical and Nuclear Chemistry 147, 41-50.

3. Albright, D., Kramer, K., 2004. Bull Atom Sci 14.

4. Allard, B., Kipatsi, H., Liljenzin, O., 1980. Expected species of uranium, neptunium and plutonium in neutral solutions. Journal of Inorganic Nuclear Chemistry 42, 1015-1027.

5. Anschutz, A.J., Penn, R.L., 2005. Geochem Trans 6.

6. Artinger, R., Buckau, G., Zeh, P., Geraedts, K., Vancluyse, J., Maes, A., Kim, J.I., 2003. Humic colloid mediated transport of tetravalent actinides and technetium. Radiochimica Acta 91, 743-750.

7. Avogadro, A., Marsily, G.D., 1984. The Role of Colloids in Nuclear Waste Disposal. Mat. Res. Soc. Symp. Proc. 26, 495-505.

8. Baalousha, M., 2009. Aggregation and disaggregation of iron oxide nanoparticles: Influence of particle concentration, pH and natural organic matter. Sci Total Environ 407, 2093-2101.

9. Baalousha, M., Maniculea, A., Cumberland, S., Kendall, K., Lead, J.R., 2008. Aggregation and Surface Properties of Iron Oxide Nanoparticles: Influence of pH and Natural Organic Matter. Environmental Toxicology and Chemistry 27, 1875-1882.

10. Banik, N.L., Buda, R.A., Burger, S., Kratz, J.V., Trautmann, N., 2007. Sorption of tetravalent plutonium and humic substances onto kaolinite. Radiochimica Acta 95, 569-575.

11. Begg, J.D., Zavarin, M., Kersting, A.B., 2014. Plutonium Desorption from Mineral Surfaces at Environmental Concentrations of Hydrogen Peroxide. Environmental Science & Technology 48, 6201-6210.

12. Begg, J.D., Zavarin, M., Zhao, P.H., Tumey, S.J., Powell, B., Kersting, A.B., 2013. Pu(V) and Pu(IV) Sorption to Montmorillonite. Environmental Science & Technology 47, 5146-5153.

13. Berg, J.C., 2010. An Introduction to Interfaces and Colloids, The Bridge to Nanoscience. World Scientific Publishing Company, Hackensack, New Jersey.

14. Blinova, O., Novikov, A., Perminova, I., Goryachenkova, T., Haire, R., 2007. Redox interactions of Pu(V) in solutions containing different humic substances. Journal of Alloys and Compounds 444, 486-490.

15. Bowen, S.M., Finnegan, D.L., Thompson, J.L., Miller, C.M., Baca, P.L., Olivas, L.F., Geoffrion, C.G., Smith, D.K., Goishi, W., Esser, B.K., Meadows, J.W., Namboodiri, N., Wild, J.F., 2001. Nevada Test Site Radionuclide Investory, 1951-1992. Los Alamos National Laboratory, Los Alamos, NM.

16. Buddemeier, R.W., Hunt, J.R., 1988. Transport of colloidal contaminants in groundwater: radionuclide migration at the Nevada Test Site. Applied Geochemistry 3, 535-548.

17. Buesseler, K.O., Kaplan, D.I., Dai, M., Pike, S., 2009. Source-Dependent and Source-Independent Controls on Plutonium Oxidation State and Colloid Associations in Groundwater. Environ Sci Technol 43, 1322-1328.

18. Buffle, J., Wilkinson, K.J., Stoll, S., Filella, M., Zhang, J., 1998. A Generalized Description of Aquatic Colloidal Interactions: The Three-colloidal Component Approach. Environmental Science and Technology 32.

19. Cantrell, K.J., 2009. Transuranic contamination in sediment and groundwater at the U.S. DOE Hanford site. Pacific Northwest National Laboratory, Richland, WA.

20. Carlton, W.H., Evans, A.G., Murphy, C.E., Pinder, J.E., Strom, R.N., 1992. Assessment of plutonium in the Savannah River site environment (U), in: Company, W.S.R. (Ed.), Aiken, SC.

21. Choppin, G.R., 2006. Actinide speciation in aquatic systems. Marine Chemistry 99, 83-92.

22. Choppin, G.R., 2007. Actinide speciation in the environment. Journal of Radioanalytical and Nuclear Chemistry 273, 695-703.

23. Choppin, G.R., Allard, B., 1985. Complexes of actinides with naturally occurring organic compounds.

24. Contardi, J.S., Turner, D.R., Ahn, T.M., 2001. Modeling colloid transport for performance assessment. J Contam Hydrol 47, 323-333.

25. Dai, M., Kelley, J.M., Buesseler, K.O., 2002. Sources and Migration of Plutonium in Groundwater at the Savannah River Site. Environ Sci Technol 36, 3690-3699.

26. Degueldre, C., Baeyens, B., Goerlich, W., Riga, J., Verbist, J., Stadelmann, P., 1989. Colloids in water from a subsurface in granitic rock. Geochimica et Cosmochimica Acta 53, 603-610.

27. Degueldre, C., Pfeiffer, H.-R., Alexander, W., Wernli, B., Bruetsch, R., 1996. Colloid properties in granitic groundwater systems. I. Sampling and characterization. Applied Geochemistry 11, 677-695.

28. Degueldre, C., Triay, I., Kim, J.-I., Vilks, P., Laaksoharju, M., MIekeley, N., 2000. Groundwater colloid properties: a global approach. Applied Geochemistry 15, 1043-1051.

29. Derjaguin, B.V., Landau, L.D., 1941. The theory of stability of highly charge lyophobic sols and coalescence of highly charged particles in electrolyte solutions. Acta Physicochim 14, 633-652.

30. Duff, M.C., Hunter, D.B., Triay, I.R., Bertsch, P.M., Reed, D.T., Sutton, S.R., Shea-McCarthy, G., Kitten, J., Eng, P., Chipera, S.J., Vaniman, D.T., 1999. Mineral Associations and Average Oxidation States of Sorbed Pu on Tuff. Environ Sci Technol 33, 2163-2169.

31. Dunnivant, F.M., 1992. Transport of naturally-occurring dissolved organic-carbon in laboratory columns containing aquifer material. Soil science society of america journal 56, 437-444.

32. Dunphy Guzman, K.A., Finnegan, M.P., Banfield, J.F., 2006. Influence of Surface Potential on Aggregation and Transport of Titania Nanoparticles. Environmental Science & Technology 40, 7688-7693.

33. Elimelech, M., Gregory, J., Jia, X., Williams, R.A., 1995. Particle deposition and aggregation: Measurement, modeling and simulation. Butterworth-Heinemann, Woburn, MA.

34. Elimelech, M., Ryan, J.N., 2002. Interactions between soil particles and microorganisms: impact on the terrestrial ecosystem. John Wiley and Sons, New York.

35. Ewing, R.C., Runde, W., Albrecht-Schmitt, T.E., 2010. MRS Bulletin 35, 859.

36. Felmy, A.R., Cantrell, K.J., Conradson, S.D., 2010. Plutonium contamination issues in Hanford soils and sediments: Discharges from the Z-Plant (PFP) comples. Phys Chem Earth 35, 292-297.

37. Gamerdinger, A.P., Kaplan, D.I., 2001. Colloid transport and deposition in water-saturated Yucca mountain tuff as determined by ionic strength. Environmental Science and Technology 35, 3326-3331.

38. Geckeis, H., Schaefer, T., Hauser, W., Rabung, T., Missana, T., Degueldre, C., Mori, A., Eikenberg, J., Fierz, T., Alexander, W.R., 2004. Results of the colloid and radionuclide retention experiment (CRR) at the Grimsel test site, Switzerland - impact of reaction kinetics and speciation of radionuclide migration. Radiochimica Acta 92, 765.

39. Gilbert, B., Ono, R.K., Ching, K.A., Kim, C.S., 2009. The effects of nanoparticle aggregation processes on aggregate structure and metal uptake. J Colloid Interface Sci 339, 285-295.

40. Grolimund, D., Barmettler, K., Borkovec, M., 2001a. Release and transport of colloidal particles in natural porous media: 2. Experimental results and effects of ligands. Water Resources Research 37, 571-582.

41. Grolimund, D., Borkovec, M., 2001. Release and transport of colloidal particles in natural porous media: 1. Modeling. Water Resources Research 37, 559-570.

42. Grolimund, D., Borkovec, M., 2005. Colloid-Facilitated Transport of Strongly Sorbing Contaminants in Natural Porous Media: Mathematical Modeling and Laboratory Column Experiments. Environ Sci Technol 39, 6378-6386.

43. Grolimund, D., Borkovec, M., 2006. Release of colloidal particles in natural porous media by monovalent and divalent cations. J Contam Hydrol 87, 155-175.

44. Grolimund, D., Elimelech, M., Borkovec, M., 2001b. Aggregation and deposition kinetics of mobile colloidal particles in natural porous media. Colloids and Surfaces A: Physicochemical and Engineering Aspects 191, 179-188.

45. Gu, B., Schmitt, J., Chen, Z., Liang, L., McCarthy, J.F., 1995. Adsorption and desorption of different organic matter fractions on iron oxide. Geochimica et Cosmochimica Acta 2, 219-229.

46. Hassellov, M., Readman, J.W., Ranville, J.F., Tiede, K., 2008. Nanoparticle analysis and characterization methodologies in environmental risk assessment of engineered nanoparticles. Ecotoxicology 17, 344-361.

47. He, Y.T., Wan, J., Tokunaga, T., 2008. Kinetic stability of hematite nanoparticles: the effect of particle sizes. J Nanoparticle Res 10, 321-332.

48. Hixon, A.E., Arai, Y., Powell, B.A., 2013. Examination of the effect of alpha radiolysis on plutonium(V) sorption to quartz using multiple plutonium isotopes. J Colloid Interface Sci 403, 105-112.

49. Hixon, A.E., Hu, Y.J., Kaplan, D.I., Kukkadapu, R.K., Nitsche, H., Qafoku, O., Powell, B.A., 2010. Influence of iron redox transformations on plutonium sorption to sediments. Radiochimica Acta 98, 685-682.

50. Hixon, A.E., Powell, B.A., 2014. Observed changes in the mechanism and rates of Pu(V) reduction on hematite as a function of total plutonium concentration. Environmental Science and Technology submitted.

51. Hochella, M.F., Lower, S.K., Maurice, P.A., Penn, R.L., Sahai, N., Sparks, D.L., Twining, B.S., 2008. Nanominerals, Mineral Nanoparticles, and Earth Systems. Science 319, 1631-1635.

52. Honeyman, B.D., 1999. Colloidal culprits in contamination. Nature 397, 23-24.

53. Kanti Sen, T., Khilar, K.C., 2006. Review on subsurface colloids and colloid-associated contaminant transport in saturated porous media. Adv Colloid Interface Sci 119, 71-96.

54. Kaplan, D.I., Bertsch, P.M., Adriano, D.C., Orlandini, K.A., 1994. Actinide association with groundwater colloids in a coastal plain aquifer. Radiochimica Acta 66/67, 181-187.

55. Kaplan, D.I., Powell, B.A., Demirkanli, D.I., Fjeld, R.A., Molz, F.J., Serkiz, S.M., Coates, J.T., 2004. Influence of Oxidation States on Plutonium Mobility during Long-Term Transport through an Unsaturated Subsurface Environment. Environ Sci Technol 38, 5053-5058.

56. Keeney-Kennicutt, W.L., Morse, J.W., 1985. The redox chemistry of Pu(V)O2+ interaction with common mineral surfaces in dilute solutions and seawater. Geochimica et Cosmochimica Acta 49, 2577-2588.

57. Kersting, A.B., 2013. Plutonium Transport in the Environment. Inorganic Chemistry 52, 3533-3546.

58. Kersting, A.B., Efurnd, D.W., Finnegan, D.L., Rokop, D.J., Smith, D.K., Thomspon, J.L., 1999. Migration of plutonium in groundwater at the Nevada Test Site. Nature 397, 56-59.

59. Kim, J.I., 1991. Actinide colloid generation in groundwater. Radiochimica Acta 52/53, 71-81.

60. Kim, J.I., 1994. Actinide colloids in natural aquifer systems. MRS Bulletin 19, 47-53.

61. Kim, J.I., Delakowitz, B., Zeh, P., Klotz, D., Lazik, D., 1994. A column experiment for the study of colloidal radionuclide migration in Gorleben aquifer systems. Radiochimica Acta 66/67, 165-171.

62. Knopp, R., Neck, V., Kim, J.I., 1999. Solubility, Hydrolysis and Colloid Formation of Plutonium (IV). Radiochimica Acta 86, 101-108.

63. Kosmulski, M., 2002. The pH-dependent surface charging and the points of zero charge. J Colloid Interface Sci 253, 77-87.

64. Kosmulski, M., 2011. The pH-dependent surface charging and points of zero charge: V. Update. J Colloid Interface Sci 353, 1-15.

65. Kretzschmar, R., 1995. The influence of natural organic matter on colloid transport through saprolite. Water Resources Research 31, 435-445.

66. Kretzschmar, R., Sticher, H., 1997. transpot of humic-coated iron oxide colloids in a sandy soil: influence of Ca2+ and trace metals. Environmental Science and Technology 31, 3497-3504.

67. Leenheer, J.A., Huffman, E.W.D., 1976. Classification of organic solutes in water by using macroreticular resins. U.S. Geological Survey Journal of Research 4, 737-751.

68. Lemire, R.J., Fuger, J., Nitsche, H., Potter, P., Rand, M.H., Rydberg, J., Spahiu, K., Sullivan, J.C., Ullman, W.J., Vitorge, P., Wanner, H., 2001. Chemical Thermodynamics of neptunium and plutonium. El Sevier 4.

69. Litaor, M.I., Barth, G., Zika, E.M., Litus, G., Moffitt, J., Daniels, H., 1998. The Behavior of Radionuclides in the soils of Rocky Flats, Colorado. J. Environ. Radioactivity 38, 17-46.

70. Litaor, M.I., Ibrahim, S.A., 1996. Plutonium association with selected solid phases in soils of Rocky Flats, Colorado, using sequential extraction technique. J Environ Qual 25, 1144-1152.

71. Lu, N., Cotter, C.R., Kitten, H.D., Bentley, J., Triay, I.R., 1998. Reversibility of Sorption of Plutonium-239 onto Hematite and Goethite Colloids. Radiochimica Acta 83, 167-173.

72. Lu, N., Reimus, P.W., Parker, G.R., Conca, J.L., Triay, I.R., 2003. Sorption kinetics and impact of temperature, ionic strength and colloid concentration on the adsorption of plutonium-239 by inorganic colloids. Radiochimica Acta 91, 713-720.

73. Madden, A.S., Hochella, M.F., Luxton, T.P., 2006. Insights for size-dependent reactivity of hematite nanomineral surfaces through Cu2+ sorption. Geochimica et Cosmochimica Acta 70, 4095-4104.

74. Marley, N.A., Gaffney, J.S., Orlandini, K.A., Cunningham, M.M., 1993. Evidence for Radionuclide Transport and Mobilization in a Shallow, Sandy Aquifer. Environ Sci Technol 27, 2456-2461.

75. Marquardt, C.M., Seibert, A., Artinger, R., Denecke, M., Kuczewski, B., Schild, D., Fanghanel, T., 2004. The redox behavior of plutonium in humic rich groundwater. Radiochimica Acta 92, 617-623.

76. McCarthy, J.F., Czerwinski, K.R., Sanford, W.E., Jardine, P.M., Marsh, D.J., 1998a. Mobilization of transuranic radionuclides from disposal trenches by natural organic matter. J Contaminant Hydrology 30, 49-77.

77. McCarthy, J.F., Degueldre, C., 1993. In Characterization of Environmental Particles:

78. Sampling and characterization of colloids in groundwater for studying their role in contaminant transport. Lewis Publishers, Chelsea, MI.

79. McCarthy, J.F., Sanford, W.E., Stafford, P.L., 1998b. Lanthanide Field Tracers Demonstrate Enhanced Transport of Transuranic Radionuclides by Natural Organic Matter. Environ Sci Technol 32, 3901-3906.

80. McCarthy, J.F., Zachara, J.M., 1989. Subsurface transport of contaminants. Environ Sci Technol 23, 496-502.

81. McCubbin, D., Leonard, K.S., Emerson, H.S., 2002. Influence of thermal and photochemical reactions upon redox cycling of Pu between solid and solution phases in seawater. Marine Chemistry 80, 61.

82. McKnight, D.M., Bencala, K.E., Zellweger, G.W., Aiken, G.R., Feder, G.L., Thorn, K.A., 1992a. Sorption of dissolved organic carbon by hydrous aluminum and iron oxides occurring at the confluence of Deer Creek with the Snake River, summit County, Colorado. Environmental Science and Technology 26, 1388-1395.

83. McKnight, D.M., Wershaw, R.L., Bencala, K.E., Zellweger, G.W., Feder, G.L., 1992b. Humic substances and trace metals associated with Fe and Al oxides deposited in an acidic mountain stream. The science of the total environment 117/118, 485-498.

84. Mercier, F., Moulin, V., Barre, N., Casanova, F., Toulhoat, P., 2001. Study of the repartition of metallic trace elements in humic acids colloids: potentialities of nuclear microprobe and complementary techniques. Anal Chimica Acta 427, 101-110.

85. Mills, W.B., Liu, S., Fong, F.K., 1991. Literature Review and Model (COMET) for Colloids/Metals Transport in Porous Media. Groundwater 29, 99-208.

86. Missana, T., García-Gutiérrez, M., Alonso, Ú., 2004. Kinetics and irreversibility of cesium and uranium sorption onto bentonite colloids in a deep granitic environment. Applied Clay Science 26, 137-150.

87. Mladenov, N., Zheng, Y., Miller, M.P., Nemergut, D.R., Legg, T., Simone, B., Hageman, C., Ahmed, K.M., McKnight, D.M., 2010. Dissolved organic matter sources and consequences for iron and arsenic mobilization in Bangladesh aquifers. environmental Science and Technology 44, 123-128.

88. Moulin, V., Ouzounian, G., 1992. Role of colloids and humic substances in the transport of radio-elements through the geosphere. Applied Geochemistry 1, 179-186.

89. Moulin, V.M., Moulin, C.M., Dran, J.C., 1996. Role of Humic Substances and Colloids in the Behavior of Radiotoxic Elements in Relation to Nuclear Waste Disposal, in: Gaffney, J.S., Marley, N.A., Clark, S.B. (Eds.), Humic and Fulvic Acids: Isolation, Structure and Environmental Role. American Chemical Society, Washington, D.C.

90. Murphy, R.J., Lenhart, J.J., Honeyman, B.D., 1999. The sorption of thorium (IV) and uranium (VI) to hematite in the presence of natural organic matter. Colloids and Surfaces 157, 47-62.

91. Navrotsky, A., Mazeina, L., Majzlan, J., 2008. Size-driven structural and thermodynamic complexity in iron oxides. Science 319, 1635-1638.

92. Neck, V., Altmaier, M., Seibert, A., Yun, J.I., Marquardt, C.M., Fanghänel, T., 2007. Solubility and redox reactions of Pu(IV) hydrous oxide: Evidence for the formation of PuO2+x(s, hyd). Radiochimica Acta 95, 193-207.

93. Neck, V., Kim, J.I., 2001. Solubility and hydrolysis of tetravalent actinides. Radiochimica Acta 89, 1-16.

94. Novikov, A.P., Kalmykov, S.N., Goryachenkova, T.A., Myasoedov, B.F., 2011. Colloid transport of radionuclides in soils. Russian Journal of General Chemistry 81, 2018-2028.

95. Novikov, A.P., Kalmykov, S.N., Kuzovkina, E.V., Myasoedov, B.F., Fujiwara, K., Fujiwara, A., 2009. Evolution of actinide partitioning with colloidal matter collected at PA "Mayak" site as studied by sequential extraction. Journal of Radioanalytical and Nuclear Chemistry 280, 629-634.

96. Novikov, A.P., Kalmykov, S.N., Utsunomiya, S., Ewing, R.C., Horreard, F., Merkulov, A., Clark, S.B., Tkachev, V.V., Myasoedov, B.F., 2006. Colloid Transport of Plutonium in the Far-Field of the Mayak Production Association, Russia. Science 314, 638-641.

97. Nyhan, J.W., Drennon, B.J., Abeele, W.V., Wheeler, M.L., Purtymun, W.D., Trujillo, B., Herrera, W.J., Booth, J.W., 1985. Distribution of Plutonium and Americium Beneath a 33-yr-old Liquid Waste Disposal Site. Journal of Environment Quality 14, 501-509.

98. Penrose, W.R., Polzer, W.L., Essington, E.H., Nelson, D.M., Orlandini, K.A., 1990. Mobility of Plutonium and Americium through a Shallow Aquifer in a Semiarid Region. Environ Sci Technol 24, 228-234.

99. Powell, B.A., Dai, Z., Zavarin, M., Zhao, P., Kersting, A.B., 2011. Stabilization of plutonium nano-colloids by epitaxial distortion on mineral surfaces. Environ Sci Technol 45, 2698-2703.

100. Powell, B.A., Duff, M.C., Kaplan, D.I., Fjeld, R.A., Newville, M., Hunter, D.B., Bertsch, P.M., Coates, J.T., Eng, P., Rivers, M.L., Serkiz, S.M., Sutton, S.R., Triay, I.R., Vaniman, D.T., 2006. Plutonium oxidation and subsequent reduction by Mn(IV) minerals in Yucca Mountain Tuff. Environmental Science and Technology 40, 3508-3514.

101. Powell, B.A., Fjeld, R.A., Kaplan, D.I., Coates, J.T., Serkiz, S.M., 2004. Pu(V)O2+ adsorption and reduction by synthetic magnetite (Fe3O4). Environmental Science and Technology 38, 6016-6024.

102. Powell, B.A., Fjeld, R.A., Kaplan, D.I., Coates, J.T., Serkiz, S.M., 2005. Pu(V)O2+ adsorption and reduction by synthetic hematite and goethite. Environmental Science and Technology 39, 2107-2114.

103. Reiller, P., Moulin, V., Casanova, F., Dautel, C., 2002. Retention behavior of humic substances onto mineral surfaces and consequences upon thorium (IV) mobility: case of iron oxides. Applied Geochemistry 17, 1551-1562.

104. Reiller, P., Moulin, V., Casanova, F., Dautel, C., 2003. On the study of Th(IV)-humic acid interactions by competition sorption studies with silica and determination of global interaction constants. Radiochimica Acta 91, 513-524.

105. Righetto, L., Bidoglio, G., Azimonti, G., Bellobono, I.R., 1991. Competitive Actinide Interactions in Colloidal Humic Acid-Mineral Oxide Systems. Environ Sci Technol 25, 1913-1919.

106. Roberts, K.A., Santschi, P.H., Leppard, G.G., West, M.M., 2004. Characterization of organic-rich colloids from surface and ground waters at the actinide-contaminated Rocky Flats Environmental Technology Site (RFETS), Colorado, USA. Colloids and Surfaces A: Physicochemical and Engineering Aspects 244, 105-111.

107. Romanchuk, A.Y., Kalmykov, S.N., Aliev, R.A., 2011. Plutonium sorption onto hematite colloids at femto- and nanomolar concentrations. Radiochimica Acta 99, 137-144.

108. Romanchuk, A.Y., Kalmykov, S.N., Egorov, A.V., Zubavichus, Y.V., Shiryaev, A.A., Batuk, O.N., Conradson, S.D., Pankratov, D.A., Presnyakov, I.A., 2013. Formation of crystalline PuO2+x·nH2O nanoparticles upon

sorption of Pu(V,VI) onto hematite. Geochimica et Cosmochimica Acta 121, 29-40.

109. Roy, S.B., Dzombak, D.A., 1996. Colloid release and transport processes in natural and model porous media. Colloids and Surfaces 107, 245-262.

110. Runde, W., Neu, M.P., 2010. The Chemistry of the Actinides and Transactinides, 4th ed. Springer, Dordrecht, The Netherlands.

111. Ryan, J.N., Elimelech, M., 1996. Colloid mobilization and transport in groundwater. Colloids and Surfaces 107, 1-56.

112. Sanchez, A.L., Murray, J.W., Sibley, T.H., 1985. The adsorption of plutonium IV and V on goethite. Geochimica et Cosmochimica Acta 49, 2297.

113. Santschi, P.H., Roberts, K.A., Guo, L.D., 2002. Organic mature of colloidal actinides transported in surface water environments. Environmental Science & Technology 36, 3711-3719.

114. Schafer, T., Artinger, R., Dardenne, K., Bauer, A., Schuessler, W., Kim, J.I., 2003. Colloid-Borne Americium Migration in Gorleben Groundwater: Significance of Iron Secondary Phase Transformation. Environ Sci Technol 37, 1528-1534.

115. Schmidt, M., Wilson, R.E., Lee, S.S., Soderholm, L., Fenter, P., 2012. Adsorption of plutonium oxide nanoparticles. Langmuir 28, 2620-2627.

116. Schrick, B., Hydutsky, B.W., Blough, J.L., Mallouk, T.E., 2004. Delivery vehicles for zerovalent metal nanoparticles in soil and groundwater. Chem. Mater. 16, 2187-2193.

117. Schwertmann, U., 1991. SOLUBILITY AND DISSOLUTION OF IRON-OXIDES. Plant and Soil 130, 1-25.

118. Seaman, J.C., Bertsch, P.M., Miller, W.P., 1995. Chemical controls on colloid generation and transport in a Sandy aquifer. Environmental Science and Technology 29, 1808-1815.

119. Seijo, M., Ulrich, S., Filella, M., Buffle, J., Stoll, S., 2009. Modeling the Adsorption and Coagulation of Fulvic Acids on Colloids by Brownian Dynamics Simulations. Environ Sci Technol 43, 7265-7269.

120. Sen, T.K., Mahajan, S.P., Khilar, K.C., 2002. Colloid-associated contaminant transport in porous media: 1. Experimental Studies. Environmental and Energy Engineering 48, 2366-2374.

121. Shaughnessy, D.A., Nitsche, H., Booth, C.H., Shuh, D.K., Waychunas, G.A., Wilson, R.E., Gill, H., Cantrell, K.J., Serne, R.J., 2003. Molecular interfacial relations between Pu(VI) and manganese oxide minerals manganite and hausmannite. Environmental Science and Technology 37, 3367-3374.

122. Shcherbina, N., Perminova, I.V., Kalmykov, S.N., Kovalenko, A.N., Haire, R.G., Novikov, A.P., 2007. Redox and complexation interactions of neptunium(V) with quinonoid-enriched humic derivatives. Environmental Science and Technology 41, 7010-7015.

123. Short, S.A., Lowson, R.T., Ellis, J., 1988. 234U/238U and 230Th/234U activity ratios in the colloidal phases of aquifers in lateritic weathered zones. Geochimica et Cosmochimica Acta 52, 2555.

124. Silva, R.J., Nitsche, H., 1995. Actinide Environmental Chemistry. Radiochimica Acta 70/71, 377-396.

125. Smith, P.A., Degueldre, C., 1993. Colloid-facilitated transport of radionuclides through fractured media. Journal of Contaminant Hydrology 13, 143-166.

126. Stumm, W., 1977. Coagulation and filtration in water and wastewater treatment become more efficient by modifying the chemical variables to improve the efficiency of collisions between particles and filter grans. Environ Sci Technol 11, 1066-1070.

127. Tanaka, K., Suzuki, Y., Ohnuki, T., 2009. Sorption and Oxidation of Tetravalent Plutonium on Mn Oxide in the Presence of Citric Acid. Chemistry Letters 38, 1032-1033.

128. Thurman, E.M., 1986. Organic Geochemistry of Natural Waters. Martinus Nijhoff/Dr W. Junk Publishers, Dordrecht.

129. Tinnacher, R.M., Zavarin, M., Powell, B.A., Kersting, A.B., 2011. Kinetics of neptunium(V) sorption and desorption on goethite: An experimental and modeling study. Geochimica et Cosmochimica Acta 75, 6584-6599.

130. Turner, N.B., Ryan, J.N., Saiers, J.E., 2006. Effect of desorption kinetics on colloid-facilitated transport of contaminants: Cesium, strontium, and illite colloids. Water Resources Research 42, 1-17.

131. Utsunomiya, S., Kersting, A.B., Ewing, R.C., 2009. Groundwater Nanoparticles in the Far-Field at the Nevada Test Site: Mechanisms for Radionuclide Transport. Environ Sci Technol 43, 1293-1298.

132. Verwey, E.J.W., Overbeek, J.T.G., Van Nes, K., 1948. Theory of the stability of lyophobic colloids: the interaction of sol particles having an electric double layer. El Sevier, New York.

133. Vilks, P., Baik, M.-H., 2001. Laboratory migration experiments with radionuclides and natural colloids in a granite fracture. Journal of Contaminant Hydrology 47, 197-210.

134. Vilks, P., Caron, F., Haas, M.K., 1998. Potential for the formation and migration of colloidal material from a near-surface waste disposal site. Applied Geochemistry 13, 31-42.

135. Vilks, P., Cramer, J.J., Shewchuk, T.A., Larocque, J.P.A., 1988. Colloid and particulate matter in Cigar Lake natural analog program. Radiochimica Acta 44/45, 305-310.

136. Vilks, P., Frost, L.H., Bachinski, D.B., 1997. Field-scale colloid migration experiments in a granite fracture. Journal of Contaminant Hydrology 26, 203-214.

137. Xie, J.C., Lin, J.F., Zhou, X.H., Li, M., Zhou, G.Q., 2014a. Plutonium partitioning in three-phase systems with water, colloidal particles, and granites: New insights into distribution coefficients. Chemosphere 99, 125-133.

138. Xie, J.C., Lin, J.F., Zhou, X.H., Li, M., Zhou, G.Q., 2014b. Plutonium partitioning in three-phase systems with water, granite grains, and different colloids. Environmental Science and Pollution Research 21, 7219-7226.

139. Xie, J.C., Lu, J.C., Lin, J.F., Zhou, X.H., Li, M., Zhou, G.Q., Zhang, J.H., 2013. The dynamic role of natural colloids in enhancing plutonium transport through porous media. Chemical Geology 360, 134-141.

140. Xie, J.C., Lu, J.C., Lin, J.F., Zhou, X.H., Xu, Q.C., Li, M., Zhang, J.H., 2014c. Insights into transport velocity of colloid-associated plutonium relative to tritium in porous media. Scientific Reports 4, 8.

141. Zanker, H., Hennig, C., 2014. Colloid-borne forms of tetravalent actinides: a brief review. J Contam Hydrol 157, 87-105.

142. Zhao, P., Zavarin, M., Leif, R.N., Powell, B.A., Singleton, M.J., Lindvall, R.E., Kersting, A.B., 2011. Mobilization of actinides by dissolved organic compounds at the Nevada Test Site. Applied Geochemistry 26, 308-318.

143. Zimmerman, T., Zavarin, M., Powell, B.A., 2014. Influence of humic acid on plutonium sorption to gibbsite: Determination of Pu-humic acid complexation constants and ternary sorption studies. Radiochimica Acta 102, 629-643.

144. Zvikelsky, O., Weisbrod, N., 2006. Impact of particle size on colloid transport in discrete fractures. Water Resources Research 42, 1-12.

CHAPTER TWO

PAPER ONE: CHARACTERIZATION OF PHYSICAL TRANSFORMATIONS OF IRON OXIDE AND SILVER NANOPARTICLES FROM AN INTERMEDIATE FIELD TRANSPORT STUDY

Status

Published in *Journal of Nanoparticle Research*

Authors

Hilary P. Emerson, Ashley E. Hart, Jonathon A. Baldwin, Tyler C. Waterhouse, Christopher L. Kitchens, O. Thompson Mefford, and Brian A. Powell

Introduction

The use of nanomaterials in industrial and commercial applications has increased dramatically in the past 10 years with silver nanoparticles (NPs) currently being the most widely used nanomaterial in consumer products (WWC 2013) and with emerging uses for iron oxide NPs in medical imaging and drug delivery (Kim et al. 2001), environmental remediation (Shipley et al. 2011), and industrial applications as ferrofluids (Raj et al. 1995) among others. Several reviews have called for a better understanding of the fate and transport capabilities of nano-sized materials in order to better understand the end of life stage and refine risk assessment models for future releases of synthetic NPs (Wiesner et al. 2009; Abbott and Maynard 2010; Asmatulu et al. 2012) as well as for a better understanding of the likelihood of colloid-facilitated transport of relatively immobile contaminants (McCarthy and Zachara 1989; Hochella et al. 2008). Understanding NP transport in subsurface environments is necessary for

quantitatively evaluating the risk to human health and the environment due to use and disposal of NP containing products as well as colloid-facilitated contaminant transport on naturally- occurring nano-sized particles. Some of the major exposure pathways to soils include accidental spills, landfill leachate and biosolids (Blaser et al. 2008; Mueller and Nowack 2008), soil remediation (Zhang and Elliott 2006; Klaine et al. 2008), and airborne deposition with exposure through application of biosolids from wastewater treatment plants suggested as the major pathway (Gottschalk et al. 2009). Gottschalk et al. (2009) and team estimated that the concentrations of metallic and metal oxide NPs could increase from several nanograms to micrograms per kilogram of soil per annum due to the increasing use of nanomaterials worldwide.

The physical/chemical mechanisms controlling nanomaterial transport through the vadose zone (i.e. subsurface environment unsaturated with respect to water) are likely different than within saturated subsurface environments due to the cycling between wetting and drying conditions. For example, Gao et al. (2006) observed accumulation of latex nanospheres at the air–water interface of insular air bubbles within a flow cell packed with silica particles. Studies of NP transport can also help in understanding the transport of naturally occurring NPs (i.e. colloids). In natural environments, several studies have documented colloid-facilitated transport of contaminants on naturally occurring colloidal materials under field conditions (Kersting et al. 1999; Novikov et al. 2006; Hochella et al. 2008) including a study of colloid-facilitated transport of plutonium on iron oxides with transport greater than 2.15 km in groundwater (Novikov et al. 2006). However, there have been relatively

few studies examining the chemical/physical behavior of engi- neered NPs once released into natural systems. While some mesocosm studies have begun to investigate environmental toxicity and bioaccumu- lation of NPs (Ferry et al. 2009; Colman et al. 2013) and with some discussion of environmental trans- formations under environmentally relevant condi- tions has begun (Kim et al. 2012a, b; Lowry et al. 2012), only one field-scale study and modeling calibration was found investigating NP transport in wetland mesocosms (Lowry et al. 2012; Dale et al. 2013).

The objective of this study was to use a unique, 1-year field experiment with lysimeters to investigate the vadose zone, unsaturated transport of metallic and metal oxide NPs in an environmentally relevant, sandy soil. The NPs investigated were iron oxide as bare NPs and coated with Suwanee River natural organic matter (SR-NOM) and silver NPs capped with citrate ($C_6H_8O_7$), SR-NOM, or dodecanethiol with average particle sizes of 10 and 30 nm for the iron oxide and silver particles, respectively. Characterization of lysimeter source materials after 1 year of exposure shows that nanomaterial transport through unsaturated media is controlled by wet–dry cycling and heteroaggregation of NPs with colloidal-sized soil coatings. The following experiments described below represent a novel approach to better understanding complex environmental systems. While a mechanistic reactive transport model of NP behavior in natural systems is desired, that effort is beyond the scope of this work. These experiments are intended to provide observational data describing the physical and chemical transformations of NPs in environmental systems. These

data can be used to test and/or validate different conceptual models within a reactive transport modeling framework. Therefore, many of the qualitative results and observations in this work are described using results and conclusions from previous laboratory studies on simpler systems to corroborate conceptual models and conclusions. The major findings from this work are that interactions with soil coatings are the primary mechanism limiting subsurface migration of NPs and that the character of the coating ligand can also influence the mobility of the NP.

Materials and Methods

Field column setup

The experimental setup shown in Fig. 1a incorporated six separate zero-tension lysimeters with an outer diameter of 4" and a length of 22" with drainage of rainwater effluent into 1-L collection bottles. A control lysimeter was prepared without NPs for establishment of back- ground iron and silver concentrations and for monitoring of soil moisture content and temperature every 15 min throughout the experiment (5TE probes and EM50 datalogger by Decagon Services). Because, the large probes on the devices (shown in Fig. 2.1b) would have impacted the flow through the NP lysimeters; the devices were fi only to the control lysimeter on the bottom, middle, and top sections and 10" below the ground for comparison. The soil temperature fluctuation as com- pared to the ground was within ±5 °C with a maximum variation of 7 °C during the hottest part of the day during the summer months (see *Supplementary Material A* for the complete monitoring datasets in Figs. S2, S3).

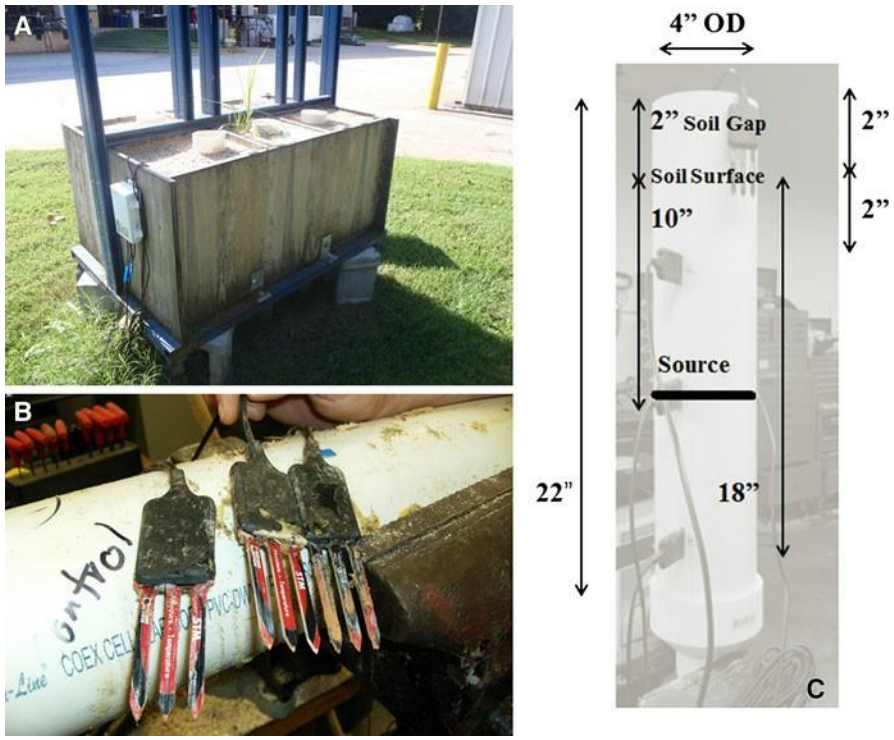

Figure 2.1: (a) Lysimeter containment setup with data storage box (*top left*), (b) photo of data collection probes from control lysimeter (*bottom left*), and (c) schematic of lysimeters (*right*).

The lysimeters were packed with a sandy soil (particles with a diameter greater than 2,000 µm removed) that was determined to be 98.8 % sand and0.9 % clay and 0.4 % silt as determined by mechanical sieve analysis and hydrometer method for the fraction <0.06 mm based on Stoke's law (Gee and Bauder 1986) and consisted mostly of silica sand particles coated with clays and iron oxides. Kaolinite clay, hydroxyl interlayered vermiculite, gibbsite, goethite, and hematite are expected to be the dominant clay fraction minerals based on analysis of soils from the same location reported previously by Kaplan et al. (2004). Table 2.1 elaborates on the soil characterization with a summary of the major soil parameters and components (Fig.

S4 of the *Supplementary Material A* shows TEM imaging of soil coatings). After packing each lysimeter halfway, the NP sources for bare iron oxide, SR-NOM coated iron oxide, citrate coated silver, SR-NOM coated silver, and dodecanethiol coated silver were placed in the middle before further packing up to 2" below the top edge of the columns to allow for the percolation of rainwater. NPs were prepared with some modifications to previous methods as described in the *Supplementary Materials A* S2 and S3 sections with additional characterization shown in Table B1 and Fig. S1 (Lefevure et al. 1998; Brown et al. 2000; Jana et al. 2001). Sources were placed in the middle of the lysimeters to allow for protection of the NPs from sunlight as transformations due to light could have further complicated results. For example, previous work has shown that silver NPs exposed to the 300 nm ultraviolet light wavelength exhibit surface-mediated transformations leading to a shell of oxidized silver, a decrease in diameter, and occasional aggregation (Gorham et al. 2012). Iron oxide NPs have been shown to be redox sensitive in the presence of natural light as some iron oxides like hematite are semiconductors that are capable of electron-hopping within the wavelengths of visible light (Waite 1990; McCubbin et al. 2002; Williams and Scherer 2004). Powell et al. (2005) demonstrated changes in redox properties based on increased reduction of an adsorbed species, and Wang et al. (2012) measured an elevated reaction time for reduction of Fe(III) to Fe(II) in the presence of a light source when utilizing the Fenton reaction. In addition, source materials were placed in the middle of the lysimeter columns for consideration of upward mobility of NPs based on capillary action and to rule out transport due to disturbance of the surface layers during heavy rain events.

Table 2.1: Summary of major soil characteristics.

pH_{eq}	4.56
Effective size (mm)	0.18
Hydraulic conductivity (m/sec)	0.025
Soil Type	Sand
Bulk soil density (g/cm^3) wet/dry	1.82/1.52
Sand/Clay/Silt (% by mass)	98.8/0.9/0.4
Major Clay components	kaolinite > goethite > hematite > gibbsite > HIV*
Organic Carbon (% by mass)	0.35
Aluminum, total/DCB extractable (mg/kg)	7040/425
Iron, total/DCB extractable (mg/kg)	6720/510
Manganese, DCB extractable (mg/kg)	2.2

* HIV = hydroxyl-interlayered vermiculite (Kaplan et al., 2006)

The sources were prepared by equilibrating NP suspensions with 60 g of soil for 4 days and separating the aqueous phase by centrifugation before emplacement 10" below the top of the lysimeters as a homogenous, wet paste on top of a 4" diameter Whatman cellulose ashless grade 42 filter paper. The filter paper was used only as a marker for the location of the source materials. Resistance calculations were completed for both the filters (based on published flow rates by Whatman) and the soil (based on measurements performed using a minidisk infiltrometer by Decagon Devices). The values were estimated at $2x10^{-8}$ and $2x10^{-4}$ sec^{-1}, respectively, demonstrating that it is unlikely that fl was impacted by the filters. In addition, it did not serve as a significant sink for the NPs as shown by source filter paper digestion of Ag-Cit, Ag- NOM, and bare Fe source materials with recovery of <0.5 %. Because filter papers were mixed together with sediments during the coring process, Ag-Thiol, and Fe- NOM source filters were not recoverable as a separate entity from sediments. Due to the synthesis of silver dodecanethiol sources in hexane and the hydrophobic nature of the surface coating, these

sources were prepared by mixing the 60 g of soil with the particle solution followed by evaporation of the hexane at room temperature. It is unsure how the evaporation of the silver dodecanethiol source affected the stability; how- ever, it is significant that these particles were initially hydrophobic while all others were initially hydrophilic.

Because of potential differences in the affinity of the NPs for the minerals in the sediments, the mass loadings were determined through microwave digestion in concentrated nitric acid (BDH Falcon Aristar Plus) of approximately 0.5 g of each source per EPA Method 3051A (2007) with measurement of iron and silver on an inductively coupled plasma mass spectrometer (ICP-MS) in 2% nitric acid (Thermo Scientific X Series 2). Additional work by Cornelius et al. (2010) noted that nitric acid digestion of silver NPs was superior to a combination of nitric and hydrochloric acid because the recoveries were greater due to the avoidance of insoluble silver chloride complexes and ease when coupled with an ICP-MS. Total iron and silver concentrations in the control soil were background subtracted to determine the total concentrations of NPs added to the sources. It is important to note that this method does not differentiate among different phases of silver. Specific determinations among solid, aqueous, and NP fractions were not attempted within the soils as any efforts to re-suspend or filter may have significantly altered the source materials. The mass loadings for each lysimeter were as follows: bare iron oxide (5.86 g), SR-NOM–iron oxide (10.08 g), SR-NOM–silver (0.88 g), citrate-silver (0.61 g), and dodecanethiol-silver (0.2 g; see *Supplementary Material A* for imaging of original source materials in Fig. S5). The loadings for the iron oxide NPs are significantly higher than the silver particles in

order to overcome the relatively high iron background in the soil.

Lysimeter sampling and characterization

Throughout the year that the lysimeters were exposed to the environment, the aqueous effluents were collected periodically from each of the columns and analyzed for iron and silver content via ICP-MS. To evaluate the extent of NP transport within the soil columns, each lysimeter was cored after 1 year by extrusion of the soil and segmentation into 1-cm slices. The slices were mixed by hand with Teflon rods in glass beakers to homogenize the segmented soil, and the iron and silver contents were measured by microwave digestion per EPA Method 3051A (2007) in triplicate with the limitations and methods described above. In some cases, large aggregates of NPs were observed in the source region indicating a large degree of heterogeneity. These aggregates were removed from the soil, segmented by hand, and processed separately. The low recoveries for silver citrate and silver dodecanethiol are most likely due to heterogeneities in source materials upon coring leading to large error in the sources due to aggregation and to the analytical detection limits (0.2 lg/g for silver). Additional characterization of NP source materials was completed via digital imaging during coring, scanning electron microscopy (SEM) and transmission electron microscopy (TEM), and elemental mapping of soils by energy dispersive X-ray (EDX) analysis on Hitachi microscopes (SU6600 SEM, HD2000 TEM, and HRTEM 9500). Prior to preparation of grids (Ted Pella lacey carbon, 300 mesh copper), samples were removed after the homogenization step and prior to drying during the lysimeter coring process and stored in 50 mL centrifuge vials purged with high purity nitrogen gas (Air Gas National

Welders) in the laboratory refrigerator (4 °C). Grids were prepared for TEM by pipetting a suspension of soil sample mixed with distilled deionized water and were allowed to dry overnight in a desiccator (Secador). Images collected on the SU6600 were collected at using a pressure of 25 Pa and an accelerating voltage of 20 keV using the backscatter electron detector. Images collected on the HD2000 TEM were collected with an accelerating voltage of 200 keV in SE mode while those collected on the HRTEM 9500 were at 300 keV. Images collected on both the SU6600 SEM and HD2000 TEM were analyzed using EDX mapping (Hitachi).

Results and Discussion

Throughout the year of exposure to the environment, periodic sampling of the rainwater effluent showed insignificant breakthrough of NPs with respect to the total masses of particles added to each system (Table 2.2). With an average wet bulk soil density of 1.82 g/cm^3, 5.2 ± 0.6 pore volumes of rainwater went through the lysimeters (based on the average and standard deviation of total pore volumes through the bottom half of all six lysimeters). Thus, transport of the NPs out of the column would have occurred if any of the NPs exhibited a retardation factor less than 5.8. It must be noted that there was no rainfall for the first 2 weeks after the NPs were placed in the lysimeters. However, sources did not completely dry out as the soil moisture content in the control lysimeter middle probe remained at or above 0.055 prior to the first rain event while the probe near the top of the control lysimeter consistently measured a dry moisture content of 0.044–0.046 prior to the first rain event.

Table 2.2: Recovery of aqueous and solid phases from lysimeter columns.

Sample ID	Effluent Recovery	Solid Phase Recovery
Bare Fe	0 %	84.2%
Fe-NOM	$1.5x10^{-4}$ %	56.3%
Ag-NOM	$5x10^{-5}$ %	23.5%
Ag-Cit	$4x10^{-5}$ %	6.5%
Ag-thiol	$1.2x10^{-4}$ %	68.5%

After 1 year of exposure, 99 % of the particles moved less than 5 cm as shown in the profiles in Figs. 2.2 and 2.3 with the recovery from the soil listed as the solid phase recovery in Table 2.2. It is notable that the transport of each of these particles is quite similar in terms of overall movement. Visible transport of both the iron oxide and silver particles capped with SR-NOM of 2 and 3 cm below the source, respectively, was observed during coring due to a change in soil coloration and confirmed by TEM imaging in Figs. 4 and 5. Therefore, a small but measureable fraction of the SR-NOM coated silver and iron oxide particles were transported within the column without undergoing chemical transformation.

Because transport of NPs through the soil columns was minimal, it was expected that extensive transformation of NPs occurred. Homoaggregation of the NPs with themselves and heteroaggregation of the NPs with colloidal-sized soil coatings appear to have been the most notable transformations and was logged in the bare iron oxide, iron oxide SR-NOM, silver citrate, and silver dodecanethiol NP sources visibly in digital photos taken during coring as shown in Fig. 6 and on a much smaller scale via TEM shown in Figs. 5 and 7. One of the most striking aspects of this experiment

was the heterogeneity of the NPs and aggregates within the source after 1 year. It is necessary to note that the sources were originally homogenous due to their preparation as aqueous suspensions as discussed previously.

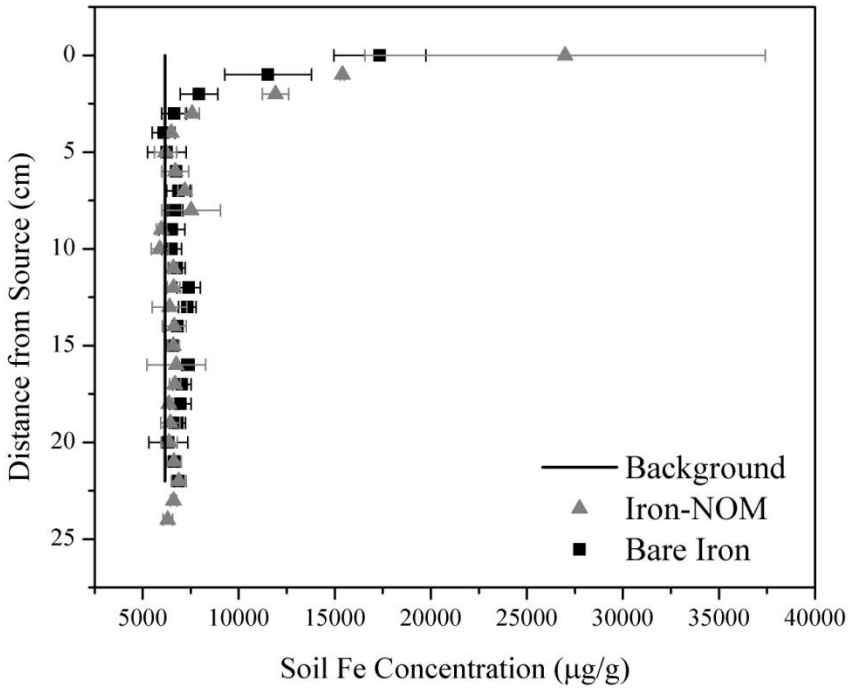

Figure 2.2: Transport profiles of bare iron oxide (a) and iron oxide SR-NOM (b) nanoparticles through columns, solid black line represents average control concentration, with (c) comparing the two types of iron oxide.

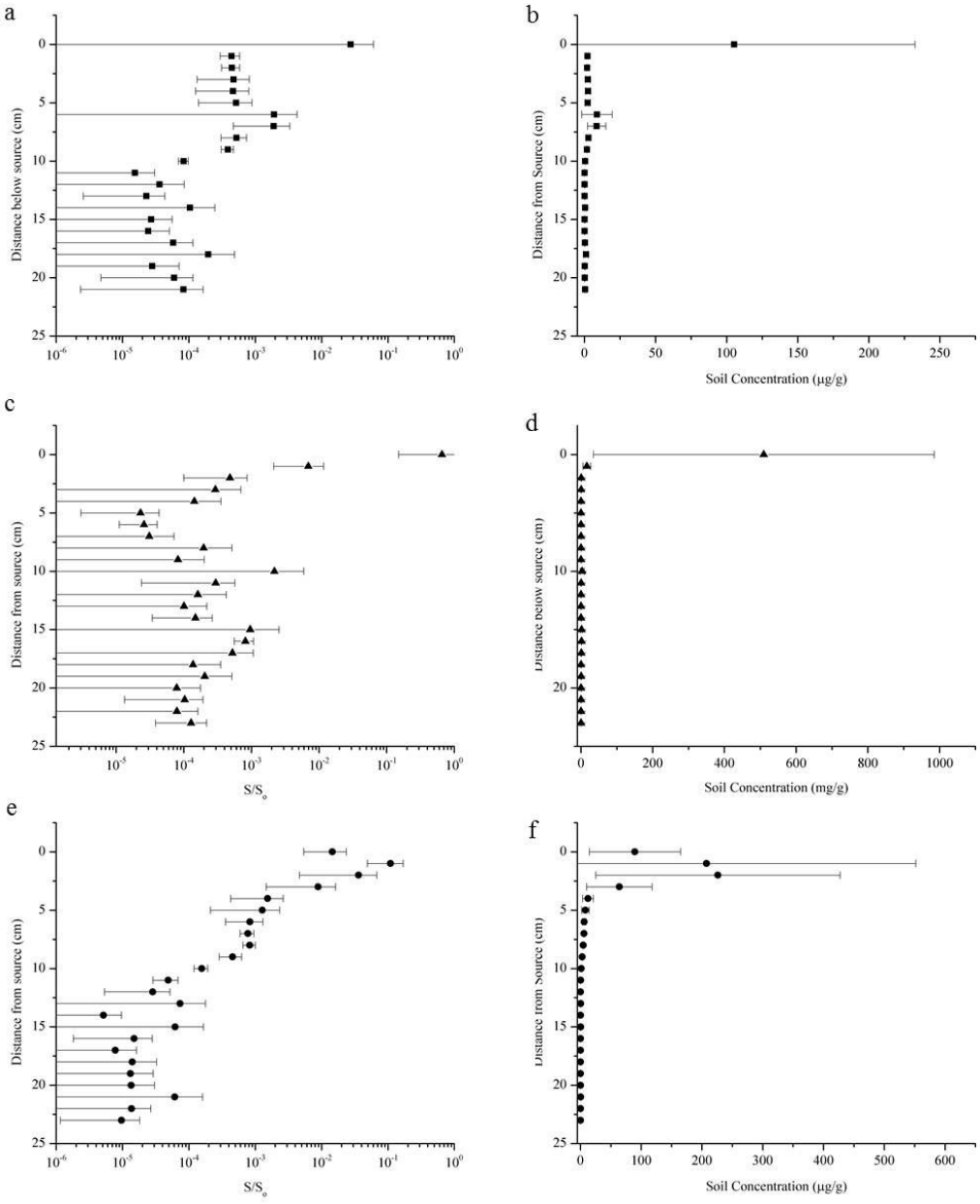

Figure 2.3: Transport profiles of silver citrate (a) and (b), silver dodecanethiol (c) and (d) and silver SR-NOM (e) and (f). Plots a, c, and e show the measured soil concentration (S) normalized to the source concentration (S_o) and plots b, d, and f show the actual measured concentration as a function of downward distance from the source.

There are different interactions expected including sorption, complexation, aggregation, oxidation/reduction reactions, and dissolution/precipitation. It is also possible that local concentrations of NPs could play a role in the type of aggregation occurring. For example, the aqueous concentrations of the iron oxide NPs may have been high enough for homoaggregation to dominate with the iron particles as compared to heteroaggregation being the dominant mechanism at lower concentrations with the silver particles. Quik et al. (2012) previously proposed a concentration dependency for heteroaggregation versus homoaggregation of aggregation for CeO_2 NPs, but still concluded that heteroaggregation was the dominant mechanism. Figures 2.5-2.7 show aggregates of the iron oxide NPs within and below the source materials. EDX mapping of iron oxide aggregates from both sources in Fig. 7a, b does not show significant amounts of aluminum or silica from the aluminosilicate clays present in soil coatings. While it is difficult to confirm the presence or absence of the naturally occurring colloidal particles with the larger iron oxide aggregates imaged by TEM and EDX mapping due to the high concentration of iron oxide, Fig. 5 illustrates the association of smaller iron oxide NPs aggregates with goethite rods and kaolinite clay sheets present in the soil coatings. Within the silver source materials, larger aggregates were not composed entirely of silver. SEM imaging and EDX mapping shown in Fig. 8 and microwave digestion followed by ICP-MS analysis of a 0.67 g aggregate from the silver citrate source materials shows that it is composed of <1 % silver with the remainder composed of clay coatings as confirmed by EDX point analysis with greater than 45 % by mass of aluminum and silicon. These

analyses provide further evidence for a possible concentration dependence on aggregation.

Aggregation of the particles can also be influenced by the ionic strength of the pore waters and divalent cations like calcium has a greater effect on stability than monovalent cations (El Badaway et al. 2010). In addition, Kretzschmar and Sticher (1997) report hematite ($a\text{-}Fe_2O_3$) breakthrough peaks before tracer peaks for systems with $>10^{-3}$ M calcium present due to ion exclusion. These studies would indicate inter- actions with dissolved ions have the potential to enhance NP stability and migration. However, Stebounova et al. (2011) reported experimental results and DLVO calculations showing that increasing ionic strength can lead to reduced stability in suspension. Chloride ions especially impact silver NP behavior by forming low concentrations of AgCl complexes with oxidized silver ions followed by precipitation of AgCl(s) as these complexes significantly decrease solubility (El Badaway et al. 2010; Levard et al. 2012; Sagee et al. 2012). Thus, the chloride ions could both enhance and retard silver migration by forming either a soluble or insoluble product, respectively. Chloride ions could also interact specifically with iron oxides but will not form insoluble complexes (Kosmulski 2002). Sulfur can also form iron complexes that make up a major fraction of the dissolved metal load in sedimentary, anoxic oceans, freshwaters, and ocean vents (Luther and Rickard 2005). While chloride and sulfide ions could interact specifically with silver and iron, neither was detected in association with NPs during EDX mapping. It is possible that the slight increase in silver concentrations between 5 and 10 cm below the silver citrate source, shown in Fig.

3, is due to the dissolution of an insoluble silver complex that would be depressed by SR-NOM or dodecanethiol ligands in the other silver sources.

The unsaturated conditions complicate the system further, where additional transformations can include capture by air–water interfaces (Gao et al. 2006), agglomeration due to drying (Rabani et al. 2003; Gilbert et al. 2009), and drastic changes in pore water chemistry due to intermittent drying and rehydrating of soils which can enhance the interactions expected under saturated conditions due to pH, ionic strength, and counter ion concentrations (Gilbert et al. 2009; El Badaway et al. 2010). Interactions within the unsaturated zone are not as well understood for NPs due to the lack of laboratory-scale transport studies under unsaturated conditions, however, a study by Gao et al. (2006) observed capture of polystyrene latex micro- spheres at air–water interfaces in laboratory flow cells. Due to these expected transformations, it is notable that discrete silver NPs were imaged up to 3 cm below the source in these experiments. Our working hypotheses are that NP aggregation occurred due to drastic fluctuations in soil pore water ionic strength, concentration of particles at air–water interfaces, and interactions between the NPs and soil coatings that prevented transport of much of the NPs in the field experiment.

It is significant that the silver SR-NOM-capped particles are the only sources without macroscopically visible aggregation after 1 year of exposure. Previous work has shown that organic carbon coatings can enhance the stability of iron (Kretzschmar and Sticher1997; Schrick et al. 2004; Baalousha et al. 2008; Baalousha 2009) and silver (Liu and Hurt 2010; Levard et al. 2012) NPs. It is also important to note that

there were significant differences in aggregation between the sources. While the aggregates in all sources imaged by TEM were generally less than 1 lm as shown in Figs. 6 and 7 shows varying levels of aggregation on the macroscopic scale throughout. For the silver sources, no visible aggregation of the silver SR-NOM source was noted during coring, while a large (0.67 g) aggregate was documented within the silver citrate source. Aggregation was also observed macroscopically in the silver dodecanethiol source, but the aggregates were small and distributed through- out the source. The macroscopic differences between the silver citrate and the silver SR-NOM particle sources and the confirmation of silver NPs 3 cm below the source in the SR-NOM but not the citrate source confirm that the ligand coating is a dominant factor controlling aggregation and transport of NPs as previously proposed (Zhou et al. 2012).

For the iron oxide NP sources, there were large mm-size aggregates throughout the bare iron oxide source and a single large aggregate noted within the SR-NOM source (Fig. 4). It is possible that macro- scale aggregation occurred in the iron SR-NOM and not the silver SR-NOM because of differences in the mass ratio loading of SR-NOM (1:6 silver to SR-NOM and 1:60 iron oxide to SR-NOM) added during synthesis and complexation affinity with SR-NOM or a dependence on NP concentration as the iron oxide mass loading was more than an order of magnitude greater than the silver NP loading. Because previous laboratory-scale studies have demonstrated that an increase in NOM can lead to an increase in transport (Kretzschmar and Sticher 1997; Schrick et al. 2004; Baalousha et al. 2008; Baalousha

2009), the latter is the more logical explanation. While the SR-NOM does appear to have prevented aggregation to some extent, it is imperative to note that the increased stability provided by the ligand did not result in a significant increase in transport of NPs.

Further examination of the underlying mechanisms of aggregation is warranted since aggregation appears to have been the dominant influence limiting transport and Cornelius et al. (2010) noted that further investigation of interactions of silver NPs with soil constituents was warranted due to the strong interactions of dissolved silver with soil constituents (i.e. clays and organic matter). Previous work has shown that colloid-sized clay particles can enhance aggregation of silver citrate (Zhou et al. 2012) and nano-zerovalent iron (Kim et al. 2012a, b) NPs at pH \7, which is applicable to the systems examined in the current work as the soil can be conceptualized as quartz particles coated with iron oxides and kaolinite clay with an equilibrium pH of 4.6 and an average effluent pH & 5.4. TEM images confirm that NPs stick to the edges of the clay sheets and goethite rods which are naturally present in the soil as seen previously in laboratory-scale experiments (Kim et al. 2012a, b; Zhou et al. 2012).

We have also observed interactions between colloidal-sized soil coatings and silver citrate NPs in batch sorption experiments mixed over 2 weeks resulting in approximately 80 % sorption with the same soils under the following conditions: 25 g/L soil, 1,000 ppm Ag, and 0.01 M NaCl. The NPs appeared to create a ‘‘floc’’ with the soil coatings that remained suspended significantly longer than colloidal particles

naturally created by suspending the soil as shown by screen captures of a 1.5 h video of particles settling in Figure S6 of *Supplementary Materials A*. The presence of the ''floc'' was found to be due to NPs interacting with the dissolved soil coatings as shown in Fig. 9, which is presumably due to electrostatically stabilized particles comprised the NPs and soil coatings. Similar NP aggregates are shown in Figure 8 for the silver citrate aggregate within the lysimeter source materials. While silver associated with soil coatings in this work are present as NPs, previous work by Kim et al. (2012a, b) found silver associated with TiO_2 NPs in biosolids that did not appear to be present as NPs. The Kim et al. (2012a, b) study mixed silver NPs (polyvinylpyrrolidone coated) with biosolids produced from a waste- water treatment plant that had titanium dioxide (TiO_2) NPs present and exposed the biosolids in slurry to local sediments.

The larger size fraction of soil which is primarily sand appeared to be ''bleached'' after this interaction consistent with removal of the soil coatings. The ''bleaching'' of the soils was also noted in the field lysimeters in the silver citrate and SR-NOM sources visible macroscopically in images in Fig. 6 was likely manifested by the same mechanisms. TEM imaging of the residual, ''bleached'' sand and remaining homogenized soil within the silver citrate source shows that fewer silver NPs are present in the residual sand and non-aggregated soil coatings. The silver NPs associated with the residual sand appear to be associated with the few remaining clay and iron coatings as shown in the *Supplementary Material A* in Figure S7. It is possible that the silver dodecanethiol particles did not mobilize soil coatings due to their hydrophobic nature causing them to be less reactive with the hydrated soils.

However, previous research has also shown that organic acids like citrate can cause an increase in the dissolution rate of kaolinite, the major clay component, of up to 12.1 times that of acetic acid at similar pH (Wang et al. 2005). Therefore, the ligand coating may have been interacting with the soil coatings as opposed to the NP. Our results and previous work by Wang et al. (2005) led to the most likely conclusion that the citrate in the silver NPs and not the silver caused the dissolution of the soil coatings, because the synthesis of silver citrate and silver SR-NOM NPs requires the use of citrate while the silver dodecanethiol particles are synthesized with an entirely different method as described in the *Supplementary Material A* in S2 "Silver NP synthesis methods" section. The dissolution of the soil coatings seen in batch sorption studies as well as the field lysimeters may have also promoted the aggregation as the macroscopic aggregates were much larger in the citrate and SR-NOM silver sources as compared to the dodecanethiol.

This field study demonstrates the importance of the NP coatings and colloidal-sized soil constituents in the mobility of NPs. Similar transport for both silver and iron oxide NPs including a slight decrease in aggregation of iron oxide and silver NPs associated with SR-NOM was observed. It appears that the coating of the NP, rather than the actual composition of the particle, plays a greater role in the aggregation and mobility of the NPs. However, the aggregation of the particles with soil components appears to be the dominant mechanism in this system. TEM analysis supports association of both metallic and metal oxide particles with the edges of clay sheets and goethite rods naturally present in soil coatings, visual observation verifies that the

silver citrate and silver SR- NOM particles can break apart soil coatings, and aggregate digestion confirms that the silver citrate particles aggregated with the colloids naturally present in the soils. The aggregation of the NPs by soil coatings led to [99 % of the NPs moving less than 5 cm over 1 year under vadose zone conditions. These observations imply that NP and natural colloid transport, in unsaturated, environmental systems will be significantly hindered relative to the expected transport based on laboratory experiments with quartz, silica, or other pure mineral phases within the columns and reinforce the need to perform experiments under environmentally relevant conditions. Future laboratory work which may validate these field based observations should focus on characterization of NP interactions with soil coatings and behavior during wet–dry cycling. Both of these processes appear to have major impacts on NP mobility, but have not been sufficiently examined in recent experiments.

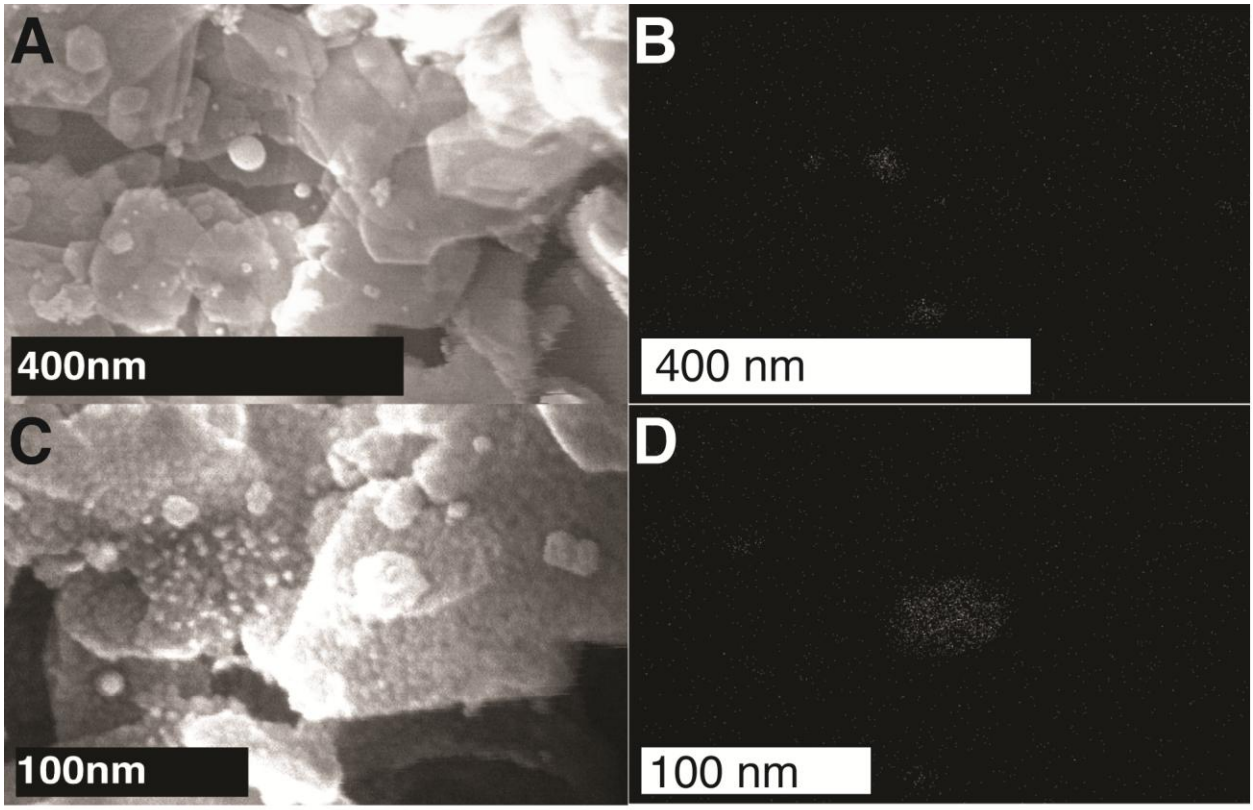

Figure 2.4: HD2000 TEM imaging of silver SR-NOM nanoparticles 3 cm below the source with silver nanoparticles present [as small, round, bright particles] in (a) and (c) as confirmed by EDX mapping for silver in (b) and (d) with mapping in (b) representing the micrograph in (a) and (d) representing (c).

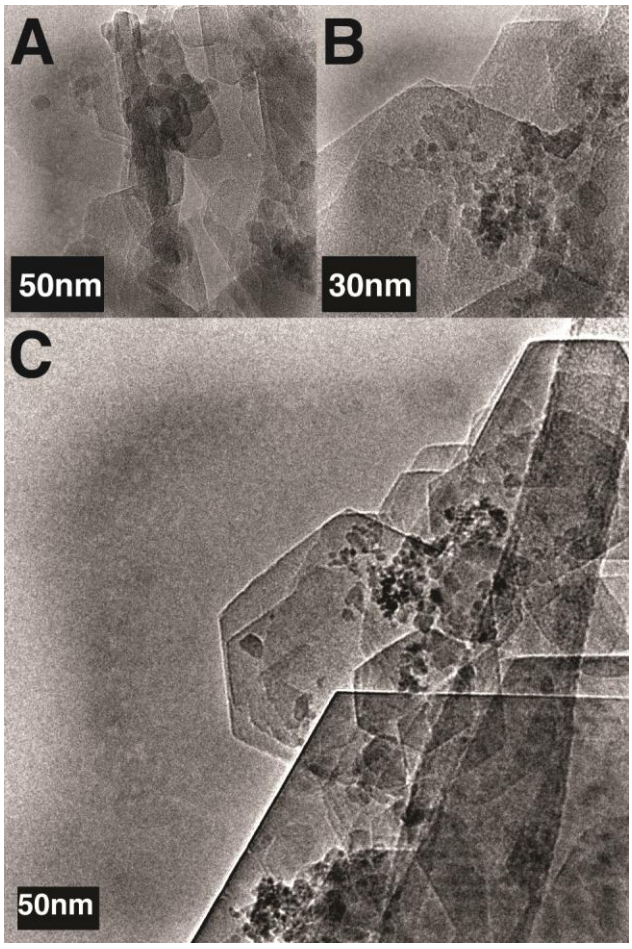

Figure 2.5: HRTEM 9500 imaging of iron oxide SR-NOM nanoparticles [small, dark and round aggregates] associated with (a) goethite rods and (b) surrounding clay sheets both within the lysimeter source materials and with (c) clay sheets located 2 cm below the source materials.

Figure 2.6: Lysimeter source materials after one year, images taken upon coring (a) Control, (b) Bare Iron oxide, (c) SR-NOM Iron oxide, (d) SR-NOM Silver, (e) Citrate Silver and (f) Dodecanethiol Silver. Note: heterogeneous distribution and aggregation of nanoparticles within all source materials after one year and soil transformations in silver NOM and citrate sources (d and e).

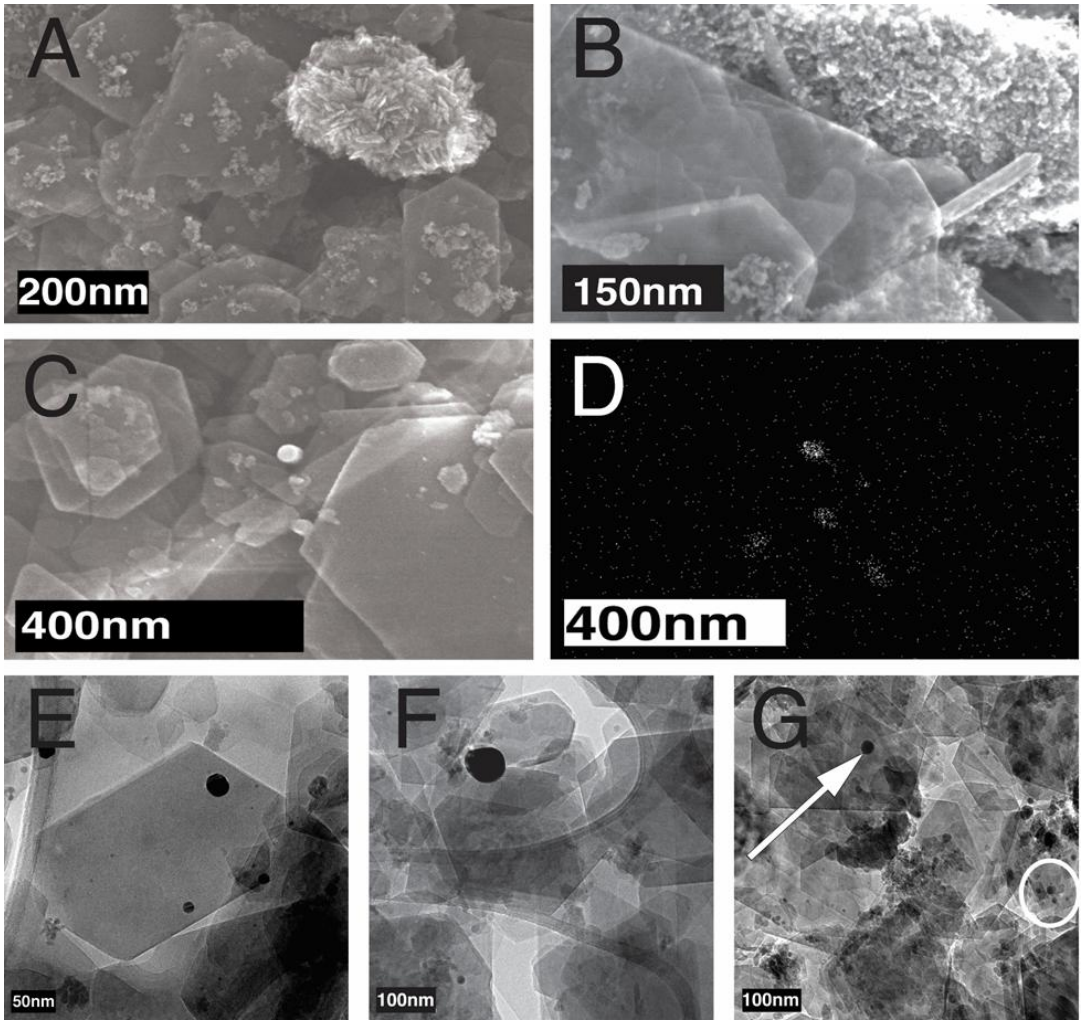

Figure 2.7: HD2000 TEM images of (a) Bare iron oxide source nanoparticle aggregates and (b) iron oxide SR-NOM source nanoparticle aggregates shown as bright area with many smaller particles surrounded by clay sheets, (c) silver SR-NOM nanoparticles in source [appear as bright, round particles] with (d) EDX mapping for silver to confirm presence of silver nanoparticles in "c", and HRTEM 9500 TEM images of (e) silver dodecanethiol nanoparticles in source, (f) silver citrate nanoparticles in source, and (g) silver SR-NOM nanoparticles 3 cm below source materials [appear as dark, round particles].

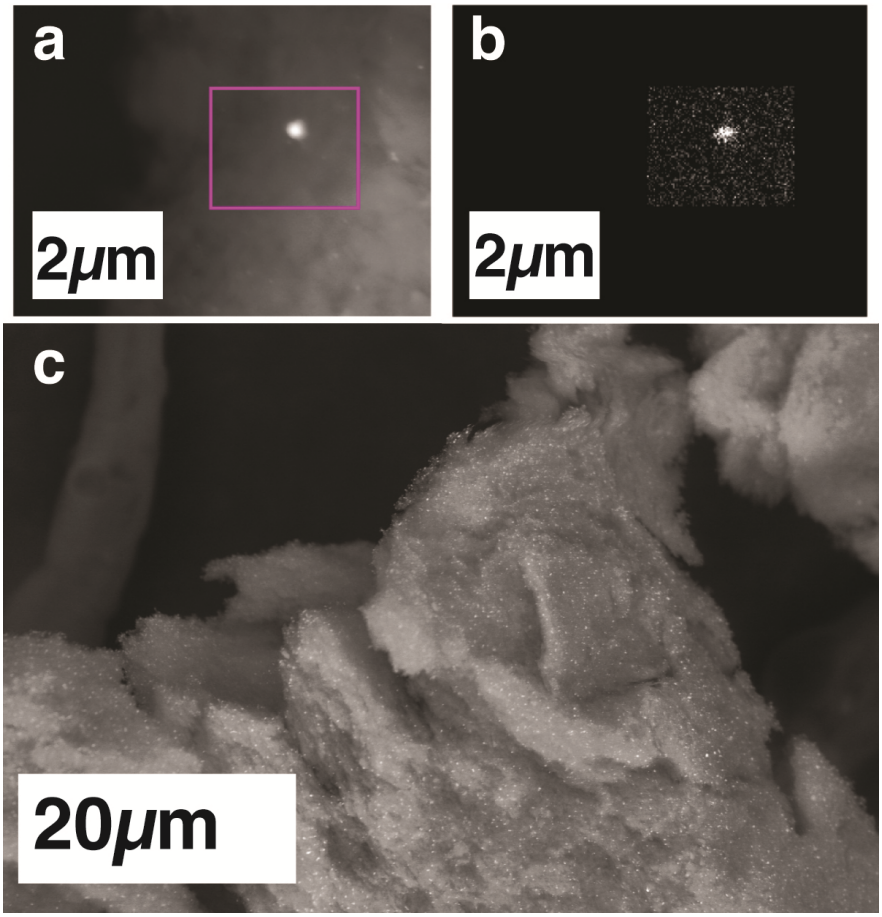

Figure 2.8: SU6600 SEM and EDX analysis of 0.67g aggregate within the silver citrate source containing less than 1% silver by mass as confirmed by total acid digestion, (a) and (b) confirm that the bright spots within the aggregate are silver nanoparticles by EDX mapping (b) of micrograph in (a), and (c) shows that particles are distributed throughout the aggregate.

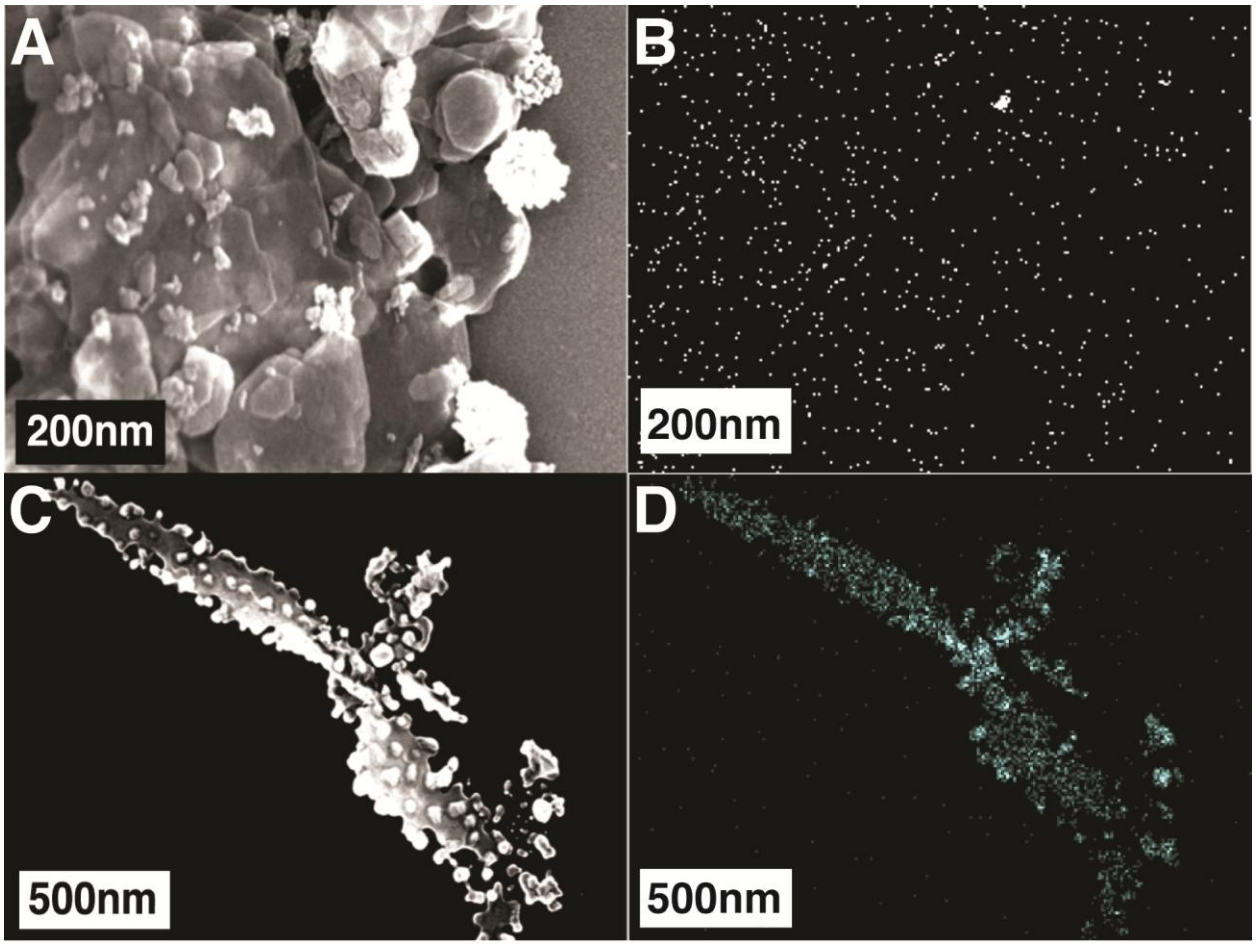

Figure 2.9: HD2000 TEM imaging of batch sorption studies of silver citrate nanoparticles to sediment suspensions [25 g/L] with [Ag]=1000 ppm and [NaCl]=0.01 M with average sorption of 70%, noted formation of a new "floc" that the silver nanoparticles sorbed to in addition to sorption to sediments, first proof of silver nanoparticles breaking up sediment coatings, with (A) TEM image of sediment after exposure to silver nanoparticles, (B) EDX map for silver of soil in "A", (C) TEM image of new "floc" created after exposure of sediment to silver nanoparticles, (D) EDX map for silver of soil in "C".

References

1. Abbott LC, Maynard AD (2010) Exposure assessment of engineered nanomaterials. Risk Anal 30(11):1634–1644. doi:10.1111/j.1539-6924.2010.01446.x

2. Asmatulu E, Twomey J, Overcash M (2012) Life cycle and nano-products: end-of-life assessment. J Nanopart Res 14(720):1–8. doi:10.1007/s/11051-012-0720-0

3. Baalousha M (2009) Aggregation and disaggregation of iron oxide nanoparticles: influence of particle concentration, pH, and natural organic matter. Sci Total Environ 407(6):2093–2101. doi:10.1016/j.scitotenv.2008.11.022

4. Baalousha M, Maniculea A, Cumberland S, Kendall K, Lead JR (2008) Aggregation and surface properties of iron oxide nanoparticles: influence of pH and natural organic matter. Environ Toxicol Chem 27(9):1875–1882. doi:10.1897/07- 559.1

5. Blaser SA, Scheringer M, MacLeod M, Hungerbuhler K (2008) Estimation of cumulative aquatic exposure and risk due to silver: contribution of nano-functionalized plastics. Sci Total Environ 390–396. doi:10.1016/J.SCITOTENV.2007. 10.010

6. Brown KR, Walter DG, Natan MJ (2000) Seeding of colloidal Au nanoparticle solutions. 2. Improved control of particle size and shape. Chem Mater 12:306–313. doi:10.1021/ cm980065p

7. Colman BP, Arnaout CL, Anciaux S, Gunsch CK, Hochella MR, Kim B, Lowry GV, McGill BM, Reinsch BC, Richardson CJ, Unrine JM, Wright JP, Yin L, Bernhardt ES (2013) Low concentrations of silver nanoparticles in biosolids cause adverse ecosystem responses under realistic field scenario. PLoS ONE 8(2):1–10. doi:10.137/journal.pone. 0057189

8. Cornelius G, Kirby JK, Beak D, Chittleborough D, McLaughlin MJ (2010) A method for determination of retention of silver and cerium oxide manufactured nanoparticles in soils. Environ Chem 7:298–308. doi:10.1071/EN10013

9. Dale AL, Lowry GV, Casman EA (2013) Modeling nanosilver transformations in freshwater sediments. Environ Sci Technol 47:12920–12928. doi:10.1021/es402341t

10. El Badaway AM, Luxton TP, Silva RG, Scheckel KG, Suidan MT, Tolamat TM (2010) Impact of environmental conditions (pH, ionic strength, and electrolyte

type) on the surface charge and aggregation of silver nanoparticles suspensions. Environ Sci Technol 44(4):1260–1266. doi:10.1021/es902240k

11. Environmental Protection Agency (2007) Method 3051A: microwave assisted acid digestion of sediments, sludges, soils, and oils

12. Ferry JL, Craig P, Hexel C, Sisco P, Frey F, Pennington PL, Fulton MH, Scott G, Decho AW, Kashiwada S, Murphy CJ, Shaw TJ (2009) Transfer of gold nanoparticles from the water column to the estuarine food web. Nat Nanotechnol 4:441–444. doi:10.1038/nnano.2009.157

13. Gao B, Saiers JE, Ryan J (2006) Pore-scale mechanisms of colloid deposition and mobilization during steady and transient flow through unsaturated granular media. Water Resour Res 42(1):1–9. doi:10.1029/2005WR004233

14. Gee GW, Bauder JW (1986) Particle-size analysis. In: Methods of soil analysis, Part 1, 2nd edn. Agronomy number 9. American Society of Agronomy, Madison

15. Gilbert B, Ono RK, Ching KA, Kim CL (2009) The effects of nanoparticles aggregation processes on aggregate structure and metal uptake. J Colloid Interface Sci 339:285–295. doi:10.1016/j.jcis.2009.07.058

16. Gorham JM, MacCuspie RI, Klein KL, Fairbrother DH, Hol- brook RD (2012) UV-induces photochemical transforma- tions of citrate-capped silver nanoparticles suspensions. J Nanopart Res 14(1139):1–16. doi:10.1007/s11051-012- 1139-3

17. Gottschalk F, Sonderer T, Scholz RW, Nowack B (2009) Modeled environmental concentrations of engineered nanomaterials (TiO_2, ZnO, Ag, CNT, fullerenes) for dif- ferent regions. Environ Sci Technol 43:9216. doi:10.102/ ES9015553

18. Hochella MF, Lower SK, Maurice PA, Penn RL, Sahai N, Sparks DL, Twining BS (2008) Nanominerals, mineral nanoparticles, and earth systems. Science 319(5870): 1631–1635. doi:10.1126/science.1141134

19. Jana NR, Gearheart L, Murphy CJ (2001) Seeding growth for size control of 5–40 nm diameter gold nanoparticles. Langmuir 17:6782–6786

20. Kaplan DI, Powell BA, Demirkanli DI, Fjeld RA, Molz FJ, Serkiz SM, Coates JT (2004) Influence of oxidation states on plutonium mobility during long-term transport through an unsaturated subsurface environment. Environ Sci Technol 38:5053–5068. doi:10.1021/es049406s

21. Kersting AB, Efurd DW, Finnegan DL, Rokop DJ, Smith DK, Thompson JL (1999) Migration of plutonium in ground- water at the Nevada Test Site. Nature 397(6714):56–59. doi:10.1038/16231

22. Kim DK, Zhang Y, Kehr J, Klason T, Bjelke B, Muhammed M (2001) Characterization and MRI study of surfactant- coated superparamagnetic nanoparticles administered into the rat brain. J Magn Magn Mater 225:256–261. doi:10. 1016/S0304-8853(00)01255-5

23. Kim B, Murayama M, Colman BP, Hochella MF (2012a) Characterization and environmental implications of nano- and larger TiO_2 particles in sewage sludge, and soils amended with sewage sludge. J Environ Monit 14(4):1129–1137. doi:10.1039/c2em10809g

24. Kim H, Phenrat T, Tilton RD, Lowry GV (2012b) Effect of kaolinite, silica fines, and pH on transport of polymer- modified zero valent iron nano-particles in heterogeneous porous media. J Colloid Interface Sci 370:1–10. doi:10. 1016/j.jcis.2011.12.059

25. Klaine SJ, Alvarez PJJ, Batley GE, Fernandes TF, Handy RD, Lyon DY, Mahendra S, McLaughlin MJ, Lead JR (2008) Nanomaterials in the environment: behavior, fate, bio- availability, and effects. Environ Toxicol Chem 27:1825. doi:10.1897/-8-090.1

26. Kosmulski M (2002) pH dependent surface charging and points of zero charge. J Colloid Interface Sci 253(1):77–87. doi:10.1006/jcis.2002.8490

27. Kretzschmar R, Sticher H (1997) Transport of humic-coated

28. iron oxide colloids in a sandy soil: influence of $Ca^{?2}$ and

29. trace metals. Environ Sci Technol 31(12):3497–3504. doi:10.1021/es970244s

30. Lefebure S, Dubois E, Cabuil V, Neveu S, Massart R (1998) Monodisperse magnetic nanoparticles: preparation and dispersion in water and oils. J Mater Res 13:2975–2981. doi:10.1557/JMR.1998.0407

31. Levard C, Hotze EM, Lowry GV, Brown GE (2012) Environ- mental transformations of silver nanoparticles: impact on stability and toxicity. Environ Sci Technol 46(13):6900–6914. doi:10.1021/es2037405

32. Liu J, Hurt RH (2010) Ion release kinetics and particle persis- tence in aqueous nano-silver colloids. Environ Sci Technol 44(6):2169–2175. doi:10.1021/es9035557

33. Lowry GV, Espinasse BP, Badireddy AR, Richardson CJ, Reinsch BC, Bryant LD, Bone AJ, Deonarine A, Chae S, Therezien M, Colman BP, Hsu-Kim H, Bernhardt ES, Matson CW, Wiesner MR (2012) Long-term transforma- tion and fate of manufactured Ag nanoparticles in simu- lated large scale freshwater emergent wetland. Environ Sci Technol 46:7027–7036. doi:10.1021/es204608d

34. Luther GW, Rickard DT (2005) Metal sulfide cluster complexes and their biogeochemical importance in the environment. J Nanopart Res 7:389–407. doi:10.1007/s11051-005-4272-4

35. McCarthy JF, Zachara JM (1989) Subsurface transport of con- taminants. Environ Sci Technol 23(5):496–502. doi:10. 0013-936X/89/0923-0496

36. McCubbin D, Leonard KS, Emerson HS (2002) Influence of thermal and photochemical reactions upon the redox cycling of Pu between solid and solution phases in sea- water. Mar Chem 80:61–77

37. Mueller NC, Nowack B (2008) Exposure modeling of engi- neered nanoparticles in the environment. Environ Sci Technol 42:4447. doi:10.1021/ES7029637

38. Novikov AP, Kalmykov SN, Utsunomiya S, Ewing RC, Hor- reard F, Merkulov A, Clark SB, Tkachev VV, Myasoedov BF (2006) Colloid transport of plutonium in the far-field of the Mayak Production Association, Russia. Science 314(5799):638–641. doi:10.1126/science.1131307

39. Powell BA, Fjeld RA, Kaplan DI, Coates JT, Serkiz SM (2005) Pu(V)O2 adsorption and reduction by synthetic Hematite and Goethite. Environ Sci Technol 39:2107-2111

40. Quik JTK, Stuart MC, Wouterse M, Peijnenburn W, Hendriks AJ, Van de Meent D (2012) Natural colloids are the dominant factor in the sedimentation of nanoparticles. Environ Toxicol Chem 31(5):1019–1022. doi:10.1002/etc. 1783

41. Rabani E, Reichman DR, Geissler PL, Brus LE (2003) Drying- mediated self-assembly of nanoparticles. Nature 426(6964):271–274. doi:10.1038/nature02087

42. Raj K, Moskowitz B, Casciari R (1995) Advances in ferrofluid technology. J Magn Magn Mater 149:174–180. doi:10. 1016/0304-8853(95)00365-7

43. Sagee O, Dror I, Berkowitz B (2012) Transport of silver nano- particles (AgNPs) in soil. Chemosphere 88(5):670–675. doi:10.1016/j.chemosphere.2012.03.055

44. Schrick B, Hydutsky BW, Blough JL, Mallouk TE (2004) Delivery vehicles for zerovalent metal nanoparticles in soil and groundwater. Chem Mater 16(11):2187–2193. doi:10. 1021/cm0218108

45. Shipley HJ, Engates KE, Guettner AM (2011) Study of iron oxide nanoparticles in soil for remediation of arsenic J Nanopart Res 13(6):2387–2397. doi:10.1007/s11051- 010-9999-x

46. Stebounova LV, Gio E, Grassian VH (2011) Silver nanoparti- cles in simulated biological media: a study of aggregation, sedimentation, and dissolution. J Nanopart Res 13(1):233–244. doi:10.1007/s11051-0022-3

47. Waite TA (1990) Photo-redox processes at the mineral–water interface. In: Hochella MF, White AF (eds) Mineral–water interface geochemistry, vol 23. Mineralogical Society of America, Washington, DC, pp 559–601

48. Wang X, Li Q, Hu F, Zhang Z, Zhou Z (2005) Dissolution of kaolinite induced by citric, oxalic, and malic acids. J Col- loid Interface Sci 290:481–488. doi:10/1016/j.jcis.2005. 04.066

49. Wang C, Liu H, Sun Z (2012) Heterogeneous photo-Fenton reaction catalyzed by nanosized iron oxides for water treatment. Int J Photoenergy 1-10. doi:10.1155/2012/801694

50. Wiesner MR, Lowry GV, Jones KL, Hochella MF, Giulio RT, Casman E, Bernhardt ES (2009) Decreasing uncertainties in assessing environmental exposure, risk, and ecological implications of nanomaterials. Environ Sci Technol 43(17):6458–6462. doi:10.1021/es803621k

51. Williams AGB, Scherer MM (2004) Spectroscopic evidence for Fe(II)–Fe(III) electron transfer at the iron oxide–water interface. Environ Sci Technol 38:4782–4790. doi:10. 1021/es049373g

52. Woodrow Wilson Center (2013) Project on emerging nanotechnologies: inventories. http://www.nanotechproject.org/inventories/. Accessed 2 June 2013

53. Zhang W-X, Elliott D (2006) Applications of iron nanoparticles for groundwater remediation. Remediation 16:7. doi:10. 1002/REM.20078

54. Zhou D, Abdel-Fattah AI, Keller AA (2012) Clay particles destabilize engineered nanoparticles in aqueous environments. Environ Sci Technol 46(14):7520–7526. doi:10. 1021/es3004427

CHAPTER THREE

PAPER TWO: OBSERVATIONS OF SURFACE-MEDIATED REDUCTION OF PU(VI) TO PU(IV) ON HEMATITE NANOPARTICLES BY ATR FT-IR

Status

To be submitted to *Langmuir*

Authors

Hilary P. Emerson and Brian A. Powell

Keywords

Plutonium, Hematite nanoparticles, Reduction mechanisms

Abbreviations

ATR FT-IR attenuated total reflectance Fourier transform infrared spectroscopy, Fe(II) ferrous iron, HRTEM high resolution transmission electron microscopy, NP nanoparticles, Pu plutonium, SEM scanning electron microscopy, XANES x-ray absorption near edge spectroscopy

Introduction

Plutonium (Pu) is a redox sensitive element capable of existing simultaneously in oxidation states ranging from +3 to +6 in environmental systems. It has been shown previously that the reduced Pu(IV) species sorbs more strongly to pure minerals and exhibits significantly reduced transport in laboratory and field column experiments as compared with Pu(V/VI) species [1-5]. Therefore, reduction of Pu(V) or Pu(VI) to less soluble and less mobile Pu(IV) can effectively retard Pu mobility [6]. However, Pu is remarkably sensitive to these redox transformations primarily due to the similarity between the redox potentials of each oxidation state [7-9]. Because the mobility of Pu in the environment is profoundly influenced by oxidation state, it is important to understand the reduction mechanisms that may lead to immobilization of Pu in the environment.

Several studies have shown that minerals may facilitate surface-mediated reduction of Pu(V/VI) to Pu(IV/III) even on minerals that are considered oxidizing or non-reactive [10-24]. Theories proposed to describe the surface-mediated reduction of Pu are shown below [16], however disproportionation and self-reduction have been previously proven negligible at environmentally relevant pH values and concentrations of Pu [21, 23]:

1. Thermodynamic favorability of Pu(IV) hydroxide complexes [16, 22-24]
2. Self-reduction via radiolysis byproducts [3, 11, 23]
3. Presence of trace reductants such as Mn(II) and Fe(II) on the surface [3, 11, 14, 15, 17, 24]
4. Electron shuttling from semiconductor materials [10, 11, 16, 21, 24]
5. Pu disproportionation [10, 11, 23, 25, 26]

The proposed mechanisms of reduction via the presence of trace reductants and electron shuttling are the focus of this study with the use of laboratory-synthesized, hematite (α-Fe_2O_3) nanoparticles. This work takes advantage of the asymmetric stretch of the axial oxygen bonds (O=Pu=O) present in the Pu(V/VI) but not Pu(IV) to quantify reduction over time. The axial oxygen bonds present in surface bound Pu(V/VI) in the presence of water can be observed as an absorbance by attenuated total reflectance Fourier transform infrared spectroscopy (ATR FT-IR), meanwhile Pu(IV) will not display such an absorbance due to the lack of axial oxygen atoms. Thus, as Pu(VI) is reduced to Pu(V) and ultimately to Pu(IV), the peak due to the asymmetric stretch of the axial oxygens in Pu(VI) and Pu(V) will disappear. Theoretical work [27-29] estimates that the absorption peaks for the actinides will exhibit the following trend with respect to the wavelength assuming they are all in the same oxidation state: U > Np > Pu. Previous experimental work has measured the ATR FT-IR peak energies for U(VI), Np(V/VI), and Pu(VI) in aqueous solutions [27, 30-33]. The shift in peak location and shape, relative to the aqueous species, has been used to infer the mode (i.e. inner versus outer sphere) of U(VI) sorbed to hematite [34-36] and U(VI) and Np(V) sorbed to other minerals [35, 37-46] (Table 3.1). However sorbed Pu(VI) species (and the reduced Pu(IV) species following interaction with a solid phase) have yet to be measured experimentally.

Hematite is a well-characterized iron oxide mineral that is ubiquitous in the natural environment and an expected end product following oxidation of steel canisters used in nuclear waste repositories. It is a ferric oxide mineral and the absence of ferrous iron (Fe(II)) in the structure implies hematite will have little to no reduction capacity. However

the presence of trace Fe(II) has been proposed to be responsible for the reduction of Pu(V/VI) on hematite [16, 21, 22, 24]. Thus, Fe(II) is likely present in hematite but may be below analytical detection limits. However, due to the low concentrations of Pu employed in many environmental studies (10^{-10} to10^{-14} M) even a small fraction of the total Fe(II) may be sufficient for reduction of Pu(V/VI). Romanchuk et al. [21] calculated that only $4x10^{-5}$ wt.% of Fe(II) is required to reduce 10^{-9} M Pu(VI) for their experiments completed at 0.32 g/L of hematite. Recently Hixon and Powell [24] reported that regardless of the total Pu concentration in the system (ranging from 10^{-8} to 10^{-6} M and initially present as Pu(V)), after 10 hours of reaction all samples had a solid phase Pu concentration of approximately $5.3 \pm 0.2 \times 10^{-2}$ $mg_{Pu}/ g_{hematite}$. This initial fast sorption and reduction (within the first 10 hours) was proposed to be due to reaction with trace Fe(II) and thus the concentration of reduced Pu may be directly correlated to the Fe(II) content. Reduction has also been observed on other 'non-reducing' minerals including silica, goethite, manganite, and pyrolusite [11, 14, 16, 17, 23].

In addition the nano- size range has a greater surface area to volume ratio as compared to bulk hematite. This allows for more surface sites in a lesser concentration thereby increasing the ratio of surface sites to trace Fe(II) and effectively maximizing the effect of trace Fe(II) on the reduction kinetics of oxidized Pu. Previous work has shown an increase in hematite reactivity as size decreases [47]. Because hematite is also a light-sensitive semiconductor that is capable of shuttling electrons there may be increased oxidation or reduction of adsorbed species with a greater surface specific area to volume ratio as would be expected with nano-size particles [48-50]. It has been previously noted

that the band gap energy of hematite includes the wavelengths of visible light meaning that visible light may increase the shuttling of electrons leading to increased reduction of Pu(V) [21, 49]. Powell *et al.* [16] observed an increase in Pu(V) sorption and reduction on bulk hematite when the samples were exposed to fluorescent light and attributed it to shuttling of electrons from trace Fe(II).

The objective of this study is to investigate reduction and sorption of Pu on hematite NPs through conventional batch sorption experiments and ATR FT-IR spectroscopy. Using ATR FT-IR, this work directly monitors the surface-mediated sorption of Pu(V/VI) followed by reduction of Pu(V/VI) to Pu(IV) on a hydrated mineral surface. To the authors' knowledge, this is the first measurement of this type.

Table 3.1: Summary of Actinide ATR FT-IR Peak Measurements.

Species	Solid/ Aqueous	Experimental Wavenumber (cm^{-1})	Theoretical pH[a]	Wavenumber (cm^{-1})
$Pu(VI)O_2^{2+}$	α-Fe_2O_3	915-917[c]	6.99	
$U(VI)O_2^{2+}$		900-906[34, 36]	5.5-8.2	
		919-925[64], 923[c]	5-7	
U(VI)/U(IV)-mix		800[34, 64]	7.5	
U(VI)-carbonate		1530[35]	7.97	
U(VI)-carbonate		1345[b][35]	7.97	
$Np(V)O_2^{+}$		~790[c]	7.00	
$Pu(VI)O_2^{2+}$	Aqueous	940[c], 962[27]	6.99	970[28], 951[29]
$Pu(V)O_2^{+}$		835[c]	6.99	883[28], 871[29]
$U(VI)O_2^{2+}$		961-965[27, 31-33]	2.52-3.82	971[28], 1001[29]
$[U(VI)O_2]_2[OH]_2^{2+}$		943 [33]	3.12-4.44	
$[U(VI)O_2]_3[OH]_5^{2+}$		922-923 [31, 33]	4.1-4.4	
$[U(VI)O_2]_3[OH]_8^{2-}$		915-916 [31, 33]	7, 12.62	
$[U(VI)O_2](OH)_4^{2-}$		857 [33]	14.38	
$[U(VI)O_2](OH)_5^{3-}$		835 [33]	13.76-4.06	
$U(VI)O_2$-carbonate		1375-1380[b] [32]	>4.5	
$U(VI)O_2$-carbonate		1525 [32]	>4.5	
U(VI)-precipitate		~1000 [36, 63], 1062[c]	5.5-8.2	
$U(V)O_2^{+}$		NM[d]		875 [29]
$Np(VI)O_2^{2+}$		964 [40],969 [27]	3	977 [28], 983[29]
$Np(VI)O_2OH^{+}$		931 [40]	4-4.6	
$[Np(VI)O_2]_2[OH]_2^{2+}$		943 [40]	5.1	
$Np(V)O_2^{+}$		817 [40], 824 [27], 833[c]	3, 7	884 [28], 904[29]
$U(VI)O_2^{2+}$	TiO_2	908-917 [38, 42]	5	
$Np(V)O_2^{+}$		789 [40]	7.6	
$U(VI)O_2^{2+}$	AlO_3H_3	903 [43]	6	
$Np(V)O_2^{+}$		784 [45]	7.5	
$Np(V)O_2^{+}$	SiO_2	786 [40]	7.6	
$Np(V)O_2^{+}$	ZnO	792 [40]	7.6	
Compreignacite	UOH in Uranyl Minerals	980-1150 [57, 59-61]		
Schoepite		~1000 [36, 63] 1018-1072 [57, 62]		
Masuyites		1025-1180 [57, 59-61]		
Vandendriesscheite		1024-1160 [57, 58]		

[a] pH is not listed for all experimental work, but ranges are given for those works that included pH measurements

[b] All peaks are asymmetric peak unless marked with 'b'

[c] Peaks reference this work

[d] NM – not measured

Experimental

Hematite Nanoparticle Synthesis

Hematite nanoparticles (NPs) were synthesized as described previously [51] by heating a low concentration of ferric iron ($1.25x10^{-3}$ M) from $Fe(NO_3)_3$ to a temperature of 100°C to create small, homogenous particles. Characterization of the particles is summarized in Table B1 with details of analysis in *Supplementary Materials B.1*. The particle diameter was 13±7 nm based on TEM analysis of over 2300 particles with a surface area of 68 m^2/g as measured by the BET method (Figure B1, Table B1).

Actinide Working Solution Preparation

Pu(V) was synthesized from a $^{238}Pu(NO_3)_4$ (Isotopes Product Source, Valencia, CA) stock as described previously [15]. The oxidation state purity was verified prior to performing each batch sorption experiment and analyzed periodically throughout by solvent extraction and LaF_3 co-precipitation as described previously [20]. For the ATR FT-IR studies, a primarily $^{242}Pu(VI)$ solution was synthesized from ^{242}Pu (originally obtained from Idaho National Laboratory, Idaho Falls, ID). The stock solution was initially purified by ion exchange (Biorad AG 1x8, Cl^- form) using the HASL 300 method [52]. Then the solution was evaporated to dryness and reconstituted in 0.5 M HNO_3. The evaporation/reconstitution step was repeated three times to effectively oxidize the Pu to Pu(VI). The final residue was dissolved in 1 mL of deionized water (DI water, resistivity >18.2 MΩ-cm) and then diluted to a concentration of $1.5x10^{-4}$ M ^{242}Pu. $^{237}Np(V)$ (Eckert and Zeigler, Atlanta, GA), in 0.1 M HCl) and $^{238}U(VI)$ (prepared from

$UO_2(NO_3)_2 \cdot 6H_2O$, Alpha Aesar, ACS grade) were prepared at a concentration of $3x10^{-4}$ M and adjusted to pH 7.

Batch Sorption

Sorption experiments using suspensions of 6.9 mg/L hematite NP in 0.01 M NaCl and pH 3.6 ± 0.1, 5.6 ± 0.2, and 7.7 ± 0.2 were completed over a period of one week with continuous mixing on a benchtop rotary (end over end) shaker in the presence of light. A stock $^{238}Pu(V)$ solution with a concentration of 42.6 ± 0.7 cpm/μL (4.7×10^{-9} M) was used to amend each sample to ($9.2x10^{-11} \pm 2.0x10^{-12}$ M) $^{238}Pu(V)$. The stock $^{238}Pu(V)$ solution had an oxidation state distribution of: 94 ± 3% as Pu(V), 1 ± 0% Pu(IV), and 5 ± 3% Pu(VI) determined using solvent extraction. Upon sampling, the aqueous fraction was determined by centrifugation at 8000 rpm for 20 minutes (Beckman and Coulter Allegra 22R centrifuge with F2402 rotor) to remove particles >50 nm according to Stoke's law as described by Jackson [53]. This is sufficient to remove hematite particles from suspension as DLS particle size (Brookhaven 90Plus) in 0.01 M NaCl are ~300 nm at pH 3 with aggregation occurring as the pH is increased. This apparent increase in particle diameter relative to the diameter of 13 nm determined from TEM micrographs is due to particle aggregation which will increase as the pH increases towards the point of zero charge of hematite. Oxidation state analysis was initially performed on the aqueous supernatant after decanting then Pu was leached from the wet solids using 0.03 M HCl and the oxidation state of Pu in the leachate was determined. This procedure has been previously used as an indirect method to determine oxidation state of sorbed Pu and has been verified with direct X-ray absorption near edge spectroscopy measurements

(XANES) [10, 11, 15, 16, 20]. Additional experiments at pH = 6.8 ± 0.1 were performed at a concentration of 17 mg/L of hematite where the suspensions were exposed to varying light intensities for fixed time periods.

ATR FT-IR Spectroscopy

ATR FT-IR spectroscopy was used to characterize $^{242}Pu(V/VI)$ sorption and reduction on hematite NPs over time. The system conditions were: $[^{242}Pu] = 6.5 \times 10^{-5}$ M, pH 7.0, and $[\alpha\text{-}Fe_2O_3] = 0.3$ g/L. A Thermo Scientific Nicolet 6700 FT-IR spectrometer with a single bounce diamond ATR crystal (smart iTR)) was used to collect spectra from 600-4000 cm^{-1} at a resolution of 1 cm^{-1} and 32 scans per sample. The ^{242}Pu stock solution was 82.4±0.3% Pu(VI), 17.4±0.3% Pu(V) and 0.2±0.02% Pu(IV) determined using solvent extraction. Throughout the experiment five sub-samples were pulled from the original hematite-plutonium suspension at successive times (sub-samples pulled at 10 minutes, 1 hour, 9.5 hours, 26 hours, and 11 days). However, many measurements were taken over time once on the crystal. Each sub-sample was centrifuged for 5 min at 10,000 rpm to remove particles from the aqueous phase then subjected to a washing step with degassed DI water adjusted to pH 7 to remove aqueous Pu and possible Pu precipitates. This centrifugation step theoretically removes particles >80 nm. This is sufficient for removal of the hematite nanoparticles at pH 7 as aggregation is occurring as the particles reach closer to their point of zero charge (Supplementary Materials B.1, Figure B3). The average particle diameter at pH 7 is 1.3µm. The wet solids remaining in the tube were resuspended in 200 µL of DI water, sonicated for 30 seconds and centrifuged again. The ^{242}Pu concentration in the supernatant from the original

suspension, the wash solution and the aqueous fractions of Pu(V/VI) following LaF_3 coprecipitation as described previously [20] were measured using an inductively coupled plasma mass spectrometer (ICP-MS, Thermo Scientific X Series II) for each of the five sub-samples. Oxidation state was not measured by solvent extraction for the solid phase as they were immediately plated onto the ATR crystal. The solids were deposited on the ATR crystal as a wet paste using two - 5 µL aliquots. Because samples remained on the crystal to collect measurements over time, a 'humidity chamber' was made over the sample using an overturned 1L glass beaker and a smaller beaker filled with saturated KNO_3 (s) to create a relative humidity of approximately 94% in the chamber and to keep the sample partially hydrated. Experiments were also completed with $^{238}U(VI)$ and $^{237}Np(V)$ following the same method described for ^{242}Pu to confirm sorbed and aqueous absorption peaks determined previously experimentally [27, 30-36, 54, 55] and theoretically [27-29] as they are expected to be similar to Pu(V/VI) (Table 3.1).

Lefevre et al. [36] previously noted that air-dried DRIFT samples reported equivalent results as their ATR FT-IR flow cell setup leading to the conclusion that Fe_2O_3-uranyl complexes were not modified by drying and Wijnja [56] reached similar conclusions for carbonate sorption to γ-Al_2O_3. It is expected that a hydration layer will remain at the mineral surfaces. It is important to note that hydration waters (or crystallization waters) are still present in all samples as evidenced by the presence of the characteristic O-H stretch at 3650-3400 cm^{-1}. Absorption in this region has been shown to be due to molecular water that is weakly polarized by cations [57]. Therefore, it is unlikely these methods have induced artificial changes in the α-Fe_2O_3-Pu complexes with

drying. In addition, it must be noted that the sorbed Pu concentration reached 22 mg/g over the course of the experiments. While these concentrations are not environmentally relevant, the high concentration is a requirement of the ATR FT-IR technique and is used to explore potential mechanisms of Pu(V/VI) reduction at solid water interfaces as previously observed and discussed below [10-12, 14, 16, 17, 21-24].

Results and Discussion

The aqueous fraction of Pu as measured through batch sorption experiments at an initial concentration of 9.2×10^{-11} M ^{238}Pu over time at pH≈ 3.6, 5.6 and 7.7 are shown in Figure 3.1 below and oxidation state distributions versus time are shown in Figure B4-5 in *Supplementary Materials B.2*). At a pH of 3.6, there is almost no sorption or reduction for any sample over 200 hours of sampling and the aqueous phase remained as Pu(V). However, at pH 7.7, nearly 100% sorption occurred within 2 hours and at pH 5.6 approximately 20% sorption occurred although there was significant scatter in the data likely due to small changes in the pH as this is near the region of the Pu(V) sorption edge on hematite. Both the sorption and reduction rates of Pu(V) increase with increasing pH as seen in previous studies with hematite [16, 21, 22, 24]. While there were not enough data points prior to equilibrium to calculate adsorption rates constants (k_{ads}) for pH 3.6 and 5.6 (eqn. 1), a sorption rate constant of 5.41 day^{-1} was estimated for the hematite data for pH 7.7 (*Supplementary Materials B.6, Figure B11-12 and Table B2*). In addition, the aqueous phase was dominated by Pu(V) with less than 1% Pu(IV) indicating that reduction of Pu(V/VI) is not occurring in the aqueous phase and is surface-mediated as discussed previously [10-12, 14, 16, 17, 21-24].

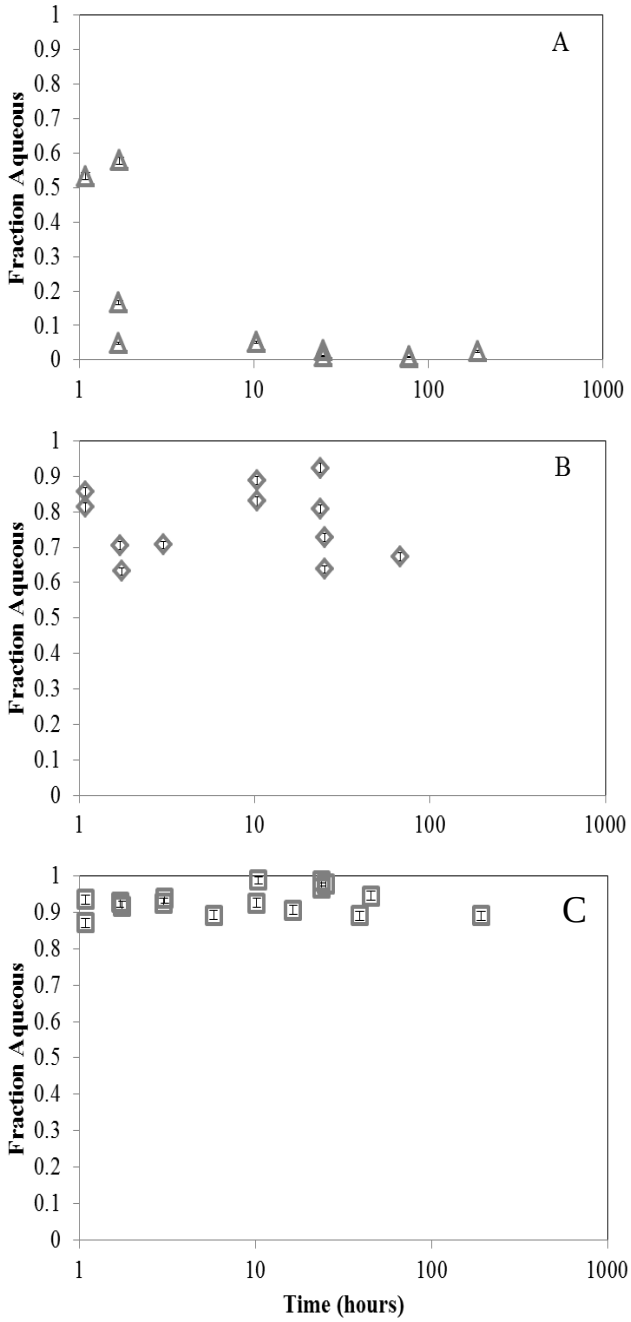

Figure 3.1: Comparison of the aqueous fraction of ^{238}Pu for hematite at (a) pH = 7.7 ± 0.2, (b) 5.6 ± 0.2 , and (c) 3.6 ± 0.1 over time at $^{238}Pu = 9.2x10^{-11}$ M, 0.01 M NaCl, 7 mg/L hematite NPs.

Prior to discussion of the ATR FT-IR measurements compiled for ^{242}Pu(V/VI), ^{238}U(VI) and ^{237}Np(V), a discussion of the methods is warranted as these data are collected at high solids loadings (22 $mg_{Pu}/g_{hematite}$, 100 $mg_{Np}/g_{hematite}$, 200 $mg_{U}/g_{hematite}$). Figure 3.2a compares two ^{238}U(VI) samples analyzed following one hour of sorption with one being subjected to the wash step described above and one plated onto the ATR FT-IR crystal immediately following the first centrifuge step. The unwashed sample shows a peak near 1062 cm^{-1}. Previous work investigating uranium sorption to pure minerals has identified peaks in this range (1034-1080 cm^{-1}) and attributed the absorption peak to changes in the mineral surface upon sorption of uranyl [40, 42, 44-46]. In addition the γ-U-O-H plane bending vibration occurs in this region (980-1180 cm^{-1}) on various uranyl minerals (Table 3.1) [57-62]. It is likely that the peak seen in this work is due to the UOH vibration. From this work it cannot be confirmed if the peak is due to a vibration caused by a UOH precipitate or by a uranyl adsorbed to a hydroxide group at the hematite surface. However, ^{238}U(VI) precipitation on the hematite surface was confirmed by scanning electron microscopy (Hitachi SU 6600 SEM) and energy dispersive x-ray mapping (EDX) (Figure 3.2b-c). It is important to note that the specific crystal phase of the U(VI) precipitate forming as the aqueous solution dried has not been identified, but similar ATR FT-IR peaks have been previously observed as U(VI) precipitates identified near 1000 cm^{-1} [36, 63]. Previous work has also ruled out the formation of uranyl nitrate ternary complexes [36]. However, it is important to note that the peak disappears (Figure 3.2a-c) with the washing step described in the Methods and Materials section. There is a high likelihood of precipitation due to the high concentrations of actinides in the aqueous

phase and the neutral pH of the experiments. Therefore, the washing methods described above were employed for all other data shown for ^{238}U(VI), ^{237}Np(V) and ^{242}Pu sorption to hematite NPs.

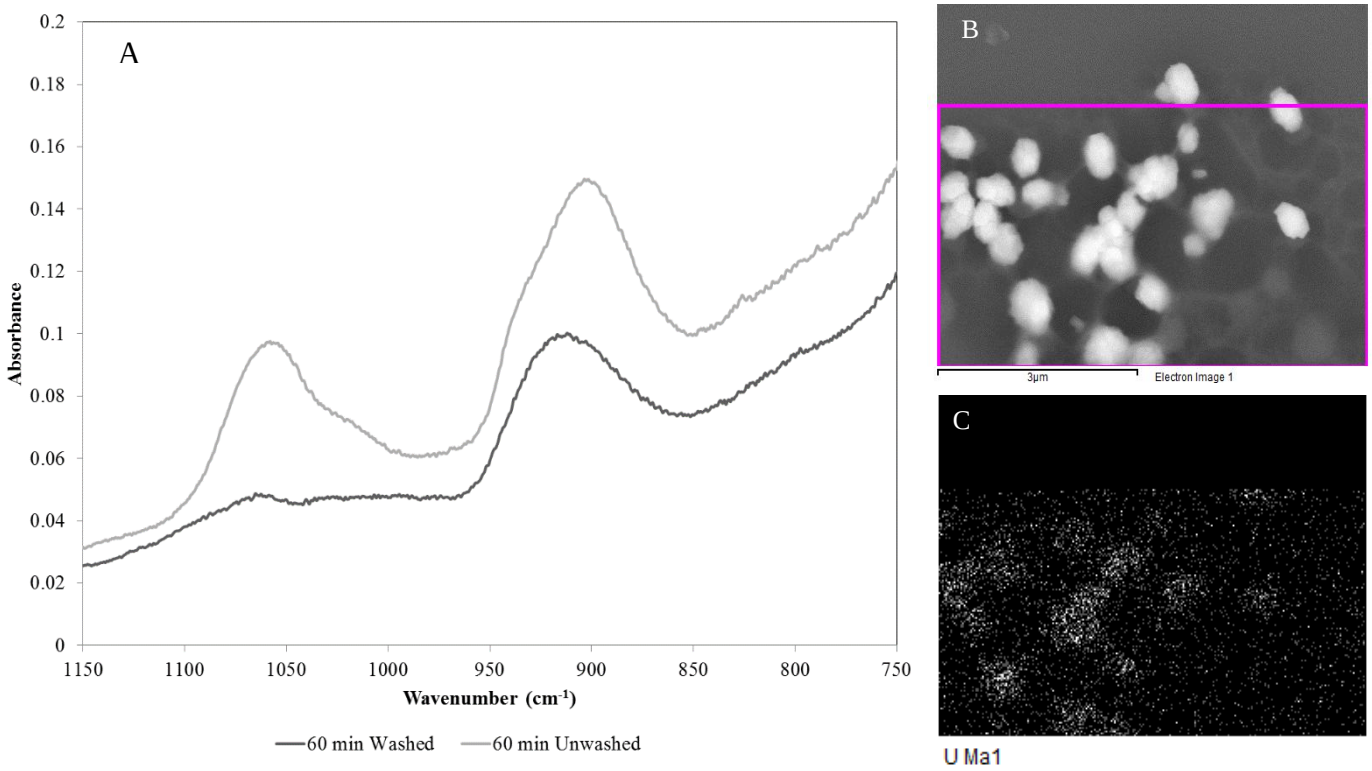

Figure 3.2: (a) ATR FT-IR spectra of $^{238}U(VI)$ sorbed onto Fe_2O_3 nanoparticles after 60 minutes at pH 7, $^{238}U = 1.5x10^{-4}$ M, 0.2 g/L hematite NPs. Sample washed as described in Methods and Materials is shown in black and sample plated onto crystal immediately following initial centrifuge step is shown in gray, (b) SEM image of uranium precipitate formed on unwashed samples (c) EDX mapping of image 'b' for uranium.

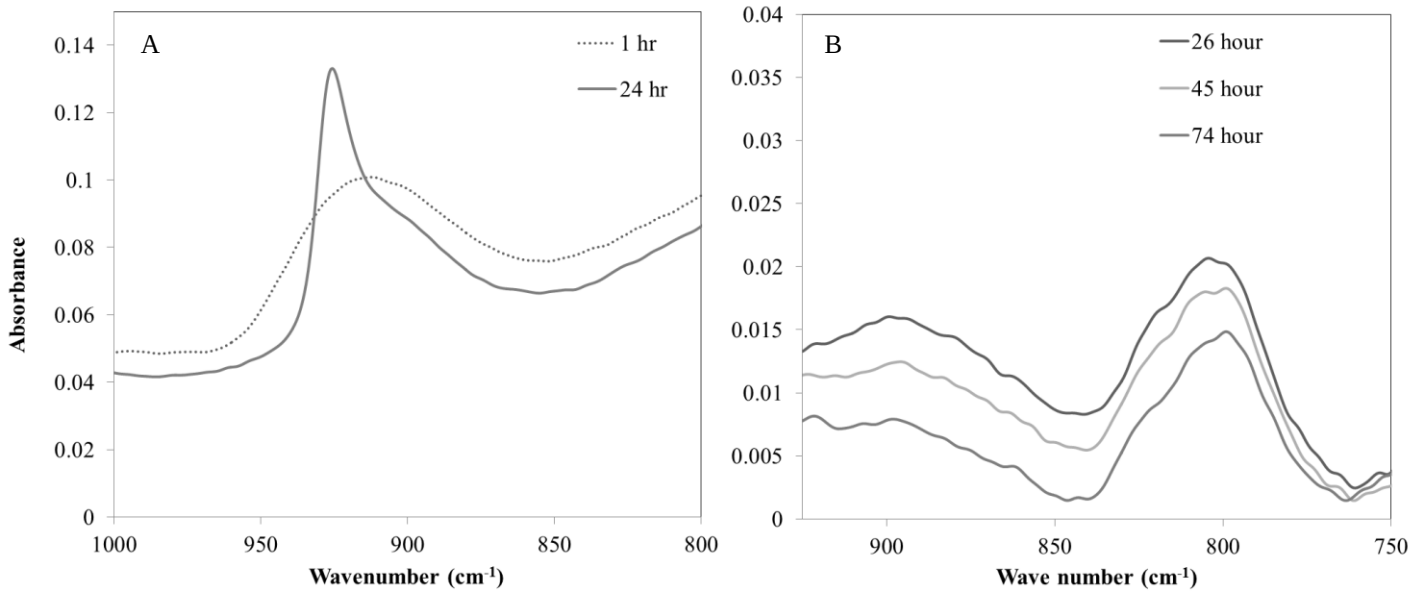

Figure 3.3: ATR FT-IR spectra of $^{238}U(VI)$ (at 923 cm^{-1}) and $^{237}Np(V)$ (at ~790 cm^{-1}) sorption to hematite NPs over time at pH 7. (a) $^{238}U(VI)$ = 1.5 x 10^{-4} M and 0.2 g/L hematite NPs and (b) $^{237}Np(V)$ = 1.7 x 10^{-4} M and 0.2 g/L hematite NPs. Note: spectra were obtained after samples reached incipient dryness on the ATR crystal.

ATR FT-IR measurements of $^{238}U(VI)$ and $^{237}Np(V)$ were completed first to validate the methods prior to measurements with $^{242}Pu(V/VI)$. The ATR FT-IR peak for $^{238}U(VI)$ sorbed to hematite measured at 923 cm^{-1} is shifted significantly compared to the peaks from aqueous UO_2^{2+} at 961 to 965 cm^{-1} previously determined [28, 29, 31-33], but it is similar to previous measurements of U(VI) on hematite [34, 36, 64] (Table 3.1). In addition, it is important to note that the peak becomes narrower with time suggesting that the sorbed complex becomes more ordered with time (Figure 3.3a). However, the peak area does not decrease suggesting that reduction of U(VI) does not occur on hematite nanoparticles under the conditions and the time span of this study (24 hours, Figure 3.3a). This was expected as previous studies on bulk hematite have not shown reduction of U(VI) under oxidizing conditions. Previous work by Liger et al. [34] have shown ferrous iron must be present in order for U(VI) to reduce on hematite under anoxic conditions (experimental conditions 160 μM U(VI), 0.53 g/L hematite and 160 μM aqueous Fe(II)). The aqueous $^{238}U(VI)$ measurement shows the primary peak around 938 cm^{-1} (*Supplementary Materials B.4 Figure B7,* Table 3.1). This peak most likely contains the absorbance for two previously identified aqueous U(VI) hydrolysis species $(UO_2)_2(OH)_2^{2+}$ at 943 cm^{-1} and $(UO_2)_3(OH)_5^{2+}$ at 922-923 cm^{-1}) [31-33].

For both U(VI) and Np(V) studies, a similar shift in the peak position to lower wavenumbers and no evidence of reduction to a tetravalent state (without axial oxygen bonds) was observed. Over 74 hours the fraction of $^{237}Np(V)$ sorbed to hematite increased to 53%. The sorbed Np(V) was difficult to differentiate as it fell into a region of high absorbance from the hematite and thus was difficult to distinguish above the

hematite peaks (Figure 3.3b). However, based on previous experimental measurements and theoretical estimates of the aqueous Np(V) species, our measurement around 790 cm^{-1} is comparable to previous observations [27-29, 32] (Table 3.1). In addition, reduction of Np(V) was not observed over the time scale of this work as the peaks did not decrease (74 hours). The aqueous, asymmetric Np=O stretch was observed at 833 cm^{-1} in this work and is in agreement previous experimental and theoretical work described above (Table 3.1) [27-29, 40].

The ATR FT-IR absorption peak for the asymmetric axial oxygen stretch of Pu(VI) sorbed to hematite was measured between 915-917 cm^{-1} throughout the experiments (i.e. pH 7.0, 0.3 g/L hematite and 6.5 x 10^{-5} M ^{242}Pu). This is a downshift of approximately 25 cm^{-1} relative to the free plutonyl (VI) ion asymmetric stretch absorption peak measured at 940 cm^{-1}. In addition, the peak decreases with time as Pu(VI) is reduced to Pu(IV) because Pu(IV) species will not have the axial oxygen atoms that are the source of the asymmetric stretch (Figure 3.4). After five days, the peak is decreased to approximately 15% of its original area and decreases to 10% at day 18 (*Supplementary Materials B.6, Figure B13,* Figure 3.4). It is also notable that at 193 hours another peak (~836 cm^{-1}) appears briefly. Previous work with uranium has observed a similar peak near 800 cm^{-1} that is proposed to be a U(IV/VI)-mixture [26, 47]. However, given the similarity with the wavelength corresponding to the Np(V) asymetric stretch, it is likely this peak corresponds to transient Pu(V) in the system prior to reduction to Pu(IV).

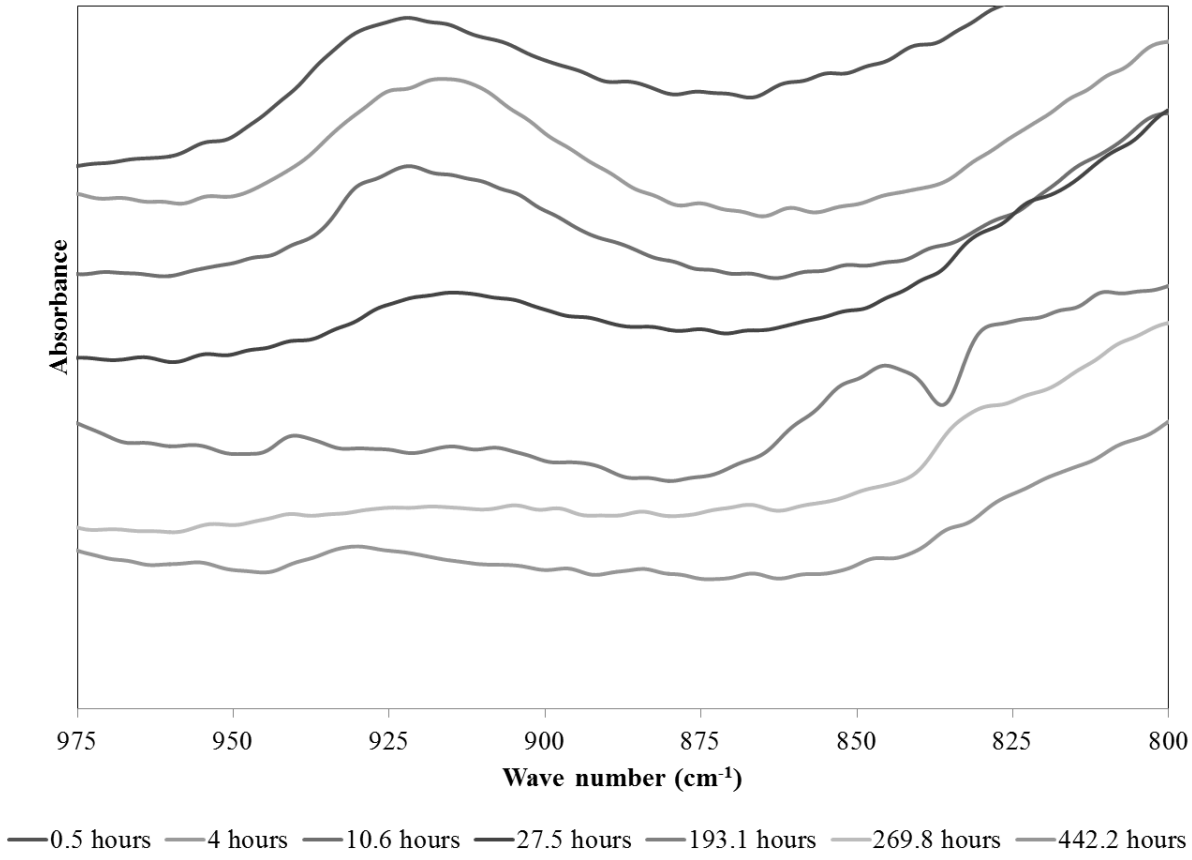

Figure 3.4: Reduction of ^{242}Pu on hematite over time, shown by a decrease of the $Pu(VI)O_2^{2+}$ asymmetric stretch peak over time as reduction to Pu(IV) occurs. System conditions: pH 7.0, 0.3 g/L hematite and 65 µM ^{242}Pu (initially as Pu(V/VI). Note: spectra were obtained after samples reached incipient dryness on the ATR crystal.

At these aqueous concentrations, precipitation during drying of an aqueous suspension can be an issue. Therefore, the washing step discussed above was employed for Pu-bearing samples. Because there were no peaks observed from 980-1180 cm^{-1} in the samples with sorbed Pu and based on previous observations with U(VI) discussed above,

the results indicate precipitation of Pu(VI) was not occurring in these samples. Measurements of the aqueous phase after reaching incipient dryness did show peaks indicating precipitation (*Supplementary Materials B.5, Figure B9*). However, previous work has also identified reduced Pu(IV) nanocolloids on goethite and hematite surfaces [22, 65] so it is possible that insoluble PuO_2 nanocolloids could form in these systems. Attempts were made to identify Pu precipitates associated with hematite using HRTEM (Hitachi HRTEM 9500) analysis but no discrete precipitates could be identified.

While no reduction of U(VI) and Np(V) was observed in previous studies or this work, reduction of Pu(V/VI) was obvious based on the decrease of the asymmetric stretch over time. Based on the decrease in the asymmetric stretch peak position of approximately 25 cm^{-1} between the aqueous U, Np, Pu and sorbed species, it is hypothesized that inner-sphere sorption is occurring. This has been previously determined for Fe_2O_3-uranyl and neptunyl complexes based on a peak shift of 20-60 cm^{-1} [34, 35] and for Np and U sorption to many other minerals [34-36, 40, 42-44, 46, 66]. Previously reported Pu-hematite adsorption and reduction kinetics measured using conventional batch sorption and oxidation state by solvent extraction agree well with the estimates presented within this work at both the batch sorption loading and ATR FT-IR loading levels ([16, 24], *Supplementary Materials B.6, Table B2 and Figures B15-16*). Therefore, it does not seem that there is a significant difference in sorption between bulk and nanoparticulate hematite for Pu when compared with respect to surface area. Although previous work has shown a greater reactivity of hematite as particle size decreases [47] and greater adsorption of U and Cu as particle size decreases [67, 68].

Normalizing the reaction rates to surface area as done in Figures B14 and B15 indicates the greater reactivity is likely due to increased surface area.

This work demonstrates surface-mediated reduction of Pu in the presence of hematite NPs by ATR FT-IR. While it does not confirm Fe(II) as the dominant reductant, previous work shows that it is likely that sufficient Fe(II) could be present in hematite to reduce environmentally relevant (i.e. 10^{-18} – 10^{-14} M Pu(V/VI)). The pseudo first order rate in experiments with 9.2 x 10^{-11} M ^{238}Pu were approximately 10x faster than that observed in systems with 6.5 x 10^{-5} M ^{242}Pu as measured previously and in this work (*Supplementary Materials B.6* Figures B15-B16) [16]. Therefore, it is proposed that reduction by Fe(II) is likely the dominant mechanism at trace Pu concentrations. In addition it appears that the rate is decreased at the high Pu loading for the ATR FT-IR samples. At these high Pu loadings, any trace Fe(II) is likely oxidized and an alternate electron source is required. As radiolysis and disproportionation have been previously dismissed [21, 23], the most likely mechanism at these high Pu loadings is that Pu(V/VI) is being reduced by water based on the thermodynamic favorability of Pu(IV)-hydroxide surface complexes and/or Pu(IV) precipitates. Direct identification of this reduction mechanism is the subject of ongoing work.

Conclusions

This work presents batch sorption experiments and ATR FT-IR work investigating Pu(V/VI) reduction on hematite. It appears that Pu is reduced on hematite regardless of the surface loading of Pu as evidenced in batch sorption experiments (10^{-3} to 10^{-4} $mg_{Pu}/g_{hematite}$) and ATR FT-IR work at high plutonium loadings (22 $mg_{Pu}/g_{hematite}$).

However, based on a reduction rate constant more than 10x lower at higher loadings, the Fe(II)-mediated reduction of Pu at higher loadings is limited by the rate of electron shuttling in the hematite and the Fe(II) content (*Supplementary Materials B.6 Table B2 and Figures B15-16*). In addition, for the first time, ATR FT-IR peaks for Pu(VI) sorbed to hematite are measured at 915-917 cm^{-1} (Figure 3.4) and the decrease in peak intensity with time provides a real-time, direct measurement of the Pu(V/VI) reduction rate (0.35 day^{-1}). This is a relatively simple method to observe the reduction of Pu with time and could be an alternative to XANES analysis though higher solid phase concentrations are required based on instrument performance.

Acknowledgements

This work was supported by the Subsurface Biogeochemical Research Program of the U.S. Department of Energy's Office of Biological and Environmental Research, DE-SC0004883. H. Emerson also acknowledges support from the U. S. Nuclear Regulatory Graduate Fellowship Program.

Author contributions

The manuscript was written through the contributions of all authors and all have given approval of the final version of the manuscript.

References

1. D.I. Kaplan, B.A. Powell, D.I. Demirkanli, R.A. Fjeld, F.J. Molz, S.M. Serkiz, J.T. Coates, Environmental science & technology 38 (2004) 5053.
2. D.I. Kaplan, D.I. Demirkanli, L. Gumapas, B.A. Powell, R.A. Fjeld, F.J. Molz, S.M. Serkiz, Environmental science & technology 40 (2006) 443.

3. B.A. Powell, A.B. Kersting, M. Zavarin, P. Zhao, Los Alamos National Laboratory (2008).

4. J.D. Begg, M. Zavarin, P. Zhao, S.J. Tumey, B. Powell, A.B. Kersting, Environmental science & technology 47 (2013) 5146.

5. B.A. Powell, D.I. Kaplan, S.M. Serkiz, J.T. Coates, R.A. Fjeld, Journal of environmental radioactivity 131 (2014) 47.

6. R.J. Silva, H. Nitsche, Radiochimica Acta 70/71 (1995) 377.

7. B. Allard, H. Kipatsi, O. Liljenzin, Journal of Inorganic Nuclear Chemistry 42 (1980) 1015.

8. M.A. Abuzwida, A.G. Maslennikov, V.F. Peretrukhim, Journal of Radioanalytical and Nuclear Chemistry 147 (1991) 41.

9. R.J. Lemire, J. Fuger, H. Nitsche, P. Potter, M.H. Rand, J. Rydberg, K. Spahiu, J.C. Sullivan, W.J. Ullman, P. Vitorge, H. Wanner, El Sevier 4 (2001).

10. W.L. Keeney-Kennicutt, J.W. Morse, Geochimica et Cosmochimica Acta 49 (1985) 2577.

11. A.L. Sanchez, J.W. Murray, T.H. Sibley, Geochimica et Cosmochimica Acta 49 (1985) 2297.

12. W.R. Penrose, D.N. Metta, J.M. Hylko, L.A. Rinckel, Journal of environmental radioactivity 5 (1987) 169.

13. M.C. Duff, D.B. Hunter, I.R. Triay, P.M. Bertsch, D.T. Reed, S.R. Sutton, G. Shea-McCarthy, J. Kitten, P. Eng, S.J. Chipera, D.T. Vaniman, Environmental science & technology 33 (1999) 2163.

14. D.A. Shaughnessy, H. Nitsche, C.H. Booth, D.K. Shuh, G.A. Waychunas, R.E. Wilson, H. Gill, K.J. Cantrell, R.J. Serne, Environmental Science and Technology 37 (2003) 3367.

15. B.A. Powell, R.A. Fjeld, D.I. Kaplan, J.T. Coates, S.M. Serkiz, Environmental Science and Technology 38 (2004) 6016.

16. B.A. Powell, R.A. Fjeld, D.I. Kaplan, J.T. Coates, S.M. Serkiz, Environmental Science and Technology 39 (2005) 2107.

17. B.A. Powell, M.C. Duff, D.I. Kaplan, R.A. Fjeld, M. Newville, D.B. Hunter, P.M. Bertsch, J.T. Coates, P. Eng, M.L. Rivers, S.M. Serkiz, S.R. Sutton, I.R. Triay, D.T. Vaniman, Environmental Science and Technology 40 (2006) 3508.

18. D.I. Kaplan, B.A. Powell, M.C. Duff, D.I. Demirkanli, M.E. Denham, R.A. Fjeld, F. Molz, Environmental Science and Technology 41 (2007) 7417.

19. Q.H. Hu, T.P. Rose, M. Zavarin, D.K. Smith, J.E. Moran, P.H. Zhao, Journal of environmental radioactivity 99 (2008) 1617.

20. A.E. Hixon, Y.J. Hu, D.I. Kaplan, R.K. Kukkadapu, H. Nitsche, O. Qafoku, B.A. Powell, Radiochimica Acta 98 (2010) 685.

21. A.Y. Romanchuk, S.N. Kalmykov, R.A. Aliev, Radiochimica Acta 99 (2011) 137.

22. A.Y. Romanchuk, S.N. Kalmykov, A.V. Egorov, Y.V. Zubavichus, A.A. Shiryaev, O.N. Batuk, S.D. Conradson, D.A. Pankratov, I.A. Presnyakov, Geochimica et Cosmochimica Acta 121 (2013) 29.

23. A.E. Hixon, Y. Arai, B.A. Powell, Journal of colloid and interface science 403 (2013) 105.

24. A.E. Hixon, B.A. Powell, Environmental Science and Technology submitted (2014).

25. H. Furuya, K. Idemitsu, Y. Inagaki, T. Arima, T. Sasaki, Y. Kuroda, S. Uchikawa, S. Mitsugashira, Y. Suzuki, Sci rep RITU A45 (1997) 89.

26. W. Runde, S.D. Conradson, D.W. Efurnd, N. Lu, C. VanPelt, C.D. Tait, Applied Geochemistry 17 (2002) 837.

27. L.H. Jones, R.A. Penneman, The Journal of Chemical Physics 21 (1953) 542.

28. J. Hay, R.L. Martin, G. Schreckenbach, Journal of Physical Chemistry A 104 (2000) 6259.

29. G.A. Shamov, G. Schreckenbach, J Phys Chem A 109 (2005) 10961.

30. S. Siegel, H.R. Hoekstra, Inorganic & Nuclear Chemistry Letters 7 (1971) 497.

31. K. Muller, V. Brendler, H. Foerstendorf, Inorganic chemistry 47 (2008) 10127.

32. K. Muller, H. Foerstendorf, S. Tsushima, V. Brendler, G. Bernhard, Journal of Physical Chemistry 113 (2009) 6626.

33. F. Quiles, C. Nguyen-Trung, C. Carteret, B. Humbert, Inorganic chemistry 50 (2011) 2811.

34. E. Liger, L. Charlet, E. Van Cappellen, Geochimica et Cosmochimica Acta 53 (1999) 2939.

35. J.R. Bargar, R. Reitmeyer, J.A. Davis, Environmental Science and Technology 33 (1999) 2481.

36. G. Lefevre, S. Noinville, M. Fedoroff, Journal of colloid and interface science 296 (2006) 608.

37. S. Lehmann, G. Geipel, H. Foerstendorf, G. Bernhard, Journal of Radioanalytical and Nuclear Chemistry 275 (2007) 633.

38. G. Lefevre, J. Kneppers, M. Fedoroff, Journal of colloid and interface science 327 (2008) 15.

39. A. Barkleit, H. Foerstendorf, K. Heim, S. Sachs, G. Bernhard, Applied Spectroscopy 62 (2008) 798.

40. K. Muller, H. Foerstendorf, V. Brendler, G. Bernhard, Environmental Science and Technology 43 (2009) 7665.

41. M.J. Comarmond, T.E. Payne, J.J. Harrison, S. Thiruvoth, H.K. Wong, R.D. Aughterson, G.R. Lumpkin, K. Muller, H. Foerstendorf, Environmental science & technology 45 (2011) 5536.

42. K. Müller, H. Foerstendorf, T. Meusel, V. Brendler, G. Lefèvre, M.J. Comarmond, T.E. Payne, Geochimica et Cosmochimica Acta 76 (2012) 191.

43. K. Gückel, A. Rossberg, V. Brendler, H. Foerstendorf, Chemical Geology 326-327 (2012) 27.

44. H. Foerstendorf, K. Heim, A. Rossberg, Journal of colloid and interface science 377 (2012) 299.

45. K. Guckel, A. Rossberg, K. Muller, B. Vinzenz, G. Bernhard, H. Foerstendorf, Environmental Science and Technology 47 (2013) 14418.

46. H. Foerstendorf, N. Jordan, K. Heim, Journal of colloid and interface science 416 (2014) 133.

47. Y.T. He, J. Wan, T. Tokunaga, Journal of Nanoparticle Research 10 (2007) 321.

48. T.D. Waite, Reviews in Mineralogy 23 (1990) 559.

49. D. McCubbin, K.S. Leonard, H.S. Emerson, Marine Chemistry 80 (2002) 61.

50. A.G.B. Williams, M.M. Scherer, Environmental Science and Technology 38 (2004) 4782.

51. W. Wang, J.Y. Howe, B. Gu, Journal of Physical Chemistry 112 (2008) 9203.

52. M.D. Erickson, in: N.A. Chieco, (Ed.)^(Eds.)Pu-11-RC Plutonium Purification - Ion Exchange Technique; U.S. Department of Homeland Security, New York, 1997.

53. M.L. Jackson, in: (Ed.)^(Eds.)Soil Chem. Anal.-Adv. course; Parallel Press, Madison, WI, 1985.

54. H. Geckeis, J. Lutzenkirchen, R. Polly, T. Rabung, M. Schmidt, Chemical reviews 113 (2013) 1016.

55. L.H. Jones, The Journal of Chemical Physics 23 (1955) 2105.

56. H. Wijnja, C.P. Schulthess, Spectrochimica acta. Part A, Molecular and biomolecular spectroscopy 55 (1999) 861.

57. J. Cejka, in: P.C. Burns, R. Finch, (Ed.)^(Eds.)Uranium: Mineralogy, Geochemistry, and the Environment; Mineralogical Society of American, 1999, p 521.

58. P.C. Burns, American Mineralogist 82 (1997) 1176.

59. D. Dothee, Univ. Besancon, Fr (1980) 148.

60. D. Dothee, M. Camelot, (1982).

61. D. Dothee, B. Fahys, M. Camelot, (1982).

62. Z. Urbanec, J. Čejka, Collection of Czechoslovak Chemical Communications 44 (1979) 1.

63. P.G. Allen, J.J. Bucher, D.K. Shuh, N.M. Edelstein, T. Reich, Inorganic chemistry 36 (1997) 4676.

64. P. Wersin, M.F. Hochella, Jr., P. Persson, G. Redden, J.O. Leckie, D.W. Harris, Geochimica et Cosmochimica Acta 58 (1994) 2829.

65. B.A. Powell, Z. Dai, M. Zavarin, P. Zhao, A.B. Kersting, Environmental science & technology 45 (2011) 2698.

66. D.C.-K. Hsi, D. Langmuir, Geochimica et Cosmochimica Acta 49 (1985) 1931.

67. H. Zeng, A. Singh, S. Basak, K.-U. Ulrich, M. Sanu, P. Biswas, J.G. Catalano, D.E. Giammar, Environmental Science and Technology 43 (2009) 1373.

68. A.S. Madden, M.F. Hochella, T.P. Luxton, Geochimica et Cosmochimica Acta 70 (2006) 4095.

CHAPTER FOUR

PAPER THREE: EXAMINATION OF THE EFFECTS OF AGING ON (DE)SORPTION OF PLUTONIUM FROM 32-YEAR OLD PLUTONIUM CONTAMINATED SEDIMENTS USING MULTIPLE PLUTONIUM ISOTOPES

Status

To be submitted to *Radiochimica Acta*

Authors

Hilary P. Emerson and Brian A. Powell

Introduction

Plutonium (Pu) has been released to the environment due to activities including nuclear weapons testing and past accidents, spills from the nuclear arms race and the early nuclear power industry. Estimated inventories of Pu at U.S. Department of Energy sites includes 3.1×10^{16} Bq in the subsurface due to underground weapons testing at the Nevada National Security Site[1], 6.1×10^{11} Bq released to streams and unlined seepage basins at the Savannah River site[2], 3.7×10^{11} Bq released to unlined seepage basins at Los Alamos[3], and 4.4×10^{14} Bq as liquid waste at Hanford in Washington.[4-6] In addition, Pu inventories by 70-75 metric tons per year from spent nuclear fuel worldwide and must be maintained for thousands of years due to the long half-lives of many of the plutonium isotopes.[6-8] Because Pu represents a long term environmental hazard, it is necessary to understand the role sorption and desorption processes may play in limiting plutonium mobility in environmental systems.

There have been several studies in the past noting that the reversibility of sorption for actinide elements including Pu decreases over time as the adsorbed complexes age.[9-16] For example, Lu *et al*. demonstrated a low reversibility of Pu sorption to hematite with <1% desorption after 150 and 293 days and concluded that desorption is a much slower process than sorption [12, 17]. Powell *et al*. reported that greater than 80% of Pu(IV) was not leachable (acidified to pH 1.5 with $HClO_4$ for 15 minutes) within days of sorption to magnetite[16]. However, work by Wang *et al*. concluded that the americium fraction irreversibly sorbed to humic acid coated gibbsite did not change with aging time within a period of 2 hours to 5 months.[18] Previous work has noted that adsorption rates may be significantly faster than desorption rates due to differences in activation energies.[11] Tinnacher *et al*. defines three major theories to describe changes in (de)sorption kinetics:

(1) Aging – secondary sorption processes that may cause changes in contaminant surface speciation with time, resulting in increased K_ds with time

(2) Hysteresis – thermodynamic changes in sorption based on the overall direction of reactions

(3) Irreversible sorption – a process where a residual fraction remains adsorbed even after desorption equilibrium is reached

These aging processes may lead to theoretical problems as equilibrium K_d values (partition coefficients) which are typically used in performance assessments are assumed to be linear, reversible values. This may lead to an over prediction of transport due to an under prediction of adsorbed fractions or an under prediction of transport where sorption to colloids is considered in risk assessment models.[6, 19] Further complicating Pu transport

processes, some studies have suggested that groundwater components like natural organic matter (NOM)[20-22] or naturally produced hydrogen peroxide[14] can play a role in mobilizing actinide elements by increasing solubility. Field and laboratory experiments have shown that natural organic matter may increase the mobility of the actinides.[23-29] Begg *et al*. reported desorption of 33.4% of adsorbed Pu from goethite with 50 µM H_2O_2 although re-adsorption did occur with time.[14] This is significantly greater than desorption observed without H_2O_2 by Lu *et al*.[12, 17] Therefore it is possible that the presence or introduction of ligands and redox active chemicals may lead to a reversal enhanced desorption and potentially a reversal of aging processes.

In these studies sorption/desorption experiments and selective iron extractions were used to investigate the effects of desorption processes and aging of plutonium in the presence of a subsurface clayey sediment from an 11 year lysimeter experiment completed at the Savannah River Site 21 years ago (sediments have now aged in the presence of $^{239/240}$Pu for a total of 32 years).[9, 30] The previous lysimeter experiments reported very little movement of plutonium of variable initial oxidation states with greater than 95% remaining within 1.25 cm of the source in an unsaturated columns exposed to the elements for 11 years.[9, 30, 31] In the current experiments, two isotopes of plutonium are used to simultaneously measure desorption of plutonium aged on SRS sediments after for 32 years ($^{239/240}$Pu) and sorption of freshly added plutonium (^{242}Pu).

Materials and Methods

Materials

^{242}Pu (Idaho National Laboratory, Idaho Falls, ID was initially purified by ion exchange (Biorad AG 1x8, Cl^- form) using the HASL 300 method [32]. Then the solution was evaporated to dryness and reconstituted in 0.5 M HNO_3. The evaporation/reconstitution step was repeated three times to effectively oxidize the Pu to Pu(VI). The final residue was dissolved in 1 mL of deionized water (DI water, resistivity >18.2 MΩ-cm) and then diluted to a concentration of 1.5 x 10^{-4} M ^{242}Pu to allow for auto-reduction to Pu(V). The oxidation state was confirmed by solvent extraction and LaF_3 co-precipitation as described previously [33] and measured by inductively coupled plasma mass spectrometer (ICP-MS, Thermo Scientific X Series II). The final stock solution was 94±1% Pu(V), 4±1% Pu(VI) and 0±3% Pu(IV). The sediment, which is representative of historical SRS burial ground sediments, was obtained from previous lysimeter experiments completed at the Savannah River Site [9, 30]. The sediment was originally sieved to remove particles >2mm. The sediment has ~2 µg/g $^{239/240}$Pu and has been stored dry at room temperature since completion of the experiments (aged with Pu ~32 years). Additional characterization has been published previously [9, 30]. In addition, control sediment (without Pu amended) from the previous experiments was also obtained from SRS and has similar physical and mineralogical characteristics.

Batch desorption experiments from aged SRS lysimeter sediments

Desorption experiments were conducted on aged source materials (~2 $\mu g/g_{sediment}$ of $^{239/240}$Pu, pH of 6.4±0.4) by mixing the sediment in 2.0 mL centrifuge tubes

(polypropylene, VWR) in the presence of one of the following organic ligands, salts, oxidants or reductants at variable concentrations.

- Salts: NaCl (BDH, ACS grade, >99% purity), $CaCl_2$ (Acros Organics, >98% purity), Na_2PO_4 (Fisher, ACS grade), or NaF (EM, ACS grade, >99% purity) from 0.1. 1.0 or 10 mM
- Organic ligands: Citric Acid (Alfa Aesar, ACS grade, >99% purity), Suwanee River Fulvic Acid (SRFA, Standard II from IHSS), or deferoxamine mesylate salt (DFOB, Sigma Aldrich, >92.5% purity) from 0.05, 0.5 or 5 mg_{carbon}/L
- Oxidant: H_2O_2 (ACS Reagent grade, VWR) from 0.01, 0.1 or 1% (3 to 300 mM)
- Reductant: $NH_2OH{\cdot}HCl$ (Fisher Scientific) at 1 mM

After 3, 7, 28 or 168 days of mixing, the aqueous phase in each tube was decanted. The 3 day desorption experiments were carried out in duplicate for only the highest ligand or salt concentration described above and with the addition of ~3.7 ppb ^{242}Pu at a soil concentration of 70±1.4 $g_{sediment}/L$. The addition of ^{242}Pu allowed for simultaneous measurement of sorption and desorption of Pu. Following the collection of 3 day sorption and desorption data, selective extractions were completed on the samples as described below. The 7 and 28 day desorption experiments were carried out with each of the ligands and concentrations mentioned above without the addition of ^{242}Pu at a soil concentration of 47.9±0.4 $g_{sediment}/L$. The 7 day desorption was completed in triplicate. Following the first 7 day desorption period, the aqueous phase was decanted and fresh solution was added for the next desorption. The 28 day desorption was completed following the three 7 day desorption periods. Finally, the 168 day experiments were

carried out as described for the 3 day dataset but without the selective extractions following. $^{239/240}$Pu was measured by liquid scintillation counting (LSC, TriCarb) of the alpha emissions with 1 mL of sample mixed with 19 mL of HiSafe III LSC cocktail with a one hour count time. The error for 3 and 168 day measurements is based on the standard deviation of duplicate measurements. The error for the 7 day measurements is based on the standard deviation of triplicate measurements. The error for the 28 day measurements is calculated based on one sigma of counting statistics for $^{239/240}$Pu and for ^{242}Pu is based on triplicate measurements by ICP-MS because multiple measurements are not taken.

Selective extractions for total and amorphous iron

Selective extractions for total free iron and amorphous iron oxides were completed on source sediment suspensions following the 3 day dual isotope sorption (^{242}Pu) and desorption ($^{239/240}$Pu) experiment. The $^{239/240}$Pu contaminated sediment suspensions were reacted with 3.7 µg/L of ^{242}Pu for 3 days and were prepared in duplicate in the presence of 10 mM NaCl, 10 mM $CaCl_2$, 10 mM Na_2PO_4, 10 mM NaF, 5 mg C/L Citric Acid, 5 mg C/L Suwanee River Fulvic Acid, 5 mg C/L DFOB, 1% H_2O_2, or 1 mM $NH_2OH{\cdot}HCl$ prior to selective extraction. In this manner, desorption of $^{239/240}$Pu and sorption of ^{242}Pu in the presence of these ionic strengths or ligands were analyzed in addition to their association with the amorphous and crystalline iron fractions in the sediments. $^{239/240}$Pu samples were analyzed by LSC and ^{242}Pu was analyzed by ICP-MS as described above. Error in these measurements is determined based on one sigma error of duplicate measurements. This soil also has relatively high levels of naturally occurring

^{232}Th so select samples were also prepared for alpha spectroscopy to confirm that total alpha activity analyzed by LSC was due only to 239/240 and 242 isotopes of plutonium. Alpha spectroscopy samples were prepared by cerium fluoride micro-precipitation (Eichrom Method SPA01) and counted for four days on the alpha spectrometer (Octete PC).

Total extractable iron was determined by the citrate bicarbonate dithionite method.[34] Briefly, 0.5 grams of dry sediment is mixed with 40 mL of 0.3 M sodium citrate (Alfa Aesar, ACS grade) and 5 mL of 1 M sodium bicarbonate (Mallinckrodt, ACS grade) and heated to 75-80°C in 100 mL conical centrifuge tubes (VWR). Then 1 gram of sodium dithionite (J.T. Baker, >90% purity) is added and mixed intermittently for 10 minutes with 10 mL of saturated NaCl (BDH) solution added at the end to promote flocculation. Because a reddish brown coloring persisted in solution following centrifugation, the method was repeated prior to analysis. The amorphous extractable iron was determined by the method using ammonium oxalate in the dark.[34] Briefly, 0.5 grams of dry sediment is mixed with 30 mL of pH 3 ammonium oxalate (0.175 M ammonium oxalate + 0.1 M oxalic acid, Fisher, ACS grade) in a light-proof 50 mL centrifuge tube (polypropylene, VWR). These were allowed to mix for 2 hours on a rotary shaker and centrifuged to remove particles prior to analysis. The crystalline iron fraction was calculated by difference with the assumption that organically-bound iron is negligible in these sediments due to the low organic carbon present.[34]

Statistical Analysis

Statistical comparisons between the average K_d and fraction sorbed were completed at a 95% confidence interval by t-test.[35] When multiple datasets were compared (i.e. multiple sorption/desorption time steps and isotopes), averages were compared using Tukey's paired comparison method and Dunnett's comparison with a control[36] as they allow for pooling of the error associated with multiple pairwise comparisons rather than completing a t-test comparison for each possible comparison of the means (calculations in *Supplementary Materials*).

Results and Discussion

Batch desorption/sorption experiments at variable ligand concentrations

Results from batch desorption experiments, 47.9±0.4 $g_{sediment}$/L and pH of 6.4±0.4 over 7 and 28 days, are shown in Figure 4.1 below. Three desorption periods of 7 days each were performed as described above followed by a 28 day period. In each case the aqueous phase was removed and replaced with a Pu-free solution of similar chemical composition. The Kd values for each of the three 7 day desorption periods were similar indicating that the fraction of Pu desorbing for a fixed period of time does not change (Figure C1 in *Supplementary Materials C*). Thus, the desorption experiments are likely sampling a similar "pool" of Pu rather than removing a labile weakly bound fraction initially. Given the similarity in values, the data in Figure 4.1 for 7 days represents the average and standard deviation of the triplicate measurements. However, the 28 day data represents only a single measurement.

There is a large amount of variation within the K_ds calculated in Figure 4.1. However it is notable that the ligands or salts did not significantly increase desorption of

$^{239/240}$Pu from the SRS soil. In addition, the ligand and ionic strength concentrations cover a range of approximately three orders of magnitude without leading to a significant change in desorption capabilities. This does not agree with some previous studies indicating that hydrogen peroxide and natural organic matter can either reduce sorption or enhance desorption of Pu from pure minerals.[14, 26-29, 37-40] However, in these previous studies, a dependence on the organic matter concentration (and essentially the ratio of sorbent to organic matter) was found to influence sorption and on the order of 50 mg_C/L of organic matter was needed to maintain a significant soluble Pu concentration in experiments with only 0.01 to 1 g/L of suspended solids. In addition, hydrogen peroxide mobilization was found to be only a transient effect at near neutral pH.[14] In this work the known high affinity of Pu for soil surfaces and the higher suspended solids ratio could be outcompeting ligand complexation and minimizing the effect of the ligands. For the 7 and 28 day desorption periods the average sorbed fraction is 99.6 and 99.7% of the initial $^{239/240}$Pu, respectively (Table 4.1). The average K_ds and fraction sorbed for the 7 and 28 day desorption period are not statistically different at 95% confidence as compared by Tukey's method (Table C.2 in *Supplementary Materials C*). Thus, it appears that no further reaction occurred between 7 and 28 days. Based on Dunnett's method for comparison to a control, the 7 day, triplicate measurements were compared to the blank for each ligand and salt concentration. Average K_ds for each treatment were not significantly different at a 95% confidence interval with respect to the blank for each of the ligand and salt concentrations (comparison for the highest ligand and salt concentration in Table C.13 in *Supplementary Materials C*). This comparison could not

be made for the 28 day desorption data because multiple measurements were not collected at each concentration.

Because no statistically significant difference between 7 and 28 day $^{239/240}$Pu desorption was observed, further experiments were developed to 1) examine shorter and longer time periods of sorption and desorption and 2) examine the lability of Pu in selective extractions. Dual isotope sorption/desorption experiments for three and 168 days at a sediment concentration of 70±1.4 $g_{sediment}$/L and pH~6.4 at a ligand concentration of 25 mg_C/L or ionic strength of 0.01 M (based on the ligand or salt) are shown in Figures 4.2-4.4 below. Figure 4.2 compares desorption K_ds measured for $^{239/240}$Pu for all four desorption time periods (3, 7, 28 and 168 days). Across the suite of ligands and salts, desorption is not significantly increased for any of the ligands and salts investigated over 168 days. However, K_ds do fluctuate between sampling periods. The K_ds measured for desorption ($^{239/240}$Pu) versus sorption (^{242}Pu) are nearly an order of magnitude different when compared for each time period, Log[K_d] of 4.2 versus 3.4, respectively, for 168 day experiments (Table 4.2). A t-test by Tukey's method confirms that desorption values are statistically different with respect to isotopes (Table C.2 *Supplementary Materials C*). However, this represents an approximate sorption of 99.9% versus 99% of the Pu and more than half of the ^{242}Pu measurements are within three times the detection limits for the ICP-MS (as shown by the maximum K_ds calculated based on minimum detectable concentrations for both isotopes in Figures 4.3 and 4.4). Therefore, these values are most likely not different. However, statistical difference cannot be determined for these experiments as the maximum detection limits were

reached for ^{242}Pu. Previous batch sorption experiments at similar pH values measured after 33 days for Pu(IV) and Pu(V) on these sediments by the Savannah River Site estimated Log[K_d] values of 3.95-4.26.[41] These values without the presence of a ligand are within the range of the values determined in this work with and without the presence of ligands. To compare the statistical difference of the ligands, a matrix was designed to compare average K_ds with each ligand using Tukey's matrix (Table C.3-C.10 in *Supplementary Materials C*) and to compare average K_ds for each ligand with the blank (DDI) using Dunnett's method (Table C.12 and C.14 in *Supplementary Materials C*). At three days, values were not statistically different from the blank with the exception of the 0.01 M NaF treatment. K_d values determined for each ligand were also not statistically different from each of the other ligands at 3 days (Table C.3-C.6 in *Supplementary Materials C*). At 168 days, values for $^{239/240}$Pu desorption for each of the ligands as compared to each of the other ligands were not statistically different (Table C.7-C.10 in *Supplementary Materials C*). For the $^{239/240}$Pu comparison to the blank at 168 days, only the K_d for 1% H_2O_2 was significantly different from the blank (Table C.14 in *Supplementary Materials C*). However, the 0.01 M NaF treatment for the ^{242}Pu isotope at 168 days was statistically different from the blank (comparison by Dunnett's method) and from all other ligand treatments (comparison by Tukey's method) (*Supplementary Materials C*, Table C.9, C.10 and C.14).

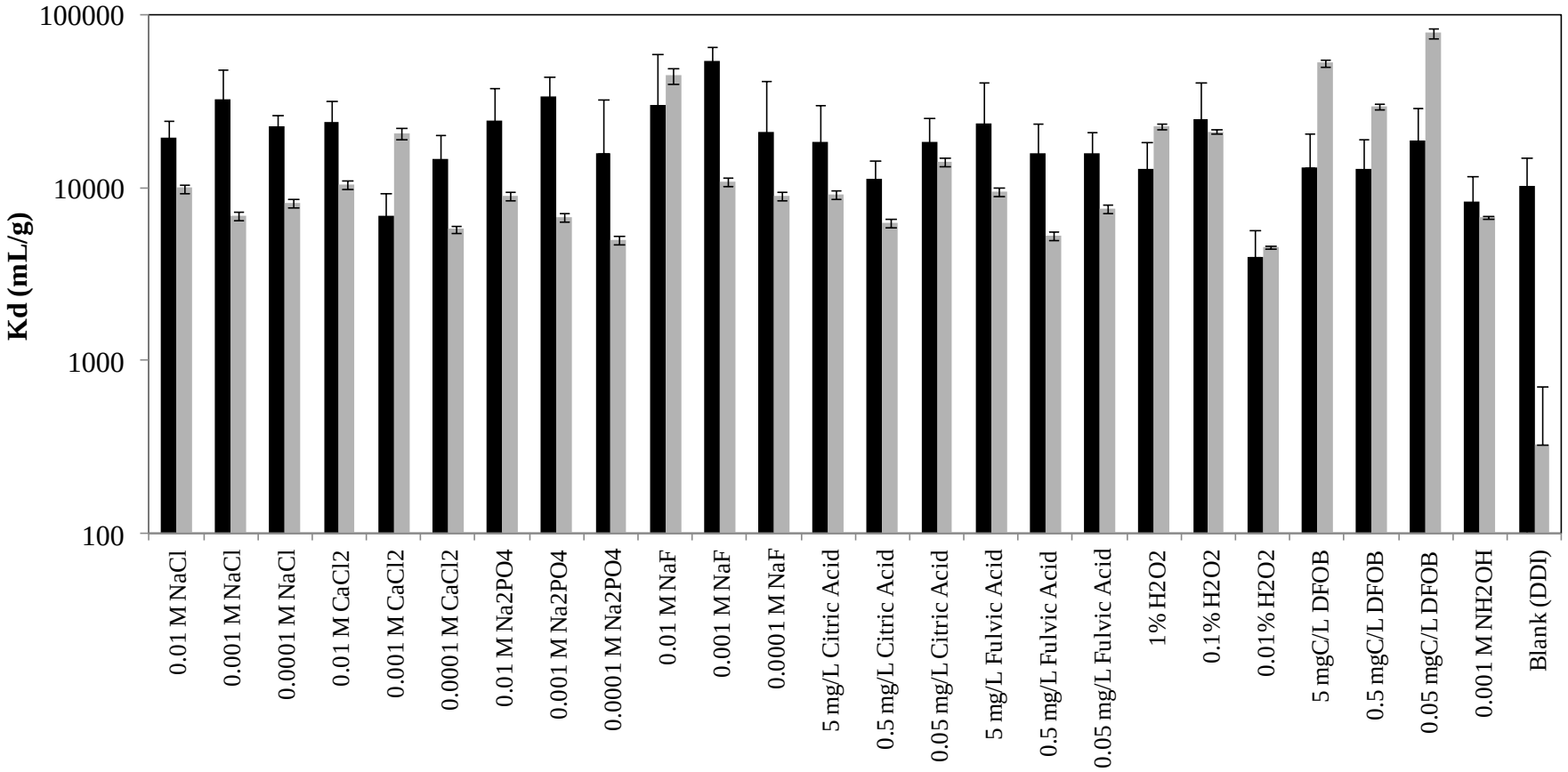

Figure 4.1: Batch desorption of ~2µg/g $^{239/240}$Pu from 50 $g_{sediment}$/L suspensions in the presence of variable ligand and ionic strength concentrations after 7 (*black*) and 28 (*gray*) days

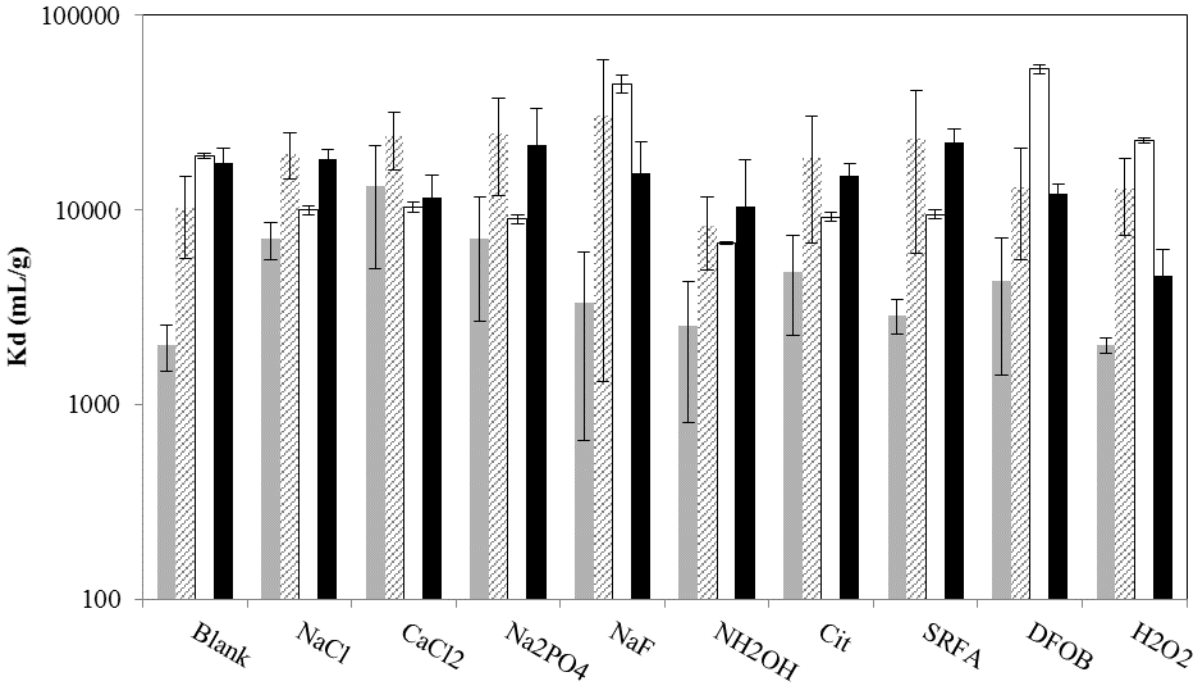

Figure 4.2: Average desorption K_ds (mL/g) for $^{239/240}$Pu for 3 (*gray*), 7 (*striped*), 28 (*white*) and 168 (*black*) day desorption experiments, average desorption K_d in the presence of 10 mM ionic strength (NaCl, $CaCl_2$, Na_2PO_4, or NaF), or 1% (300 mM) H_2O_2, or 5 mg_C/L (citrate, SRFA, or DFOB), or 1 mM NH_2OH*HCl

Table 4.1: Average K_ds (mL/g) and fraction sorbed for batch sorption (^{242}Pu) and desorption ($^{239/240}$Pu) experiments, average and standard deviation of K_ds measured in the presence of all ligands and ionic strengths investigated

Parameter	**3 days**		**7 days**	**28 days**	**168 days**	
	$^{239/240}$Pu	^{242}Pu	$^{239/240}$Pu	$^{239/240}$Pu	$^{239/240}$Pu	^{242}Pu
Log[K_d (mL/g)]	3.69±0.25	3.22±0.38	4.16±0.34	4.24±0.35	4.17±0.24	3.41±0.29
Fraction Sorbed (%)	99.6±0.3	98.6±1.6	99.4±0.6	99.7±0.3	99.6±0.2	98.7±1.6

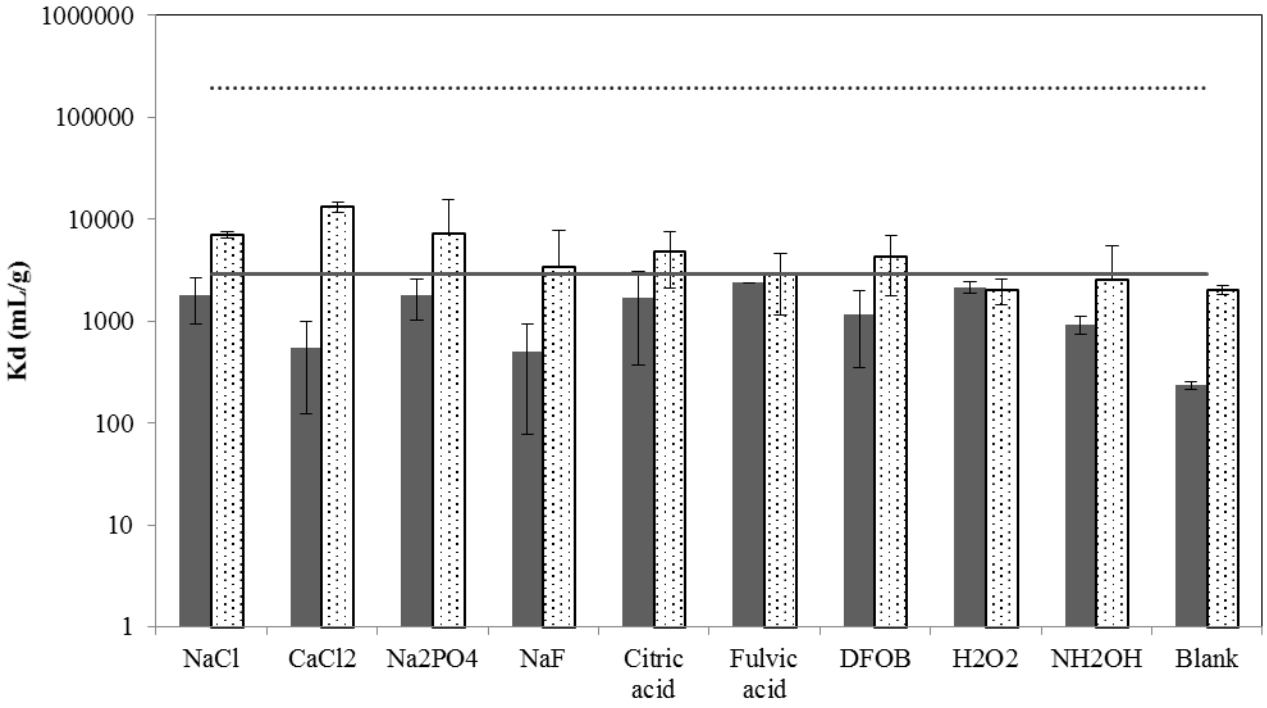

Figure 4.3: Results of dual isotope sorption (^{242}Pu, *gray*) and desorption ($^{239/240}$Pu, *black dotted*) over three days in the presence of 70 $g_{sediment}$/L, average K_d in the presence of 10 mM ionic strength (NaCl, $CaCl_2$, Na_2PO_4, or NaF), or 1% (300 mM) H_2O_2, or 5 mg_C/L (citrate, SRFA, or DFOB), or 1 mM NH_2OH*HCl, detection limits are shown by the lines for ^{242}Pu (*gray solid*) and $^{239/240}$Pu (*black dotted*)

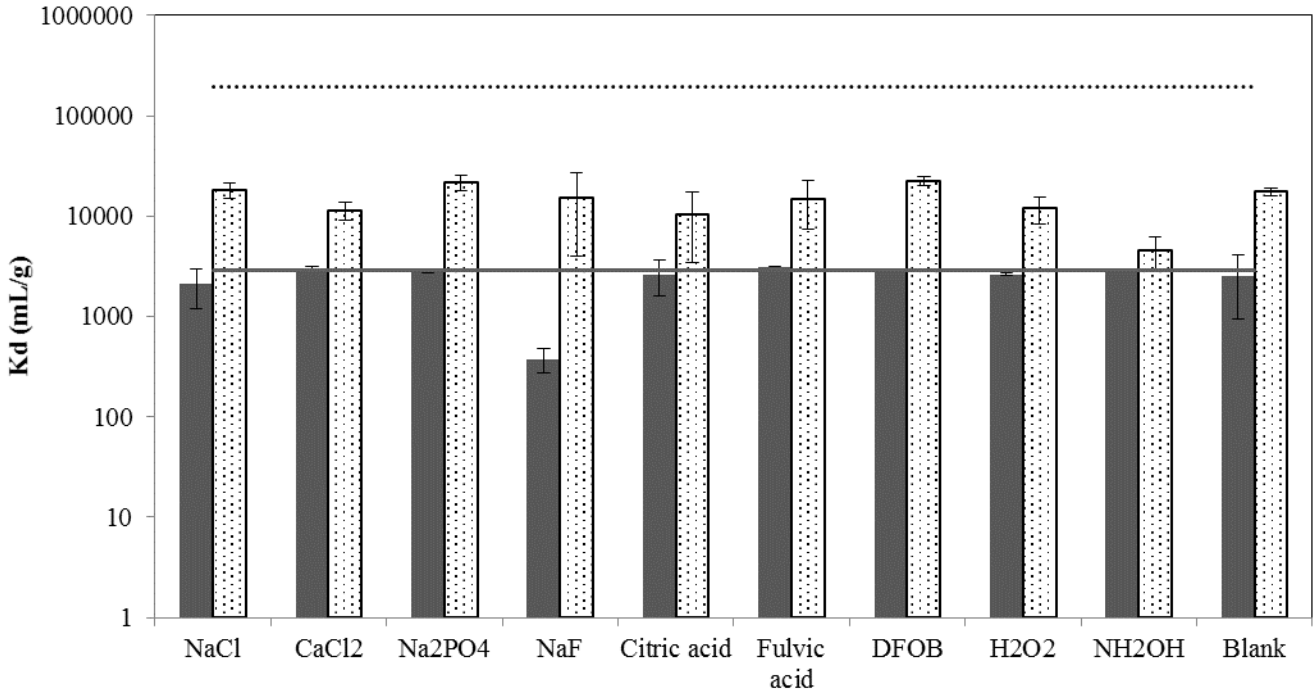

Figure 4.4: Results of dual isotope sorption (242Pu, gray solid) and desorption (239/240Pu, black dotted) over 168 days in the presence of 70 gsediment/L, average Kd in the presence of 10 mM ionic strength (NaCl, CaCl2, Na2PO4, or NaF), or 1% (300 mM) H2O2, or 5 mgC/L (citrate, SRFA, or DFOB), or 1 mM NH2OH*HCl, detection limits are shown by the lines for 242Pu (gray solid) and 239/240Pu (black dotted)

Selective extraction for total and amorphous iron

Selective extraction to remove the amorphous and total iron fractions of the soil were performed to examine the lability of Pu associated with these operationally defined phases. There were no observable effects of the different ligands and salts (Figures 4.5 and 4.6). However, there were significant differences in the two isotopes of Pu, representing aging of three days (^{242}Pu) versus 32 years ($^{239/240}$Pu). The average ^{242}Pu and $^{239/240}$Pu removed by the total free iron extraction was 91±16% and 63±5%,

respectively, and the average removed by the amorphous iron extraction was 81±8% and 42±4%, respectively. These different aging times exhibited statistically different extraction amounts as estimated by a t-test at a 95% confidence level (*Supplementary Materials C* Table C11). Since the amorphous and total iron extractions were performed on separate samples, the amount of Pu within an operationally defined 'crystalline' iron phase must be determined by the difference between the total and amorphous extractions. The average ^{242}Pu and $^{239/240}$Pu associated with the crystalline iron fraction was 11±19% and 21±14%, respectively. However, because the amorphous iron and total free iron extractions removed the majority of the ^{242}Pu in both samples, several represented a negative fraction as crystalline iron. While it is likely that the ^{242}Pu and $^{239/240}$Pu are being influenced by the specific conditions of the iron extraction solutions (i.e. reaction with oxalate or dithionite/bicarbonate) in addition to the dissolution of those targeted phases, these experiments show that the 3-day exposure (^{242}Pu) is removed much more easily than the 32-year exposure ($^{239/240}$Pu). However, if the $^{239/240}$Pu removal is representative of Pu associated with iron, it shows that the majority of the Pu is associated with iron fractions within the sediment. Previous laboratory work has shown that Pu sorbs very strongly to iron oxides.[16, 42-44] Microscopy is in progress to determine if the Pu in these sediments is strongly associated with the iron fraction as suggested by the selective extractions (described in the *Supplementary Materials*). Overall this data demonstrates that there is a difference in the lability of adsorbed Pu with time which could be explained by changes in the surface speciation of Pu. This could be explained by irreversible sorption as described above with a two-site

model. This model could represent changes in the contaminant (i.e. dehydration of the surface species or incorporation into the solid) or the surface (i.e. relaxation of the surface).

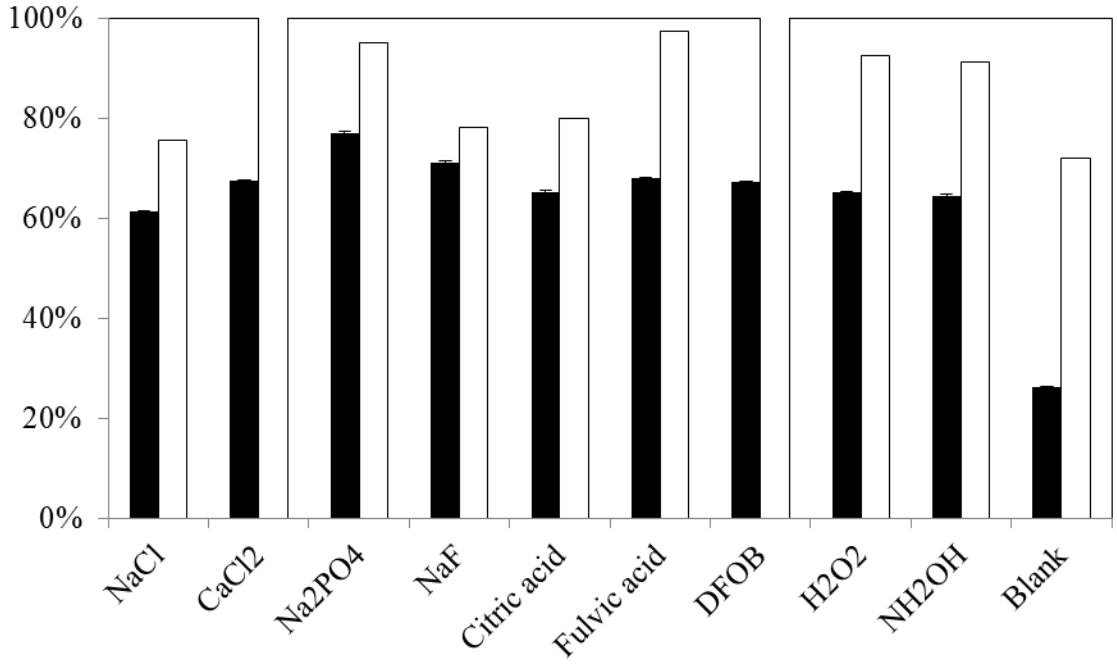

Figure 4.5: ^{242}Pu (*white*) and $^{239/240}$Pu (*black*) recovery from total free iron selective extraction as measured by the citrate bicarbonate dithionite method on 70 $g_{sediment}$/L suspensions following a 3 day sorption/desorption experiment in the presence of 10 mM ionic strength (NaCl, $CaCl_2$, Na_2PO_4, or NaF), or 1% (300 mM) H_2O_2, or 5 mg_C/L (citrate, SRFA, or DFOB), or 1 mM NH_2OH*HCl

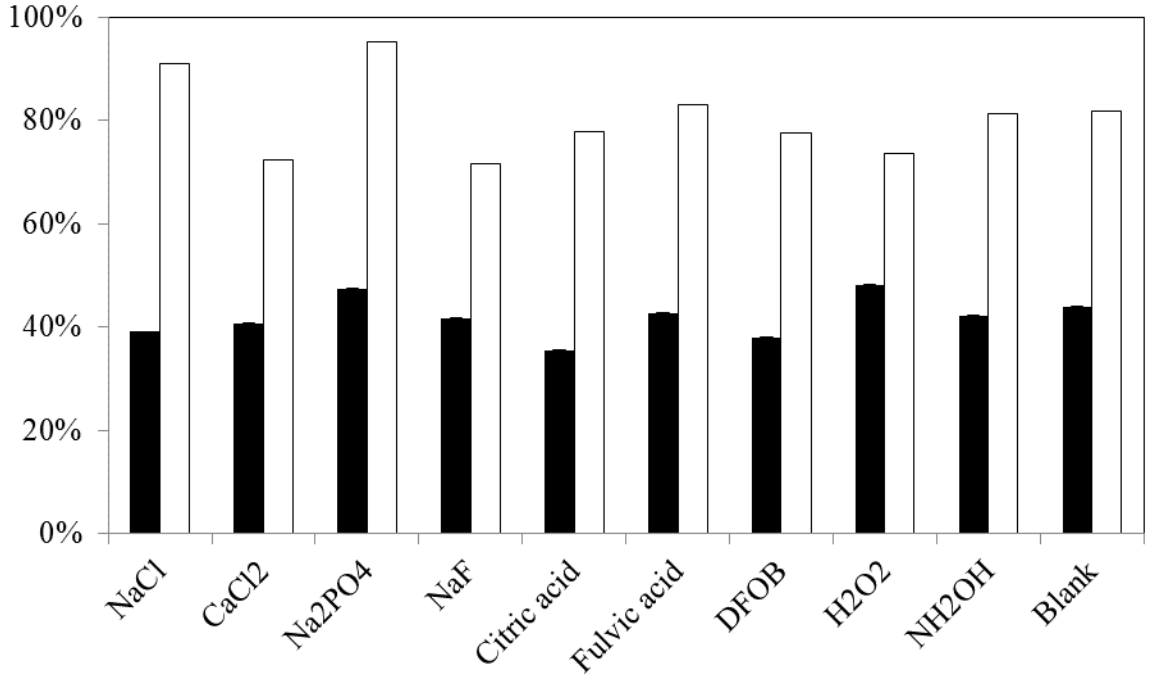

Figure 4.6: ^{242}Pu (*white*) and $^{239/240}$Pu (*black*) recovery from amorphous iron selective extraction as measured by the ammonium oxalate in the dark method on 70 $g_{sediment}$/L suspensions following a 3 day sorption/desorption experiment in the presence of 10 mM ionic strength (NaCl, $CaCl_2$, Na_2PO_4, or NaF), or 1% (300 mM) H_2O_2, or 5 mg_C/L (citrate, SRFA, or DFOB), or 1 mM NH_2OH*HCl

Conclusions

These experiments demonstrate the irreversibility of sorption of Pu to natural sediments. Within three days the majority of Pu is irreversibly adsorbed to natural sediments. This is consistent with previous work reporting extremely small fractions of Pu desorption from inorganic minerals over long periods.[9-16] In addition, this is consistent with previous work by Powell *et al.* which demonstrated that nearly 80% of Pu was unleachable from magnetite on the order of days.[16] When compared to previous batch sorption experiments

completed by the Savannah River Site without ligands for different time periods on the same sediments, similar K_d values are estimated.[41] This data provides further confirmation that the ligands did not play a significant role in desorbing Pu from sediments in these systems. While the K_ds (and adsorbed fraction) are not significantly changing within the aging and sorption/desorption time on the scale of these batch sorption experiments, there is a statistically significant difference between the aging times (3 days for ^{242}Pu versus 32 years for $^{239/240}$Pu) for selective extraction experiments. There is significantly more Pu removed after three days of aging versus 32 years for the selective extractions. Because the chemical conditions of the selective extractions are mobilizing different fractions of Pu for the different isotopes, surface species may be changing with time. This is consistent with a change in the lability of adsorbed Pu over time. These changes can be explained by the two-site sorption model. A detailed examination of changes in surface species with time using spectroscopic methods would be useful to confirm that Pu lability is changing with time.

Acknowledgements

This work was supported by the Subsurface Biogeochemical Research Program of the U.S. Department of Energy's Office of Biological and Environmental Research under project number DE-SC0004883. Thanks to Daniel Kaplan at the Savannah River Site for his aide in the formulation of experimental protocols. In addition, H. Emerson would like to thank the Nuclear Regulatory Commission for an educational fellowship.

References

1. Bowen, S. M.; Finnegan, D. L.; Thompson, J. L.; Miller, C. M.; Baca, P. L.; Olivas, L. F.; Geoffrion, C. G.; Smith, D. K.; Goishi, W.; Esser, B. K.; Meadows, J. W.; Namboodiri, N.; Wild, J. F. *Nevada Test Site Radionuclide Investory, 1951-1992*; Los Alamos National Laboratory: Los Alamos, NM, 2001.

2. Carlton, W. H.; Evans, A. G.; Murphy, C. E.; Pinder, J. E.; Strom, R. N. *Assessment of plutonium in the Savannah River site environment (U)*; Aiken, SC, 1992.

3. Nyhan, J. W.; Drennon, B. J.; Abeele, W. V.; Wheeler, M. L.; Purtymun, W. D.; Trujillo, B.; Herrera, W. J.; Booth, J. W., Distribution of Plutonium and Americium Beneath a 33-yr-old Liquid Waste Disposal Site. *Journal of Environment Quality* **1985,** *14*, (4), 501-509.

4. Cantrell, K. J. *Transuranic contamination in sediment and groundwater at the U.S. DOE Hanford site*; Pacific Northwest National Laboratory: Richland, WA, 2009.

5. Runde, W.; Neu, M. P., *The Chemistry of the Actinides and Transactinides, 4th ed*. Springer: Dordrecht, The Netherlands, 2010; Vol. 6.

6. Kersting, A. B., Plutonium Transport in the Environment. *Inorganic Chemistry* **2013,** *52*, (7), 3533-3546.

7. Albright, D.; Kramer, K., *Bull Atom Sci* **2004,** *14*.

8. Ewing, R. C.; Runde, W.; Albrecht-Schmitt, T. E., *MRS Bulletin* **2010,** *35*, 859.

9. Kaplan, D. I.; Powell, B. A.; Demirkanli, D. I.; Fjeld, R. A.; Molz, F. J.; Serkiz, S. M.; Coates, J. T., Influence of Oxidation States on Plutonium Mobility during Long-Term Transport through an Unsaturated Subsurface Environment. *Environ Sci Technol* **2004,** *38*, (19), 5053-5058.

10. Missana, T.; García-Gutiérrez, M.; Alonso, Ú., Kinetics and irreversibility of cesium and uranium sorption onto bentonite colloids in a deep granitic environment. *Applied Clay Science* **2004,** *26*, (1-4), 137-150.

11. Tinnacher, R. M.; Zavarin, M.; Powell, B. A.; Kersting, A. B., Kinetics of neptunium(V) sorption and desorption on goethite: An experimental and modeling study. *Geochimica et Cosmochimica Acta* **2011,** *75*, (21), 6584-6599.

12. Lu, N.; Cotter, C. R.; Kitten, H. D.; Bentley, J.; Triay, I. R., Reversibility of Sorption of Plutonium-239 onto Hematite and Goethite Colloids. *Radiochimica Acta* **1998,** *83*, 167-173.

13. Turner, N. B.; Ryan, J. N.; Saiers, J. E., Effect of desorption kinetics on colloid-facilitated transport of contaminants: Cesium, strontium, and illite colloids. *Water Resources Research* **2006,** *42*, 1-17.

14. Begg, J. D.; Zavarin, M.; Kersting, A. B., Plutonium Desorption from Mineral Surfaces at Environmental Concentrations of Hydrogen Peroxide. *Environmental Science & Technology* **2014,** *48*, (11), 6201-6210.

15. Shang, J.; Liu, C.; Wang, Z.; Zachara, J. M., Long-term kinetics of uranyl desorption from sediments under advective conditions. *Water Resources Research* **2014,** *50*, 855-870.

16. Powell, B. A.; Fjeld, R. A.; Kaplan, D. I.; Coates, J. T.; Serkiz, S. M., Pu(V)O2+ adsorption and reduction by synthetic magnetite (Fe3O4). *Environmental Science and Technology* **2004,** *38*, (22), 6016-6024.

17. Lu, N.; Reimus, P. W.; Parker, G. R.; Conca, J. L.; Triay, I. R., Sorption kinetics and impact of temperature, ionic strength and colloid concentration on the adsorption of plutonium-239 by inorganic colloids. *Radiochimica Acta* **2003,** *91*, 713-720.

18. Wang, X. K.; Chen, C. L.; Du, J. Z.; Tan, X. L.; Xu, D.; Yu, S. M., Effect of pH and aging time on the kinetic dissociation of Am-243(III) from humic acid-coated gamma-Al2O3: A chelating resin exchange study. *Environmental Science & Technology* **2005,** *39*, (18), 7084-7088.

19. Moulin, V.; Ouzounian, G., Role of colloids and humic substances in the transport of radio-elements through the geosphere. *Applied Geochemistry* **1992,** *1*, 179-186.

20. McCarthy, J. F.; Czerwinski, K. R.; Sanford, W. E.; Jardine, P. M.; Marsh, D. J., Mobilization of transuranic radionuclides from disposal trenches by natural organic matter. *J Contaminant Hydrology* **1998,** *30*, 49-77.

21. McCarthy, J. F.; Sanford, W. E.; Stafford, P. L., Lanthanide Field Tracers Demonstrate Enhanced Transport of Transuranic Radionuclides by Natural Organic Matter. *Environmental science & technology* **1998,** *32*, (24), 3901-3906.

22. McCarthy, J. F.; Zachara, J. M., Subsurface transport of contaminants. *Environmental science & technology* **1989,** *23*, (5), 496-502.

23. Artinger, R.; Buckau, G.; Zeh, P.; Geraedts, K.; Vancluyse, J.; Maes, A.; Kim, J. I., Humic colloid mediated transport of tetravalent actinides and technetium. *Radiochimica Acta* **2003,** *91*, 743-750.

24. Silva, R. J.; Nitsche, H., Actinide Environmental Chemistry. *Radiochimica Acta* **1995,** *70/71*, 377-396.

25. Geckeis, H.; Lutzenkirchen, J.; Polly, R.; Rabung, T.; Schmidt, M., Mineral-water interface reactions of actinides. *Chem Rev* **2013,** *113*, (2), 1016-62.

26. Banik, N. L.; Buda, R. A.; Burger, S.; Kratz, J. V.; Trautmann, N., Sorption of tetravalent plutonium and humic substances onto kaolinite. *Radiochimica Acta* **2007,** *95*, (10), 569-575.

27. Roberts, K. A.; Santschi, P. H.; Leppard, G. G.; West, M. M., Characterization of organic-rich colloids from surface and ground waters at the actinide-contaminated Rocky Flats Environmental Technology Site (RFETS), Colorado, USA. *Colloids and Surfaces A: Physicochemical and Engineering Aspects* **2004,** *244*, (1-3), 105-111.

28. Santschi, P. H.; Roberts, K. A.; Guo, L. D., Organic mature of colloidal actinides transported in surface water environments. *Environmental Science & Technology* **2002,** *36*, (17), 3711-3719.

29. Zimmerman, T.; Zavarin, M.; Powell, B. A., Influence of humic acid on plutonium sorption to gibbsite: Determination of Pu-humic acid complexation constants and ternary sorption studies. *Radiochimica Acta* **2014,** *102*, (7), 629-643.

30. Kaplan, D. I.; Demirkanli, D. I.; Gumapas, L.; Powell, B. A.; Fjeld, R. A.; Molz, F. J.; Serkiz, S. M., Eleven-Year Field Study of Pu Migration of Pu III, IV, and VI Sources. *Environ Sci Technol* **2006,** *40*, (2), 443-448.

31. Kaplan, D. I.; Powell, B. A.; Duff, M. C.; Demirkanli, D. I.; Denham, M. E.; Fjeld, R. A.; Molz, F., Influence of Sources on Plutonium Mobility and Oxidation State Transformations in Vadose Zone Sediments. *Environmental Science and Technology* **2007,** *41*, (21), 7417-7423.

32. Erickson, M. D., HASL 300, The Procedures Manual of the Environmental Measurements Laboratory, 28th ed. In *Pu-11-RC Plutonium Purification - Ion Exchange Technique*, Chieco, N. A., Ed. U.S. Department of Homeland Security: New York, 1997; Vol. 4.

33. Hixon, A. E.; Hu, Y. J.; Kaplan, D. I.; Kukkadapu, R. K.; Nitsche, H.; Qafoku, O.; Powell, B. A., Influence of iron redox transformations on plutonium sorption to sediments. *Radiochimica Acta* **2010,** *98*, (9-11), 685-682.

34. Sparks, D. L.; Page, A. L.; Helmke, P. A.; Loeppert, R. H.; Soltanpour, P. N.; Tabatabai, M. A.; Johnston, C. T.; Sumner, M. E., In *Methods of Soil Analysis, Part 3: Chemical Methods*, Soil Society of America: Madison, WI, 1996.

35. Berthouex, P. M.; Brown, L. C., Assessing the Average of Differences. In *Statistics for Environmental Engineers*, CRC Press: Boca Raton, Florida, 1994; pp 111-114.

36. Berthouex, P. M.; Brown, L. C., Multiple Paired Comparisons of k Averages. In *Statistics for Environmental Engineers*, CRC Press: Boca Raton, Florida, 1994; pp 123-128.

37. Buda, R. A.; Banik, N. L.; Kratz, J. V.; Trautmann, N., Studies of the ternary systems humic substances - kaolinite - Pu(III) and Pu(IV). *Radiochimica Acta* **2008,** *96*, (9-11), 657-665.

38. Xu, C.; Santschi, P. H.; Zhong, J. Y.; Hatcher, P. G.; Francis, A. J.; Dodge, C. J.; Roberts, K. A.; Hung, C. C.; Honeyman, B. D., Colloidal Cutin-Like Substances Cross-Linked to Siderophore Decomposition Products Mobilizing Plutonium from Contaminated Soils. *Environmental Science & Technology* **2008,** *42*, (22), 8211-8217.

39. Roberts, K. A.; Santschi, P. H.; Honeyman, B. D., Pu(V) reduction and enhancement of particle-water partitioning by exopolymeric substances. *Radiochimica Acta* **2008,** *96*, (9-11), 739-745.

40. Zhao, P. H.; Zavarin, M.; Leif, R. N.; Powell, B. A.; Singleton, M. J.; Lindvall, R. E.; Kersting, A. B., Mobilization of actinides by dissolved organic compounds at the Nevada Test Site. *Applied Geochemistry* **2011,** *26*, (3), 308-318.

41. Powell, B. A.; Fjeld, R. A.; Coates, J. T.; Kaplan, D. I.; Serkiz, S. M. *Plutonium Oxidation State Geochemistry in the SRS Subsurface Environment (U)*; WSRC-TR-2003-00035; Westinghouse Savannah River Company

1. Clemson University: Aiken, SC, 2003.

42. Hixon, A. E.; Powell, B. A., Observed changes in the mechanism and rates of Pu(V) reduction on hematite as a function of total plutonium concentration. *Environmental Science and Technology* **2014,** *submitted*.

43. Powell, B. A.; Fjeld, R. A.; Kaplan, D. I.; Coates, J. T.; Serkiz, S. M., Pu(V)O2+ adsorption and reduction by synthetic hematite and goethite. *Environmental Science and Technology* **2005,** *39*, (7), 2107-2114.

44. Romanchuk, A. Y.; Kalmykov, S. N.; Aliev, R. A., Plutonium sorption onto hematite colloids at femto- and nanomolar concentrations. *Radiochimica Acta* **2011,** *99*, (3), 137-144.

CHAPTER FIVE

PAPER FOUR: COLLOID-FACILITATED TRANSPORT OF TETRAVALENT ACTINIDES ON HEMATITE COLLOIDS IN THE PRESENCE OF SUWANEE RIVER FULVIC ACID

Status

To be submitted to *Geochimica et Cosmochimica Acta*

Authors

Hilary P. Emerson, Katherine A. Hickok, and Brian A. Powell

Introduction

Colloid-facilitated transport has been implicated in recent field studies for actinide elements and data suggest colloid-facilitated transport is primarily occurring in association with natural or pseudo-colloids (Kaplan et al., 1994; Kersting, 2012, 2013; Kersting et al., 1999; McCarthy and Zachara, 1989; Novikov et al., 2006; Penrose et al., 1990; Santschi et al., 2002; Short et al., 1988). Kersting *et al*. reported plutonium (Pu) migration in association with colloids of greater than 1.3 km at the Nevada National Security Site (Kersting et al., 1999). Los Alamos National laboratory and the Mayak nuclear facility in Russia have identified colloidal transport of Pu over 3 km (Novikov et al., 2006; Penrose et al., 1990). Work has implicated iron oxide colloids correlated with thorium (Th) (Short et al., 1988) and plutonium and uranium (Novikov et al., 2006) in previous field measurements. Plutonium has also been measured in the field in association with inorganic clay and zeolite colloids (Kersting, 2012, 2013; Kersting et al., 1999) or organic colloids (Kersting, 2013; Santschi et al., 2002). Studies of colloid

facilitated radionuclide transport are relevant at all field sites as previous research has reported that colloids are present at some concentration in all groundwater systems (Degueldre et al., 1996; McCarthy and Degueldre, 1993). While colloid-facilitated transport of contaminants in groundwater systems is not a new concept, the mechanisms of colloid-facilitated transport of actinides are still not well understood especially for ternary systems with presence of both inorganic colloids and humic substances (Kersting et al., 1999; McCarthy and Zachara, 1989; Ryan and Elimelech, 1996; Zanker and Hennig, 2014).

Tetravalent actinides are particularly susceptible to colloidal transport due to the strong sorption affinity to mineral surfaces and the ubiquitous nature of colloids in environmental systems (Geckeis et al., 2013). Further, deep groundwaters are expected to exhibit reducing conditions that would lead to the tetravalent oxidation state of the actinides being dominant (Degueldre et al., 1996; Kim and Grambow, 1999) and Pu(IV) is generally expected to be the dominant oxidation state of plutonium in natural systems (Choppin, 2007). Further the presence of humic substances has been shown to lead to reduction and stabilization of Pu in the aqueous phase in the +4 oxidation state (Andre and Choppin, 2000; Blinova et al., 2007; Choppin and Allard, 1985; Marquardt et al., 2004; Righetto et al., 1991; Shcherbina et al., 2007b). Blinova *et al.* reported that Pu(V) reduction is faster in the presence of fulvic acid as compared to humic acid, and Pu(IV) could form strong, mobile complexes with fulvic acid (Blinova et al., 2007).

Th(IV) is a common analog for the tetravalent actinides, especially Pu, even though it has no f electrons, has a larger ionic radii and has been shown to exhibit slightly weaker

complexation affinity than Pu(IV) (Choppin, 1999, 2007; Krauskopf, 1984; Neck and Kim, 2001; Schwantes and Santschi, 2010). However, Th(IV) is commonly used because it is a stable oxidation state for the investigation of tetravalent actinides whereas Pu, Np, and U can exist in multiple oxidation states in environmental systems (Choppin, 1999, 2007). Previous laboratory work with Th(IV) and Pu(IV) sorption to natural soils (Duff et al., 1999; Hixon et al., 2010; Kaplan et al., 2004; Kaplan et al., 2007; Melson et al., 2012; Powell et al., 2006), bulk minerals (Begg et al., 2013; Hixon et al., 2013; Keeney-Kennicutt and Morse, 1985; Lu et al., 2003; Powell et al., 2004, 2005; Zavarin et al., 2012), mineral colloids (Lu et al., 1998; Lu et al., 2003; Righetto et al., 1988; Romanchuk et al., 2011) and organic colloids (Artinger et al., 2003; Artinger et al., 2002; Blinova et al., 2007; Marquardt et al., 2004; Murphy et al., 1999; Reiller et al., 2008; Roberts et al., 2008; Santschi et al., 2002; Shcherbina et al., 2007b; Xu et al., 2008) have been conducted on simplified, binary systems. However, few studies have examined transport of actinides in ternary systems with both organic matter and inorganic colloids.

Batch sorption experiments for Th(IV) sorption to binary hematite-NP systems (Cromieres et al., 1998; Melson et al., 2012) have been studied previously and show that interactions are strong with a sorption edge near pH 3. Plutonium also exhibits strong sorption to iron oxide minerals (Hixon et al., 2010; Hixon and Powell, 2014; Keeney-Kennicutt and Morse, 1985; Lu et al., 1998; Lu et al., 2003; Powell et al., 2004, 2005; Romanchuk et al., 2011; Sanchez et al., 1985). Lu *et al*. reported <1% desorption from hematite colloids after 150 and 293 days leading to the conclusion that there is a strong irreversibly sorbed fraction of Pu (Lu et al., 1998; Lu et al., 2003). These studies

generally begin with an oxidized form of Pu due to the low solubility of Pu(IV) (Neck et al., 2007; Neck and Kim, 2001), but surface-mediated reduction to Pu(IV) has been observed on many minerals including the iron oxides (Duff et al., 1999; Hixon et al., 2013; Hixon et al., 2010; Hixon and Powell, 2014; Kaplan et al., 2004; Kaplan et al., 2007; Keeney-Kennicutt and Morse, 1985; Powell et al., 2006; Powell et al., 2004, 2005; Sanchez et al., 1985; Shaughnessy et al., 2003). Surface mediated reduction to Pu(IV) is consistent with the common observation of Pu(IV) as the dominant oxidation state in environmental systems when adsorbed to inorganic minerals (Begg et al., 2013; Hixon et al., 2013; Hixon et al., 2010; Hu et al., 2008; Kaplan et al., 2004; Kaplan et al., 2007; Keeney-Kennicutt and Morse, 1985; Powell et al., 2006; Powell et al., 2004, 2005; Powell et al., 2014; Romanchuk et al., 2011; Sanchez et al., 1985).

Several recent studies have examined tetravalent actinide transport in association with inorganic colloids. Xie *et al*. has completed colloid-facilitated transport experiments of Pu with natural colloids at variable colloid concentration (0-2000 mg/L), ionic strength (0.01-0.96 mol/L NaCl) and flow rate (0.472-4.56 mL/min) (Xie et al., 2013; Xie et al., 2014). The optimum colloid concentration for colloid facilitated transport of Pu was 375 mg/L with greater than 50% of Pu within the mobile fraction (Xie et al., 2013). As ionic strength increased, Pu transport decreased and the colloid zeta potential became more positive (Xie et al., 2014). Because colloid facilitated transport of plutonium increased with flow rate, the authors concluded that hydrodynamic shear forces play an important role in promoting transport (Xie et al., 2014).

Humic substances can have a significant impact on sorption and transport of contaminants on inorganic minerals (Baalousha, 2009; Baalousha et al., 2008; Davis and Leckie, 1978; Kretzschmar and Sticher, 1997; Murphy et al., 1999; Reiller et al., 2008; Reiller et al., 2002, 2003; Schrick et al., 2004). Previous work has also shown that actinides form strong complexes with humic substances (Choppin, 2007; Geckeis et al., 2002; Reiller et al., 2008; Reiller et al., 2003) and that their transport capability may be increased (Artinger et al., 2003; Silva and Nitsche, 1995). Specifically, Th(IV) and Pu(IV) have been shown to act similarly in the presence of humic substances (Artinger et al., 2003). However, complexation constants have been measured to be up to three orders of magnitude greater for plutonium (Zimmerman et al., 2014). Reiller *et al*. compares the similarity of An(IV)-humic complexation constants and notes that solubility of Th is increased 60 fold in the presence of humic acid at pH 6 (Reiller et al., 2008). Therefore, it is likely that humic acid (and other natural organic matter) could solubilize Pu and Th and reduce sorption to mineral surfaces. Both of these processes would enhance Pu and Th mobility. Humic substances may also coat inorganic colloids and increase the mobility of the colloids. If Pu and Th are associated with the colloid surface or the surface bound humic acid, then colloid facilitated transport of Th and Pu may be increase.

In addition to simple binary systems it is important to understand ternary systems with tetravalent actinides in the presence of both inorganic colloids and humic substances (Kersting, 2013; Zanker and Hennig, 2014). While several studies have investigated ternary complex formation with respect to mono-, di- and trivalent metals, the tetravalent actinides are still not well understood. Previous studies have considered actinide sorption

in ternary systems with and inorganic mineral and citrate (Tanaka et al., 2009), mineral and phosphate, and mineral and humic substances (Banik et al., 2007; Murphy et al., 1999; Reiller et al., 2002, 2003; Zimmerman et al., 2014) in batch experiments. In the presence of humic substances, actinide sorption to minerals is generally increased at low pH and decreased at high pH with respect to binary actinide-mineral systems (Banik et al., 2007; Murphy et al., 1999; Reiller et al., 2002, 2003; Righetto et al., 1991; Zimmerman et al., 2014). However, the body of knowledge for actinide-ternary systems has just begun to investigate transport in laboratory scale experiments.

This work examines the transport of strongly sorbing tetravalent actinides [Th(IV), Pu(IV)] in the presence of iron oxide colloids and Suwanee River fulvic acid through columns packed with quartz or natural soils. Few experiments have attempted to investigate these complex ternary systems and the authors chose this simplified system as a case study of conditions for optimum transport. The objective is to compare transport of tetravalent actinides in ternary systems (actinide + iron oxide colloid + fulvic acid) to transport of systems with combinations of components building up to the ternary system. Laboratory scale transport of actinides in the following systems will be studied: dissolved actinide ion, precipitated intrinsic actinide colloid, binary systems including iron oxide colloids or fulvic acid, and the ternary system.

Materials and Methods

Materials

Hematite nanoparticles (Fe_2O_3-NP) were synthesized with a low concentration ferric iron ($1.25x10^{-3}$ M) from $Fe(NO_4)_3$ at a temperature of 100°C to create a small,

homogenous size fraction (Wang et al., 2008). A fraction of the particles were labeled with ^{55}Fe by adding an aliquot of ^{55}Fe during synthesis. Characterization of the particles by HRTEM (Hitachi 9500), XRD, as well as particle size and zeta potential (Brookhaven 90Plus) is summarized in Table D1 and Figure D1-D2 in the *Supplementary Materials D*. The particle diameter was 13±7 nm at pH 3.0 based on TEM analysis of over 2300 particles and 50±10 nm based on particle size analysis of a suspension (Brookhaven 90Plus) with a surface area of 68 m^2/g as measured by the N_2(g)-BET method (at 77K, Micrometrics ASAP 2010 physisorption analyzer) (Brunhauer et al., 1938). The discrepancy between TEM imaging and 90Plus particle size is likely due to hydration of particles in suspension versus dried onto a TEM grid (Formvar, Ted Pelco). Polystyrene microspheres (Thermo Scientific) were purchased with a 100 nm diameter and blue fluorescent dye with excitation wavelengths at 365, 388 and 412 nm and emission wavelengths of 447 and 473 nm. The particle diameter and zeta potential of the solution as received was 90.6±1.0 nm and -50.7±4.0 mV, respectively. Suwanee River Fulvic Acid (SRFA) was obtained from the International Humic Substances Society (Standard I) and radiolabeled with ^{3}H to improve detection limits (minimum detection concentrations, MDC, are presented below for each set of experiments as dilutions and volumes measured are different for each). The methods for radiolabeling are based on methods described by Tinnacher and Honeyman with modifications for our laboratory apparatus (Tinnacher and Honeyman, 2007). High purity quartz was obtained from Unimin Corp with major elemental and soil sieve analysis presented in the Appendix (Iota Standard, Spruce Pine, NC, details in *Supplementary Materials D*, Table D2 and Figure D3). A

surface sandy soil was obtained from the Savannah River Site with characteristics previously reported (Powell et al., 2003; Powell et al., 2014). An additional soil sieve analysis is reported in *Supplementary Materials D*, Figure D4. ^{232}Th (High Purity Standards) and ^{230}Th (Environmental Monitoring Systems Laboratory, Las Vegas, NV) isotopes were used as received and a ^{239}Pu(IV) stock solution was prepared from solid $^{239}PuO_2$ obtained from Lawrence Berkeley National Laboratory. It was dissolved by repeatedly heating and evaporating in HNO_3 followed by heating and evaporating in HCl. An aliquot was then transferred to a 15 mL PFA vial and evaporated to dryness, the residue was then dissolved in 5 M HCl and evaporated to dryness three time. The final dried residue was dissolved in 0.5 M HCl with a few crystals of $NaNO_2$ to aide reduction. The final stock solution was 99.2% ^{239}Pu(IV) [25800 Bq/mL] as determined by solvent extraction as described previously (Hixon et al., 2010).

Batch experiments

Hematite-NP and SRFA Systems

Preliminary batch experiments examining the sorption of SRFA to hematite NPs and the particle size/zeta potential of bare and SRFA-associated hematite NPs as a function of pH were used to identify the optimum conditions for transport of hematite-NP suspensions. Particle size and zeta potential measurements (Brookhaven 90Plus) were taken at variable ionic strength (0.01 – 0.0001 M $NaClO_4$) and pH (3 – 9) for 0.03 g/L ($1.9x10^{-4}$ M) hematite-NP suspensions in the presence and absence of 25 mg_C/L SRFA. Additional experiments in 0.01 and 0.001 M NaCl yielded similar results (not shown). Further experiments utilized ^{3}H – SRFA to investigate sorption of 5 mg_C/L SRFA (6700

Bq/mL, ^{3}H) to 0.03 g/L hematite-NP at pH 4.1 – 5.9 over a three day period followed by desorption over a 28 day period (*Supplementary Materials D*, Figure D9). The fraction of SRFA sorbed to the hematite-NP was measured based on filtration through 10k MWCO filters (Pall Nanosep) which removed the hematite and any bound SRFA but allowed soluble SRFA to pass through the membrane. The SRFA concentration in the filtrate was measured via ^{3}H by liquid scintillation counting in Optiphase HiSafe III Cocktail (Perkin Elmer) with a minimum detectable concentration (MDC) of 5.6 Bq/mL or 0.02 mg_C/L (LSC, Hidex SL300). The detection limits are significantly higher for these experiments due to a greater dilution for measurements. Error bars are calculated based on counting statistics. Following the three day sorption period, hematite-NP were washed with pH adjusted ultrapure water and resuspended. Desorption samples were analyzed following filtration as described above at 20 minutes, 1 hour, 6 hours, 24 hours, 5 days, and 28 days.

Quartz – Hematite-NP – SRFA – Thorium Systems

Sorption experiments were conducted at 200 ug/L $^{232}Th(IV)$ in quadruplicate at 50 g/L (0.54 M) quartz, 45 mg hematite/L ($2.8x10^{-4}$ M), 25 mg_C/L SRFA and 0.001 M NaCl at pH 5.5 in 50 mL polypropylene tubes (VWR). Three sample sets were prepared in the presence of $^{232}Th(IV)$ including: 1) Quartz + SRFA, 2) Quartz + hematite-NP, and 3) Quartz + hematite-NP + SRFA. The aqueous phase was removed for analysis on days 1, 6 and 12 and subject to a centrifugation step for quartz or filtration step for hematite-NP as described previously. The centrifugation step included centrifugation at 8000 rpm for 20 min in a Beckman Coulter Allegra 22XR with an F2402 rotor. This is calculated to

remove particles <100 nm by Stokes law as described by Jackson (Jackson, 1985). The MDC using ICP-MS is 0.6 ppb ($2.6x10^{-9}$ M) ^{232}Th and 80 ppb ($1.4x10^{-6}$ M) ^{56}Fe under these sampling conditions. Sorption coefficients (K_d) are calculated based on equations presented in the *Supplementary Materials D*.

Column experiments

Hematite-NP – SRFA Systems

Laboratory-scale, saturated column (polycarbonate columns, 8.5 cm length x 1.5 cm ID; pore volume ~6.3 mL) experiments were conducted at a flow rate of 1 mL/min (~6.5 minute residence time) or 0.1 mL/min (~65 minute residence time) using a peristaltic pump (Masterflex, model 7720-60) and Tygon tubing (Masterflex, size 16) attached to columns packed with either high purity quartz or Savannah River Site surface sandy soil. Prior to input of approximately one pore volume spike solutions amended with hematite-NPs and/or SRFA each column was conditioned with at least 100 pore volumes of 0.001 M NaCl at pH 5.5. Following spike input the columns were flushed with at least 38 pore volumes of 0.001 M NaCl at pH 5.5. The effluent was collected into a fraction collector (Eldex) in 2 mL aliquots for the first 4-5 pore volumes followed by collection of 6 mL aliquots for the remainder of the experiments. Each spike solution contained a nonreactive tracer (rhenium at 5 ug/L or ^{3}H at 2500 Bq/mL). Eight column experiments were designed to investigate the transport of tetravalent actinides in the presence and absence of hematite-NP and SRFA (major characteristics of spike solutions in Table 5.1). Six column experiments were completed at pH 5.5 to examine ^{232}Th(IV) (at ~250 µg/L

unless otherwise noted) transport at a 1 mL/min flowrate (~6.5 minute retention time) in 0.001 M NaCl at pH 5.5:

1) 1 µg/L ^{232}Th(IV) through IOTA quartz column

2) 10 µg/L ^{232}Th(IV) through IOTA quartz column

3) ^{232}Th(IV) – hematite-NP through IOTA quartz column

4) ^{232}Th(IV) – SRFA through IOTA quartz column

5) ^{232}Th(IV) – hematite-NP – SRFA through IOTA quartz column

6) ^{232}Th(IV) – hematite-NP – SRFA through SRS sandy soil column

Due to the relatively high concentrations of stable ^{56}Fe iron in the SRS soil column, experiments were completed with NPs labeled with ^{55}Fe to improve detection limits. A total iron detection limits based on ^{55}Fe via LSC was 13 ppb compared with 80 ppb using ICPMS for determination of ^{56}Fe. Two additional columns were run at 0.1 mL/min (~65 minute retention time) to compare conditions at a lower flow rate as well as compare Th(IV) and Pu(IV) behavior:

7) ^{232}Th(IV) – hematite-NP – SRFA through IOTA quartz column

8) ^{239}Pu(IV) – hematite-NP – SRFA through IOTA quartz columnŷ

Transmission electron microscopy (Hitachi 9500 TEM and HD2000 STEM) was completed on the initial spike solutions by air-drying 10 µL of the spike solutions (Table 5.1) onto a Formvar coated or lacey carbon grids (Ted Pelco) with storage in a low humidity chamber prior to analysis.

Table 5.1: Initial spike chemical characteristics.

Spike ID[a]	Flow Rate, mL/min	Hematite, g/L [mol/L]	An(IV), ppb [mol/L]	An(IV) Isotope	SRFA, mg_C/L [^3H, Bq/mL]	Zeta Potential, mV	Diameter, nm	Dissolved Th, %
^{230Th}	0.94±0.17	0	0.72[c] [$3.1x10^{-9}$]	^{230}Th	0	NM	NM	85%
^{232}Th	0.98±0.07	0	10 [$4.3x10^{-8}$]	^{232}Th	0	NM	NM	15%
Hematite-Th	0.97±0.14	0.1 [$6.25x10^{-4}$]	289 [$1.3x10^{-6}$]	^{232}Th	0	70±4	152±1	<1%
SRFA-Th	0.94±0.02	0	274 [$1.2x10^{-6}$]	^{232}Th	25 [250]	NM	NM	NM
Hematite-SRFA-Th	1.02±0.01	0.04 [$2.5x10^{-4}$]	147 [$6.3x10^{-7}$]	^{232}Th	25 [32.6]	-42±3	190±4	24.8%
Hematite-SRFA-Th	1.01±0.02	0.1 [$6.25x10^{-4}$]	311 [$1.3x10^{-6}$]	^{232}Th	25 [64.6]	-58±3	98±6	16.1%
Hematite-SRFA-Pu	0.107±0.014	0.04 [$2.5x10^{-4}$]	56[d] [$2.3x10^{-7}$]	^{239}Pu	25 [65.6]	-43±3	172±6	10.3%
SRS Sandy - hematite-Th-SRFA	0.106±0.013	0.05[b] [$3.1x10^{-4}$]	238 [$1.0x10^{-6}$]	^{232}Th	25	-56±5	350±38	15.3%

[a]All columns except for the last column were run in columns packed with high purity quartz, the final column is packed with SRS sandy soil

[b]Concentration of ^{55}Fe of 2250 Bq/mL

[c]Concentration of ^{230}Th of 0.55 Bq/mL

[d]Concentration of ^{239}Pu of 128.4 Bq/mL

Effluent collection included analysis of ^{56}Fe and ^{232}Th via ICP-MS and ^{3}H, ^{55}Fe, ^{230}Th and ^{239}Pu using LSC as appropriate for the given experiment. In addition, samples with a sufficient concentration and remaining volume were analyzed for fraction dissolved by performing measurements on the filtrate passed through 10k MWCO filter, particle size and zeta potential (Brookhaven 90Plus). It is noteworthy that previous experiments showed that >90% of dissolved An(IV) passed through the 10k MWCO filters in the presence of 5 mg_C/L SRFA at pH 5, 7 and 9 (*Supplementary Materials D*, Table D3) (Simpkins, 2011). Effluent samples were analyzed for ^{56}Fe and ^{232}Th by ICP-MS (with an MDC of 3.8 and 0.01 ppb, respectively) and for ^{3}H, ^{230}Th, ^{239}Pu and ^{55}Fe (with an MDC of 0.02 Bq/mL for ^{239}Pu and ^{230}Th, alpha emitting radionuclides and 0.6 Bq/mL for ^{55}Fe and ^{3}H, beta emitting radionuclides). Following collection of the column effluent, columns were sectioned into 1 cm slices and leached in 8 M HNO_3 for two weeks to leach Fe and Pu from the solid phase and then measured on either ICP-MS or LSC as discussed above. Samples from the 8 M HNO_3 leach step were prepared for LSC in Ultima Gold AB (Perkin Elmer) cocktail for high acid and mineral content to reduce quench. In addition, error bars for elements analyzed by ICP-MS are based on triplicate measurements and by LSC are based on counting statistics. Retardation factors were calculated for effluent breakthrough of each component based on equations presented previously (Clark, 1996; Powell et al., 2014) and outlined in the *Supplementary Materials D.*

Polystyrene Microsphere Systems

Column experiments were carried out using the same setup described for the hematite-SRFA systems with a 1 mL/min flow rate. The experiments were run with columns packed with both high purity quartz and SRS sandy soil. The spike solutions were prepared with 0.81 g/L polystyrene microspheres and 0.001 M NaCl ionic strength at pH 5.5. Effluent breakthrough was quantified by fluorescence spectrometry (Fluoromax-4 Spectrofluorometer by Jobin Yvon Technology) with a detection limit of 0.008 g/L with respect to these experiments based on a calibration range of 0.001-0.5 g/L with an R^2 of 0.99 (*Supplementary Materials D* Figure D4). Following flushing with approximately 20 pore volumes of 0.001 M NaCl at pH 5.5, columns were sectioned in 1 cm slices. A leaching step was conducted in 0.001 M NaCl following preparation of samples for microscopy. The outlet (1 cm) was sliced with a low speed rock saw (Buehler) and embedded in EpoFix (Buehler) epoxy for analysis of the pore sizes on SEM 7600 (Hitachi). Additional fluorescence microscopy was completed with an optical microscope (Nikon AZ100) and processed with Nikon imaging software (NIS-elements).

Results

Batch Experiments

Preliminary work investigated the ability of SRFA to stabilize and adsorb to hematite-NP in suspension as well as the ability of hematite-NP and quartz to sorb ^{232}Th(IV) in the presence and absence of SRFA (*Supplementary Materials D* Figures D6-D8, Figure 5.1-2). The NP stability experiments presented in *Supplementary Materials D*, Figures D6-S8 show that minimal aggregation occurs with the SRFA at 25 mg_C/L

across the pH range (3-9) investigated. Furthermore, presence of SRFA causes the zeta potential of the hematite-NP – SRFA suspensions to flip to negative in the range of -25 – -35 mV without considerable variation with respect to ionic strength. Without the SRFA ligand, hematite-NPs' particle size increases with ionic strength and pH towards the point of zero charge near pH 7-8 (Kosmulski, 2002, 2011) and particles are no longer stable in suspension by pH 6.0. In addition, the hematite-NP zeta potential decreases with increasing pH across the range investigated. Near the point of zero charge of hematite the zeta potential of hematite-NP suspensions in the absence of SRFA reach zero and enter the negative range indicating the surface of the NPs transition from a net positive to a net negative charge. At the pH and ionic strength chosen for the column experiments presented below (5.5 and 0.001 M NaCl, respectively), the hematite-NPs in the absence of SRFA are expected to have a positive zeta potential and exhibit some aggregation. However, they were stable in suspension over the length of the experiments. The hematite-NPs in the presence of SRFA are expected to exhibit minimal aggregation and a negative zeta potential. These parameters were chosen for the column transport experiments presented below to exhibit ideal conditions for colloid-facilitated transport with conditions that could still be relevant to natural systems.

Batch sorption and desorption experiments investigating ^{3}H-SRFA sorption to 0.03 g/L hematite-NP (Figure 5.1) in the presence of 4.5 mg_C/L SRFA show that approximately 54% of the SRFA was sorbed to the hematite-NPs within three days and minimal desorption (< 15%) occurred over 28 days. Therefore, it is expected that the hematite-NPs will be coated with a monolayer SRFA as described by Seijo *et al*. using

Brownian dynamics simulations for low ionic strength systems (Seijo et al., 2009) and minimal desorption of SRFA will occur over the timescale of the column experiments presented below.

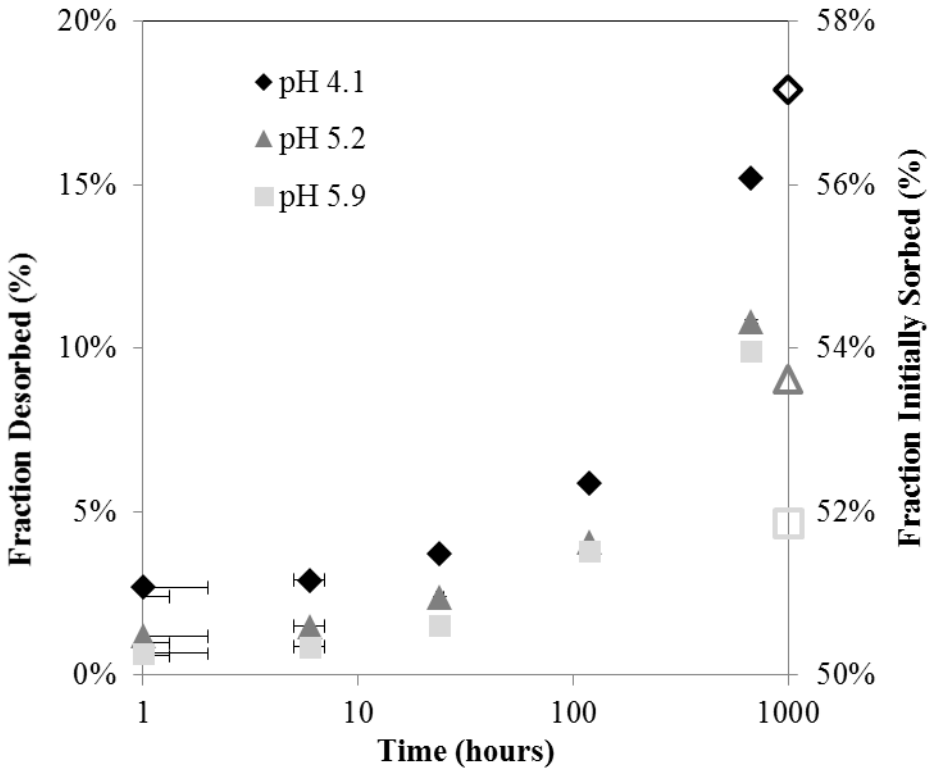

Figure 5.1: Batch sorption (3 days, *open symbols*) followed by desorption (*closed symbols*) of 4.5 mg_C/L ^{3}H-SRFA to 0.03 g/L hematite-NP at pH 4.1 (*diamonds*), 5.2 (*triangles*) and 5.9 (*squares*), error bars based on counting statistics are within the size of the symbols.

Batch sorption experiments for ^{232}Th(IV) sorption to quartz and hematite-NP at pH 5.5 in 0.001 M NaCl was reduced by at least one order of magnitude in the presence of 4.5 mg_C/L SRFA relative to SRFA-free systems (Figure 5.2). The greatest reduction

was observed with the hematite-NP as equilibrium K_ds differed by approximately two orders of magnitude at equilibrium. At equilibrium (12 days) the average K_d based on triplicate measurements for ^{232}Th(IV) sorption to hematite-NP and quartz without SRFA was 27200 and 620 L/kg, respectively. However, in the presence of SRFA, those K_d values dropped to 230 and 22 L/kg at equilibrium (12 days), respectively (K_d calculations in *Supplementary Materials D*). It must be noted that the SRFA may be capable of desorbing ^{232}Th(IV) from the hematite-NPs. Therefore, each spike solution prepared for the column experiments presented below was equilibrated for approximately three days prior to introduction to the columns for consistency with the dissolved fraction measured immediately prior to introduction to the columns presented in Table 5.1 above with 10-25% of ^{232}Th initially in the dissolved phase as determined by filtration through 10 MWCO filters as described above. It is assumed that any ^{232}Th in the dissolved fraction is associated with the SRFA.

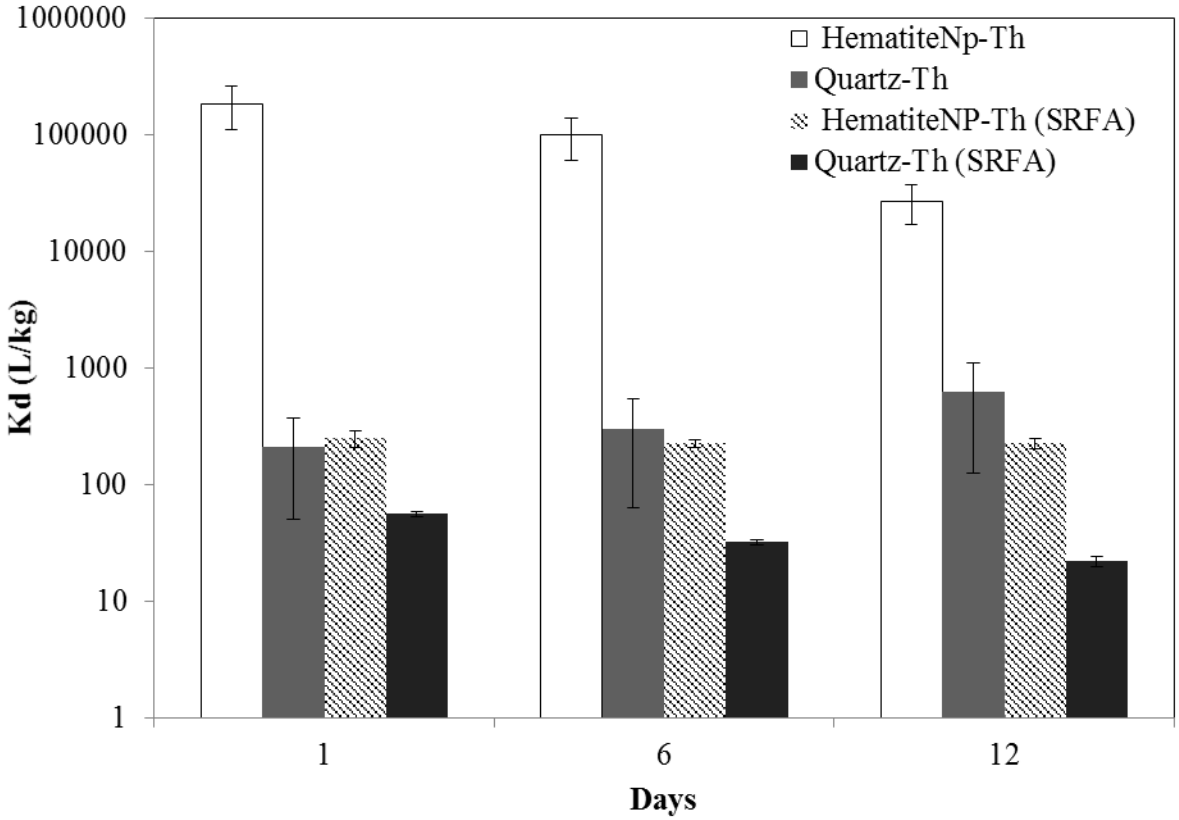

Figure 5.2: Batch sorption results for experiments at pH 5.5 in 0.001 M NaCl with the following constituents: 200 µg/L ^{232}Th, 50 g/L quartz or 45 mg/L hematite-NP, with/without 25 mgC/L SRFA, Kd (L/kg) values are calculated for systems for ^{232}Th:hematite-NP (*white*), ^{232}Th:Quartz (*gray*), ^{232}Th:hematite-NP in the presence of SRFA (*striped*), and ^{232}Th:Quartz in the presence of SRFA (*black*), error bars are based on measurement error of triplicate samples.

Column Experiments

Figure 5.3 below presents the elemental effluent breakthrough for each of the 1 mL/min columns run in high purity quartz media for Th(IV), hematite-NP as Fe, and SRFA as ^{3}H. It is important to note that each of the components (hematite as Fe, SRFA

as ^{3}H, and Th) for the columns determined through elemental analysis as described in the Materials and Methods section above have similar breakthrough times and retardation factors. Therefore, from this point the data will be represented by only the An(IV) elemental breakthrough. Nonetheless full effluent and solid phase analysis for each column is included in the *Supplementary Materials D* Figures D9-D17 and Table D4-5 and aqueous (effluent) and overall recovery are in Table 5.2 with Table 5.3 including physical parameters for each column experiment. Table 5.4 summarizes the additional effluent analysis conducted during collection for all hematite-SRFA-An(IV) columns including filtration, particle size analysis and zeta potential measurements as discussed in the Materials and Methods section (disaggregated filtration data is presented in Table D4 in the *Supplementary Materials D*). However, additional filtration and particle analysis was not completed on remaining column effluents due to lack of sufficient volume and detection limitations. For comparison, Figure 5.4 presents only the effluent Th(IV) breakthrough for all of the 1 mL/min flow rate, quartz columns. The quartz columns with SRFA present [hematite-SRFA-Th, hematite-SRFA-Pu, and SRFA-Th] have similar retardation factors of 1.0-1.6 for both 0.1 and 1.0 mL/min flow rates with effluent recovery >60% (Figure 5.3-5, Table 5.2, retardation factor calculations in *Supplementary Materials D*, retardation factors in Table D5). The SRFA led to nearly unretarded transport of both hematite-NP and An(IV) in these columns (hematite-SRFA-Th and SRFA-Th). The breakthrough of Th-SRFA is slightly earlier than hematite-SRFA-Th (retardation of 1.0 versus 1.4 at 1.0 mL/min, Table D5 in *Supplementary Materials D*). The ^{230}Th and hematite-NP – Th columns at 1 mL/min flow rate in quartz had a

retardation factor of 2.4 and 4.8 and effluent recoveries of 51.6 and 1.3%, respectively (Table 5.2 and 5.3). The ^{232}Th column did not have sufficient effluent recovery to calculate retardation factors as most aqueous measurements were below the MDC described above in the Materials and Methods.

The breakthrough for the 1.0 mL/min flow rate could be slightly earlier than at the 0.1 mL/min flow rate for the hematite-SRFA-Th input in quartz columns (retardation factors of 1.4 versus 1.5, respectively, Table D5 in *Supplementary Materials D*). However, due to the resolution of the data, it cannot be confirmed. In addition, the first datapoint for ^{239}Pu appears slightly earlier than the ^{232}Th through quartz columns with hematite-SRFA-An(IV) spike solutions at 0.1 mL/min flow rate. Possible phenomena leading to these results will be elaborated on below in the discussion section.

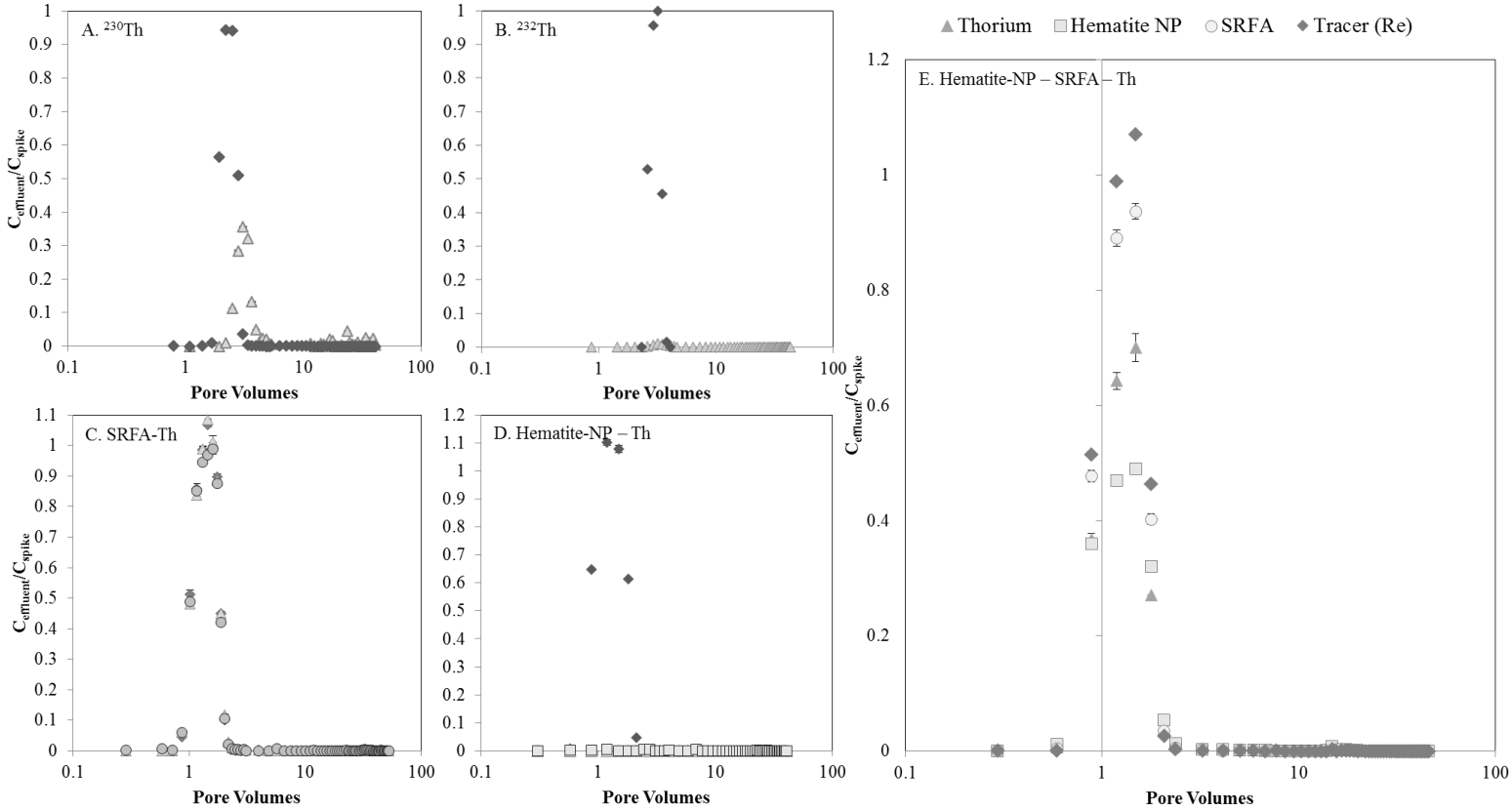

Figure 5.3: Effluent breakthrough for quartz columns under four different spike conditions (noted within the text box of each figure) at 1 mL/min flow rate at pH 5.5 and 0.001 M NaCl. The breakthrough of Th(IV) (*triangles*), hematite as ^{56}Fe (*squares*), SRFA as ^{3}H (*circles*), and Re tracer (*diamonds*): (A) ^{230}Th, (B) ^{232}Th, (C) SRFA-Th, (D) Hematite-Th, (E) Hematite-SRFA-Th.

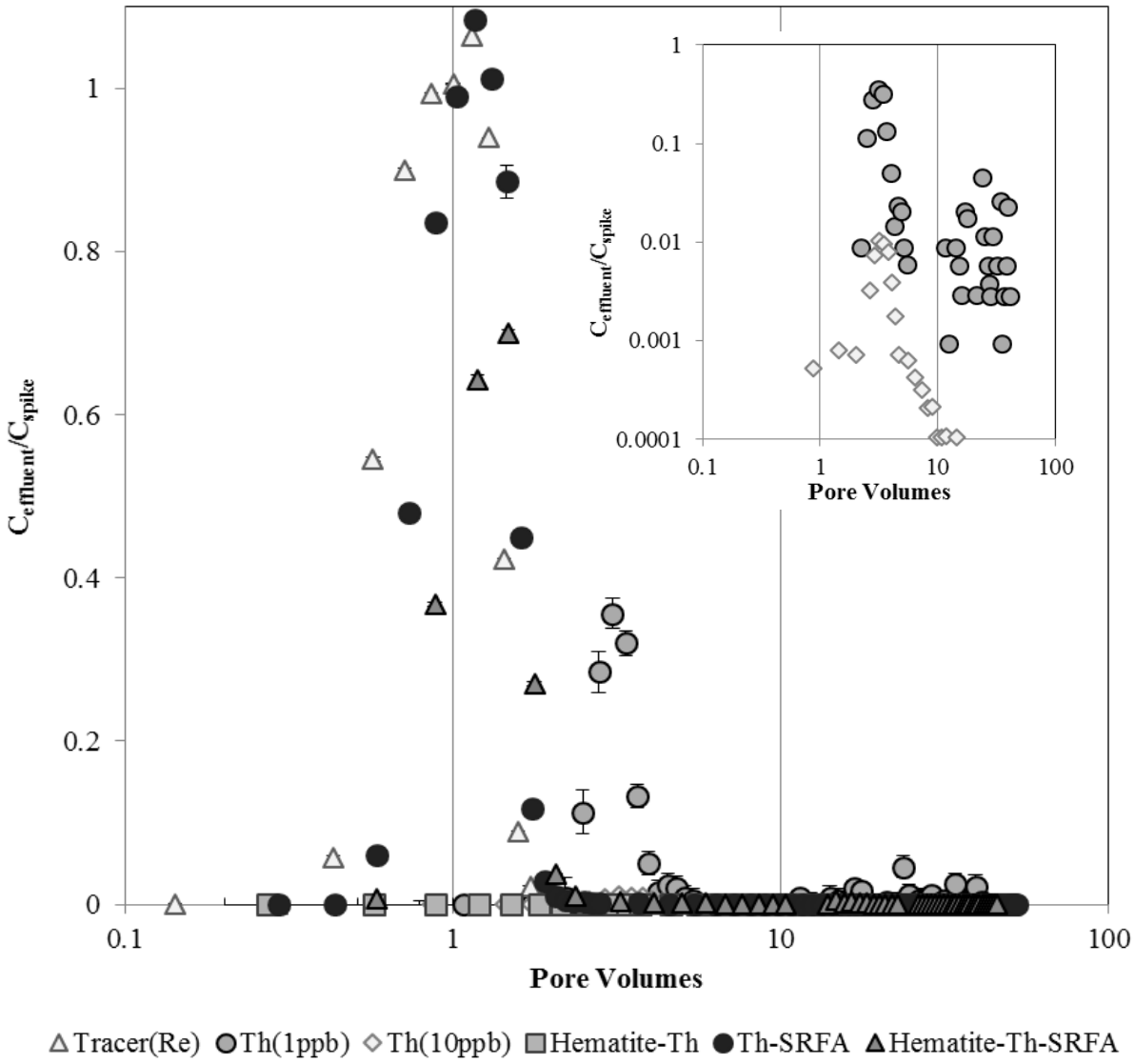

Figure 5.4: Effluent breakthrough of Th(IV) at pH 5.5 in 0.001 M NaCl within the following column experiments in high purity quartz: ^{230}Th (*gray circles*), ^{232}Th (*white diamonds*), Hematite-Th (*gray squares*), Th-SRFA (*black circles*) and Hematite-SRFA-Th (*gray triangles*) with the tracer (Re, *white triangles*) included for comparison, error bars are based on triplicate measurements for ^{232}Th and counting statistics for ^{230}Th.

The effluent recovery of the hematite-Th spike through quartz is <2% as compared to >60% recovery in the hematite-SRFA-Th spike at a 1 mL/min flow rate. In addition, the distribution of the components recovered within the solid phase of the hematite-SRFA-Th column represents a small fraction of the total input and is evenly distributed throughout the column, while the hematite-Th leaching results show the majority of influent Th was deposited within the first 2 cm from inlet (Figure 5.4). It must be noted that the NPs in the hematite-Th spike solution had not aggregated significantly prior to introduction to the column as an average particle size of 152±1 nm was measured prior to input which is similar to hematite-SRFA-An(IV) column spike solutions also at pH~5.5 (ranging from 95-190 nm, Table 5.1). However, the hematite-Th spike solution had a positive zeta potential 70±4 mV which may have been attracted towards the negatively charged quartz based on its point of zero charge near pH ~2 (Kosmulski, 2002, 2011). The hematite-SRFA-An(IV) solutions had a zeta potential of -42 to -55 mV prior to input into the columns and was expected to be repelled by the bulk quartz sand.

Table 5.2: Summary of aqueous (effluent) recovery and overall (effluent + solid phase) recovery for all column experiments.

Spike ID	Flow Rate (mL/min)	Aqueous Recovery (%)				Overall Recovery (%)		
		An(IV)	Fe	SRFA	Tracer	An(IV)	Fe	SRFA
^{230Th}	0.94 ± 0.17	51.6	N/A	N/A	96.5	97.7	N/A	N/A
^{232}Th	0.98 ± 0.07	2.1	N/A	N/A	160.4	90.6	N/A	N/A
Hematite-Th	0.97 ± 0.14	1.3	1.9	N/A	110.5	61.6	86.4	N/A
SRFA-Th	0.94 ± 0.02	97.3	N/A	98.2	94.9	97.3	N/A	98.2
Hematite-SRFA-Th	1.02 ± 0.01	60.3	70.5	92	98	99.9	84.8	92
SRS Sandy - hematite-SRFA-Th	1.01 ± 0.02	<1	<1	NM	53.6	88	78.7	NM
Hematite-SRFA-Th	0.107 ± 0.014	85.1	93.9	92.3	85.1	104.5	106.6	92.3
Hematite-SRFA-Pu	0.106 ± 0.013	77.3	82.1	94.3	106.7	92.2	93.1	97.2

Note: N/A – not applicable, NM – not measured

Table 5.3: Summary of physical column parameters.

Spike ID	Flow Rate (mL/min)	Effluent pH	# Pore Volumes	Pore Volume (mL)	Porosity
^{230Th}	0.94 ± 0.17	5.30 ± 0.06	41	6.1	0.31
^{232}Th	0.98 ± 0.07	5.52 ± 0.06	44	6.1	0.30
Hematite-Th	0.97 ± 0.14	5.59 ± 0.16	41	5.7	0.42
SRFA-Th	0.94 ± 0.02	5.80 ± 0.17	53	5.7	0.29
Hematite-SRFA-Th	1.02 ± 0.01	5.52 ± 0.11	46	6.3	0.43
SRS Sandy - hematite-SRFA-Th	1.01 ± 0.02	5.38 ± 0.17	38	4.6	0.23
Hematite-SRFA-Th	0.107 ± 0.014	5.59 ± 0.19	67	6.1	0.42
Hematite-SRFA-Pu	0.106 ± 0.013	5.59 ± 0.17	72	6.1	0.42

Table 5.4: Summary of effluent analysis for select column experiments including particle size, zeta potential and % dissolved (average of at least 3 effluent samples).

Spike ID	Flow Rate (mL/min)	Zeta (mV)	Diameter (nm)	Fraction Dissolved An(IV) (%)
Hema-SRFA-Th	1	-52 ± 12	176 ± 3	28 ± 22%
Hema-SRFA-Th	0.1	-69 ± 8	153 ± 17	18 ± 1%
Hema-SRFA-Pu	0.1	-52 ± 9	173 ± 12	15 ± 2%

The 1.0 mL/min flow rate in SRS sandy soil with the hematite-SRFA-Th spike solution did not exhibit effluent breakthrough above the MDC (Figure 5.5). However, transport of the hematite-NP and ^{232}Th was observed within the column with the largest fraction in the sections 2 and 3 cm from the influent. Additional column experiments were completed at 1 mL/min flow rate in both quartz and SRS sandy soil with polystyrene microspheres. The intent of the experiments with microspheres was to examine filtration of nonreactive polystyrene NPs to assist in differentiating between filtration and reactivity. Unretarded breakthrough of the polystyrene NPs occurred in quartz columns, but negligible breakthrough was observed in the SRS sandy soil (*Supplementary Materials D* Figure D17). Results with the polystyrene microspheres are comparable to those with hematite-SRFA-Th spike solutions in both quartz and SRS sandy soil. Fluorescence microscopy of the SRS sandy soil shows that particles are strongly associated with the coatings on the quartz grains (*Supplementary Materials D* Figure D18).

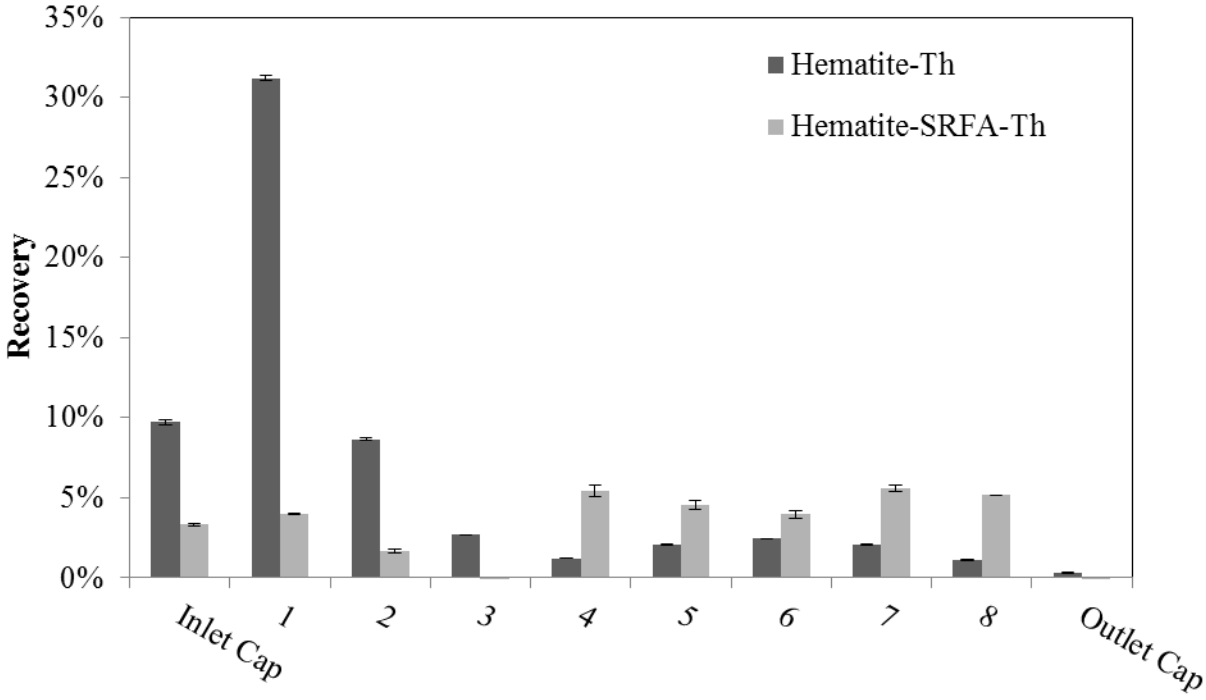

Figure 5.5: Recovery of ^{232}Th(IV) from quartz sand for hematite-Th (*black*) and hematite-SRFA-Th (*gray*) column experiments at 1 mL/min flow rate based on leaching in 8 M HNO_3, error bars based on triplicate measurements.

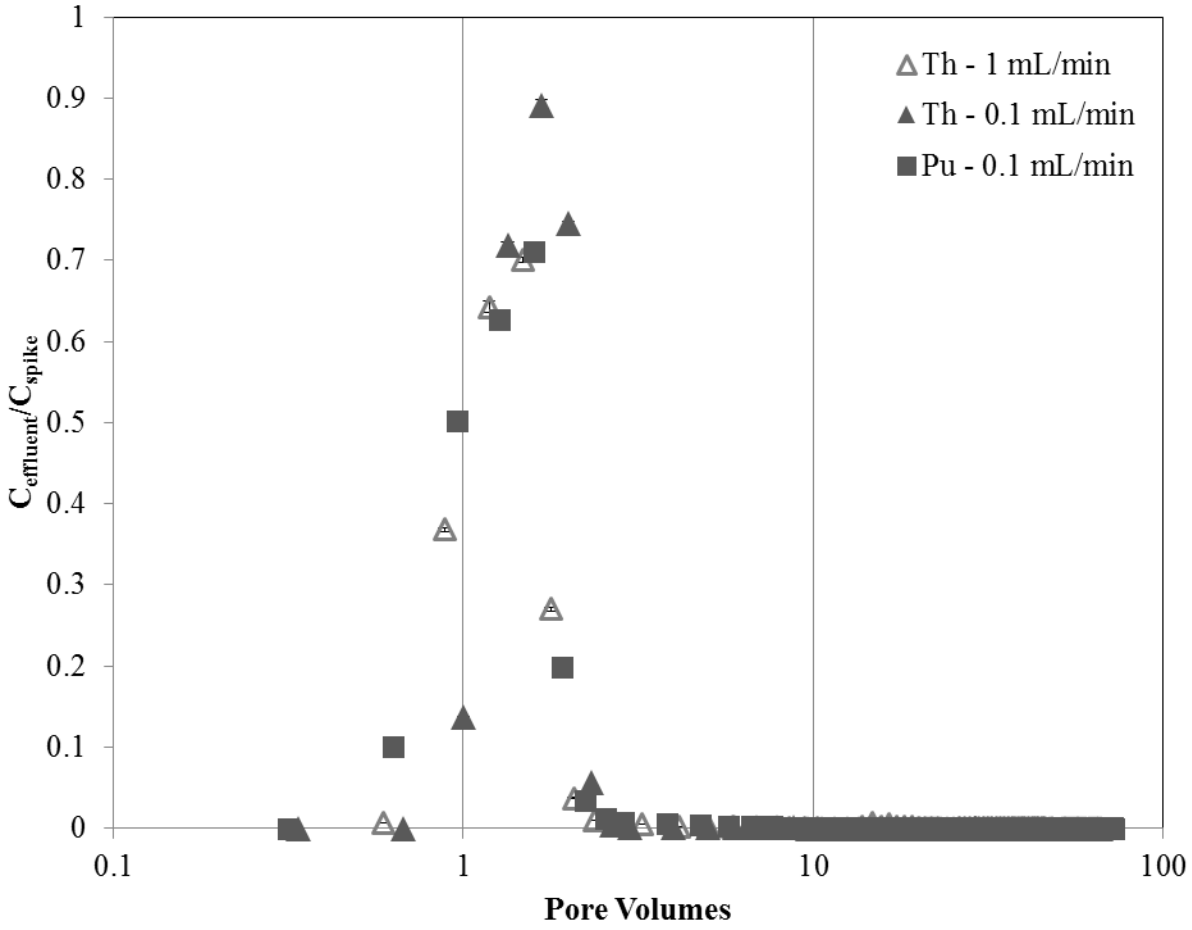

Figure 5.6: Comparison of hematite-NP facilitated transport of An(IV) [as hematite-SRFA-An(IV)] through quartz columns at 0.1 and 1.0 mL/min flow rate, 1.0 mL/min quartz column with hematite-SRFA-Th (*open triangles*), 0.1 mL/min flow rate, quartz column with hematite-SRFA-Th (*closed triangles*) and hematite-SRFA-Pu (*squares*) spike solutions, column conditions for all experiments: pH 5.5 in 0.001 M NaCl.

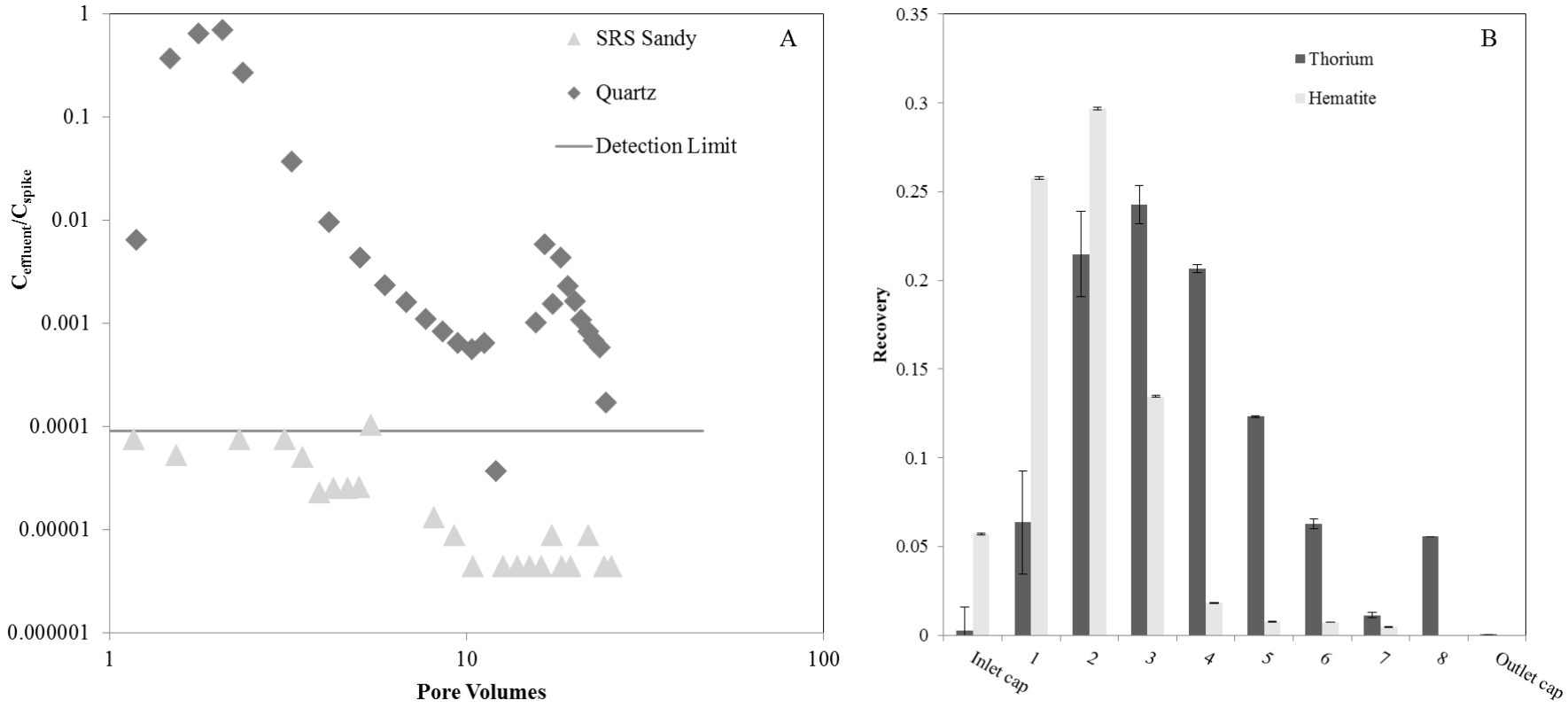

Figure 5.7: (A) Effluent ^{232}Th breakthrough comparison of hematite – SRFA – Th spike solutions through quartz (*triangles*) and SRS sand soil (*squares*) at a 1 mL/min flow rate with the MDC (*line*), error bars are based on triplicate measurements, (B) Recovery within the SRS sandy soil column for hematite-NPs as ^{55}Fe (*gray*) and ^{232}Th (*black*) following leaching in 8 M HNO_3 for hematite – SRFA – Th spike, column conditions for all experiments: pH 5.5 in 0.001 M NaCl.

Discussion

Batch Experiments

These experiments were designed to investigate the optimal conditions for colloid-facilitated transport of An(IV) on hematite-NPs. The batch experiments presented above demonstrate the ability of SRFA to stabilize hematite-NPs in suspension as seen previously with humic substances and iron oxide NPs (Baalousha, 2009; Baalousha et al., 2008; Davis and Leckie, 1978; Kretzschmar and Sticher, 1997; Reiller et al., 2008; Reiller et al., 2002, 2003; Schrick et al., 2004). Based on these and previous experiments, a low ionic strength (0.001 M NaCl) and pH of 5.5 were chosen to reduce aggregation but still represent environmentally relevant conditions. In addition, the ^{3}H-SRFA and hematite-NP batch sorption/desorption experiments proved that significant desorption of the SRFA from the hematite-NP's is not expected over the time span of these experiments as <15% desorbed over 28 days. It is expected that hematite-NPs are coated with a monolayer of SRFA at low ionic strength as described previously (Seijo et al., 2009). The batch sorption experiments for ^{232}Th showed that ^{232}Th adsorbs much more strongly to hematite-NP versus quartz. Therefore, the ^{232}Th is more likely to be associated with hematite-NPs than quartz. However, with time, the SRFA can significantly decrease the fraction of An(IV) adsorbed to hematite-NPs and quartz. Over the time span of the column experiments presented in this work, a significant fraction still remains associated with the hematite-NPs as evidenced by filtration data presented in Table 5.4.

Quartz columns at 1.0 mL/min flow rate

The overall mobility of Th through quartz columns with respect to each of the experimental conditions followed the trend:

Th – SRFA > Hematite – Th – SRFA > soluble ^{230}Th > saturated ^{232}Th > Hematite – Th

The Th – SRFA column exhibited the earliest and greatest effluent breakthrough. It is notable that the transport of Th and hematite-NPs was increased in the presence of SRFA although its breakthrough was slightly delayed as compared to Th – SRFA (1.0 versus 1.4 retardation factor). However, without SRFA present the hematite-NPs were less mobile relative to dissolved Th (^{230}Th column). A comparison of the recovery from the aqueous (effluent, Figure 5.1) and the solid phase distribution for the hematite-Th and hematite-SRFA-Th columns (Figure 5.2) demonstrates the drastic difference in transport. The effluent recovery in the hematite-Th column is <2% as compared to >60% recovery in the hematite-SRFA-Th column. The majority of the hematite-NP and Th were quickly sequestered within the column without the presence of SRFA. This is possibly due to adsorption of the hematite-Th complexes to the quartz or destabilization and aggregation of the particles in the presence of quartz due to attraction of positively charged hematite-Th complexes to negatively charged quartz. It is important to note that for these simplified systems hematite-NPs could both increase or decrease Th transport with respect to the dissolved species depending on the presence or absence of SRFA.

Because each of the components (hematite as Fe, SRFA as ^{3}H, and Th) for the columns had similar breakthrough times and retardation factors and because 70-85% of

the ^{232}Th(IV) was associated with the colloidal size fraction in the effluent and initial spike solutions (based on filtration Table 5.3) in the hematite-SRFA-Th column, it is likely that a ternary hematite-SRFA-Th complex is present and mobile in these systems. Due to the low pH and observed sorption behavior in batch studies, the ternary complex is likely a SRFA coated hematite-NP with Th bound to the SRFA coating. This ternary complex is especially likely considering the significant sorption of SRFA to hematite in preliminary experiments. In addition, greater than 99% of the ^{232}Th(IV) was associated with the hematite-NP's in the hematite-Th column spike solution and ^{56}Fe and ^{232}Th are correlated in their distribution in the solid phase leading to the conclusion that the two components were strongly associated throughout the length of the experiments (*Supplementary Materials D* Figure D13) as predicted by the preliminary K_d measurements. Therefore, in these experiments, either a mobile ternary (hematite-SRFA-Th) or an immobile binary (hematite-Th) complex exists depending on whether or not SRFA is present. In addition, it is assumed that the Th-SRFA spike input exhibited transport of a mobile binary Th-SRFA complex. It must be noted that it is not expected that the An(IV) species affected the transport of the hematite-NP in these experiments due to the low mass relative to that of the colloid (mass ratio of colloid:An(IV) of at least 150). However, previous work has shown that at high concentrations the dissolved contaminant can affect the transport of the colloids as noted with lead and kaolinite colloids (Sun et al., 2006).

The ^{230}Th and ^{232}Th columns represent both dissolved and precipitated Th(IV), respectively. Solubility calculations based on work by Neck and Kim predict a solubility

of 4.3 µg/L at pH 5.5 with $Th(OH)_2^{2+}$ as the major species with ionic strength corrections approximated using the Debye-Huckel method (*Supplementary Materials D* Figure D21) (Neck and Kim, 2001). However, it must be noted that the error on the solubility constant (K_{sp}) is 0.8 log units. Therefore, introduction of one sigma error of the K_{sp} leads to a solubility range at pH 5.5 of 0.7 to 25.3 µg/L. Insignificant breakthrough occurred for the ^{232}Th [10 µg/L] column in the presence of quartz at pH 5.5 and 0.001 M NaCl at 1 mL/min flow rate and 85% of the ^{232}Th in the initial spike solution was in the colloidal size fraction (15% in the dissolved fraction) based on filtration. Therefore, it is likely that precipitation occurred and led to immobilization of the majority of the ^{232}Th within the column. However, the ^{230}Th column [0.72 µg/L] in quartz at pH 5.5 and 0.001 M NaCl at a 1 mL/min flow rate recovered approximately 52% of the total ^{230}Th within the effluent breakthrough with 72% of the ^{230}Th associated with the dissolved size fraction in the initial spike solution. Assuming the colloidal size fraction that did not pass through the 10 MWCO filter as described in Materials and Methods is precipitated Th(IV) and that precipitated Th(IV) is not mobile within the columns, it is likely that the true solubility of Th(IV) is on the lower end of the estimated range. In addition, it is notable that a large fraction of the dissolved Th(IV) is mobile in these systems due to the fast flow rate (1 mL/min) and low reactivity with the quartz sand.

For the Th-SRFA column spike solutions where no hematite-NPs are present, it is expected that Th exists as a mobile Th-SRFA complex. Because of the strong complexation affinity of Th(IV) with both hematite-NPs and humic substances (Cromieres et al., 1998; Reiller et al., 2002, 2003) and the increased solubility of Th(IV)

in the presence of humic substances (Artinger et al., 2003; Choppin, 2007; Reiller et al., 2008), it is likely that precipitation of Th(IV) did not occur within spike solutions with hematite-NPs and/or SRFA. However, concentrations were above theoretical solubility of Th without the presence of humic substances. Yet, Reiller *et al*. estimated a 60 fold increase in Th solubility in the presence of humic acid at pH 6 (Reiller et al., 2008). With respect to the solubility range estimated above, a 60 fold increase in solubility would lead to a range of 40-1500 ppb at pH 5.5. Electron microscopy was also completed on spike solutions but could not rule out precipitation of Th due to the small size of hematite-NPs (on the same order as possible Th precipitates) and issues imaging in the presence of SRFA. While precipitation of Th cannot be ruled out in the systems with hematite NPs and SRFa present, it is not expected based on the above discussion.

Quartz Columns at 0.1 mL/min flow rate

Because the 1 mL/min flow rate resulted in a retention time of only ~6.5 minutes, additional column experiments were conducted at a 0.1 mL/min flow rate (~65 minute retention time) for comparison. These experiments were conducted to investigate whether or not the fast flow rate could be a major factor impacting transport in these systems. It was considered that the fast flow rate could induce shear forces great enough to lead to break up of sorbed or aggregated NPs followed by re-mobilization as discussed previously (Dunphy Guzman et al., 2006). Gao and team also noted that faster flow rates led to greater mobilization of colloids under unsaturated conditions (Gao et al., 2006). The similarity of hematite-NP, Th and SRFA from the the hematite-SRFA-Th spike solution through quartz columns at 0.1 and 1.0 mL/min show that it is unlikely that

shear forces affect NP transport in these systems (Figure 5.3). However, the breakthrough is slightly earlier in the 1.0 mL/min flow rate (retardation factors of 1.4 versus 1.5 for 1.0 and 0.1 mL/min flow rates, respectively, Table D5 in *Supplementary Materials D*), but the resolution of the breakthrough peaks is not great enough to confirm differences. In addition, the hematite-Th spike solution at 1.0 mL/min demonstrates that the fast flow rate was not capable of breaking up and re-mobilizing hematite-NPs with flushing of over 40 pore volumes of 0.001 M NaCl at pH 5.5.

It is notable that both the hematite-SRFA-Pu and hematite-SRFA-Th columns in quartz at 0.1 mL/min flow rate exhibit comparable transport and recoveries. While the initial ^{239}Pu spike solution was almost entirely Pu(IV) [99.2%], effluent measurements of the oxidation state were not possible due to insufficient volume and detection limits. However, because of the similarity of the data to the Th(IV) breakthrough and the presence of fulvic acid, it is expected that Pu remained in the +4 oxidation state. Further, Pu(IV) has been previously shown to be the dominant oxidation state in solution in the presence of humic substances (Choppin, 2007; Marquardt et al., 2004; Shcherbina et al., 2007a) and the dominant oxidation state in the solid phase in the presence of hematite (Hixon and Powell, 2014; Powell et al., 2005; Romanchuk et al., 2011). While Th has been shown to not be an ideal analog for Pu(IV) (Choppin, 1999; Krauskopf, 1984; Neck and Kim, 2001; Schwantes and Santschi, 2010), it is representative of Pu(IV) in these systems because of the strong sorption to the hematite-NP and SRFA. Both Th(IV) and Pu(IV) can represent the transport of other tetravalent actinides in these ternary systems. However, it does appear that the first datapoint in the effluent breakthrough curve for

^{239}Pu is slightly earlier than that for ^{232}Th. It cannot be confirmed that these are significantly different breakthroughs due to the resolution of the effluent peaks. This could be due to the significantly greater sorption of Pu to SRFA than Th as shown previously (Zavarin, et al., 2014).

SRS Sandy columns at 1.0 mL/min flow rate

It is important that the two media (quartz versus SRS sandy) exhibited dramatically different transport of the hematite-SRFA-Th spike input. A comparison of the effluent measurements for the hematite-SRFA-Th columns in both quartz and SRS sandy soil is shown in Figure 5.7. Previous work investigating dissolved Pu(IV) in the same soil from Savannah River Site and similar column setup at pH 3 reported no breakthrough of Pu(IV) and that the largest fraction of Pu was associated with the first cm of the column (Powell et al., 2014), while these experiments with the majority of the Th(IV) associated with hematite-NP and SRFA exhibit the greatest solid phase recovery in the 2nd, 3rd and 4th centimeter of the column (>20% recovery of the total in each 1 cm slice). Therefore, while significant transport of hematite-NP, Th or SRFA from the hematite-SRFA-Th spike through the SRS sandy soil column did not occur, the post-experiment solid phase analysis indicated that greater transport of the components of the hematite-SRFA-Th ternary complex occurred relative to dissolved Pu(IV) occurred than expected as compared to dissolved tetravalent actinides. Therefore, the SRS sandy column results follow the overall trend for dissolved versus hematite-SRFA-Th ternary complexes observed on the quartz although the scale of transport was significantly decreased.

Because the SRS sandy is a natural soil composed of quartz sand as well as soil coatings mostly composed of kaolinite and goethite, it is likely that the soil coatings (and not the quartz sand) led to the reduction in transport. Previous experiments with environmentally relevant soils have reached similar conclusions that naturally occurring, colloidal-sized particles can contribute to removal of NPs (Emerson et al., 2014; Quik et al., 2012). The following multiple working hypotheses have been developed to describe the mechanisms behind the reduction in transport in the SRS sandy soil relative to the quartz columns:

1. Coating-mediated aggregation or destabilization of the particles
2. Adsorption of particles to the clay-sized coating minerals
3. Physical entrapment of particles in smaller pores caused by the presence of clay-sized coatings

It is notable that previous lysimeter experiments with a similar soil from Savannah River Site investigating NP transport under unsaturated conditions reached the conclusion that the clay-sized coatings led to significant aggregation of iron oxide and silver NPs (Emerson et al., 2014). However, it is likely that these theorized mechanisms are not independent but interconnected processes leading to immobilization of the particles. Nonetheless, additional experiments were conducted with presumably non-reactive, 100 nm polystyrene NPs to further investigate these mechanisms (*Supplementary Materials D*, Figure D19). However, similar results were observed with quartz versus SRS sandy soil columns for the polystyrene microspheres as noted with the hematite-SRFA-Th columns (*Supplementary Materials D* Figure D19). Fluorescence microscopy shows that

particles are associated with the soil grains specifically with the coatings (*Supplementary Materials D*, Figure D20). Based on the microscopy results, it appears that interactions with soil coatings and possibly filtration were responsible for sequestration of the polystyrene NPs within the sandy soil columns. Filtration does not appear to be a significant mechanism for the removal of the polystyrene NPs in the quartz columns but drawing a conclusion from the SRS sandy soil columns from that data is not possible since the pore structures were not exactly matched.

Conclusions

It is noteworthy that slightly greater transport of Th-SRFA occurred versus the hematite-SRFA-Th column. Thus even at the low pH of these experiments where some sorption of organic matter is expected, enhanced mobility of Th(IV) was observed. However, the SRFA-Th experiments were only performed on the quartz columns and, as this work demonstrates, experiments using pure phases may not properly represent real soils. Furthermore, it is expected that colloids will be present in most environmental systems at some concentration (Degueldre et al., 1996; Degueldre et al., 2000; Kanti Sen and Khilar, 2006; Kim, 1991; McCarthy and Degueldre, 1993; McCarthy and Zachara, 1989; Moulin and Moulin, 2001; Moulin and Ouzounian, 1992; Vilks et al., 1998). Therefore, it is just as significant that a large fraction of the Th was transported in the hematite-SRFA-Th systems. These ternary systems should be investigated further to better understand the mechanisms of colloid facilitated transport of the tetravalent actinides. The enhanced mobilization of colloidal hematite facilitated by SRFA clearly shows the enhanced mobility of Pu or Th associated with the hematite-SRFA complex.

This work and previous work illustrates that colloids can enhance or retard transport of the actinides depending on the conditions (Sun et al., 2006; Zhu et al., 2012). Finally the transport of Th, SRFA, and hematite-NPs was dramatically decreased within the SRS sandy column as compared to the quartz sand. Based on the theories presented for the greater fraction of hematite-NPs – ^{232}Th – SRFA spike remaining within the SRS sandy column, it is likely that the hematite-NPs and polystyrene microspheres are both reacting strongly with the natural coatings on the SRS sandy soil leading to immobilization of the NPs. Therefore, future work should be concentrated on environmentally relevant soils and soil coatings to further investigate ternary systems.

Acknowledgements

The authors would like to acknowledge the Clemson light imaging facility and electron microscopy laboratory for their invaluable help imaging these systems. This work was supported by the Subsurface Biogeochemical Research Program of the U.S. Department of Energy's Office of Biological and Environmental Research. Emerson also acknowledges support from the U.S. Nuclear Regulatory Commission Graduate Fellowship Program.

References

1. Andre, C., Choppin, G.R., 2000. Reduction of Pu(V) by humic acid. Radiochimica Acta 88, 613-616.
2. Artinger, R., Buckau, G., Zeh, P., Geraedts, K., Vancluyse, J., Maes, A., Kim, J.I., 2003. Humic colloid mediated transport of tetravalent actinides and technetium. Radiochimica Acta 91, 743-750.
3. Artinger, R., Schuessler, W., Schafer, T., Kim, J.-I., 2002. A kinetic study of Am(III)/Humic colloid interactions. Environmental Science and Technology 36, 4358-4363.

4. Baalousha, M., 2009. Aggregation and disaggregation of iron oxide nanoparticles: Influence of particle concentration, pH and natural organic matter. Sci Total Environ 407, 2093-2101.

5. Baalousha, M., Maniculea, A., Cumberland, S., Kendall, K., Lead, J.R., 2008. Aggregation and Surface Properties of Iron Oxide Nanoparticles: Influence of pH and Natural Organic Matter. Environmental Toxicology and Chemistry 27, 1875-1882.

6. Banik, N.L., Buda, R.A., Burger, S., Kratz, J.V., Trautmann, N., 2007. Sorption of tetravalent plutonium and humic substances onto kaolinite. Radiochimica Acta 95, 569-575.

7. Begg, J.D., Zavarin, M., Zhao, P.H., Tumey, S.J., Powell, B., Kersting, A.B., 2013. Pu(V) and Pu(IV) Sorption to Montmorillonite. Environmental Science & Technology 47, 5146-5153.

8. Blinova, O., Novikov, A., Perminova, I., Goryachenkova, T., Haire, R., 2007. Redox interactions of Pu(V) in solutions containing different humic substances. Journal of Alloys and Compounds 444, 486-490.

9. Brunhauer, S., Emmett, P.H., Teller, E., 1938. Adsorption of gases in multimolecular layers. Journal of the American Chemical Society 60, 309-319.

10. Choppin, G.R., 1999. Utility of Oxidation State Analogs in the Study of Plutonium Behavior. Radiochimica Acta 85, 89-95.

11. Choppin, G.R., 2007. Actinide speciation in the environment. Journal of Radioanalytical and Nuclear Chemistry 273, 695-703.

12. Choppin, G.R., Allard, B., 1985. Complexes of actinides with naturally occurring organic compounds.

13. Clark, M.M., 1996. Transport Modeling for Environmental Engineers and Scientists. John Wiley and Sons, New York, NY.

14. Cromieres, L., Moulin, V., Fourest, B., Guillaumont, R., Giffaut, E., 1998. Sorption of thorium onto hematite colloids. Radiochimica Acta 82, 249-255.

15. Davis, J.A., Leckie, J.O., 1978. EFFECT OF ADSORBED COMPLEXING LIGANDS ON TRACE-METAL UPTAKE BY HYDROUS OXIDES. Environmental Science & Technology 12, 1309-1315.

16. Degueldre, C., Pfeiffer, H.-R., Alexander, W., Wernli, B., Bruetsch, R., 1996. Colloid properties in granitic groundwater systems. I. Sampling and characterization. Applied Geochemistry 11, 677-695.

17. Degueldre, C., Triay, I., Kim, J.-I., Vilks, P., Laaksoharju, M., MIekeley, N., 2000. Groundwater colloid properties: a global approach. Applied Geochemistry 15, 1043-1051.

18. Duff, M.C., Hunter, D.B., Triay, I.R., Bertsch, P.M., Reed, D.T., Sutton, S.R., Shea-McCarthy, G., Kitten, J., Eng, P., Chipera, S.J., Vaniman, D.T., 1999. Mineral Associations and Average Oxidation States of Sorbed Pu on Tuff. Environ Sci Technol 33, 2163-2169.

19. Dunphy Guzman, K.A., Finnegan, M.P., Banfield, J.F., 2006. Influence of Surface Potential on Aggregation and Transport of Titania Nanoparticles. Environmental Science & Technology 40, 7688-7693.

20. Emerson, H.P., Hart, A.E., Baldwin, J.A., Waterhouse, T.C., Kitchens, C.L., Mefford, O.T., Powell, B.A., 2014. Physical transformations of iron oxide and silver nanoparticles from an intermediate scale field transport study. Journal of Nanoparticle Research 16, 14.

21. Gao, B., Saiers, J.E., Ryan, J., 2006. Pore-scale mechanisms of colloid deposition and mobilization during steady and transient flow through unsaturated granular media. Water Resources Research 42, n/a-n/a.

22. Geckeis, H., Lutzenkirchen, J., Polly, R., Rabung, T., Schmidt, M., 2013. Mineral-water interface reactions of actinides. Chem Rev 113, 1016-1062.

23. Geckeis, H., Rabung, T.H., Ngo Manh, T., Kim, J.I., Beck, H.P., 2002. Humic colloid-borne natural polyvalent metal ions: Dissociation experiment. Environmental Science and Technology 36, 2946-2952.

24. Hixon, A.E., Arai, Y., Powell, B.A., 2013. Examination of the effect of alpha radiolysis on plutonium(V) sorption to quartz using multiple plutonium isotopes. J Colloid Interface Sci 403, 105-112.

25. Hixon, A.E., Hu, Y.J., Kaplan, D.I., Kukkadapu, R.K., Nitsche, H., Qafoku, O., Powell, B.A., 2010. Influence of iron redox transformations on plutonium sorption to sediments. Radiochimica Acta 98, 685-682.

26. Hixon, A.E., Powell, B.A., 2014. Observed changes in the mechanism and rates of Pu(V) reduction on hematite as a function of total plutonium concentration. Environmental Science and Technology submitted.

27. Hu, Q.H., Rose, T.P., Zavarin, M., Smith, D.K., Moran, J.E., Zhao, P.H., 2008. Assessing field-scale migration of radionuclides at the Nevada Test Site: "mobile" species. J Environ Radioact 99, 1617-1630.

28. Jackson, M.L., 1985. Soil Chemical Analysis - Advanced Course, 2nd ed., Soil Chem. Anal.-Adv. course. Parallel Press, Madison, WI.

29. Kanti Sen, T., Khilar, K.C., 2006. Review on subsurface colloids and colloid-associated contaminant transport in saturated porous media. Adv Colloid Interface Sci 119, 71-96.

30. Kaplan, D.I., Bertsch, P.M., Adriano, D.C., Orlandini, K.A., 1994. Actinide association with groundwater colloids in a coastal plain aquifer. Radiochimica Acta 66/67, 181-187.

31. Kaplan, D.I., Powell, B.A., Demirkanli, D.I., Fjeld, R.A., Molz, F.J., Serkiz, S.M., Coates, J.T., 2004. Influence of Oxidation States on Plutonium Mobility during Long-Term Transport through an Unsaturated Subsurface Environment. Environ Sci Technol 38, 5053-5058.

32. Kaplan, D.I., Powell, B.A., Duff, M.C., Demirkanli, D.I., Denham, M.E., Fjeld, R.A., Molz, F., 2007. Influence of Sources on Plutonium Mobility and Oxidation State Transformations in Vadose Zone Sediments. Environmental Science and Technology 41, 7417-7423.

33. Keeney-Kennicutt, W.L., Morse, J.W., 1985. The redox chemistry of Pu(V)O2+ interaction with common mineral surfaces in dilute solutions and seawater. Geochimica et Cosmochimica Acta 49, 2577-2588.

34. Kersting, A.B., 2012. Impact of colloidal transport on radionuclide migration in the natural environment. Radionuclide Behaviour in the Natural Environment: Science, Implications and Lessons for the Nuclear Industry, 384-410.

35. Kersting, A.B., 2013. Plutonium transport in the environment. Inorganic chemistry 52, 3533-3546.

36. Kersting, A.B., Efurnd, D.W., Finnegan, D.L., Rokop, D.J., Smith, D.K., Thomspon, J.L., 1999. Migration of plutonium in groundwater at the Nevada Test Site. Nature 397, 56-59.

37. Kim, J.I., 1991. Actinide colloid generation in groundwater. Radiochimica Acta 52/53, 71-81.

38. Kim, J.I., Grambow, B., 1999. Geochemical assessment of actinide isolation in a German salt repository environment. Engineering Geology 52, 221-230.

39. Kosmulski, M., 2002. The pH-dependent surface charging and the points of zero charge. J Colloid Interface Sci 253, 77-87.

40. Kosmulski, M., 2011. The pH-dependent surface charging and points of zero charge: V. Update. J Colloid Interface Sci 353, 1-15.

41. Krauskopf, K.B., 1984. Thorium as an Analogue for Plutonium and Rare-Earth Metals as Analogues for Heavier Actinides, in: Smellie, J.A.T. (Ed.), Natural Analogues to the Conditions around a Final Repository for High-Level Radioactive Waste. Swedish Geological Company, Uppsala, Sweden.

42. Kretzschmar, R., Sticher, H., 1997. transpot of humic-coated iron oxide colloids in a sandy soil: influence of Ca2+ and trace metals. Environmental Science and Technology 31, 3497-3504.

43. Lu, N., Cotter, C.R., Kitten, H.D., Bentley, J., Triay, I.R., 1998. Reversibility of Sorption of Plutonium-239 onto Hematite and Goethite Colloids. Radiochimica Acta 83, 167-173.

44. Lu, N., Reimus, P.W., Parker, G.R., Conca, J.L., Triay, I.R., 2003. Sorption kinetics and impact of temperature, ionic strength and colloid concentration on the adsorption of plutonium-239 by inorganic colloids. Radiochimica Acta 91, 713-720.

45. Marquardt, C.M., Seibert, A., Artinger, R., Denecke, M., Kuczewski, B., Schild, D., Fanghanel, T., 2004. The redox behavior of plutonium in humic rich groundwater. Radiochimica Acta 92, 617-623.

46. McCarthy, J.F., Degueldre, C., 1993. In Characterization of Environmental Particles:

47. Sampling and characterization of colloids in groundwater for studying their role in contaminant transport. Lewis Publishers, Chelsea, MI.

48. McCarthy, J.F., Zachara, J.M., 1989. Subsurface transport of contaminants. Environ Sci Technol 23, 496-502.

49. Melson, N.H., Haliena, B.P., Kaplan, D.I., Barnett, M.O., 2012. Adsorption of tetravalent thorium by geomedia. Radiochimica Acta 100, 827-832.

50. Moulin, V., Moulin, C., 2001. Radionuclide speciation in the environment: a review. Radiochimica Acta 89, 773-778.

51. Moulin, V., Ouzounian, G., 1992. Role of colloids and humic substances in the transport of radio-elements through the geosphere. Applied Geochemistry 1, 179-186.

52. Murphy, R.J., Lenhart, J.J., Honeyman, B.D., 1999. The sorption of thorium (IV) and uranium (VI) to hematite in the presence of natural organic matter. Colloids and Surfaces 157, 47-62.

53. Neck, V., Altmaier, M., Seibert, A., Yun, J.I., Marquardt, C.M., Fanghänel, T., 2007. Solubility and redox reactions of Pu(IV) hydrous oxide: Evidence for the formation of PuO2+x(s, hyd). Radiochimica Acta 95, 193-207.

54. Neck, V., Kim, J.I., 2001. Solubility and hydrolysis of tetravalent actinides. Radiochimica Acta 89, 1-16.

55. Novikov, A.P., Kalmykov, S.N., Utsunomiya, S., Ewing, R.C., Horreard, F., Merkulov, A., Clark, S.B., Tkachev, V.V., Myasoedov, B.F., 2006. Colloid Transport of Plutonium in the Far-Field of the Mayak Production Association, Russia. Science 314, 638-641.

56. Penrose, W.R., Polzer, W.L., Essington, E.H., Nelson, D.M., Orlandini, K.A., 1990. Mobility of Plutonium and Americium through a Shallow Aquifer in a Semiarid Region. Environ Sci Technol 24, 228-234.

57. Powell, B.A., Duff, M.C., Kaplan, D.I., Fjeld, R.A., Newville, M., Hunter, D.B., Bertsch, P.M., Coates, J.T., Eng, P., Rivers, M.L., Serkiz, S.M., Sutton, S.R., Triay, I.R., Vaniman, D.T., 2006. Plutonium oxidation and subsequent reduction by Mn(IV) minerals in Yucca Mountain Tuff. Environmental Science and Technology 40, 3508-3514.

58. Powell, B.A., Fjeld, R.A., Coates, J.T., Kaplan, D.I., Serkiz, S.M., 2003. Plutonium Oxidation State Geochemistry in the SRS Subsurface Environment (U). Westinghouse Savannah River Company

59. Clemson University, Aiken, SC.

60. Powell, B.A., Fjeld, R.A., Kaplan, D.I., Coates, J.T., Serkiz, S.M., 2004. Pu(V)O2+ adsorption and reduction by synthetic magnetite (Fe3O4). Environmental Science and Technology 38, 6016-6024.

61. Powell, B.A., Fjeld, R.A., Kaplan, D.I., Coates, J.T., Serkiz, S.M., 2005. Pu(V)O2+ adsorption and reduction by synthetic hematite and goethite. Environmental Science and Technology 39, 2107-2114.

62. Powell, B.A., Kaplan, D.I., Serkiz, S.M., Coates, J.T., Fjeld, R.A., 2014. Pu(V) transport through Savannah River Site soils - an evaluation of a conceptual model of surface- mediated reduction to Pu (IV). J Environ Radioact 131, 47-56.

63. Quik, J.T., Stuart, M.C., Wouterse, M., Peijnenburg, W., Hendriks, A.J., van de Meent, D., 2012. Natural colloids are the dominant factor in the sedimentation of nanoparticles. Environ Toxicol Chem 31, 1019-1022.

64. Reiller, P., Evans, N.D.M., Szabo, G., 2008. Complexation parameters for the actinides(IV)-humic acid system: a search for consistency and application to laboratory and field observations. Radiochimica Acta 96, 345-358.

65. Reiller, P., Moulin, V., Casanova, F., Dautel, C., 2002. Retention behavior of humic substances onto mineral surfaces and consequences upon thorium (IV) mobility: case of iron oxides. Applied Geochemistry 17, 1551-1562.

66. Reiller, P., Moulin, V., Casanova, F., Dautel, C., 2003. On the study of Th(IV)-humic acid interactions by competition sorption studies with silica and determination of global interaction constants. Radiochimica Acta 91, 513-524.

67. Righetto, L., Bidoglio, G., Azimonti, G., Bellobono, I.R., 1991. Competitive Actinide Interactions in Colloidal Humic Acid-Mineral Oxide Systems. Environ Sci Technol 25, 1913-1919.

68. Righetto, L., Bidoglio, G., Marcandalli, B., Bellobono, I.R., 1988. Surface Interactions of Actinides with Alumina Colloids. Radiochimica Acta 44/45, 73-75.

69. Roberts, K.A., Santschi, P.H., Honeyman, B.D., 2008. Pu(V) reduction and enhancement of particle-water partitioning by exopolymeric substances. Radiochimica Acta 96, 739-745.

70. Romanchuk, A.Y., Kalmykov, S.N., Aliev, R.A., 2011. Plutonium sorption onto hematite colloids at femto- and nanomolar concentrations. Radiochimica Acta 99, 137-144.

71. Ryan, J.N., Elimelech, M., 1996. Colloid Mobilization and Transport in Groundwater. Colloids Surface A 107, 1-56.

72. Sanchez, A.L., Murray, J.W., Sibley, T.H., 1985. The adsorption of plutonium IV and V on goethite. Geochimica et Cosmochimica Acta 49, 2297.

73. Santschi, P.H., Roberts, K.A., Guo, L.D., 2002. Organic mature of colloidal actinides transported in surface water environments. Environmental Science & Technology 36, 3711-3719.

74. Schrick, B., Hydutsky, B.W., Blough, J.L., Mallouk, T.E., 2004. Delivery vehicles for zerovalent metal nanoparticles in soil and groundwater. Chem. Mater. 16, 2187-2193.

75. Schwantes, J.M., Santschi, P.H., 2010. Mechanisms of plutonium sorption to mineral oxide surfaces: new insights with implications for colloid-enhanced migration. Radiochimica Acta 98, 737-742.

76. Seijo, M., Ulrich, S., Filella, M., Buffle, J., Stoll, S., 2009. Modeling the Adsorption and Coagulation of Fulvic Acids on Colloids by Brownian Dynamics Simulations. Environ Sci Technol 43, 7265-7269.

77. Shaughnessy, D.A., Nitsche, H., Booth, C.H., Shuh, D.K., Waychunas, G.A., Wilson, R.E., Gill, H., Cantrell, K.J., Serne, R.J., 2003. Molecular interfacial relations between Pu(VI) and manganese oxide minerals manganite and hausmannite. Environmental Science and Technology 37, 3367-3374.

78. Shcherbina, N., Perminova, I.V., Kalmykov, S.N., Kovalenko, A.N., Haire, R.G., Novikov, A.P., 2007a. Redox and complexation interactions of neptunium(V) with quinonoid-enriched humic derivatives. Environmental Science and Technology 41, 7010-7015.

79. Shcherbina, N.S., Kalmykov, S.N., Perminova, I.V., Kovalenko, A.N., 2007b. Reduction of actinides in higher oxidation states by hydroquinone-enriched humic derivatives. Journal of Alloys and Compounds 444, 518-521.

80. Short, S.A., Lowson, R.T., Ellis, J., 1988. 234U/238U and 230Th/234U activity ratios in the colloidal phases of aquifers in lateritic weathered zones. Geochimica et Cosmochimica Acta 52, 2555.

81. Silva, R.J., Nitsche, H., 1995. Actinide Environmental Chemistry. Radiochimica Acta 70/71, 377-396.

82. Simpkins, L., 2011. The Influence of Natural Organic Matter on Plutonium Sorption to Gibbsite, Environmental Engineering and Earth Science. Clemson University.

83. Sun, H., Gao, B., Tian, Y., Yin, X., Yu, C., Wang, Y., Ma, L.Q., 2006. Kaolinite and lead in saturated porous media: Facilitated and impeded transport. Journal of Environmental Engineering 136, 1305-1308.

84. Tanaka, K., Suzuki, Y., Ohnuki, T., 2009. Sorption and Oxidation of Tetravalent Plutonium on Mn Oxide in the Presence of Citric Acid. Chemistry Letters 38, 1032-1033.

85. Tinnacher, R.M., Honeyman, B.D., 2007. A new method ot radiolabel natural organic matter by chemical reduction with tritiated sodium borohydride. Environ Sci Technol 41, 6776-6782.

86. Vilks, P., Caron, F., Haas, M.K., 1998. Potential for the formation and migration of colloidal material from a near-surface waste disposal site. Applied Geochemistry 13, 31-42.

87. Xie, J.C., Lu, J.C., Lin, J.F., Zhou, X.H., Li, M., Zhou, G.Q., Zhang, J.H., 2013. The dynamic role of natural colloids in enhancing plutonium transport through porous media. Chemical Geology 360, 134-141.

88. Xie, J.C., Lu, J.C., Lin, J.F., Zhou, X.H., Xu, Q.C., Li, M., Zhang, J.H., 2014. Insights into transport velocity of colloid-associated plutonium relative to tritium in porous media. Scientific Reports 4, 8.

89. Xu, C., Santschi, P.H., Zhong, J.Y., Hatcher, P.G., Francis, A.J., Dodge, C.J., Roberts, K.A., Hung, C.C., Honeyman, B.D., 2008. Colloidal Cutin-Like Substances Cross-Linked to Siderophore Decomposition Products Mobilizing Plutonium from Contaminated Soils. Environmental Science & Technology 42, 8211-8217.

90. Zanker, H., Hennig, C., 2014. Colloid-borne forms of tetravalent actinides: a brief review. Journal of contaminant hydrology 157, 87-105.

91. Zavarin, M., Powell, B.A., Bourbin, M., Zhao, P., Kersting, A.B., 2012. Np(V) and Pu(v) ion exchange and surface-mediated reduction mechanisms on montmorillonite. Environ Sci Technol 46, 2692-2698.

92. Zhu, Y., Ma, L.Q., Gao, B., Bonzongo, J.C., Harris, W., Gu, B., 2012. Transport and interactions of kaolinite and mercury in saturated sand media. J Hazard Mater 213-214, 93-99.

93. Zimmerman, T., Zavarin, M., Powell, B.A., 2014. Influence of humic acid on plutonium sorption to gibbsite: Determination of Pu-humic acid complexation constants and ternary sorption studies. Radiochimica Acta 102, 629-643.

CHAPTER SIX

CONCLUSIONS AND FUTURE RESEARCH

Conclusions

This work investigated the mechanisms of colloid-facilitated transport in a step-wise manner with the first three papers investigating specific components necessary to understand colloid-facilitated transport of the actinides. The previously outlined conditions for colloid-facilitated transport of radionuclides were:

1) Colloids must exist in appreciable concentration
2) Colloids must be mobile and stable in the environment of interest
3) Colloids must be able to sorb radionuclides
4) Colloids and the associated radionuclides must be transported through the aquifer

Each of the papers investigated specific systems to better understand the conditions for transport with the exception of the first conditions which has been previously proven by field measurements:

Table 6.1: Summary of papers, system parameters and conditions for colloid-facilitated transport.

Paper	System	Conditions for transport
(1) "Characterization of physical transformations of iron oxide and silver nanoparticles from an intermediate scale field transport study"	Iron oxide NP transport in environmentally relevant sediments (under unsaturated conditions)	Colloids must be mobile and stable in the environment of interest (2)
(2) "On the mechanisms of Pu reduction upon interaction with hematite nanoparticles"	Plutonium sorption and surface-mediated reduction to hematite-NPs	Colloids must be able to sorb radionuclides (3)
(3) "Aging effect of sorption of 32-year-old plutonium complexes on Savannah River Site sediments"	Reversibility of sorption of plutonium following aging on environmentally relevant sediments	Colloids must be able to sorb radionuclides (3)
(4) "Experimental evidence for colloid-facilitated transport of tetravalent actinides on hematite colloids in the presence of Suwanee River fulvic acid"	Tetravalent actinide transport on fulvic acid coated hematite-NPs	Colloids and the associated radionuclides must be transported through the aquifer (4)

The final paper combined each of the components into a laboratory-scale colloid-facilitated transport study and, therefore, addressed all of the conditions for transport.

In the first paper, the transport of iron oxide nanoparticles in Savannah River Site sandy sediment was investigated in unsaturated columns and found that the mobility of iron oxide nanoparticles was most significantly affected by soil coatings. The iron oxide nanoparticles were shown to be aggregated with soil coatings with greater than 99% of nanoparticles remaining within 5 cm of the source after one year. In addition, the ligand

coatings of the nanoparticles rather than the particle composition was the primary component dictating the mobility and aggregation of the particles with the composition of the particles playing a secondary role. The second paper includes the first demonstration of reduction of plutonium on the surface of hematite-NPs based on the loss of the asymmetric Pu=O stretch in ATR FT-IR. In addition, it confirms the strong association of plutonium with iron oxide nanoparticles and the dominance of Pu(IV) as the solid phase oxidation state. This study demonstrated similar sorption and reduction kinetics as compared to previous studies when normalized to the surface concentrations of Pu. This demonstrates that the reactivity of Pu at solid:water interfaces can be scaled with Pu concentration. The third paper shows the irreversibility of plutonium sorption to environmentally relevant sediments. In this work, there were no significant changes in sorption of plutonium with respect to ligands and time. Despite reaction times ranging from years to days, Pu was strongly associated with the soil with greater than 98% sorbed. However, selective extraction experiments leached a greater amount of Pu from soil when interacted for only days relative to the originally added Pu which reacted for approximately 32 years. This demonstrated a change in lability of adsorbed plutonium with time possibly due to a change of surface species.

The final paper incorporated concepts from the previous systems to investigate colloid-facilitated transport of tetravalent actinides on hematite-NPs in the presence of fulvic acid. This work confirmed that SRFA can stabilize and mobilize hematite-NPs most likely by coating NPs under saturated conditions as suggested by previous work. In addition, transport of tetravalent actinides was significantly increased in the presence of

SRFA with or without hematite-NPs in quartz columns. However, significant transport of tetravalent actinides occurred in the presence of hematite-NPs and SRFA with greater than 70% of the actinide associated with the colloidal size fraction, likely as a ternary complex. However, transport of the hematite-NP – An(IV) complex was significantly decreased with the presence of SRFA. The transport of the hematite-NP – An(IV) complex without SRFA was less than transport of the dissolved An(IV) indicating that colloids may indeed reduce the mobility of actinides without a ligand to stabilize the nanoparticles in the aqueous phase. Despite the observations of highly mobile Pu-facilitated transport by SRFA coated hematite-NPs discussed from above experiments with high purity quartz packed columns, transport of the ternary hematite-NP – An(IV) – SRFA complex was insignificant through columns of a Savannah River site sandy sediment. The reduced sorption is hypothesized to be due to interactions with clay and metal oxide coatings on the soil surface.

This work emphasizes the importance of experiments investigating environmentally relevant systems. Observations on systems with pure quartz, silica or other pure minerals will not accurately predict environmental transport of contaminants. This is shown by experiments in the first and fourth paper demonstrating that soil coatings can play a significant role in mobility of iron oxide nanoparticles. Three theories have been presented to explain the mechanisms:

1) Coating-mediated aggregation or destabilization of the particles

2) Adsorption of particles to the clay-sized coating materials

3) Physical entrapment of particles in smaller pores caused by the presence of clay-sized coatings

However, it will be important to remember that these processes may be occurring simultaneously. Therefore, these are working hypotheses of which one may not be solely responsible for decreased mobility of nanoparticles in the presence of natural soil coatings.

The first and fourth paper alsoestablish the importance of ligand coatings on environmental transport of nanoparticles and colloids. In the first paper, it is suggested that the organic matter may have slightly increased mobility of iron oxide nanoparticles in Savannah River Site sandy soil in unsaturated columns. However, the work presented in the fourth paper shows that transport of hematite-NPs was drastically increased in the presence of SRFA in quartz columns. In addition, when the transport of hematite-NP – An(IV) – SRFA is compared to dissolved Pu(IV) and Pu(V) transport (previous work by Powell et al. 2013), the ternary actinide complex moves further within columns of Savannah River site sediments. Therefore, the presence organic matter in environmental systems will play an important role in transport of iron oxide colloids.

The second and third paper demonstrate the strong (largely irreversible) sorption of plutonium to inorganic minerals and the prevalence of the reduced Pu(IV) species in environmental systems. Because of the low solubility of tetravalent actinides, especially plutonium, and strong sorption, these elements are an ideal contaminant for colloid-facilitated transport. If plutonium is adsorbed to a mobile colloid then it is likely that it may transport large distances as desorption is expected to be limited based on these

experiments. While K_ds were decreased for thorium sorption to hematite-NPs in the presence of SRFA in the fourth paper, it is likely that organic matter concentrations will be lower in groundwater environments. In addition, sorption to an inorganic mineral in the presence of an organic ligand is likely kinetically different than desorption from an inorganic mineral by addition of an organic ligand, i.e. the source term will play a role in transport.

Colloids have been previously shown to be ubiquitous in environmental systems. However, transport of contaminants in the presence of inorganic colloids can be increased or decreased depending on the conditions. For example, if a colloid with sorbed/associated An(IV) is mobilized by a coating of natural organic matter as was demonstrated in the fourth paper with hematite-NP – An(IV) – SRFA complexes in quartz columns, transport of the actinides can be significantly increased. Nonetheless, a contaminant's transport may be significantly decreased due to the presence of a colloid as shown by the hematite-NP – An(IV) complexes in quartz columns. Transport of actinides as ternary actinide – ligand – inorganic colloid complexes may be a significant transport mechanism through irreversible sorption of the actinide to an inorganic colloid followed by stabilization of the colloid by organic ligands naturally present or anthropogenically-produced in environmental systems.

Future Work

The research presented in this dissertation has identified several knowledge gaps within the nanoparticle/colloid transport area as well as in environmental actinide chemistry. Both the first and fourth paper identified the need to better understand colloid and nanoparticle interactions with soil coatings as they appear to be a limiting factor in environmental transport. In addition, the second and third paper identify knowledge gaps in our understanding of speciation of adsorbed actinide species and their (ir)reversibility with time. Finally, the fourth paper recognizes a lack of understanding of ternary actinide systems as research has only recently begun investigating these complex systems. The future needs for research in these areas is described in further detail below:

1) Colloid interactions with natural soil coatings
    - Experiments under unsaturated conditions are needed to examine behavior during wet-dry cycling, particularly with a focus on colloid interactions at air:water interfaces
    - Systematic investigation of aggregation/destabilization of colloids in the presence of pure minerals present in soil coatings
    - Kinetics of sorption of different types of colloids to minerals and soil coatings
2) Actinide adsorption to inorganic minerals and sediments
    - Further investigation of Pu reduction kinetics on minerals by ATR FT-IR methods

- Identification of peaks for additional plutonium species by ATR FT-IR and Raman (i.e. Pu-carbonate or Pu-hydroxide peaks)
- Investigation of speciation changes of adsorbed plutonium with time using EXAFS (to clarify changes in lability with time)

3) Actinides in ternary systems
    - Study of ternary complex formation mechanisms and kinetics
    - Model development for transport of ternary actinide complexes

APPENDICES

Appendix A: Supplementary Materials for Paper One

A.1 Supplementary Tables and Figures

Table A.1: Summary of zeta potential and particle size for stock nanoparticle solutions, average of 5 measurements.

Nanoparticle	Particle Diameter (nm)	Zeta Potential (mV)
Magnetite	NM	-37.5±1.9
Magnetite SR-NOM	NM	-37.0±2.3
Silver SR-NOM	33.0±0.9	-36.9±3.7
Silver Citrate	34.3±0.3	-33.2±3.1

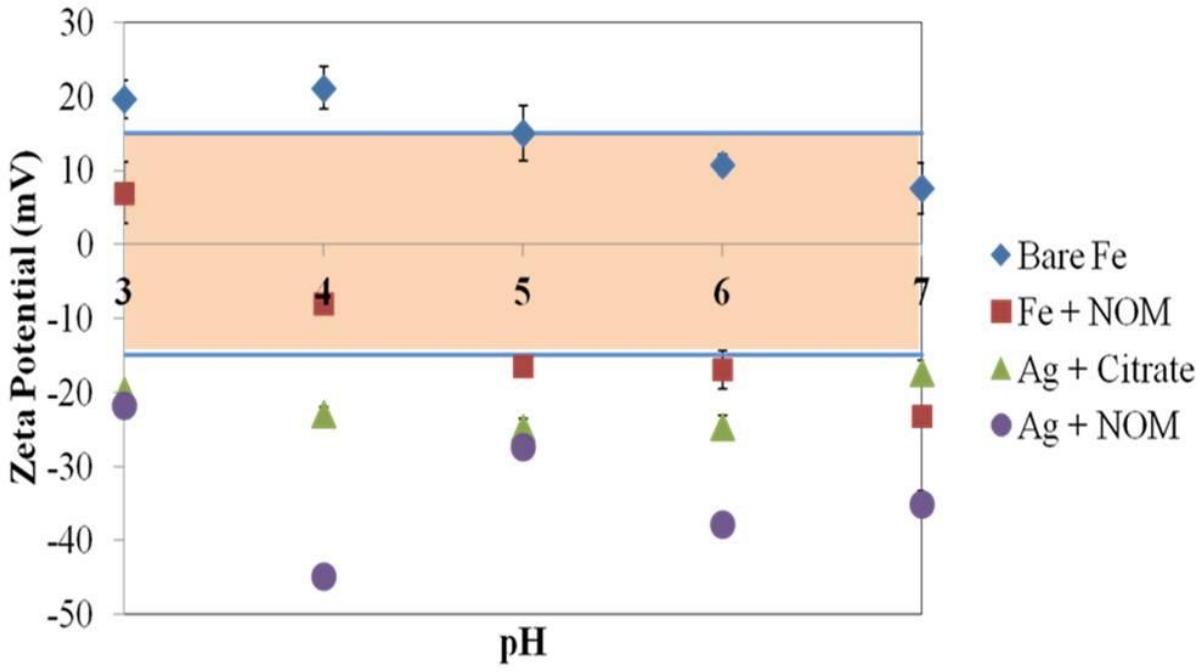

Figure A1: Zeta potential (mV) versus pH for a solution at 0.01 M NaCl, representative of the ionic strength of groundwater for the area in which the soil samples were collected where the colored area represents the area of zeta potential in which particles would be considered unstable in suspension. Results show that both types of silver nanoparticles should be electrostatically stable in suspension, while the iron nanoparticles are borderline. It is assumed that a particle that is stable in suspension will be more mobile than a particle that is not.

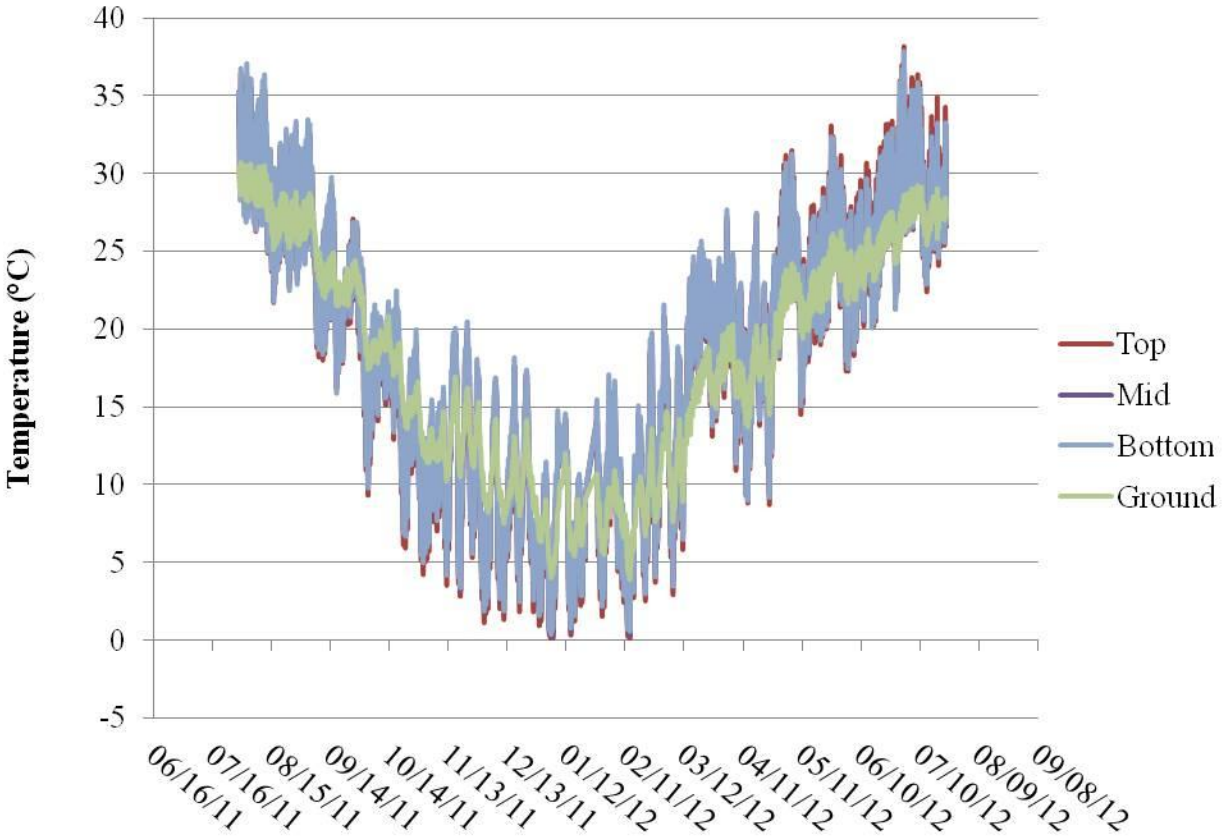

Figure A2: Temperature monitoring for probes at the top, middle, and bottom of the control lysimeter and 10" below the ground surface. While there is a fluctuation of approximately ±5°C for the lysimeter column versus the ground temperature, the average temperature follows that of the ground.

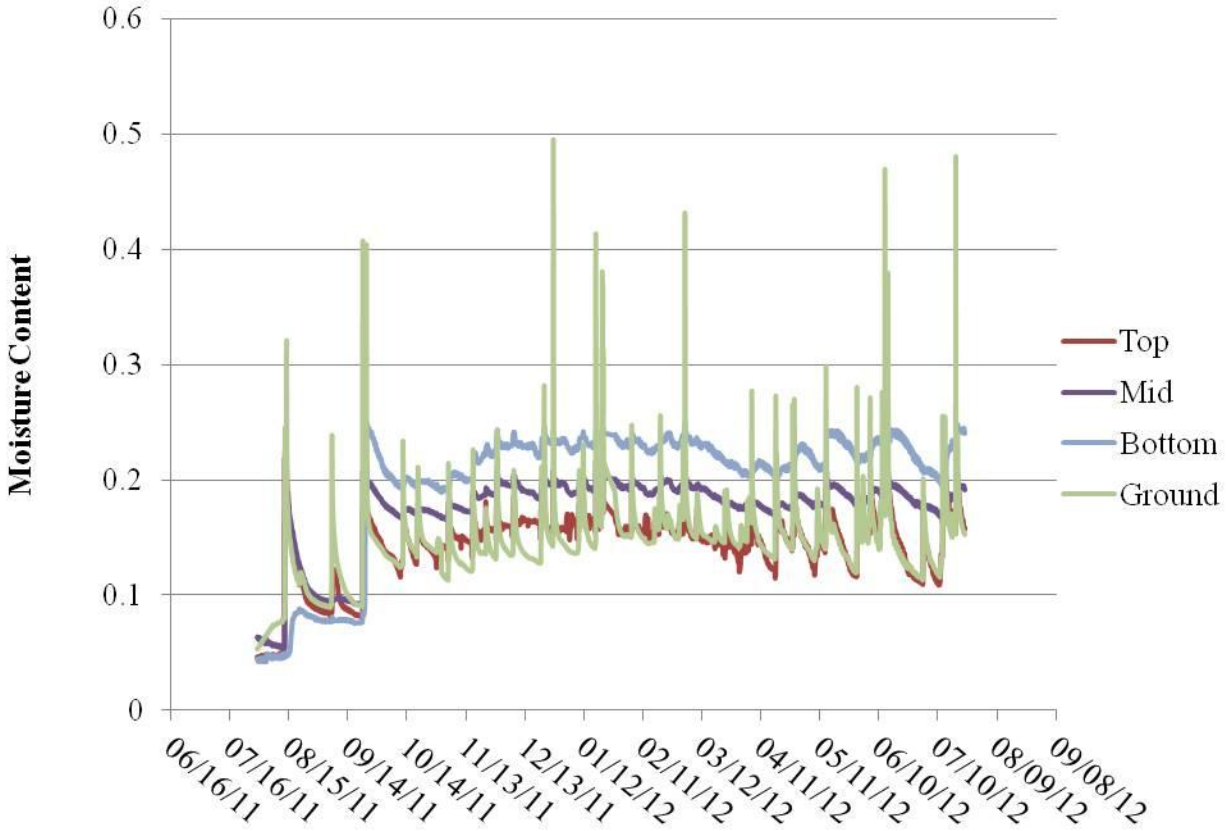

Figure A3: Soil moisture content for probes in the top, middle, and bottom of the control lysimeter and 10" below the ground surface. Each of the "spikes" in the data that are greater than a water content of ≈0.3 represent rain events that were significant enough for breakthrough of rainwater. It is important to note that after the first few rain events, the middle and bottom probes were consistently more saturated, showing that the columns did not dry out over the year of measurements.

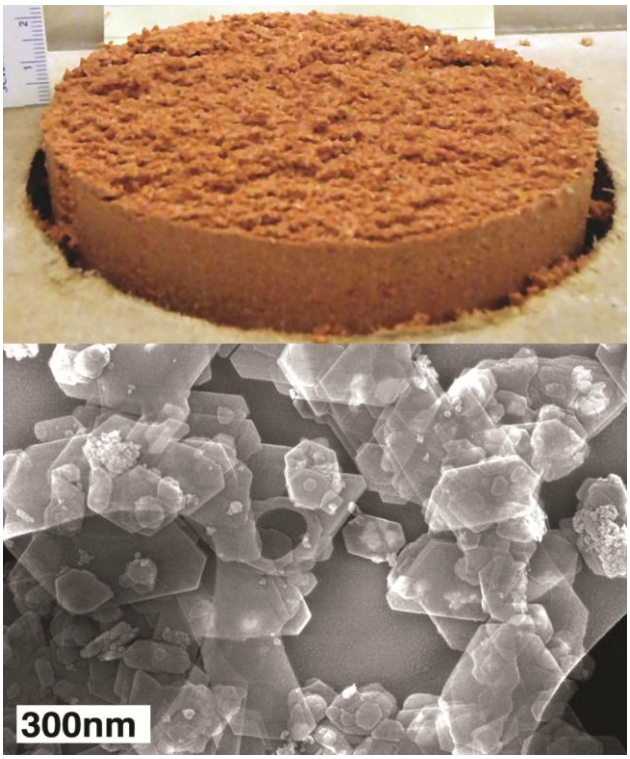

Figure A4: TEM Imaging of the Control lysimeter and clean sediments. The top image shows that the soil was loaded with a homogenous distribution throughout the columns while the lower image shows colloidal-sized kaolinite clay sheet and iron oxide coatings on the soils.

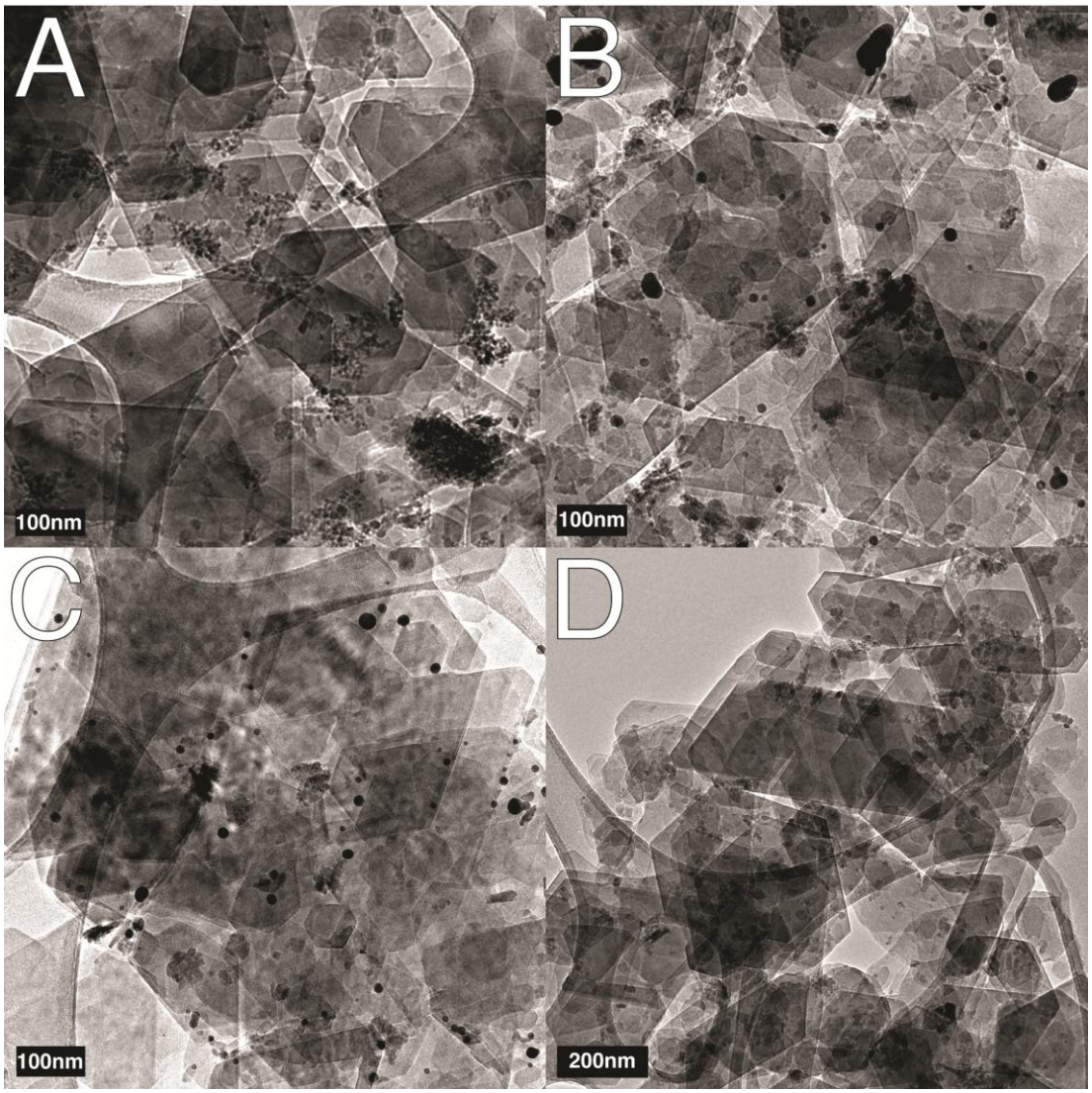

Figure A5: TEM Imaging of the source initial sediments showing the nanoparticles distributed throughout the sediment in the sources, (a) Magnetite SR-NOM, (b) Silver Citrate, (c) Silver SR-NOM, and (d) Silver Dodecanethiol [Bare Magnetite not pictured].

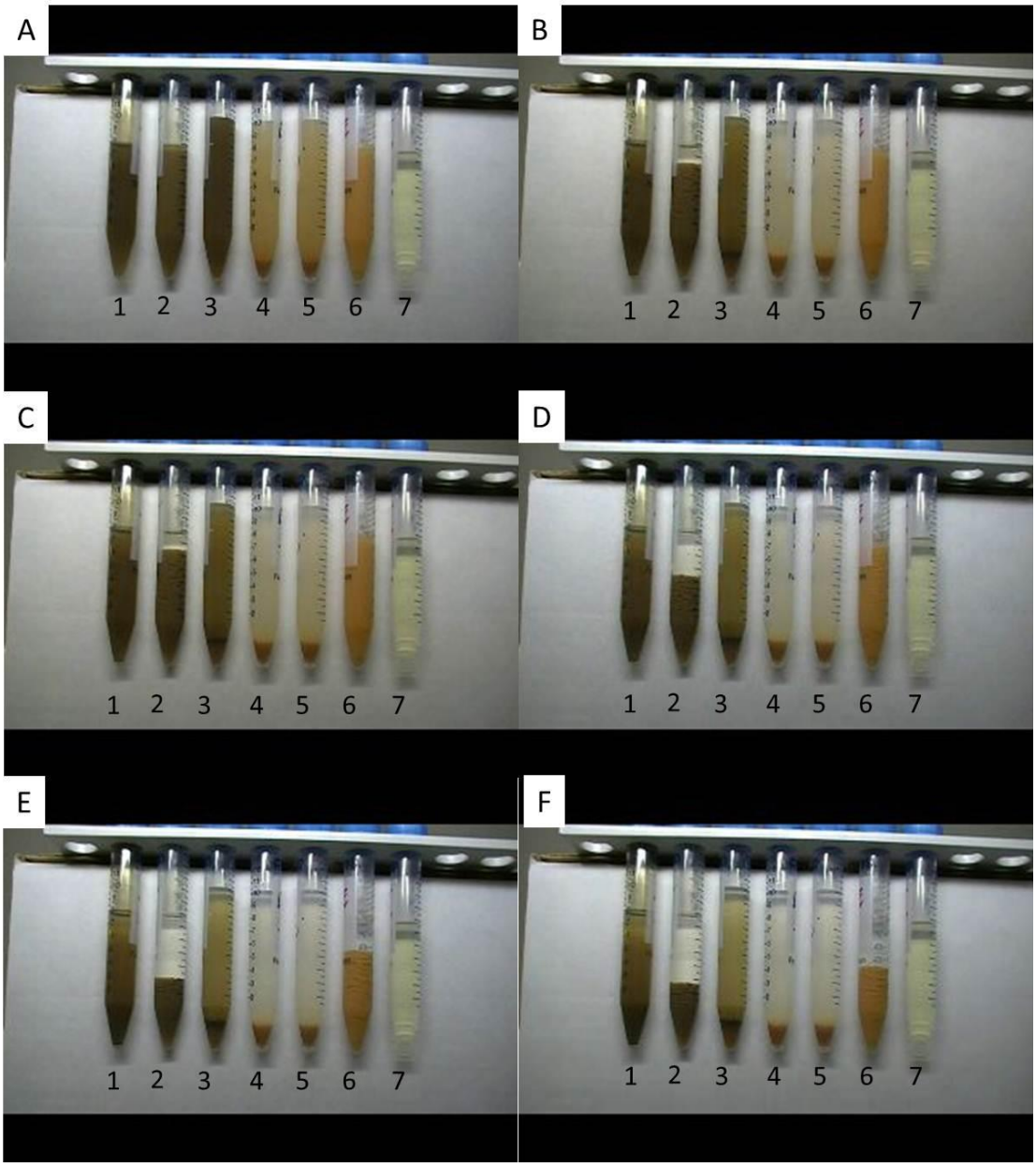

Figure A6: Screen capture images of a video demonstrating "floc" formation in aqueous suspensions containing bare iron and silver-citrate nanoparticles after L to R: 1) Fe particles, no soil, mixed for 2 weeks; 2) Fe particles, soil, mixed for 2 weeks; 3) Fe particles, soil, no mixing; 4) No particles, soil, mixed for 2 weeks; 5) Ag particles, soil, no mixing; 6) Ag particles, soil, mixed for 2 weeks; 7) Ag particles, no soil, mixed for 2

weeks. Screen capture images taken after a) 1 minute, b) 5 minutes, c) 10 minutes, d) 20 minutes, e) 40 minutes, and f) 60 minutes. The video showed that the Ag and Fe oxide nanoparticles associated with the sediment for two weeks causing a "floc" to generate as noted by the remaining suspension in samples 2 and 6. The "floc" was not observed within the soil suspension without nanoparticles mixed for two weeks (sample 4), soil suspensions with nanoparticles added just before making the video (samples 3 and 5), or the nanoparticles in the absence soil (samples 1 and 7). Therefore, it is the reaction of the nanoparticles with the soil coatings that appears to be causing this effect.

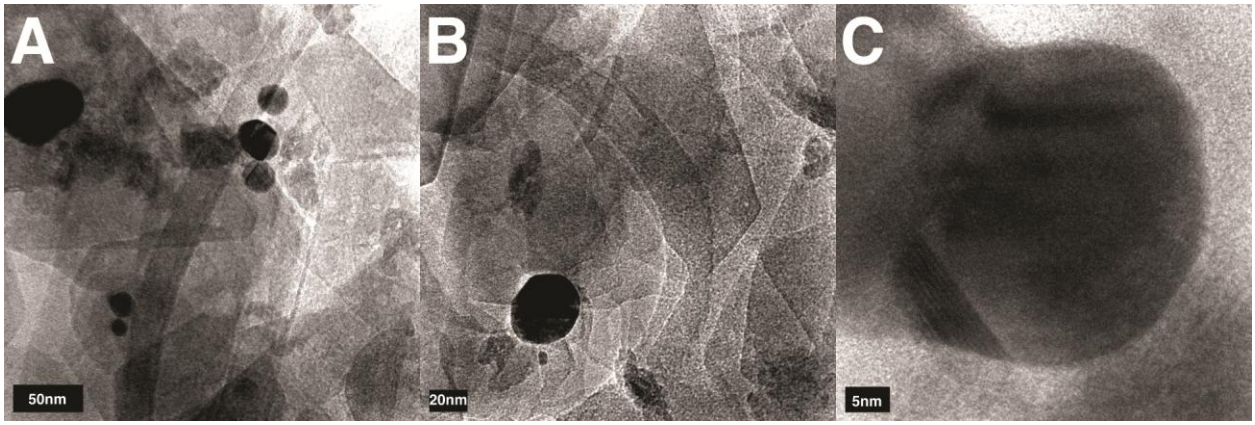

Figure A7: HRTEM imaging of silver citrate lysimeter source materials after one year with (a) and (b) representing the "Bleached" sand materials with the dark spots representing the silver nanoparticle aggregates and (c) a magnification of a single particle associated with remaining clay sheets within the "bleached" sand within the source materials. These images confirm that the silver nanoparticles are associated with the few remaining soil coatings in the "bleached" materials.

A.2 Silver Nanoparticle Synthesis Methods

Materials

Silver nitrate [$AgNO_3$] of 99.995% purity, 99.0% crystalline trisodium citrate dihyrdrate [$C_6H_9Na_3O_9$] and 98+% purity tetra-n-octylammoinum bromide (ToAB) [$C_{32}H_{68}BrN$] were purchased from Alfa Aesar and sodium borahydride [$NaBH_4$] was purchased from EMD Chemicals and Dodecanethiol (DDT) [$CH_3(CH_2)_{10}CH_2SH$] was purchased from TCI corporation. Toluene [C_7H_8] and Chloroform [$CHCl_3$] were purchased BDH. Suwanee River natural organic matter (SR-NOM) was purchased from the International Humic Substances Society.

Synthesis

Silver citrate nanoparticles were synthesized using a method described previously[1, 2]. The synthesis was scaled up to produce 0.6g of silver citrate nanoparticles. In short, a 2.5 L solution of 2.5mM silver nitrate and trisodium citrate dihydrate was prepared in distilled deionized (DDI) water. While mixing, 156 mL of iced, 0.05 M aqueous sodium borahydride was added to the silver nitrate and citrate solution. The solution turned a bright yellow color and was mixed for 15 minutes, then dialyzed for 24 hours to remove excess ligand. Natural organic matter, SR-NOM, stabilized particles were synthesized with the same method; with the addition of 0.124 g of NOM. Silver dodecanethiol nanoparticles were synthesized with a scaled up biphasic synthesis method previously described by Brust[3]. In short, 0.94g of AgNO3 in 180 mL of DI H2O was mixed with 13.4 g of ToAB in 122 mL of chloroform. After one hour of mixing, the aqueous phase was discarded and 1.192 mL of DDT was added. After 15 minutes of mixing, 2.48 g of

NaBH4 in 150 mL of DDI was added and stirred for 12 hours. The aqueous phase was then discarded and the nanoparticle with were washed twice with ethanol and centrifugation. The particles were then redispersed in 50 mL of fresh toluene.

References

1. Brown, K.R., Walter, D. G., Natan, M. J., *Seeding of Colloidal Au Nanoparticle Solutions. 2. Improved Control of Particle Size and Shape.* Chemical Materials, 2000. **12**: p. 306-313.

2. Jana, N.R., Gearheart, L., Murphy, C. J. , *Seeding Growth for Size Control of 5-40 nm Diameter Gold Nanoparticles.* Langmuir, 2001. **17**: p. 6782-6786.

3. Brust, M., Walker, M., Bethell, D., Schiffrin, D. J., Whyman, R., Chemical Communications, 1994: p. 801.

A.3 Iron Oxide Nanoparticle Synthesis Methods

Materials

Ferric chloride ($FeCl_3$) and ferrous chloride ($FeCl_2$) (both from Sigma-Aldrich) were stored under nitrogen in a desiccator and used as received. Distilled deionized (DDI) water was deoxygenated by bubbling nitrogen through the solution for over 30 minutes prior to synthesis. Sodium hydroxide (Sigma-Aldrich, 50%, v/v, aqueous) and hydrochloric acid (Sigma-Aldrich, 6M) were used as received.

Synthesis

Iron oxide nanoparticles were synthesized by the chemical precipitation of iron salts based on techniques developed by Massart[1]. Iron(III) chloride (10.4 g, 64.1 mmol) and iron(II) chloride (4 g, 31.5 mmol) were charged into a round bottom flask along with 48.28 mL of deoxygenated deionized water 1.45 mL of 6M hydrochloric acid. The iron salt solution was then slowly added into a solution containing 60 mL of 50% sodium

hydroxide and 440mL of DDI water and stirred via a magnetic stirrer. Careful attention was paid to maintain an oxygen-free environment by purging the reaction vessel with a heavy flow of nitrogen throughout synthesis. The resulting black suspension of particles were then centrifuged at 6000 rpm and washed with DDI water until the pH of the suspension was neutral.

To produce the SR-NOM coated iron oxide nanoparticles, 6 grams of the iron oxide nanoparticles suspended in 85 mL of DDI water were combined with 99.4 mg of SR-NOM. The resulting suspension was stirred overnight and then dialyzed with DDI water for 48 hours to remove any of the unbound ligand.

References

1. Lefebure, S., Dubois, E., Cabuil, V., Neveu, S., Massart, R. (1998) "Monodisperse magnetic nanoparticles: Preparation and dispersion in water and oils." *Journal of Materials Research*, **13**, 2975-2981.

Appendix B: Supplementary Materials for Paper Two

B.1 Hematite Nanoparticle Characterization

Nanoparticles were characterized via Brookhaven 90Plus particle size and zeta potential analysis, XRD, SEM, EDX, and HRTEM. In addition, total Fe and Fe(II) were determined spectrophotometrically via methods outlined in *Standard Methods for the Examination of Water and Wastewater (Clesceri, Eaton et al. 1996)* and the particle surface area was measured per the N_2(g)-BET method at 77K using a Micromeritics ASAP 2010 physisorption analyzer (Brunhauer, Emmett et al. 1938). A summary of the two particles is presented in Table 1 below. Particle size and zeta potential are reported at a pH=3.15, as determined from 10 consecutive measurements (with 10 cycles per measurement) on the Brookhaven 90Plus particle size and zeta potential analyzer. TEM grids were prepared on copper coated Formvar or Lacy carbon grids (EMS) by air drying 5-10 µL of aqueous suspensions. TEM particle size was estimated using ImageJ software with analysis of over 2300 particles on a Hitachi 9500 HRTEM (Figure B1, Table B1). The discrepancy between TEM imaging and 90Plus particle size is mostly likely due to hydration of particles and aggregation in suspension (Figure B1). The isoelectric point pH_{iep} (pH of zero zeta potential) is around pH 9.0 as approximated from a zeta potential titration from pH 3.2 to 9.6 completed on the Brookhaven 90Plus software as shown in Figure B2. It is within range of the values reported for hematite (7.0-9.3) in literature as compiled by Kosmulski (Hsi and Langmuir 1985, Liger, Charlet et al. 1999, Kosmulski 2002, Kosmulski 2011).

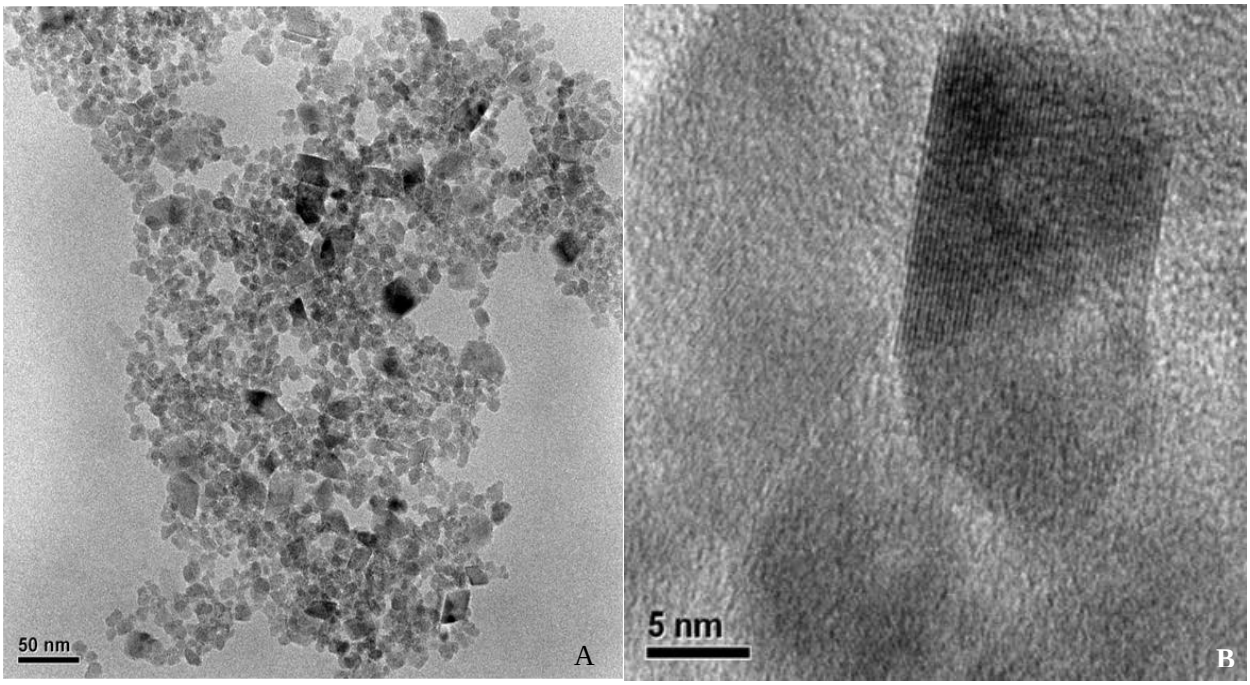

Figure B1: A.) Overview of aerated hematite particles, B.) High resolution image of aerated hematite particles.

Table B1: Characteristics of Fe_2O_3 NP Stocks.

Parameter	**Aerated**	**NonAerated**
Stock Concentration (by ICP-MS) (mg/L)	43.9	26.2
DLS Particle Size (nm)	109±1 nm	202±6 nm
TEM Particle Size (nm)	12.9±6.5 nm	13.7±9.5 nn
BET Surface Area (m^2/g)	68 m^2/g	ND
Fe(II) Content (%)	0.9±0.4%	2.4±0.6%

*ND – not determined

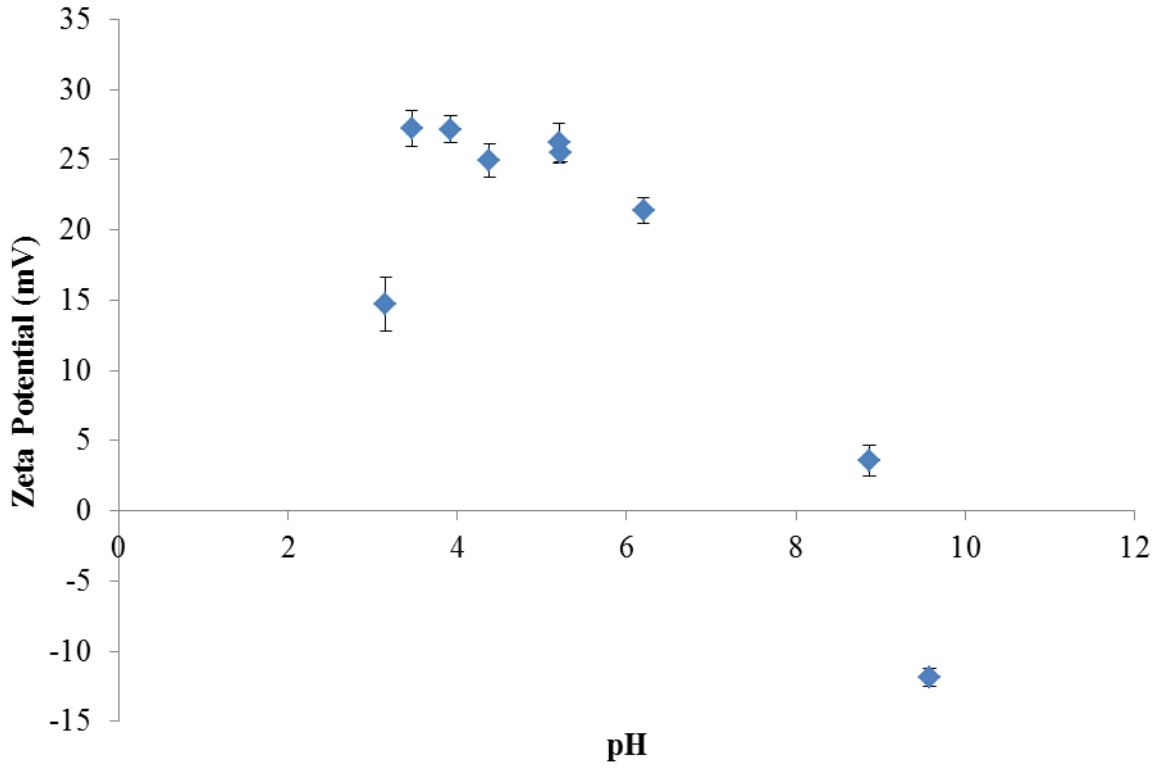

Figure B2: Zeta potential titration of hematite nanoparticles on Brookhaven 90Plus particle size and zeta potential analyzer with error bars representing the standard deviation of ten measurements.

B.2 Oxidation State Analysis for Batch Sorption Experiments

The following figures S3 and S4 show the total (aqueous + solid phase) oxidation state analysis over time at pH 3.6, 5.6, and 7.7 based on solvent extraction and LaF_3 coprecipitation as discussed previously (Hixon, Hu et al. 2010). Error bars are calculated from the propagation of error based on nuclear counting statistics. Figure B5 summarizes the total fraction as Pu(IV) for the batch sorption experiments at pH 6.8 with variable light.

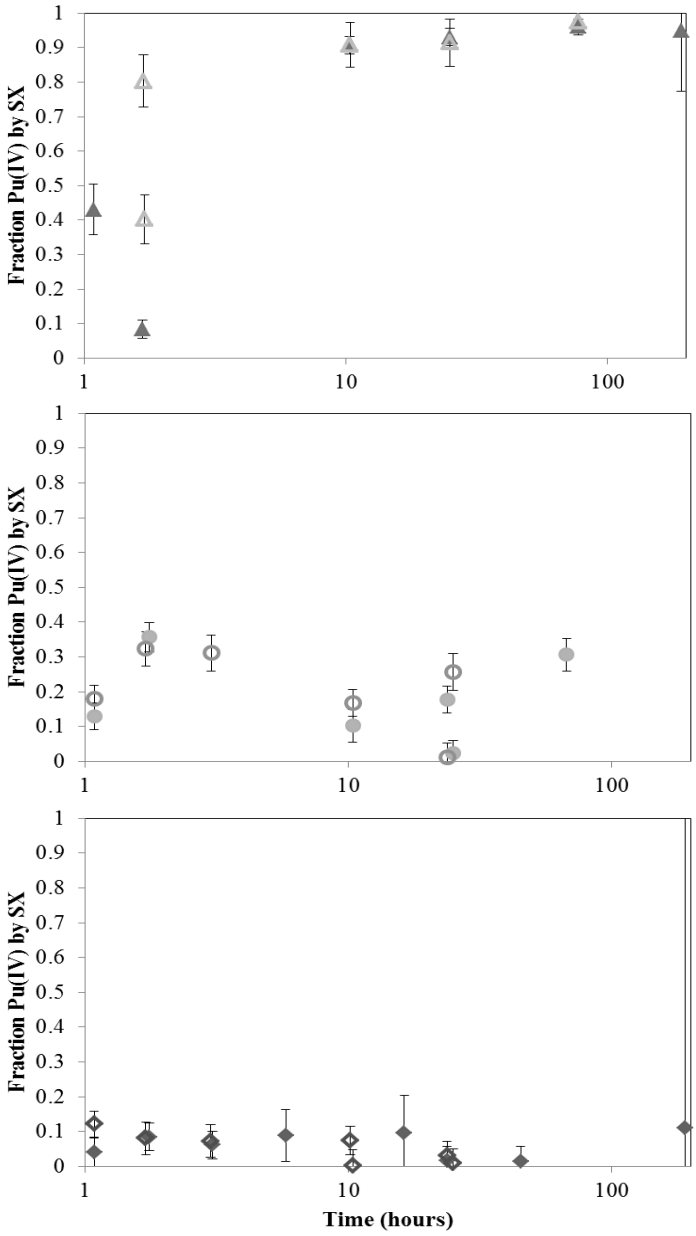

Figure B3: Total Pu(IV) [aqueous + solid phase] throughout batch sorption experiments with respect to time and pH as determined by solvent extraction with Aer-hematite (filled) and NonAer-hematite (unfilled), (1) pH 7.7, (2) pH 5.6, and (3) pH 3.6 over time at $^{238}Pu = 9.2x10^{-11}$ M, 0.01 M NaCl, 7 mg/L hematite NPs.

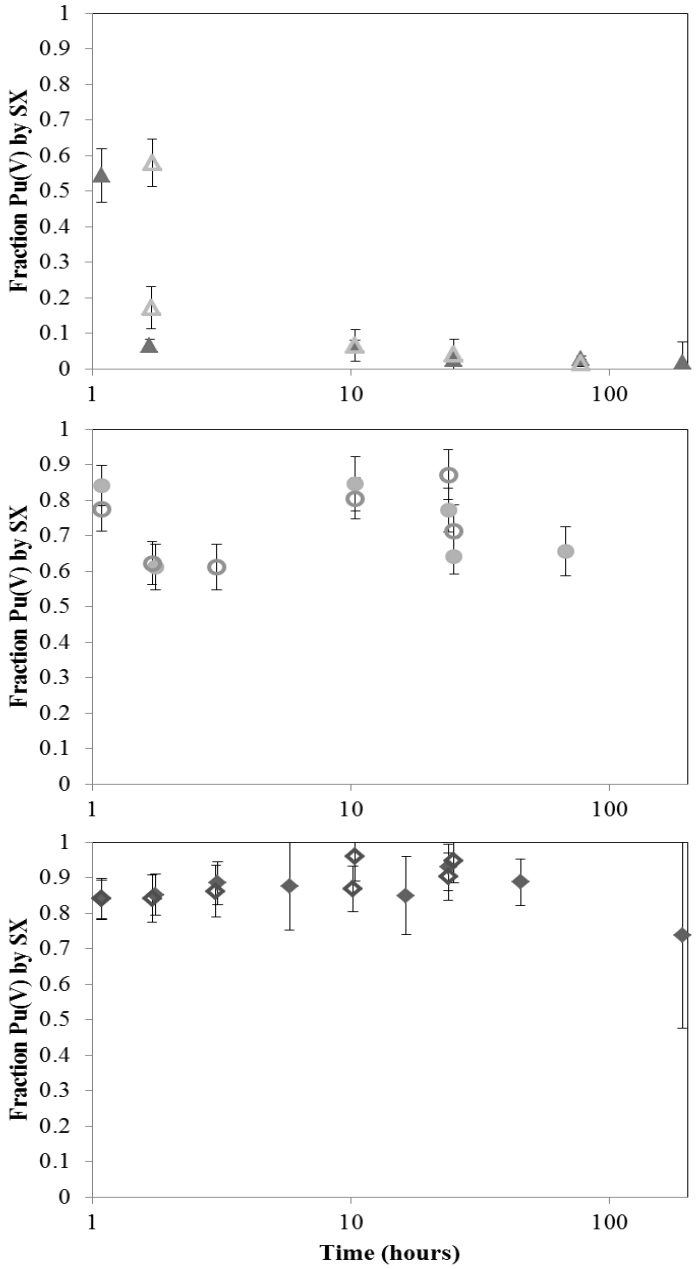

Figure B4: Total Pu(V) [aqueous + solid phase] throughout batch sorption experiments with respect to time and pH as determined by solvent extraction with Aer-hematite (filled) and NonAer-hematite (unfilled), (1) pH 7.7, (2) pH 5.6, and (3) pH 3.6 over time at $^{238}Pu = 9.2x10^{-11}$ M, 0.01 M NaCl, 7 mg/L hematite NPs.

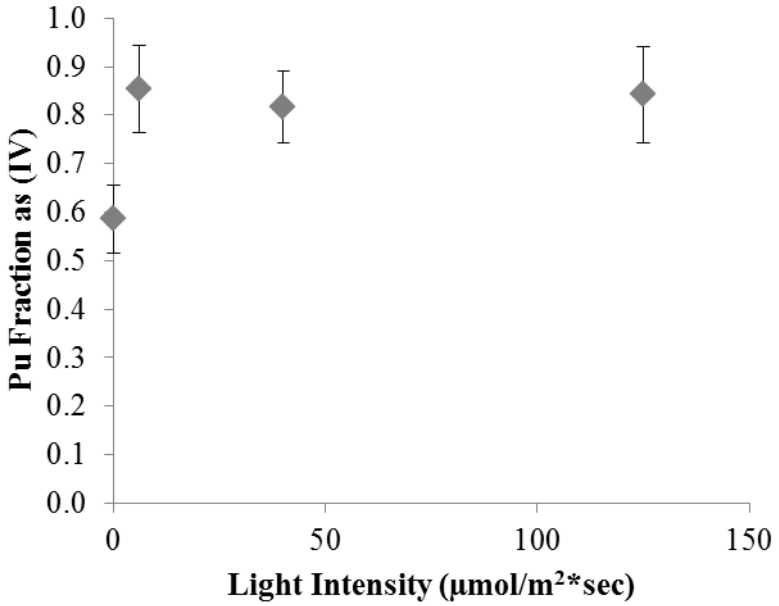

Figure B5: Batch results for ^{238}Pu ($9.2x10^{-11}$ M) reduction in the presence of 17 mg/L Aer-Fe_2O_3 over time with variable light intensity at pH 6.8±0.1.

B.3 Statistical Analysis of Batch Sorption Experiments

Statistical analysis (Table B2) is based on the F_{test} statistic calculated from the variances (s^2) of both the aerated and nonaerated datasets as shown in Eq.1 (van Reeuwijk and Houba 1998). The variance is calculated based on a nonlinear regression of the total Pu(IV) in the system over time at each pH and is compared to the F_{stat} statistic based on the degrees of freedom (DOF) for each dataset. The F-statistic is based on a 95% confidence level.

$$F = \frac{{S_{nonaer}}^2}{{S_{aer}}^2} \quad \text{Eq. 1}$$

Table B2: Statistical Comparison of Batch Sorption Datasets based on F-test.

pH	Aerated variance	NonAerated variance	F_{test}	F_{stat} (by DOF)(van Reeuwijk and Houba 1998)	Significance
7.7	0.046	0.054	1.2	5.19	No
5.6	0.014	0.012	1.2	5.05	No
3.6	0.001	0.002	1.5	3.79	No

B.4 ATR FT-IR for $^{237}Np(V)$ and $^{238}U(VI)$ on Fe_2O_3 Nanoparticles

Batch sorption experiments of $^{238}U(VI)$ and $^{237}Np(V)$ at pH 7 in 0.2 g/L suspensions of Fe_2O_3 nanoparticles were analyzed over time on the FTIR-ATR in order to estimate peak locations for plutonium sorption to Fe_2O_3 nanoparticles and to compare with previous studies on bulk Fe_2O_3. To prepare sub samples for the FTIR-ATR, each sample was centrifuged at 10,000 rpm for 5 minutes, washed with ultrapure (UP, 18 MΩ) water adjusted to pH 7 and centrifuged again to concentrate the solid phase and prevent precipitation of the actinides from the aqueous phase following plating onto the ATR FT-IR crystal. Figure 2 compares two $^{238}U(VI)$ samples analyzed after one hour of sorption with one being subjected to the wash step described above and one plated onto the ATR FT-IR crystal immediately following the first centrifuge step. It is clear that precipitation of $^{238}U(VI)$ results in a peak at 1052 cm^{-1}. This seems to be consistent with precipitation which was previously identified as being near 1000 cm^{-1} (Allen, Bucher et al. 1997, Lefevre, Noinville et al. 2006). Figure B6 shows the aqueous phase ATR FT-IR measurements.

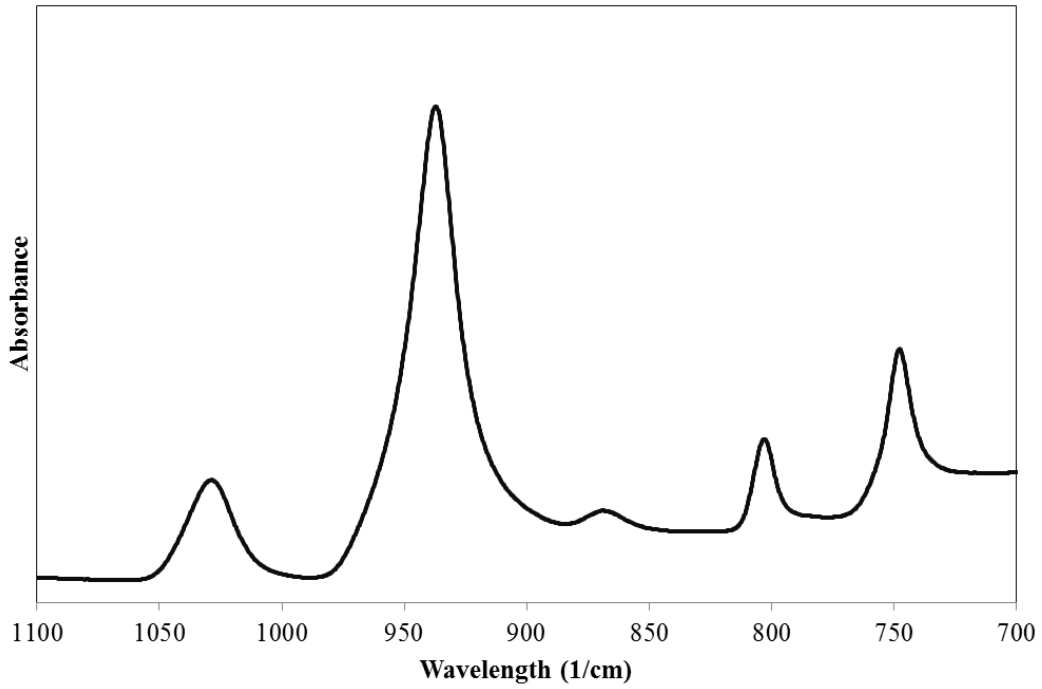

Figure B6: ATR FT-IR spectra of the aqueous stock solution of $^{238}U(VI)$ at 150 µM at pH 7.

^{237}Np batch sorption experiments were also completed at a concentration of 173 µM $^{237}Np(V)$ and 0.2 g/L Fe_2O_3 nanoparticles at pH 7 and analyzed in the same manner as the $^{238}U(VI)$ samples. Over 74 hours the fraction of ^{237}Np sorbed to the Fe_2O_3 increased to 53%. Unfortunately the sorbed Np(V) was difficult to differentiate as it fell into a region of high background from the solid phase (Figure 3). However, based on previous experimental measurements and theoretical estimates of the aqueous Np(V) species, our measurement around 790 cm^{-1} is within range (Jones and Penneman 1953, Hay, Martin et al. 2000, Shamov and Schreckenbach 2005, Muller, Foerstendorf et al. 2009). From Figure B10, the aqueous $Np(V)O_2^+$ peak is near 833 cm^{-1} which is near previous

experiment and theoretical work. The strong absorbance near 1350 cm^{-1} is consistent with residual NO_3 (Figure B7).

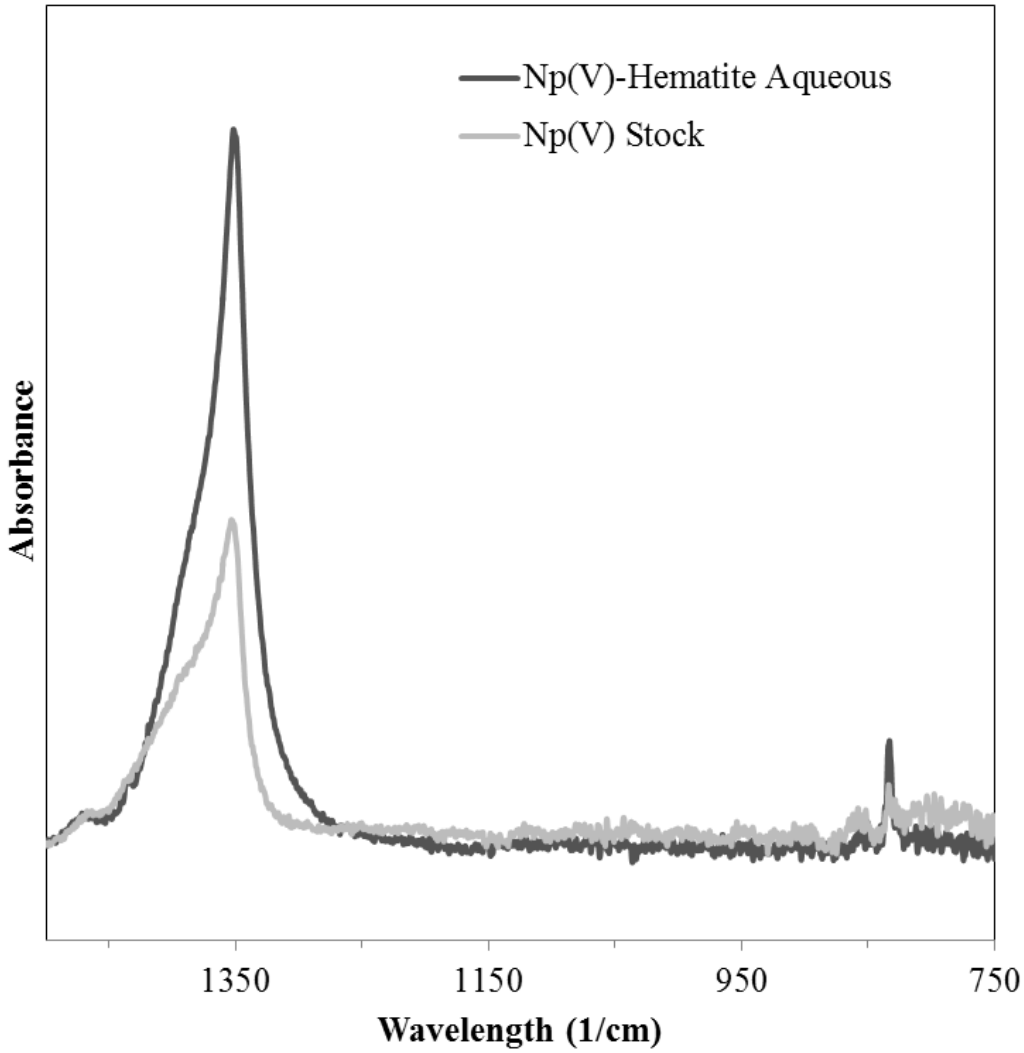

Figure B7: ATR FT-IR spectra of the aqueous stock solution of $^{232}Np(V)$ at 150 µM at pH 7.

B.5 ATR FT-IR of the aqueous phase of batch sorption experiments for Pu(V/VI) on Fe_2O_3 nanoparticle

The following (Figure B8-9) presents the ATR FT-IR absorbance spectra for the aqueous phase of 65 µM ^{242}Pu batch samples prepared at pH 6.99 and the 150 µM ^{242}Pu stock solution. The strong peaks around 1100 cm^{-1} are consistent with precipitation as the aqueous solution is dried on the crystal similar to that noted with U(VI). It appears the drying process will induce precipitation in these aqueous samples. For this reason and to minimize the potential of an experimental artifact, all hematite suspensions were washed to remove aqueous Pu prior to drying on the ATR crystal.

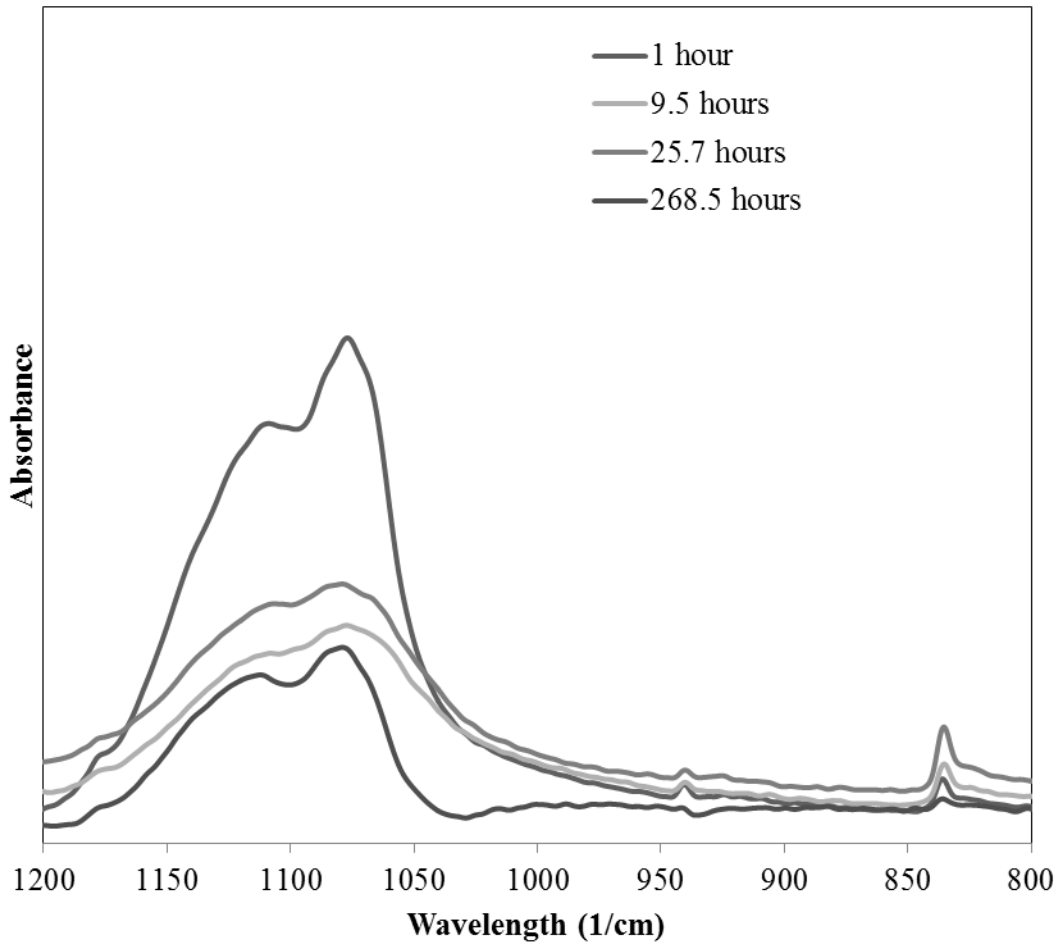

Figure B8: Aqueous ^{242}Pu(V/VI) ATR FT-IR absorbance with time for 65 µM ^{242}Pu.

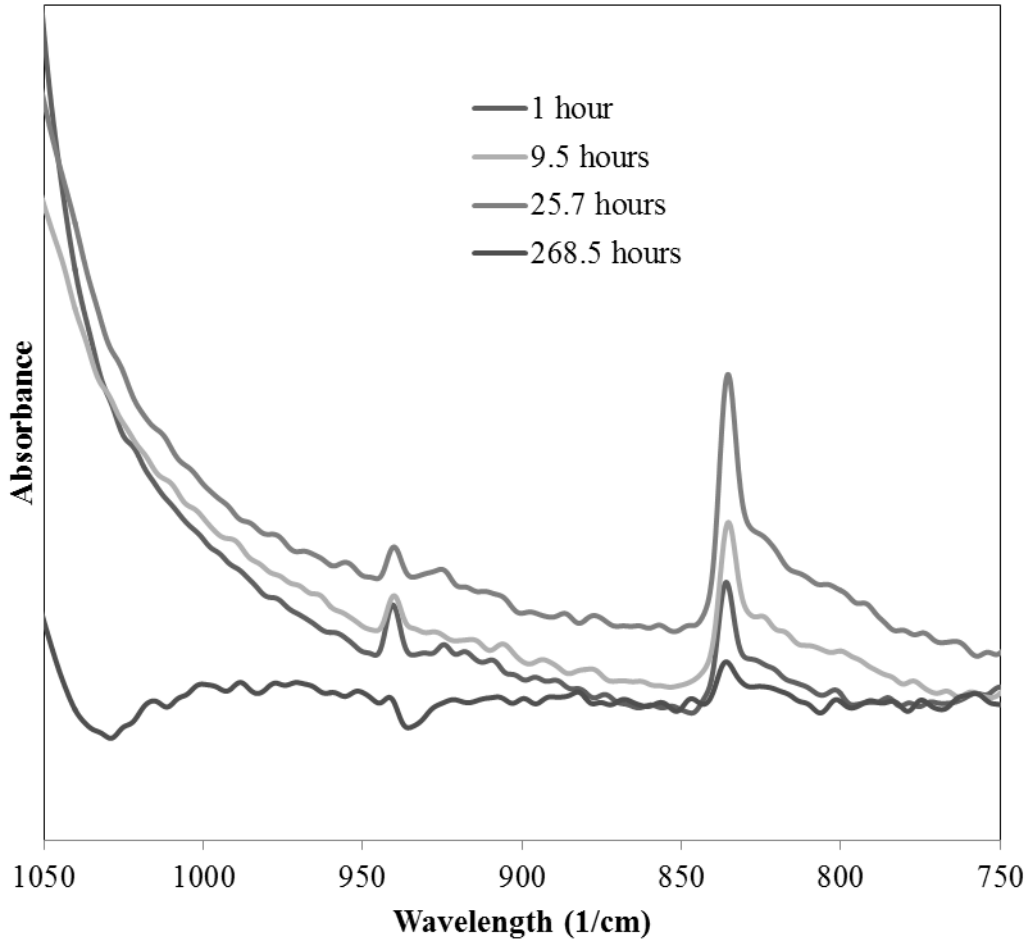

Figure B9: Aqueous ^{242}Pu(V/VI) ATR FT-IR absorbance with time for 65 µM ^{242}Pu reacted with 0.06 g/L Fe_2O_3.

B.6 Kinetic analysis of Pu(V/VI) reduction to Pu(IV) on Fe_2O_3 Nanoparticles

Two kinetic parameters can be determined from the data presented in this study including an adsorption and a reduction rate constant for Pu. First-order adsorption rate constants (k_{ads}) describe the adsorption of plutonium to the solid phase and are based upon measurement of the aqueous plutonium concentration. First-order reduction rate

constants (k_{red}) describe the reduction of Pu(V) to Pu(IV) on the hematite surface and are based upon results from the oxidation state analysis procedure described above. In this work, it is assumed that all kinetic rates follow a first order model.

First-order adsorption rate constants were obtained from

$$\frac{d[Pu]_{aq}}{dt} = -k_{ads}[Pu]_{aq} \qquad \text{Eqn. 2}$$

Equation 2 was integrated so that a plot of $\ln([Pu]_{aq,t}/[Pu]_{aq,0})$ versus time yields the first-order adsorption rate constant (k_{ads}) as the slope. Pseudo-first order adsorption rate constants were estimated based on the change in aqueous Pu concentrations over time for the batch sorption experiments at pH 7.7 (^{238}Pu at 4.7 x 10^{-9} M, 6.9 mg/L hematite, 0.01 M NaCl) using Eqn. 2. There was insufficient adsorption at pH 3.6 and 5.6 to estimate the adsorption rate. It must be noted that it has been previously determined that at low plutonium concentrations (< 10^{-7} M Pu) the adsorption step (not reduction) is the rate limiting step [16, 24]. However, at higher concentrations (>10^{-6} M Pu) reduction is the rate limiting step in the reaction kinetics. Thus, the reaction rates determined based the sorption rate at low Pu concentrations are indeed a reduction rate. However, at higher Pu concentrations, such as those for the ATR FT-IR data described here, where sorbed Pu(V) or Pu(VI) persists for an observable time, a true reduction rate can be determined based on the loss of Pu(V/VI) from the system.

$$\frac{df_s^{ox}}{dt} = -k_{red}f_s^{ox} \qquad \text{Eqn. 3}$$

Where f_s^{ox} is the fraction of Pu(V/VI) in the solid phase. Equation 3 was integrated so that a plot of $ln(f_{s,t}^{ox}/f_{s,0}^{ox})$ versus time yields the first-order reduction rate constant (k_{red}) as the slope. First order reduction rate constants were estimated based on the ATR FT-IR data for Pu based on the integration of Eqn. 3 (further explanation within *Supplementary Materials F*), where f_{ox} represents the total oxidized fraction of Pu(V/VI) and k_{red} is the reduction rate (day^{-1}). It is important to note that for this work f_{ox} is the baseline and ATR corrected PuO_2^{2+} peak area (fit using Grams software) at a given time normalized to the initial peak area. Using the peak areas in this quantitative sense assumes that the same mass of hematite and Pu was deposited on the ATR crystal for each sample measurement. Routinely the peak would be normalized to a consistent, known peak to account for changes in sample mass deposited on the crystal. However, such a peak was not available in the spectra. The consistency in sample manipulation and deposition on the ATR crystal provides some assurance that a similar mass was applied each time. The reduction rate constant is determined based on data gathered up to 5 days (utilizing only the first two sub-samples) as the peak effectively decreases back to the baseline after this time point.

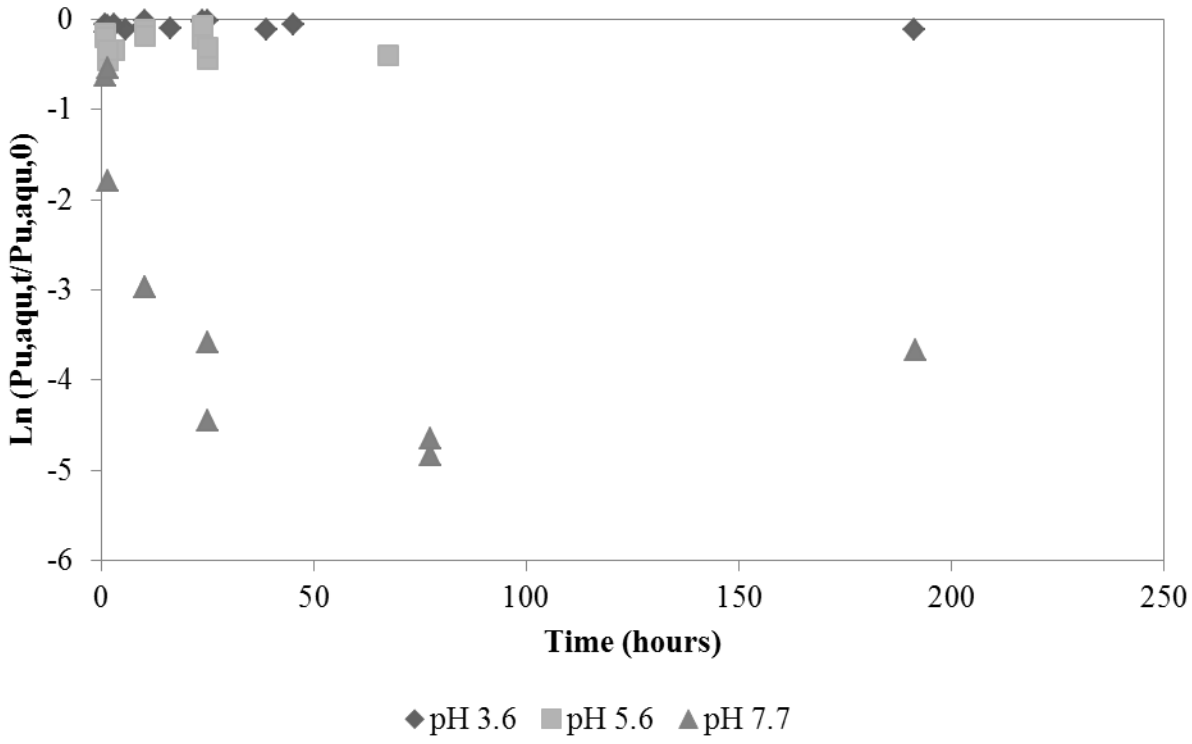

Figure B10: $Ln(Pu_{aqu,t}/Pu_{aqu,0})$ graphed with respect to time and shown for pH 3.6 (diamonds), 5.6 (squares) and 7.7 (triangles) at $9.2x10^{-11}$ M ^{238}Pu and 7 mg/L hematite.

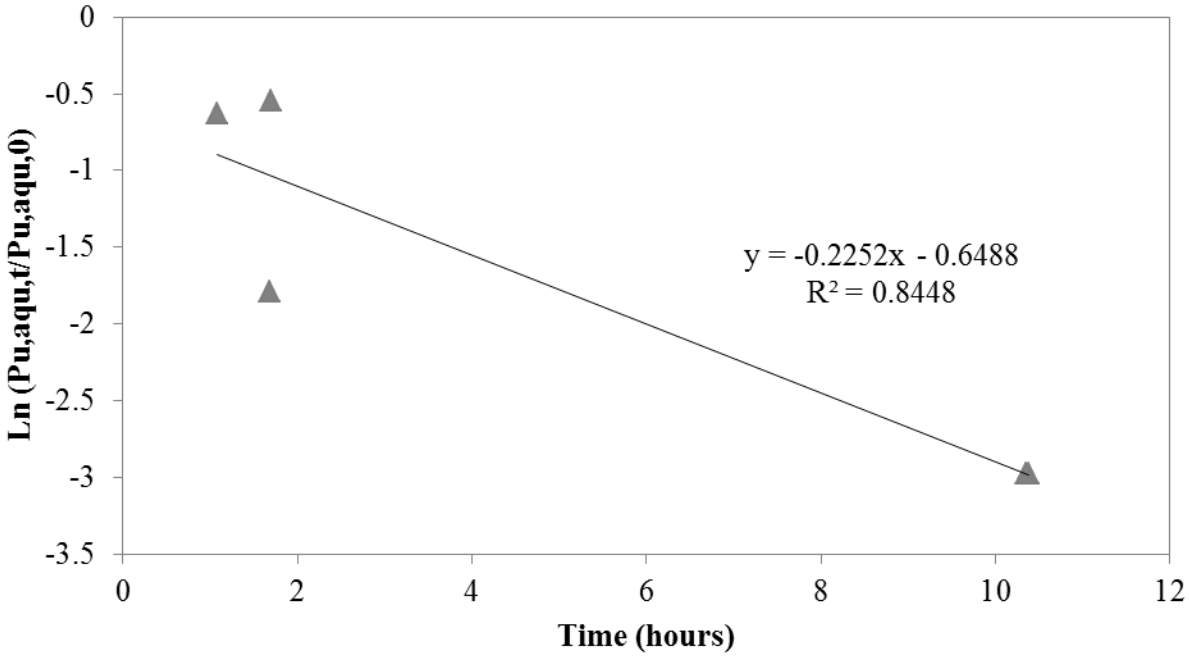

Figure B11: Linear (first order) fit for the K_{abs} at pH 7.7, where slope = K_{abs} = 0.23 $hour^{-1}$ for sorption of $9.2x10^{-11}$ M ^{242}Pu to 7 mg/L Fe_2O_3.

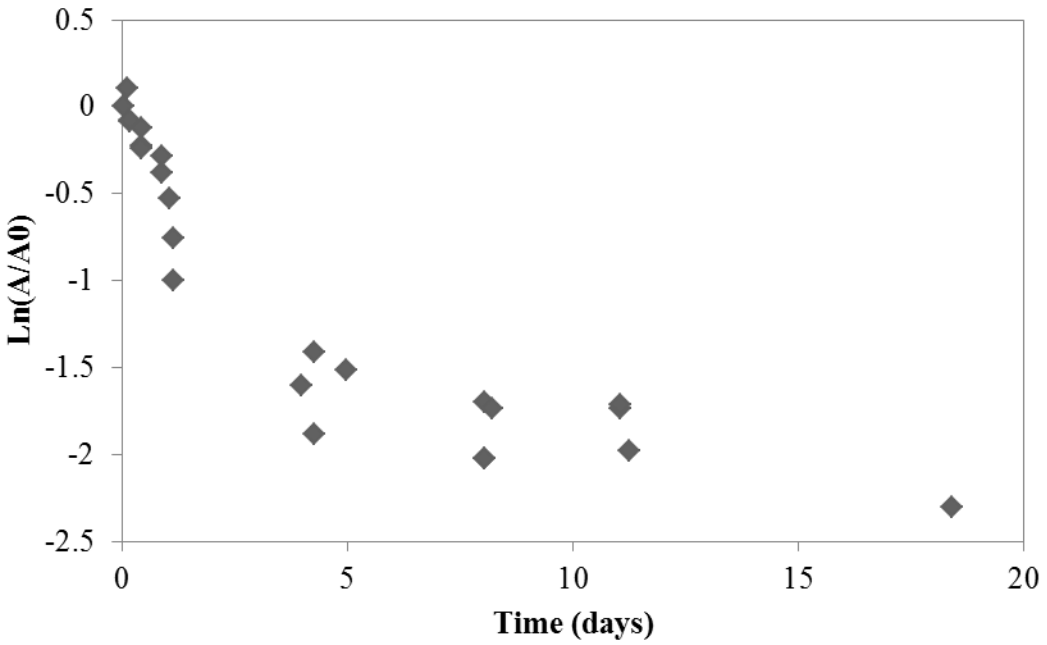

Figure B12: ATR FT-IR data in terms of peak area change [$Ln(A_t/A_0)$] for sorption of 65 µM ^{242}Pu sorption to 0.06 g/L Fe_2O_3 at pH 6.99.

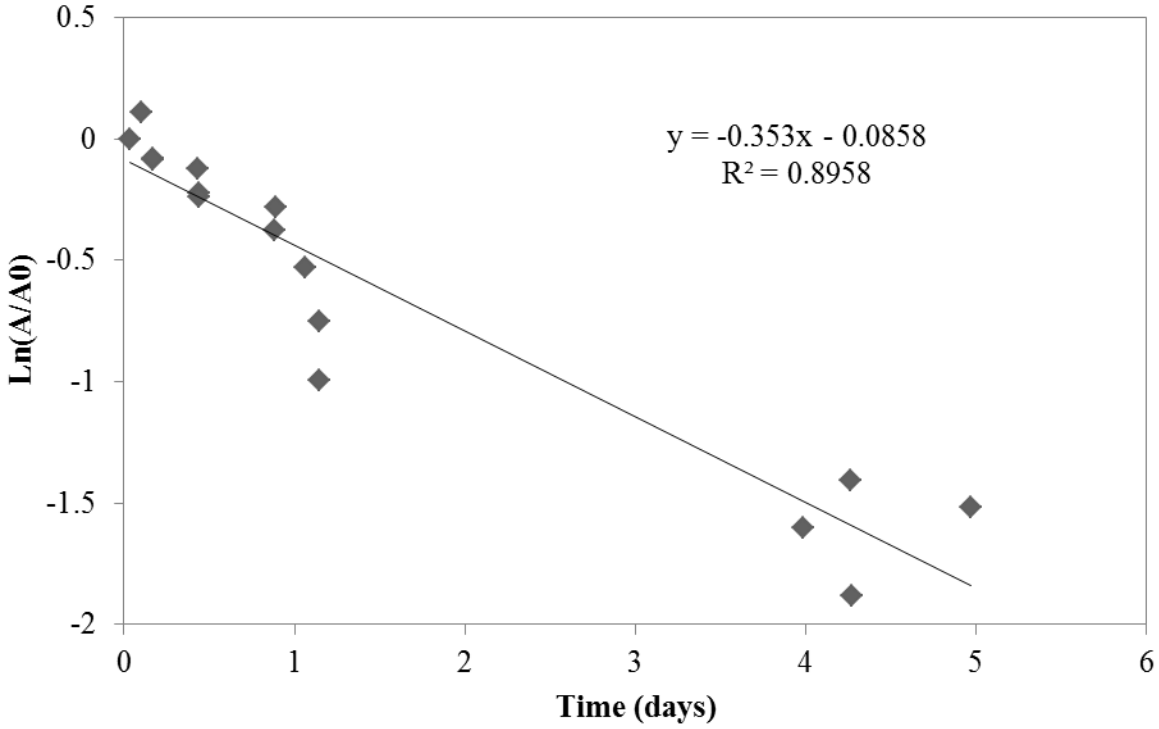

Figure B13: Linear (first order) fit for the K_{red} at pH 6.99, where slope = K_{red} = 0.353 $hour^{-1}$ for sorption of $9.2x10^{-11}$ M ^{242}Pu to 7 mg/L Fe_2O_3.

Table B3: First order kinetic rates determined in this study.

pH	K (1/day)	Pu (mol/L)	Hematite (m^2/L)	Hematite (g/L)
6.99	0.353	6.5E-05	4.08	0.06
7.7±0.2	5.405	9.2E-11±2.0E-12	0.48±0.13	0.007

The following figures S14-15 compare the kinetic parameters determined in this study to those determined at similar concentrations in previous works on Fe_2O_3. Figure B14 compares data for K_{ads} at a lower Pu/solid ratio and Figure B15 compares the high loading ATR FT-IR K_{red} to K_{ads} constants determined at a lower solids loading. While Figure B15 is comparing different kinetic constants, it is important to note that Hixon and Powell showed that the rates are similar at these higher Pu/solid loadings (Hixon and Powell 2014).

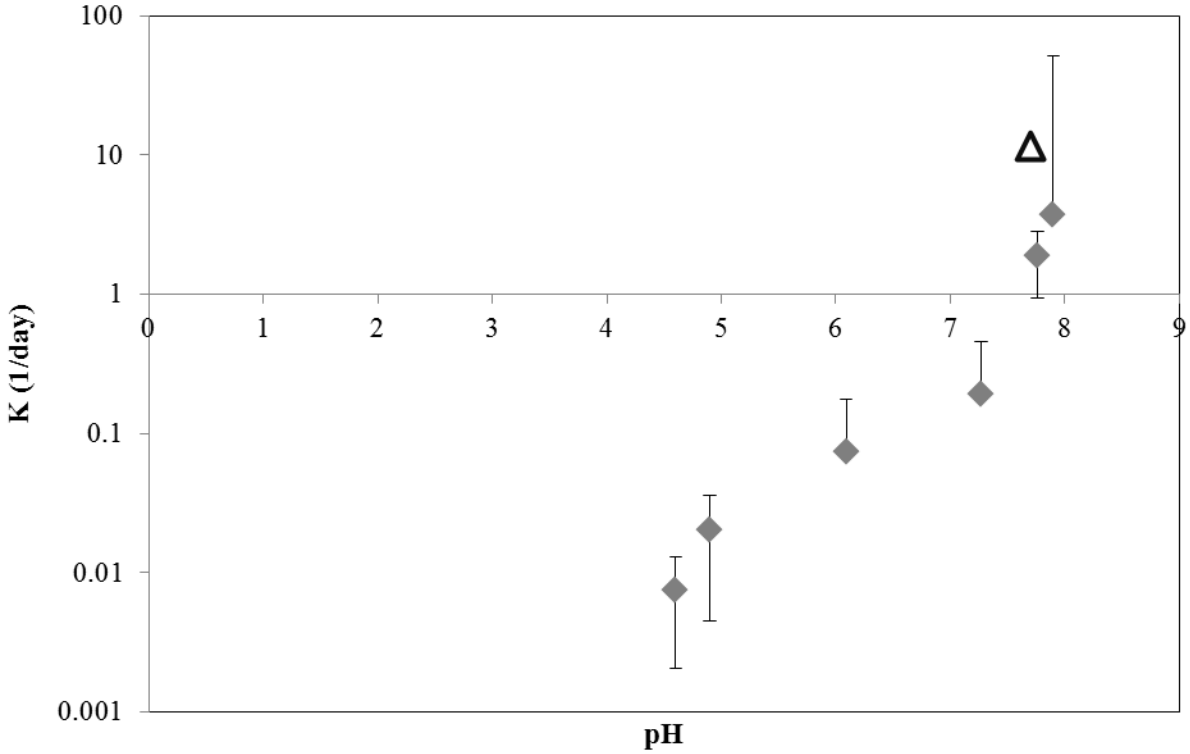

Figure B14: Kinetic absorption parameters determined previously by Powell et al. (Powell, Fjeld et al. 2005) (diamonds) on bulk Fe_2O_3 as compared to this work (triangle) for Fe_2O_3 nanoparticles. Rate constants were normalized to the surface area concentration of hematite and are plotted as L m^{-2} d^{-1}. Both datasets has similar solid phase Pu concentrations ranging from $1.3x10^{-3}$ to $1.3x10^{-4}$ mg_{Pu}/g_{Fe2O3}.

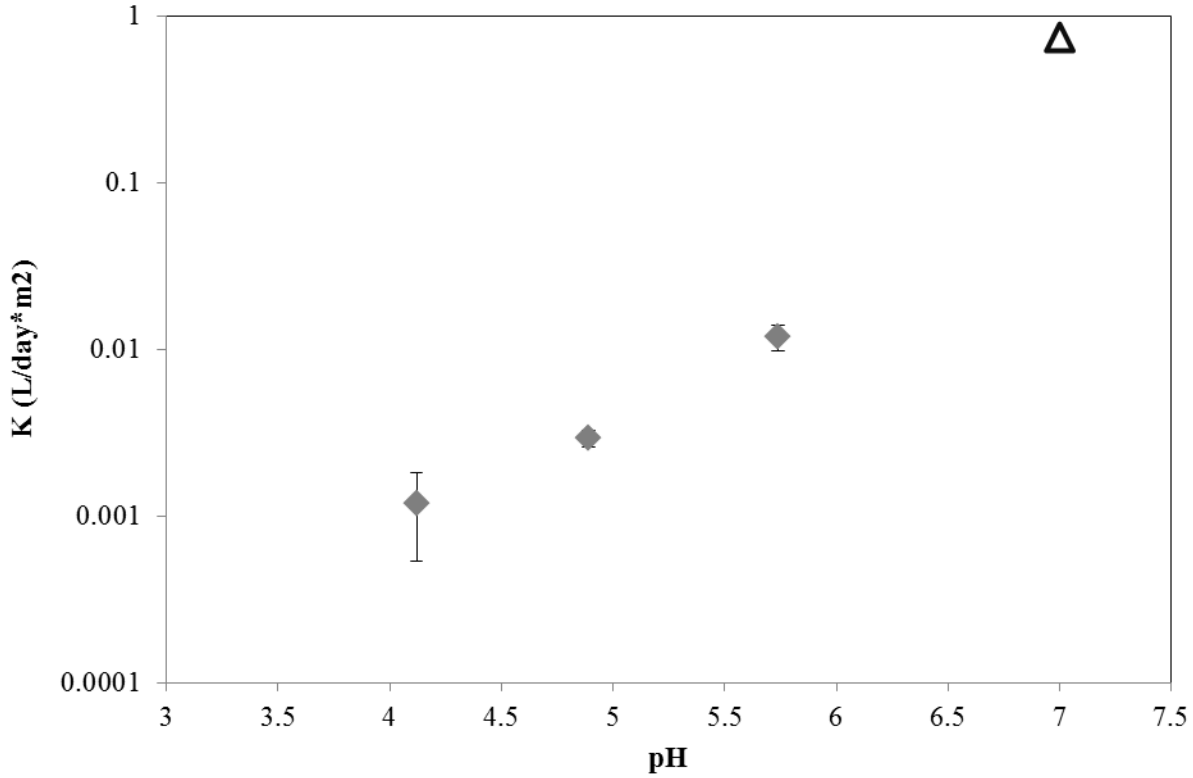

Figure B15: Reduction kinetic rates normalized to surface area at pH 7 for this work (*triangle*) at solids loading of 95-180 mg_{Pu}/g_{Fe2O3} based on the decrease in area of FTIR-ATR peak for sorbed $Pu(VI)O_2^{2+}$ compared to batch sorption data at lower pH and solids loading ≈2.4 mg_{Pu}/g_{Fe2O3} from Hixon and Powell(Hixon and Powell 2014) (*squares*).

B References

1. Allen, P. G., J. J. Bucher, D. K. Shuh, N. M. Edelstein and T. Reich (1997). "Investigation of aquo and chloro complexes of UO22+, NpO2+, Np4+, and Pu3+ by X-ray absorption fine structure spectroscopy." Inorganic Chemistry **36**(21): 4676-4683.

2. Brunhauer, S., P. H. Emmett and E. Teller (1938). "Adsorption of gases in multimolecular layers." Journal of the American Chemical Society **60**: 309-319.

3. Clesceri, L. S., A. D. Eaton, A. E. Greenberg and M. A. H. Franson (1996). Standard Methods for the Examination of Water and Wastewater, 19th ed.

4. Hay, J., R. L. Martin and G. Schreckenbach (2000). "Theoretical studies of the properties and solution chemistry of AnO22+ and AnO2+ Aquo complexes for An = U, Np, and Pu." Journal of Physical Chemistry A **104**: 6259-6270.

5. Hixon, A. E., Y. J. Hu, D. I. Kaplan, R. K. Kukkadapu, H. Nitsche, O. Qafoku and B. A. Powell (2010). "Influence of iron redox transformations on plutonium sorption to sediments." Radiochimica Acta **98**(9-11): 685-682.

6. Hixon, A. E. and B. A. Powell (2014). "Observed changes in the mechanism and rates of Pu(V) reduction on hematite as a function of total plutonium concentration." Environmental Science and Technology **submitted**.

7. Hsi, D. C.-K. and D. Langmuir (1985). "Adsorption of uranyl onto ferric oxyhydroxides: Application of the surface complexation site-binding model." Geochimica et Cosmochimica Acta **49**: 1931-1941.

8. Jones, L. H. and R. A. Penneman (1953). "Infrared Spectra and Structure of Uranyl and Transuranium (V) and (VI) Ions in Aqueous Perchloric Acid Solution." The Journal of Chemical Physics **21**(3): 542.

9. Kosmulski, M. (2002). "The pH-dependent surface charging and the points of zero charge." J Colloid Interface Sci **253**(1): 77-87.

10. Kosmulski, M. (2011). "The pH-dependent surface charging and points of zero charge: V. Update." J Colloid Interface Sci **353**(1): 1-15.

11. Lefevre, G., S. Noinville and M. Fedoroff (2006). "Study of uranyl sorption onto hematite by in situ attenuated total reflection-infrared spectroscopy." J Colloid Interface Sci **296**(2): 608-613.

12. Liger, E., L. Charlet and E. Van Cappellen (1999). "Surface catalysis of U(VI) reduction by Fe(II)." Geochimica et Cosmochimica Acta **53**(19/20): 2939-2955.

13. Muller, K., H. Foerstendorf, S. Tsushima, V. Brendler and G. Bernhard (2009). "Direct spectroscopic characterization of Aqueous Actinyl(VI) species: A comparative study of Np and U." Journal of Physical Chemistry **113**: 6626-6632.

14. Powell, B. A., R. A. Fjeld, D. I. Kaplan, J. T. Coates and S. M. Serkiz (2005). "Pu(V)O2+ adsorption and reduction by synthetic hematite and goethite." Environmental Science and Technology **39**(7): 2107-2114.

15. Shamov, G. A. and G. Schreckenbach (2005). "Density functional studies of actinyl aquo complexes studies using small-core effective core potentials and a scalar four-component relativistic model." J Phys Chem A **109**(48): 10961-10974.

16. van Reeuwijk, L. P. and V. J. G. Houba (1998). Guidelines for Quality Management in Soil and Plant Laboratories. FAO Soils Bulletin - 74. Rome, Italy, Food and Agriculture Organization of the United Nations.

Appendix C: Supplementary Materials for Paper Three

C.1 Statistical Analysis of Samples

T-test: Comparison of Two Averages[1]

The following equations were utilized to calculate the 95% confidence interval of the difference of two means based on a null hypothesis that the difference in the means is zero. Equation 1 is used to calculate the difference in the measured means, E.

$$E = \eta_a - \eta_b \quad \text{Eqn. 1}$$

The variance (V) of each sample set (i) is calculated based on equation 2 below where σ_i is the standard deviation and n_i is the number of samples within the sample set.

$$V_i = \frac{{\sigma_i}^2}{n_i} \qquad \text{Eqn. 2}$$

The pooled estimate of the variance (s_{pooled}^2) is then calculated based on the variances calculated in equation 2.

$${s_{pooled}}^2 = \frac{(n_a-1){V_a}^2+(n_b-1){V_b}^2}{n_a+n_b-2} \qquad \text{Eqn. 3}$$

Finally the estimated variance of the difference (V_d) is estimated based on equation 4 below.

$$V_d = {s_{pooled}}^2\left(\frac{1}{n_a}+\frac{1}{n_b}\right) \qquad \text{Eqn. 4}$$

The square root of the variance of the difference is then multiplied by the t statistic (determined based on the degrees of freedom and confidence interval) to determine the confidence interval for the difference in the two means. Table C.1 represents a comparison at 95% confidence level of desorption Kd values for 28 and 168 day periods for $^{239/240}$Pu.

Table C.1: Comparison of means for Kd values at 28 and 168 day desorption periods

Desorption Ligand	CI-statistic	Difference
0.1 NaF	129294	29243
5 mg_C/L DFOB	47862	40892
1% H_2O_2	27099	18111

Tukey's Paired Comparison of Multiple Averages[2]

Tukey's paired comparison method can be used to more accurately compare the averages of multiple datasets. The variance and pooled variance are calculated as described above for the T-test method with the exception that all dataset variances are pooled in the calculation of the pooled variance. The degrees of freedom are calculated based on the difference between the total number of samples pooled between all of the datasets minus the number of samples in one dataset. Instead of a T-statistic, Tukey's method utilizes a q-statistic which is based on the calculated degrees of freedom and number of datasets. The final confidence limits for comparison of the difference in the means is calculated based on equation 5 below.

$$\eta_i - \eta_j \pm \left(\frac{q}{\sqrt{2}}\right) s_{pooled} \sqrt{\left(\frac{1}{n_i} + \frac{1}{n_j}\right)} \qquad \text{Eqn. 5}$$

All variables are compared with 95% confidence for consistency. Table C2 summarizes the comparison of average Log[Kd] and fraction sorbed where all data for each isotope and time is averaged. Tables C3-C10 compare the different ligands with eachother for each isotope and the 3 and 168 day time period. Each value represents the difference between the two ligands on the table. The 28 day values are not compared to eachother in this manner because multiple measurements were not collected. All values that are

statistically different (i.e. values are outside of the maximum distance) are marked in ***bold italics*.** Table C11 compares the two isotopes' selective extraction removal percentages.

Table C.2: Comparison of calculated 95% confidence interval (CI) with difference in average Log[Kd], Kd and sorbed fractions, values marked in bold italics are outside of the permitted difference (confidence interval) and reject the null hypothesis

	Statistic	Isotopes		Pu-239/240			Pu-242
	CI	3 days	168 days	3vs7	3vs28	3vs168	3vs168
Log[Kd]	0.685	-0.476	***0.756***	-0.581	-0.545	-0.545	0.198
Kd	26302	-3299	12260	-13904	-12572	-12572	954
Sorbed%	0.441	***-0.985***	***0.935***	-0.182	-0.141	-0.141	0.138

Table C.3: Comparison matrix of difference in 3 day desorption K_d ($^{239/240}$Pu) to Tukey's maximum difference at a 95% confidence interval, the maximum difference is 4207 mL/g, values marked in ***bold italics*** are outside of the permitted difference (confidence interval) and reject the null hypothesis

	NaCl	$CaCl_2$	Na_2PO_4	NaF	Citric	SRFA	DFOB	H_2O_2	NH_2OH
NaCl	0								
$CaCl_2$	349	0							
Na_2PO_4	655	306	0						
NaF	2289	1940	1634	0					
Citric acid	-449	-798	-1104	-2738	0				
Fulvic acid	289	-60	-366	-2000	738	0			
DFOB	1079	730	424	-1210	1528	790	0		
H_2O_2	1284	936	630	-1004	1733	996	206	0	
NH_2OH	2055	1706	1400	-234	2503	1766	976	770	0
Blank	1632	1283	977	-657	2081	1343	553	347	-423

Note: no values are statistically different

Table C.4: Comparison matrix of difference in 3 day fraction desorbed ($^{239/240}Pu$) to Tukey's maximum difference at a 95% confidence interval, the maximum difference is 0.0223, values marked in ***bold italics*** are outside of the permitted difference (confidence interval) and reject the null hypothesis

	NaCl	$CaCl_2$	Na_2PO_4	NaF	Citric	SRFA	DFOB	H_2O_2	NH_2OH
NaCl	0								
$CaCl_2$	-0.0007	0							
Na_2PO_4	0.0004	0.0012	0						
NaF	0.0043	0.0050	0.0038	0					
Citric acid	0.0014	0.0021	0.0010	-0.0029	0				
Fulvic acid	0.0030	0.0037	0.0025	-0.0013	0.0016	0			
DFOB	0.0022	0.0029	0.0018	-0.0021	0.0008	-0.0008	0		
H_2O_2	0.0048	0.0056	0.0044	0.0006	0.0034	0.0019	0.0026	0	
NH_2OH	0.0051	0.0059	0.0047	0.0009	0.0037	0.0021	0.0029	0.00029	0
Blank	0.0032	0.0040	0.0028	-0.0010	0.0018	0.0003	0.0010	-0.0016	-0.0019

Note: no values are statistically different

Table C.5: Comparison matrix of difference in 3 day sorption K_d (^{242}Pu) to Tukey's maximum difference at a 95% confidence interval, the maximum difference is 2180 mL/g, values marked in ***bold italics*** are outside of the permitted difference (confidence interval) and reject the null hypothesis

	NaCl	$CaCl_2$	Na_2PO_4	NaF	Citric	SRFA	DFOB	H_2O_2	NH_2OH
NaCl	0								
$CaCl_2$	1253	0							
Na_2PO_4	-6	-1259	0						
NaF	1298	45	1304	0					
Citric acid	94	-1159	100	-1204	0				
Fulvic acid	-566	-1819	-560	-1864	-660	0			
DFOB	629	-624	635	-669	535	1194	0		
H_2O_2	-337	-1590	-331	-1635	-431	229	-966	0	
NH_2OH	875	-378	881	-423	781	1441	246	1212	0
Blank	1572	319	1578	274	1478	2138	943	1909	697

Table C.6: Comparison matrix of difference in 3 day fraction sorbed (^{242}Pu) to Tukey's maximum difference at a 95% confidence interval, the maximum difference is 0.0494, values marked in ***bold italics*** are outside of the permitted difference (confidence interval) and reject the null hypothesis

	NaCl	$CaCl_2$	Na_2PO_4	NaF	Citric	SRFA	DFOB	H_2O_2	NH_2OH
NaCl	0								
$CaCl_2$	0.0268	0							
Na_2PO_4	-0.0002	-0.0270	0						
NaF	0.0333	0.0065	0.0335	0					
Citric acid	0.0032	-0.0237	0.0033	-0.0301	0				
Fulvic acid	-0.0029	-0.0297	-0.0027	-0.0362	-0.0061	0			
DFOB	0.0071	-0.0198	0.0072	-0.0263	0.0039	0.0100	0		
H_2O_2	-0.0024	-0.0293	-0.0023	-0.0357	-0.0056	0.0005	-0.0095	0	
NH_2OH	0.0063	-0.0205	0.0065	-0.0270	0.0032	0.0092	-0.0007	0.0087	0
Blank	0.0495	0.0226	0.0496	0.0162	0.0463	***0.0524***	0.0424	***0.0519***	0.0432

Table C.7: Comparison matrix of difference in 168 day desorption K_d ($^{239/240}Pu$) to Tukey's maximum difference at a 95% confidence interval, the maximum difference is 17875 mL/g, values marked in ***bold italics*** are outside of the permitted difference (confidence interval) and reject the null hypothesis

	NaCl	$CaCl_2$	Na_2PO_4	NaF	Citric	SRFA	DFOB	H_2O_2	NH_2OH
NaCl	0								
$CaCl_2$	6743	0							
Na_2PO_4	-3481	-10224	0						
NaF	2849	-3895	6329	0					
Citric acid	3241	-3502	6722	393	0				
Fulvic acid	-4085	-10828	-604	-6934	-7326	0			
DFOB	6181	-562	9662	3333	2940	10266	0		
H_2O_2	13625	6882	17106	10777	10384	17710	7444	0	
NH_2OH	7869	1126	11350	5021	4628	11954	1688	-5756	0
Blank	769	-5974	4250	-2080	-2472	4854	-5412	-12856	-7100

Note: no values are statistically different

Table C.8: Comparison matrix of difference in 168 day fraction sorbed ($^{239/240}Pu$) to Tukey's maximum difference at a 95% confidence interval, the maximum difference is 0.0075, values marked in ***bold italics*** are outside of the permitted difference (confidence interval) and reject the null hypothesis

	NaCl	$CaCl_2$	Na_2PO_4	NaF	Citric	SRFA	DFOB	H_2O_2	NH_2OH
NaCl	0								
$CaCl_2$	-0.0015	0							
Na_2PO_4	0.0008	0.0023	0						
NaF	0.0001	0.0015	-0.0007	0					
Citric acid	-0.0005	0.0009	-0.0013	-0.0006	0				
Fulvic acid	0.0008	0.0022	0.0000	0.0007	0.0013	0			
DFOB	-0.0010	0.0005	-0.0018	-0.0010	-0.0004	-0.0017	0		
H_2O_2	-0.0022	-0.0007	-0.0030	-0.0023	-0.0017	-0.0030	-0.0012	0	
NH_2OH	-0.0026	-0.0011	-0.0034	-0.0026	-0.0020	-0.0033	-0.0016	-0.0004	0
Blank	0.0001	0.0015	-0.0007	0.0000	0.0006	-0.0007	0.0010	0.0023	0.0026

Note: no values are statistically different

Table C.9: Comparison matrix of difference in 168 day sorption K_d (^{242}Pu) to Tukey's maximum difference at a 95% confidence interval, the maximum difference is 1446 mL/g, values marked in ***bold italics*** are outside of the permitted difference (confidence interval) and reject the null hypothesis

	NaCl	$CaCl_2$	Na_2PO_4	NaF	Citric	SRFA	DFOB	H_2O_2	NH_2OH
NaCl	0								
$CaCl_2$	-911	0							
Na_2PO_4	-720	191	0						
NaF	***1722***	***2632***	***2442***	0					
Citric acid	***-1595***	-685	-876	***-3317***	0				
Fulvic acid	-1045	-135	-325	***-2767***	550	0			
DFOB	-877	33	-158	***-2599***	718	168	0		
H_2O_2	-792	119	-72	***-2514***	804	254	86	0	
NH_2OH	-533	378	187	***-2255***	1062	512	344	259	0
Blank	-400	511	320	***-2122***	1196	645	478	392	133

Table C.10: Comparison matrix of difference in 168 day fraction sorbed (^{242}Pu) to Tukey's maximum difference at a 95% confidence interval, the maximum difference is 0.0169, values marked in ***bold italics*** are outside of the permitted difference (confidence interval) and reject the null hypothesis

	NaCl	$CaCl_2$	Na_2PO_4	NaF	Citric	SRFA	DFOB	H_2O_2	NH_2OH
NaCl	0								
$CaCl_2$	0.0041	0							
Na_2PO_4	0.0036	-0.0005	0						
NaF	***-0.0458***	***-0.0499***	***-0.0494***	0					
Citric acid	0.0056	0.0015	0.0019	***0.0514***	0				
Fulvic acid	0.0046	0.0006	0.0010	***0.0505***	-0.0009	0			
DFOB	0.0045	0.0004	0.0009	***0.0503***	-0.0011	-0.0001	0		
H_2O_2	0.0039	-0.0002	0.0003	***0.0497***	-0.0017	-0.0008	-0.0006	0	
NH_2OH	0.0031	-0.0009	-0.0005	***0.0490***	-0.0024	-0.0015	-0.0013	-0.0007	0
Blank	0.0009	-0.0032	-0.0027	***0.0467***	-0.0046	-0.0037	-0.0036	-0.0030	-0.0022

Table C.11: Comparison of difference in ^{242}Pu versus $^{239/240}Pu$ removal for selective extractions for total iron and amorphous iron

	Measured Difference	Calculated (t-test) Difference
Total Fe	***28%***	5%
Amorphous Fe	***39%***	2%

Dunnett's Comparison with a Control[2]

Dunnett's is a similar comparison method to Tukey's with the exception that it uses a modified t-test statistic instead of the q-value. This method allows for comparison of multiple treatments with a control or standard treatment. In this case, the blank (DDI H_2O) treatment is considered the control and is compared to all other ligands. Tables C12-C14 compare the 3, 7 and 168 day data, respectively. 28 day desorption data is not compared because multiple measurements were not collected for each ligand and concentration.

Table C.12: Comparison to the blank (DDI) treatment for 3 day data, difference of averages (Blank – treatment X) shown for Kd and fraction sorbed, values marked in ***bold italics*** are statistically different at the 95% confidence level because difference is greater than that calculated with the test statistic (bottom row) for Dunnett's comparison, Note: data only shown for $^{239/240}Pu$

	Fsorb	Kd
NaCl	0.0017	1632
$CaCl_2$	0.0016	1283
Na_2PO_4	0.0011	977
NaF	***-0.0159***	-657
Citric acid	0.0014	2081
Fulvic acid	0.0007	1343
DFOB	-0.0015	553
H_2O_2	-0.0004	347
NH_2OH	-0.0045	-423
Calc Diff	0.0140	2662

Table C.13: Comparison to the blank (DDI) treatment for 7 day data, difference of averages for highest ligand concentrations (Blank – treatment X) shown for Kd, Log[Kd] and fraction sorbed, values marked in ***bold italics*** are statistically different from the blank at the 95% confidence level because difference is greater than that calculated with the test statistic (bottom row) for Dunnett's comparison

	Kd	Log[Kd]	Fsorb
NaCl	9246	0.36	0.004
$CaCl_2$	13647	0.30	0.003
Na_2PO_4	14433	0.43	0.005
NaF	20107	0.40	0.004
citric	8301	0.20	-0.002
SRFA	13125	0.31	0.003
DFOB	2825	0.11	0.002
H_2O_2	2659	0.12	0.002
NH_2OH*HCl	-1981	-0.07	0.000
Calc Diff	27180	0.59	0.010

Note: no values are statistically different

Table C.14: Comparison to the blank (DDI) treatment for 168 day data, difference of averages (Blank – treatment X) shown for Kd and fraction sorbed, values marked in ***bold italics*** are statistically different at the 95% confidence level because difference is greater than that calculated with the test statistic (bottom row) for Dunnett's comparison

	F_{sorb} $^{239/240}Pu$	Kd $^{239/240}Pu$	F_{sorb} ^{242}Pu	Kd ^{242}Pu
NaCl	0.0001	769	-0.0009	400
$CaCl_2$	0.0015	-5974	0.0032	-511
Na_2PO_4	-0.0007	4250	0.0027	-320
NaF	0.0000	-2080	***-0.0467***	***2122***
Citric acid	0.0006	-2472	0.0046	***-1196***
Fulvic acid	-0.0007	4854	0.0037	-645
DFOB	0.0010	-5412	0.0036	-478
H_2O_2	0.0023	***-12856***	0.0030	-392
NH_2OH	0.00	-7100	0.0022	-133
Calc Diff	0.0047	11310	0.0107	915

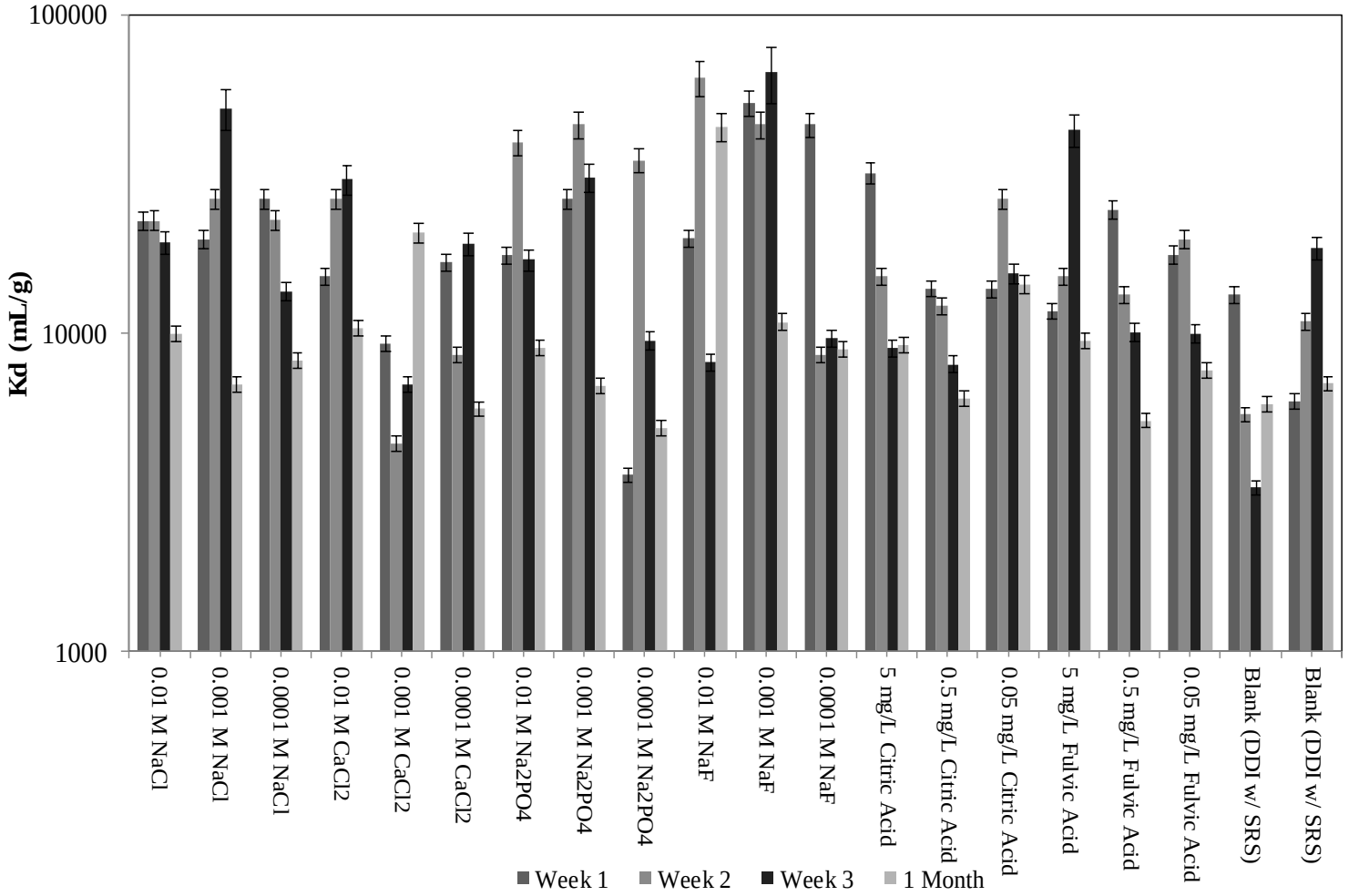

Figure C1: Batch desorption of 2 µg/gsediment 239/240Pu from 50 gsediment/L suspension in the presence of variable ligands and salts, sediments aged in the presence of Pu for 32 years

Future TEM and Electron Microprobe Microscopy

Electron microprobe and high resolution TEM will be conducted to investigate which minerals Pu is likely to associate with within these sediments and whether there are differences between Pu aged for weeks (^{242}Pu) versus years ($^{239/240}$Pu). Analyses are to be completed at the Environmental Molecular Sciences laboratory (EMSL, Richland WA) for SRS lysimeter sediments aged for 32 years in the presence of ~6 ppm $^{239/240}$Pu and control SRS lysimeter sediments amended with ~100 ppm ^{242}Pu aged on the order of weeks. To ensure that soil samples sent for analysis contain the highest fraction of plutonium possible, alpha radiography (polyalkyl diglycol plastic) was completed to isolate fractions with greater plutonium content. After exposure to the soil samples, the plastic film is placed into 6M NaOH to etch areas impacted by alpha emissions from the soils. Total and clay/silt fractions of the sediment were also dissolved in 8M HNO_3 and analyzed by LSC to confirm total activity associated with each fraction. Because alpha radiography and soil dissolution experiments confirmed a strong association of the $^{239/240}$Pu with the clay/silt size fraction (>98.9% of total activity in this fraction), samples prepared for microscopy include the total sediment and clay/silt-sized fractions of both the 'aged' and 'amended' SRS sediments. Prior to analysis, sediments were air-dried and ~15 mg of sediment were mixed with EpoFix resin and hardener (Buehler) and poured into 1 inch diameter cups (Buehler). Following drying at room temperature within a vacuum (to remove bubbles), samples were polished in an air-filled glovebox (Unilab MBraun) with a magnetic, hand polisher (Pace Technologies Mano 1000T) equipped with 8 inch Satyn and Micro magnetic backed polishing disks (Buehler).

C References

1. Berthouex, P. M.; Brown, L. C., Assessing the Average of Differences. In *Statistics for Environmental Engineers*, CRC Press: Boca Raton, Florida, 1994; pp 111-114.

2. Berthouex, P. M.; Brown, L. C., Multiple Paired Comparisons of k Averages. In *Statistics for Environmental Engineers*, CRC Press: Boca Raton, Florida, 1994; pp 123-128.

Appendix D: Supplementary Materials for Paper Four

D.1 Figures and Tables

Table D1: Major characteristics of Fe_2O_3-NP

Parameter	**Hematite NP**
DLS Particle Size (nm)	25±1 nm
TEM Particle Size (nm)	12.9±6.5 nm
BET Surface Area (m^2/g)	68 m^2/g

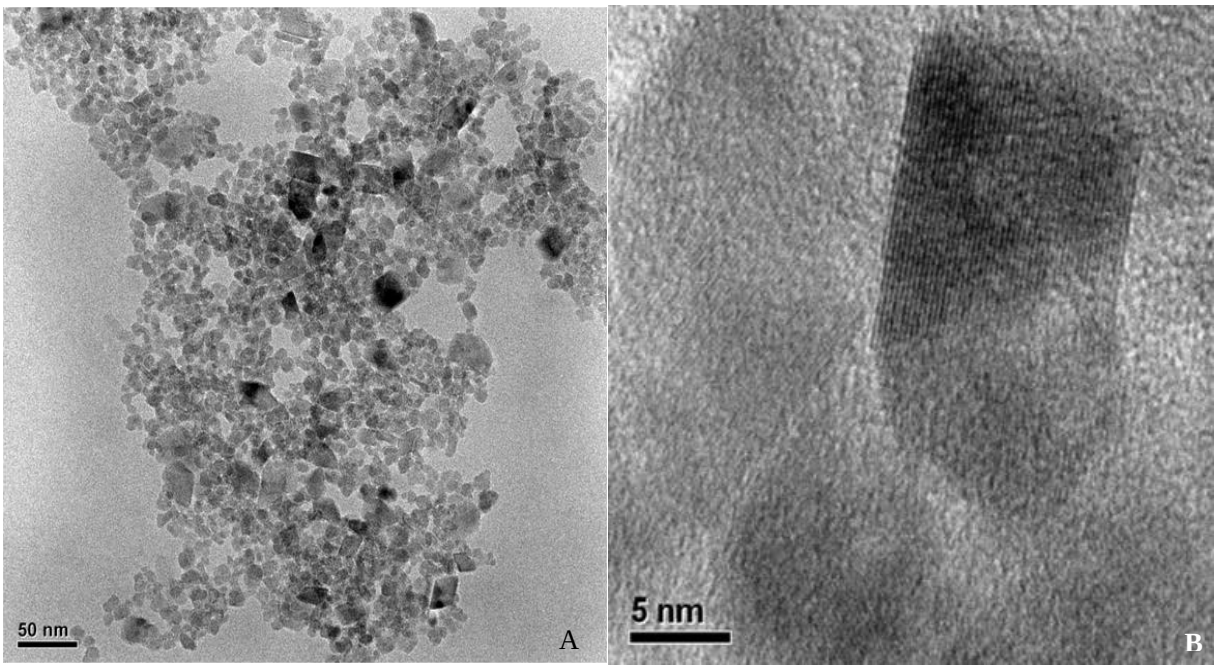

F-igure D1: Images of Fe_2O_3-NP (Hitachi 9500 HRTEM), *left* – low resolution image of particles, *right* – high resolution image of particles.

Table D2: Chemical analysis (ppm) of trace elements in high purity quartz, manufacturer provided (Unimin Corp).

Element	Concentration (ppm)
Al	14.6
Ca	0.5
Cu	0.0
Fe	0.3
Ge	0.5
K	0.5
Li	0.6
Mg	0.0
Mn	0.0
Na	0.8
Ni	0.0
Ti	1.2
Zn	0.0
Zr	0.7

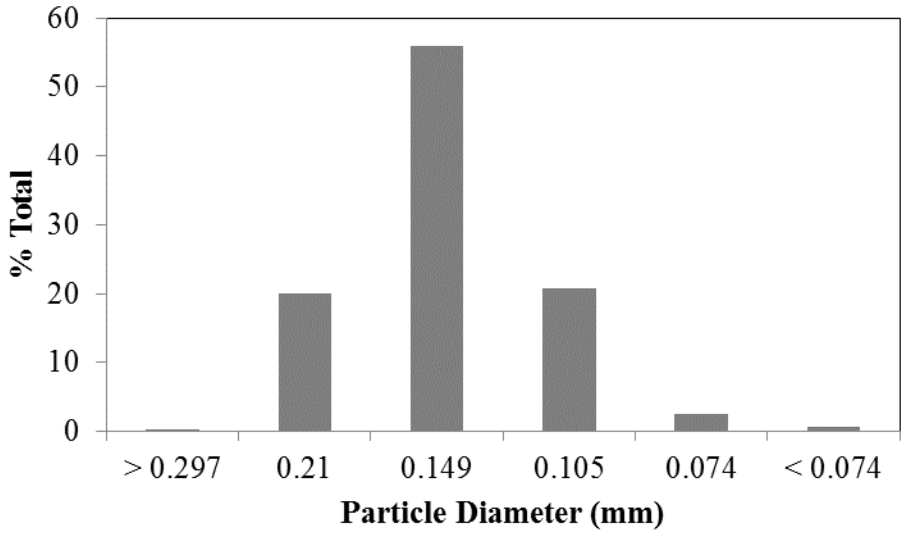

Figure D2: Soil sieve analysis of high purity quartz (Iota Standard, Unimin Corp).

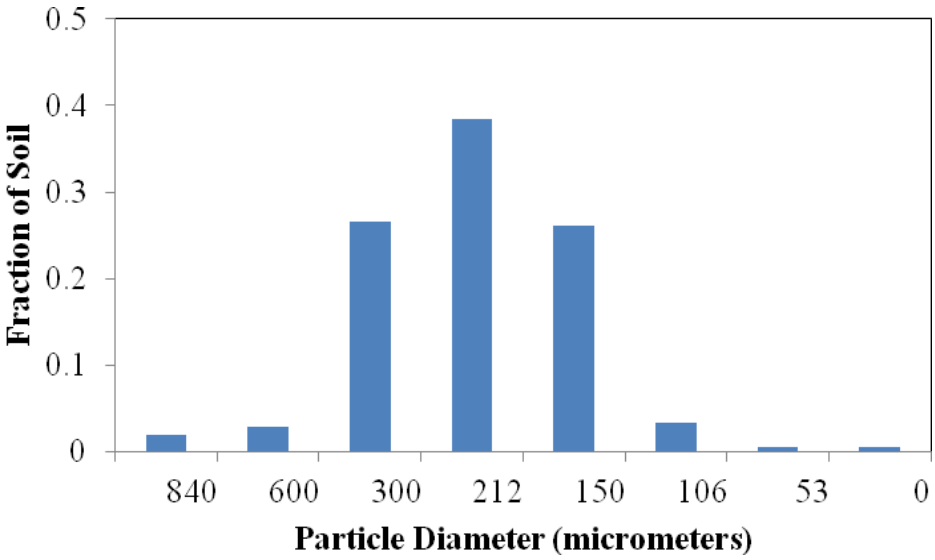

Figure D3: Soil sieve analysis of Savannah River Site sandy.

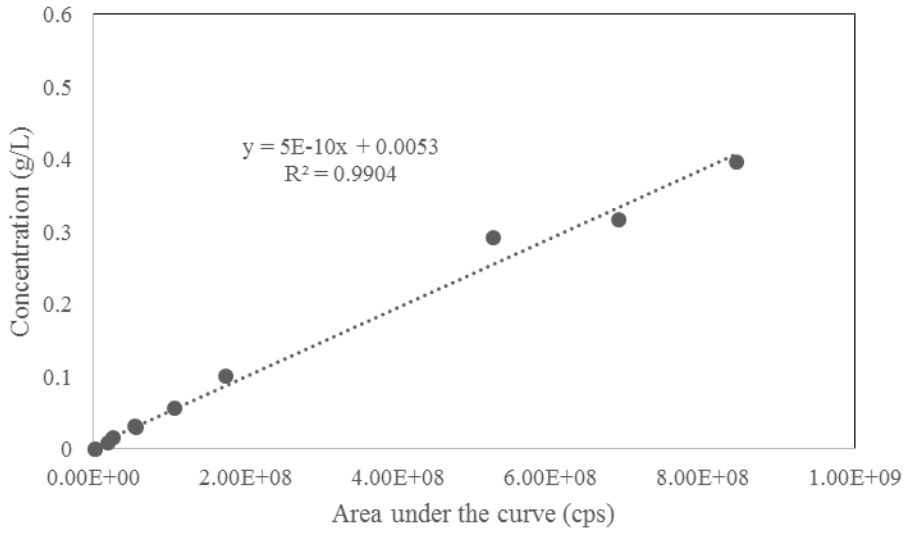

Figure D4: Calibration curve for blue fluorescent, polystyrene microspheres.

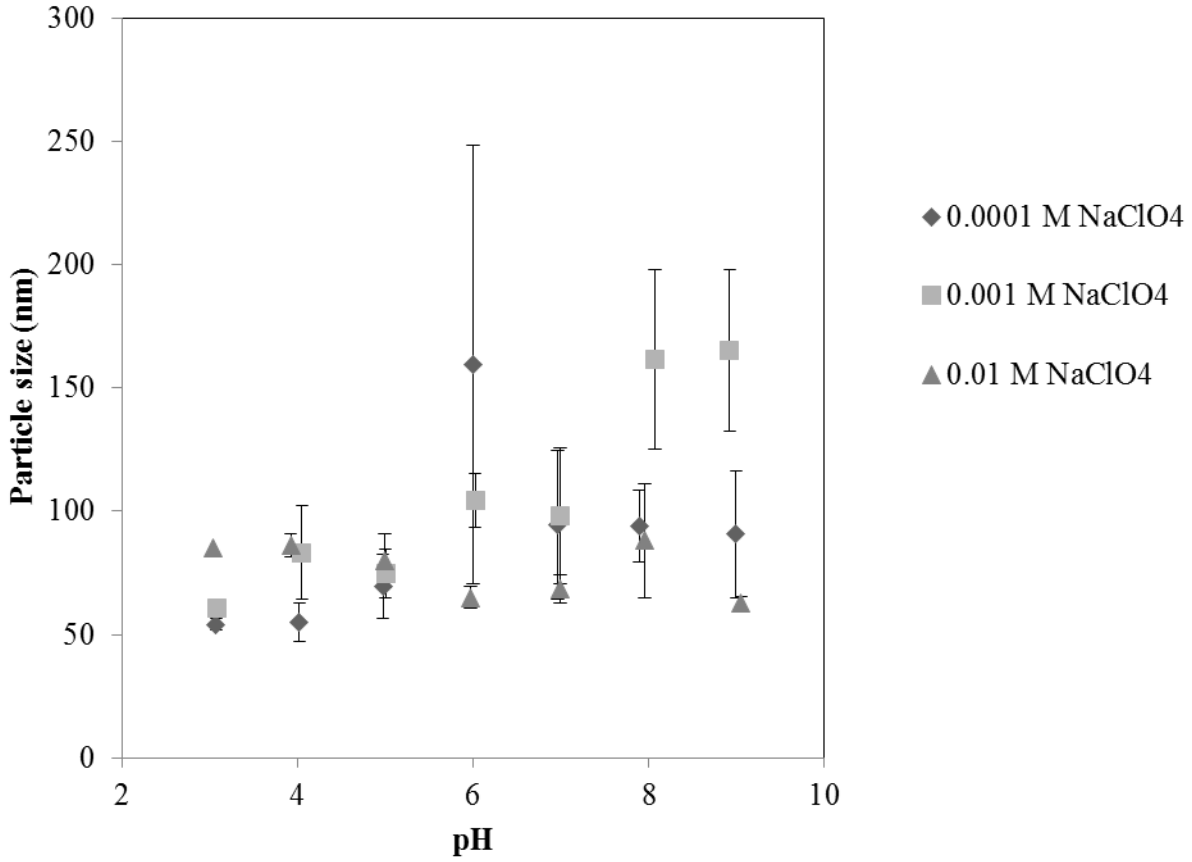

Figure D5: Particle diameter (nm) with respect to pH and ionic strength of 0.03 g/L Fe_2O_3-NP suspensions in the presence of 25 mgC/L SRFA, error bars represent the average of 5 consecutive measurements.

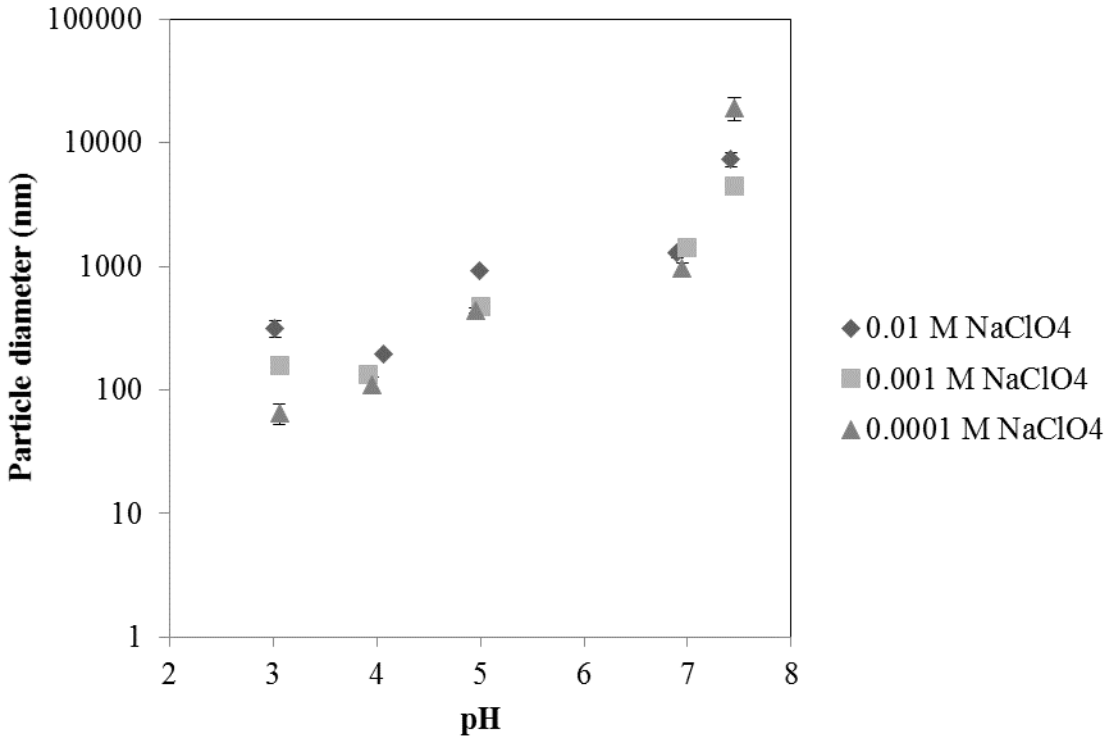

Figure D6: Particle diameter (nm) with respect to pH and ionic strength of 0.03 g/L Fe_2O_3-NP suspensions in the absence of SRFA, error bars represent the average of 5 consecutive measurements.

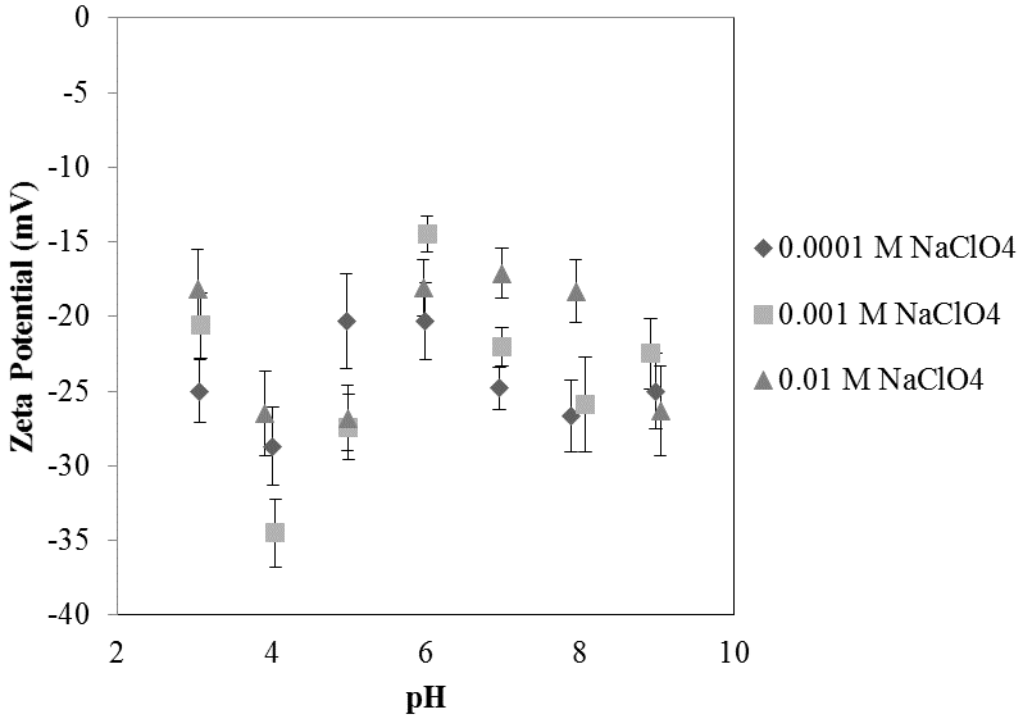

Figure D7: Zeta potential (mV) with respect to pH and ionic strength of 0.03 g/L Fe_2O_3-NP suspensions in the presence of 25 mgC/L SRFA, error bars represent the average of 5 consecutive measurements, Note: at pH 3, SRFA without Fe_2O_3-NP is -16.8±2.5.

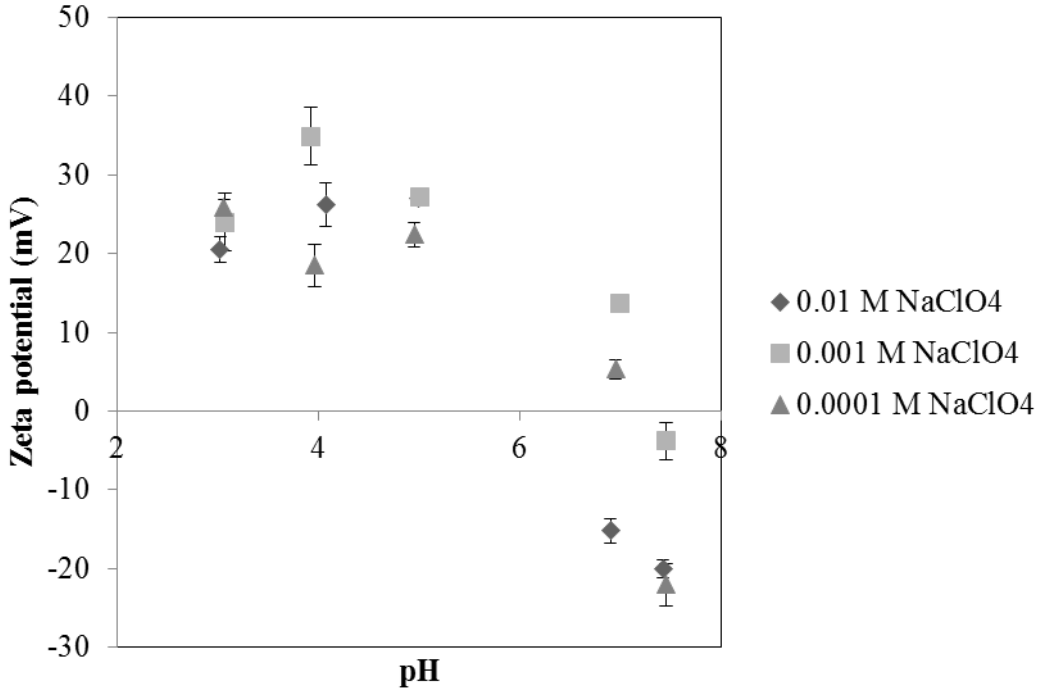

Figure D8: Zeta potential (mV) with respect to pH and ionic strength of 0.03 g/L Fe_2O_3-NP suspensions in the absence of SRFA, error bars represent the average of 5 consecutive.

Table D3: Fraction of 5 mgC/L Suwanee River Fulvic Acid passing through 30k, 10k and 5k MWCO filter (Pall, Nanosep) at pH 5, 7, 9 in 0.01 M NaCl (Simpkins 2011).

pH	30k	10k	3k
5	93.5%	91.1%	69.8%
7	98.1%	92.8%	77.1%
9	102.3%	96.7%	80.9%

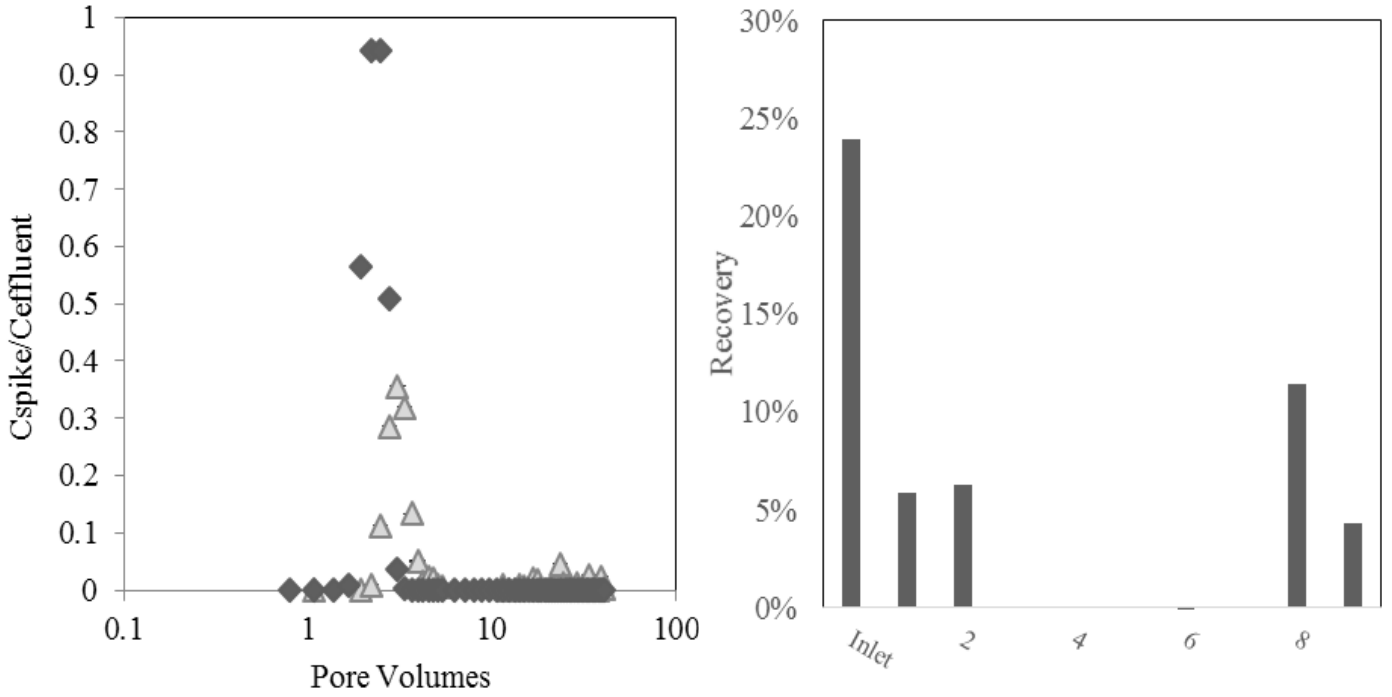

Figure D9: ^{230}Th column in high purity quartz at 1 mL/min flow rate at pH 5.5 with 5 µg/L Re and 0.72 µg/L ^{230}Th in 0.001 M NaCl, *left* – effluent results for ^{230}Th and tracer (Re) and *right* – solid phase results within the column following leaching step in 8 M HNO_3.

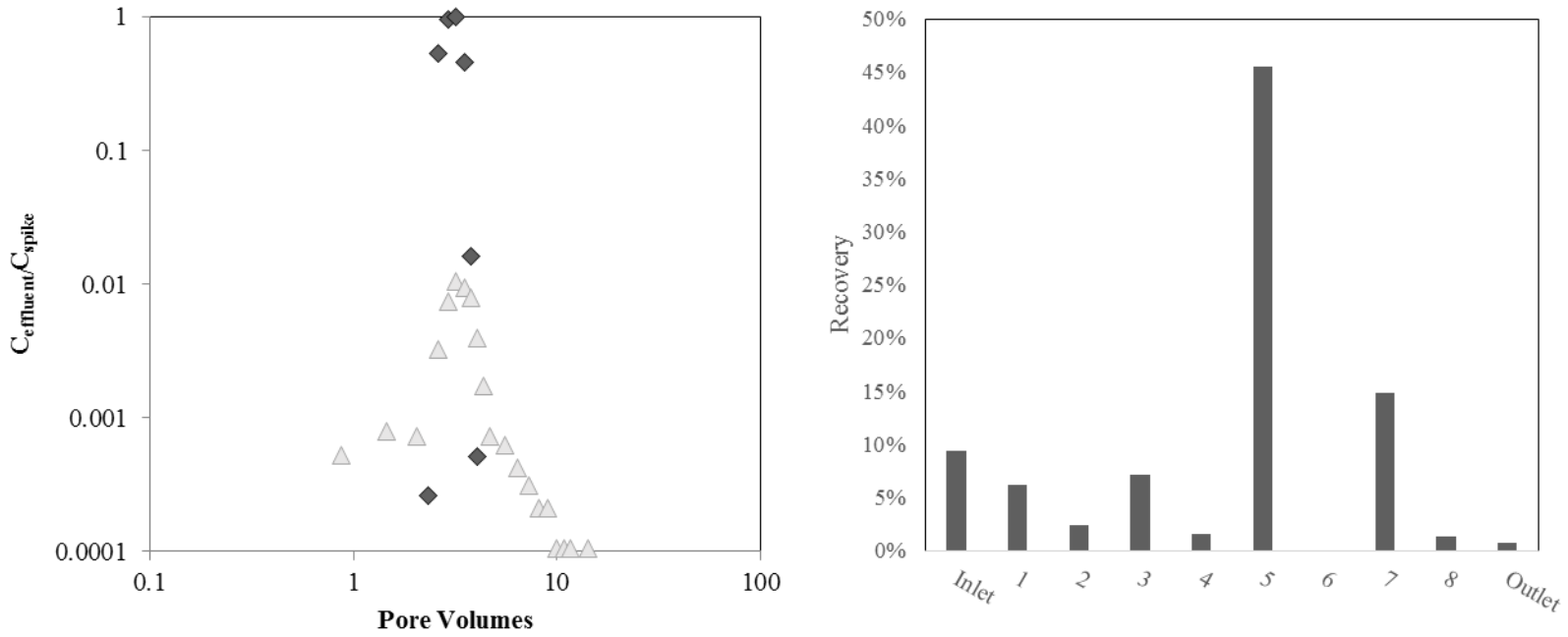

Figure D10: ^{232}Th column in high purity quartz at 1 mL/min flow rate at pH 5.5 with 5 µg/L Re and 10 µg/L ^{232}Th in 0.001 M NaCl, *left* – effluent results for ^{232}Th and tracer (Re) and *right* – solid phase results within the column following leaching step in 8 M HNO_3.

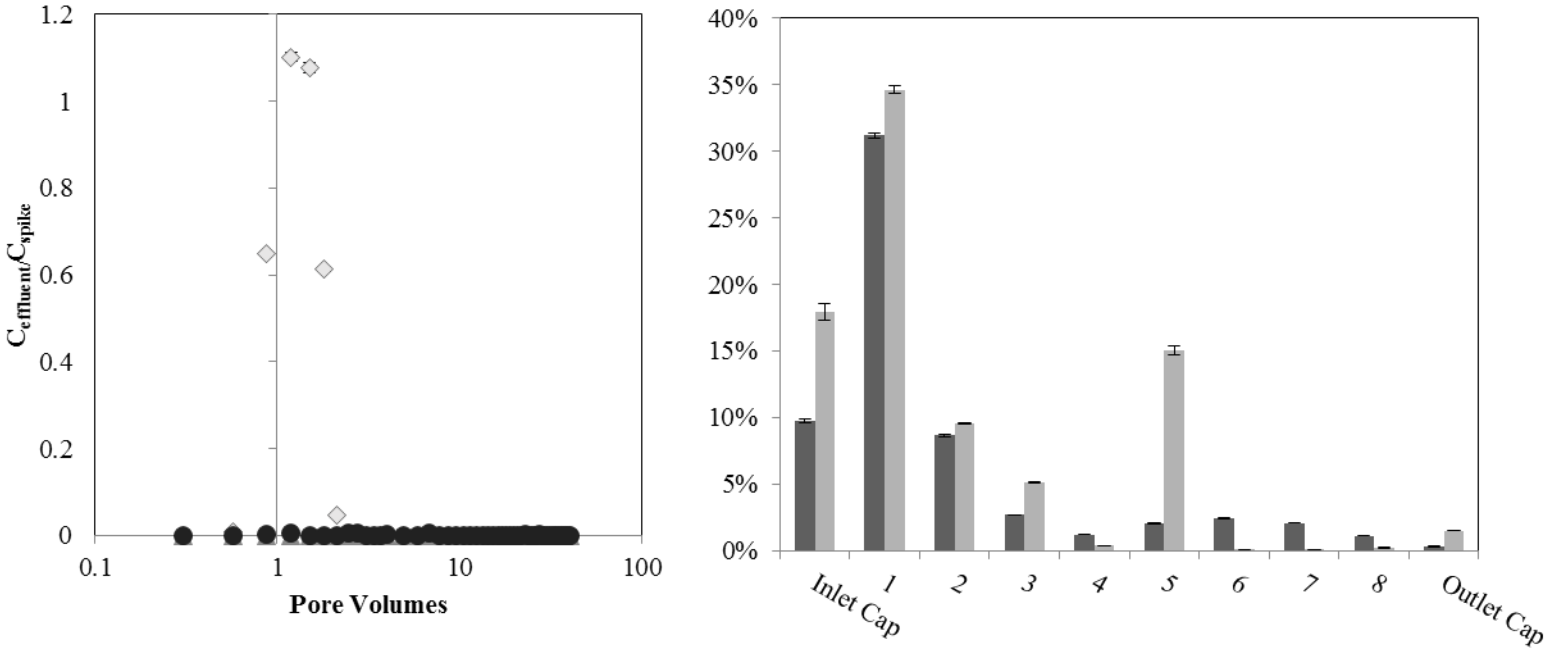

Figure D11: Hematite-Th column in high purity quartz at 1 mL/min flow rate at pH 5.5 with 5 µg/L Re, 289 µg/L ^{232}Th, and 0.1 g/L Hematite-NP in 0.001 M NaCl, *left* – effluent results for ^{232}Th (*triangles*), Hematite-NP as ^{56}Fe (*circles*), and tracer (*diamonds*, Re) and *right* – solid phase results within the column following leaching step in 8 M HNO_3 for Hematite as ^{56}Fe (*gray*) and ^{232}Th (*black*).

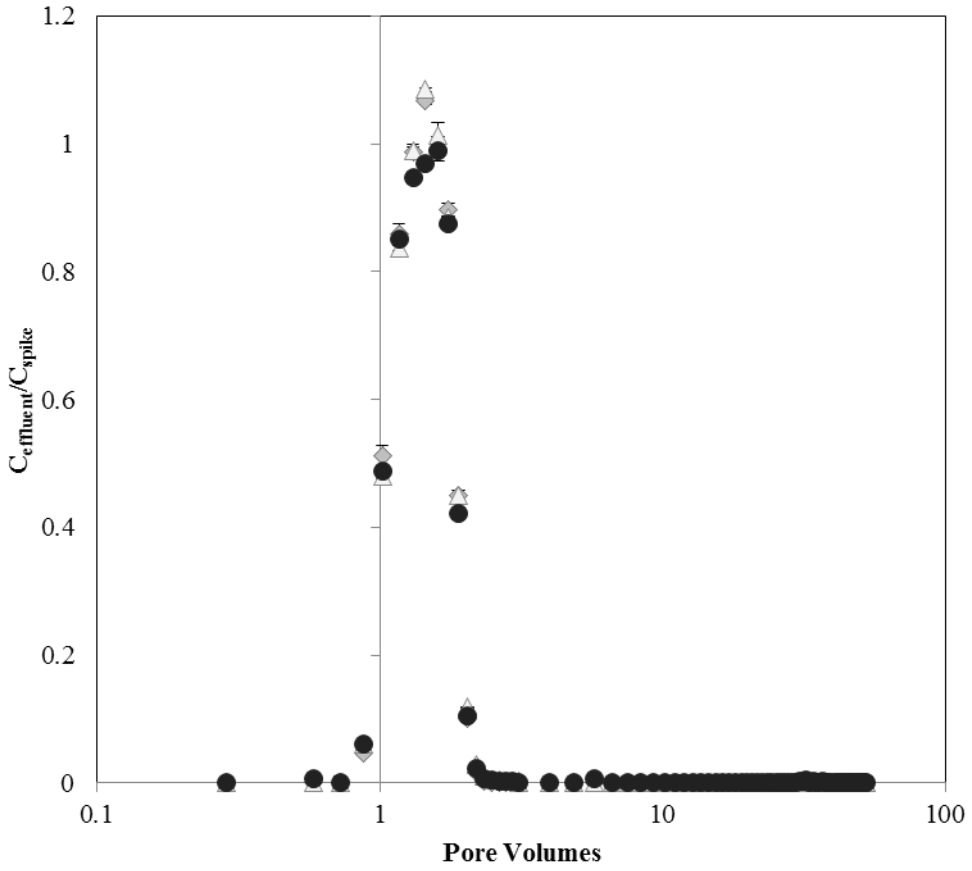

Figure D12: SRFA-Th column in high purity quartz at 1 mL/min flow rate at pH 5.5 with 5 µg/L Re, 274 µg/L ^{232}Th, and 25 mg_C/L SRFA in 0.001 M NaCl, effluent results for ^{232}Th (*triangles*), SRFA as ^{3}H (*circles*), and tracer (Re, *diamonds*), Note: no recovery of constituents within the solid phase leaching step.

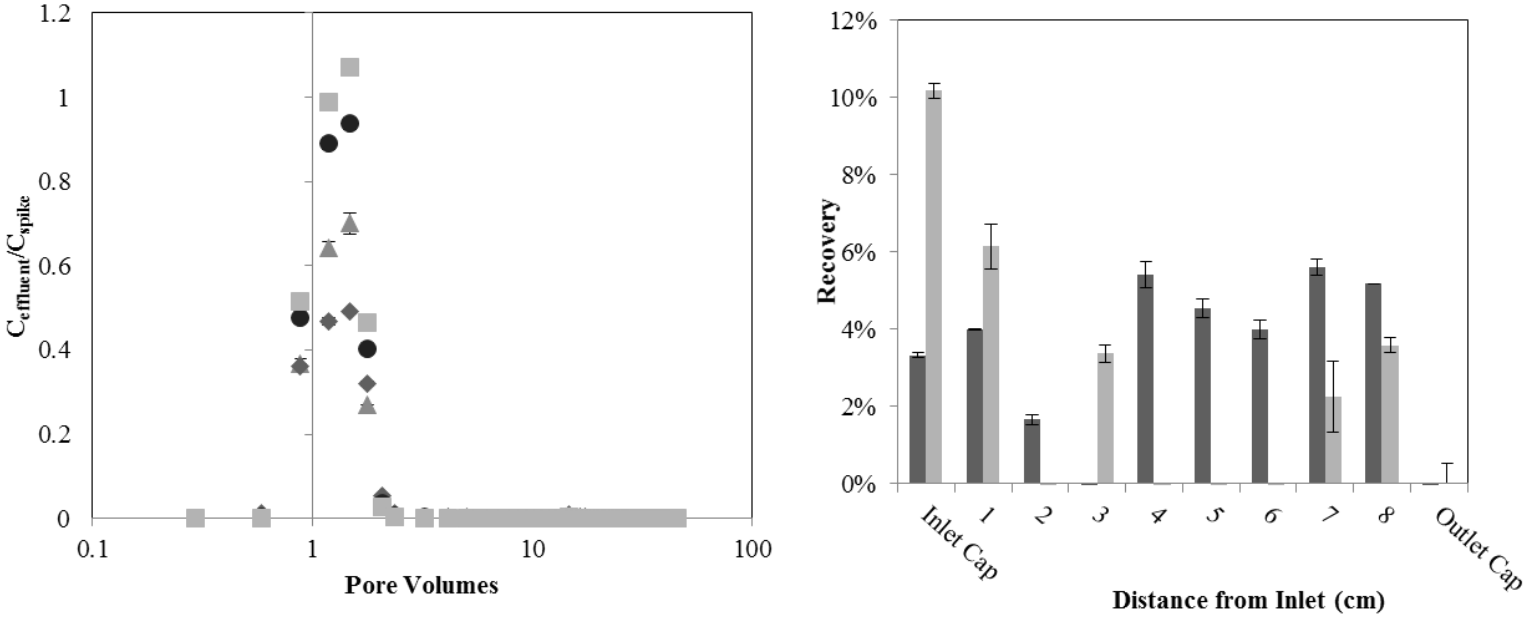

Figure D13: Hematite-SRFA-Th column in high purity quartz at 1 mL/min flow rate at pH 5.5 with 5 µg/L Re, 147 µg/L ^{232}Th, 0.04 g/L Hematite-NP and 25 mg_C/L SRFA in 0.001 M NaCl, *left* – effluent results for ^{232}Th (*triangles*), Hematite-NP as ^{56}Fe (*diamonds*), SRFA as ^{3}H (*circles*), and tracer (Re, *squares*) and *right* – solid phase results within the column following leaching step in 8 M HNO_3 for Hematite as ^{56}Fe (*gray*) and ^{232}Th (*black*), Note: no recovery of SRFA in the solid phase.

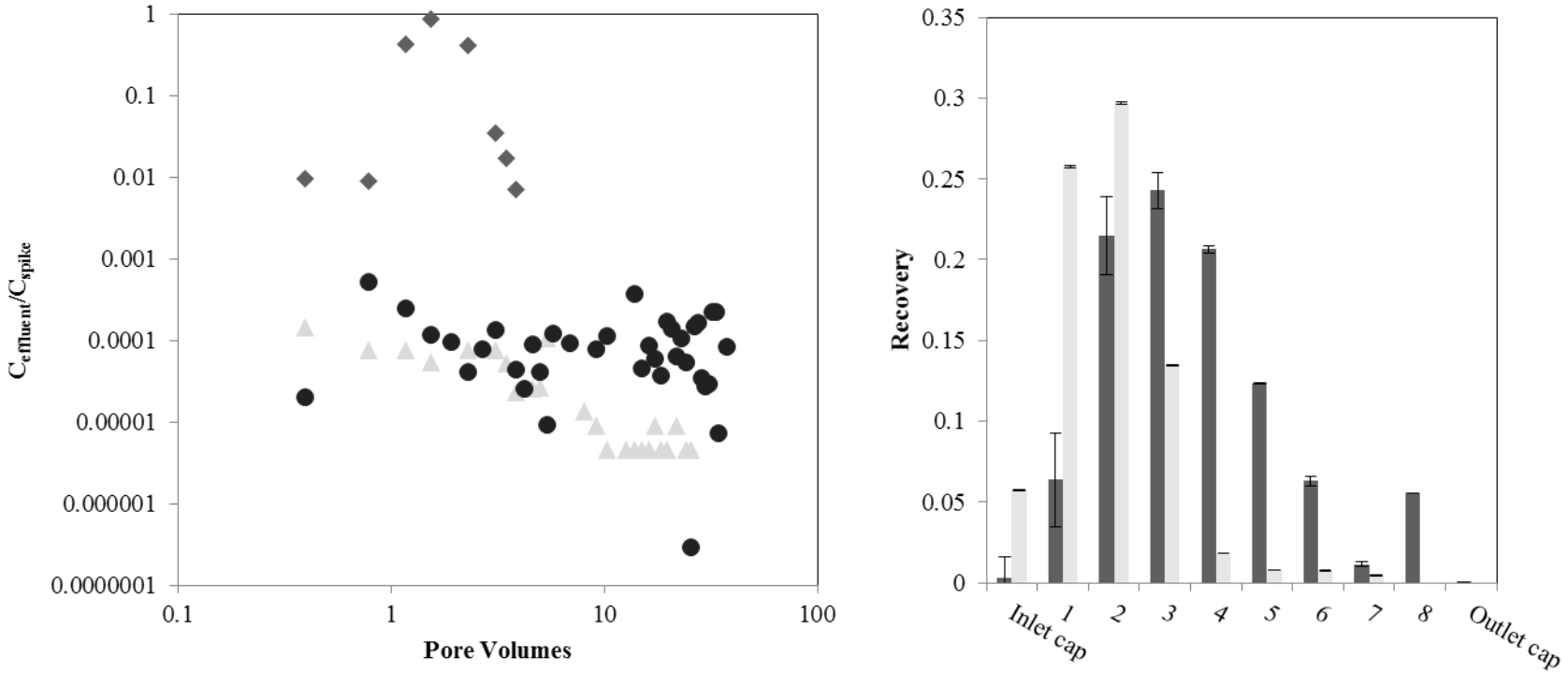

Figure D14: Hematite-SRFA-Th column in SRS sandy at 1 mL/min flow rate at pH 5.5 with 5 µg/L Re, 238 µg/L 232Th, 0.05 g/L Hematite-NP and 25 mgC/L SRFA in 0.001 M NaCl, left – effluent results for 232Th (triangles), Hematite-NP as 55Fe (circles), and tracer (Re, diamonds) and right – solid phase results within the column following leaching step in 8 M HNO3 for 232Th (black) and Hematite as 55Fe (gray), Note: SRFA not analyzed due to inability to differentiate between 3H and 55Fe by LSC (experiment run without 3H-SRFA).

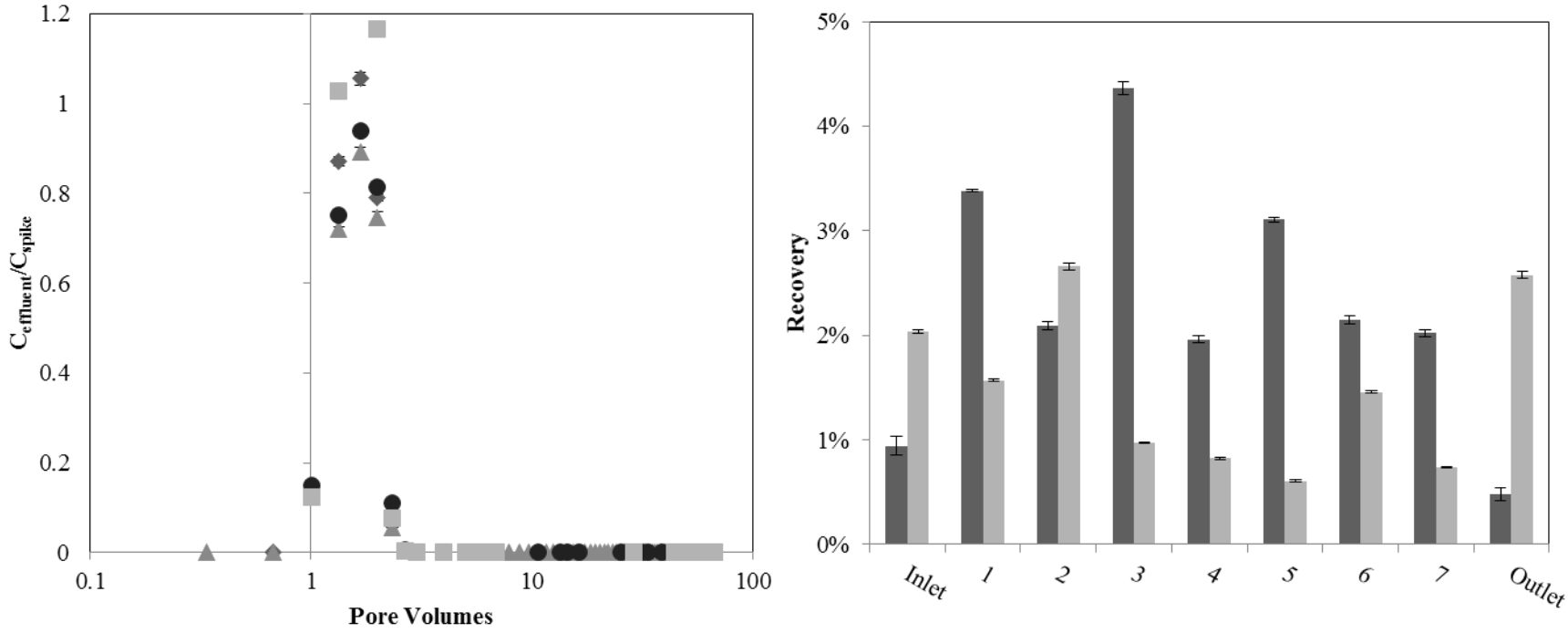

Figure D15: Hematite-SRFA-Th column in quartz at 0.1 mL/min flow rate at pH 5.5 with 5 µg/L Re, 311 µg/L ^{232}Th, 0.1 g/L Hematite-NP and 25 mg_C/L SRFA in 0.001 M NaCl, *left* – effluent results for ^{232}Th (*triangles*), Hematite-NP as ^{56}Fe (*diamonds*), SRFA as ^{3}H (*circles*), and tracer (Re, *squares*) and *right* – solid phase results within the column following leaching step in 8 M HNO_3 with ^{232}Th (*black*) and Hematite as ^{56}Fe (*gray*).

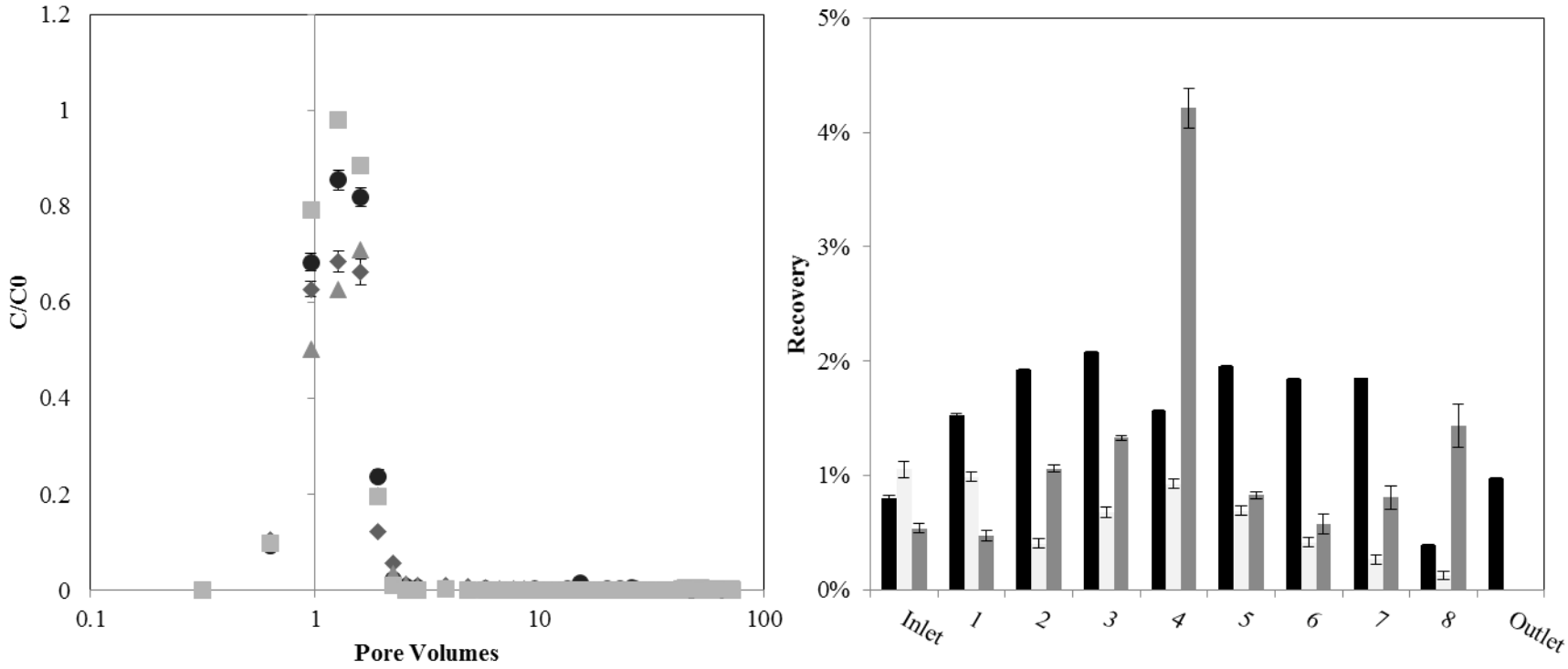

Figure D16: Hematite-SRFA-Pu column in quartz at 0.1 mL/min flow rate at pH 5.5 with 5 µg/L Re, 56 µg/L ^{239}Pu, 0.04 g/L Hematite-NP and 25 mg_C/L SRFA in 0.001 M NaCl, *left* – effluent results for ^{239}Pu (triangles), Hematite-NP as ^{56}Fe (diamonds), SRFA as ^{3}H (circles), and tracer (Re, squares) and *right* – solid phase results within the column following leaching step in 8 M HNO_3 with ^{239}Pu (*black*), SRFA as ^{3}H (*white*) and Hematite as ^{56}Fe (*gray*).

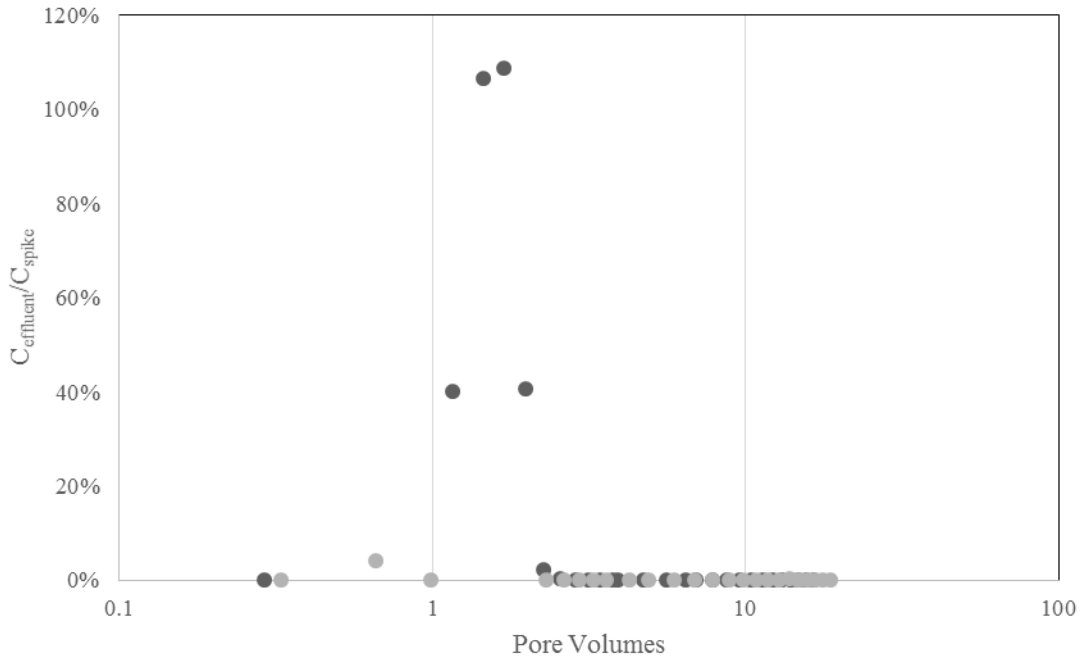

Figure D17: Comparison of effluent breakthrough for polystyrene microspheres [0.8 g/L] at pH 5.5 in 0.001 M NaCl for quartz (*black*) versus SRS sandy (*gray*) columns.

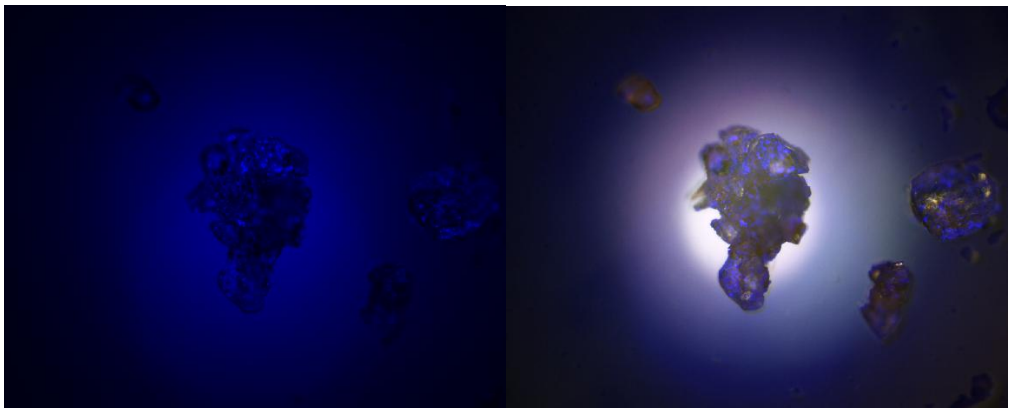

Figure D18: Fluorescence microscopy (Nikon AZ100) of SRS sandy column inlet soil grains following input of the polystyrene microsphere solution [0.8 g/L microspheres, 0.001 M NaCl, pH 5.5] with *left* – image of blue fluorescent particles on soil grain at 10x magnification and *right* – overlay of image of blue fluorescent particles onto color image of soil grains.

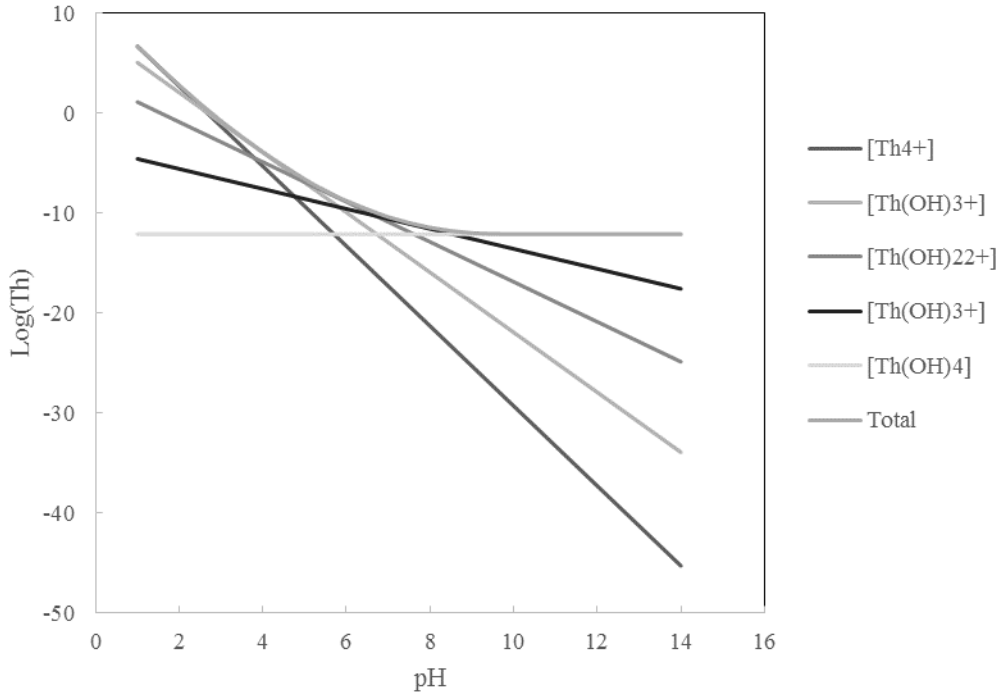

Figure D19: Solubility of Th with respect to pH at 0.001 M NaCl ionic strength, based on solubility constants from Neck and Kim, 2001 and adjusted for ionic strength using Debye-Huckel theory.

Table D4: Raw filtration data from column effluents.

Column ID	Displaced Pore Volumes (DPV)	Effluent An(IV), as ^{232}Th (ppb) or ^{239}Pu (cpm/mL)	An(IV) % Soluble	Effluent Fe, ppm	Fe % Soluble	Effluent ^{3}H, cpm/mL	SRFA % Soluble
Hematite-SRFA-Th - 1 mL/min - A	0.88	66	31.1	10.4	0	NM	NM
Hematite-SRFA-Th - 1 mL/min - B	1.19	115	28	13.5	0.04	NM	NM
Hematite-SRFA-Th - 1 mL/min - C	1.48	126	0	14.1	0	NM	NM
Hematite-SRFA-Th - 1 mL/min - D	1.78	49	52.9	9.2	0.09	NM	NM
Hematite-SRFA-Th - 0.1 mL/min - A	1.34	224	16.5	11.7	6.1	NM	NM
Hematite-SRFA-Th - 0.1 mL/min - B	1.67	277	19.2	12.2	6	NM	NM
Hematite-SRFA-Th - 0.1 mL/min - C	2	232	18.3	10.4	7	NM	NM
Hematite-SRFA-Pu - 0.1 mL/min - A	0.63	780	12.1	0.05	5.9	367	61.4
Hematite-SRFA-Pu - 0.1 mL/min - B	0.96	3871	17.3	0.28	1.1	2690	75
Hematite-SRFA-Pu - 0.1 mL/min - C	1.27	4835	17.1	0.31	1.1	3368	78.1
Hematite-SRFA-Pu - 0.1 mL/min - D	1.6	5472	14.3	0.3	1	3228	76.5
Hematite-SRFA-Pu - 0.1 mL/min - E	1.91	1526	15.4	0.06	5.1	936	72.9

Note: NM – not measured

Table D5: Calculated retardation factors.

Flow Rate (mL/min)	Column	Retardation Factor (R)			
		Th	Fe	SRFA	Tracer
1.0	230Th	2.1	N/A	N/A	2.3
	232Th	4.3	N/A	N/A	3.6
	Hema-Th	BDL	4.8	N/A	1.2
	SRFA-Th	1	N/A	0.9	1
	Hema-SRFA-Th	1.4	1.43	1.36	1.35
	SRS Sandy	N/A	N/A	N/A	N/A
0.1	Hema-SRFA-Th	1.51	1.52	1.54	1.55
	Hema-SRFA-Pu	1.62	1.52	1.54	1.19

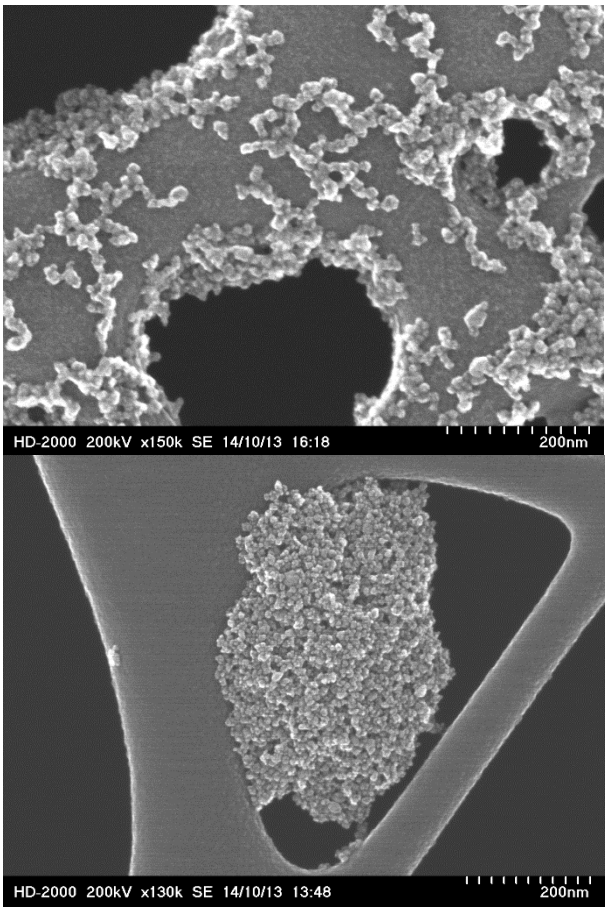

Figure D20: Representative HD2000 TEM images of spike solutions air-dried onto TEM grids, *left* – Hematite-SRFA-Th and *right* – Hematite-Th, significantly greater aggregation is noted for Hematite-SRFA-Th spike solutions.

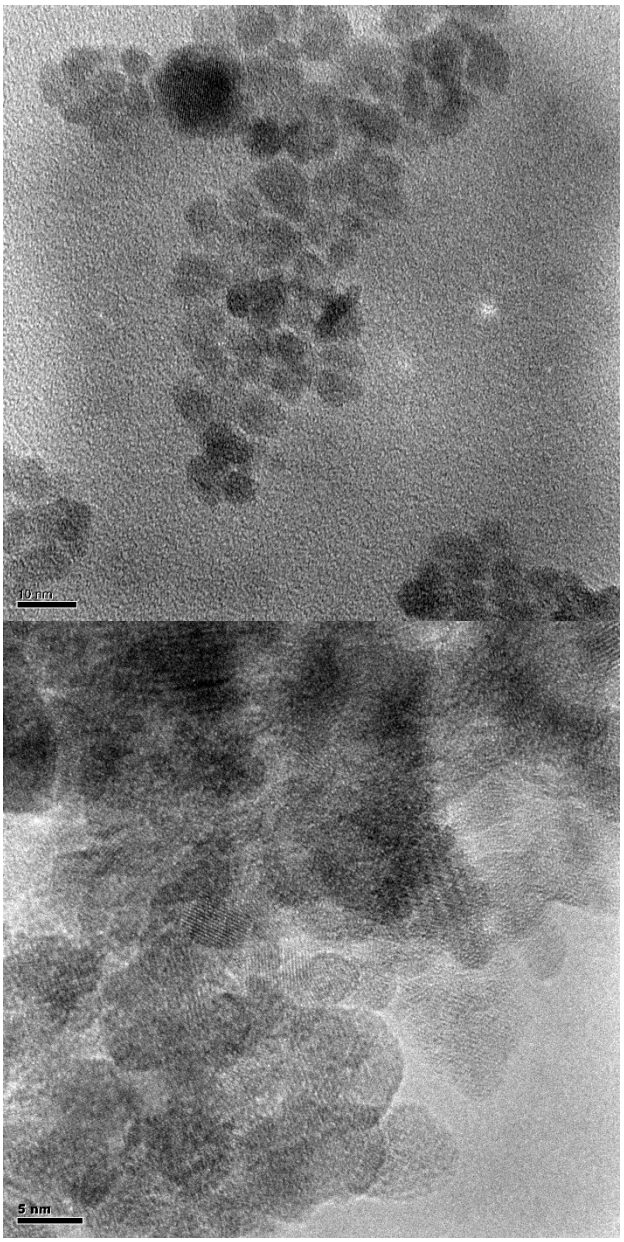

Figure D21: Representative HRTEM 9500 images of spike solutions air-dried onto TEM grids, *left* – clean Hematite-NPs and *right* – Hematite-SRFA-Th spike solutions, due to the small size of hematite-NPs and presence of SRFA, Th precipitates cannot be ruled out.

D.2 Technical Calculations

Batch sorption experiments – Sorption coefficients

A sorption partitioning coefficient (Kd) was calculated based on the sediment concentration (eqn. 1) and the aqueous concentration (measured). The sediment concentration was calculated using the following equation:

$$[C]_{sed} = \frac{([C]_{aq,i} - [C]_{aq,t})V_L}{m_{sed}} \qquad \text{Eqn. 1}$$

where: $[C]_{sed}$= total iodine concentration in sediment, ppb
$[C]_{aq,i}$= initial total aqueous iodine concentration, ppb
$[C]_{aq,t}$= total aqueous iodine concentration at time, t, ppb
V_L= sample liquid volume, mL
m_{sed}= sample sediment mass, g

The sediment-water partitioning coefficient, K_d, was calculated using the following equation:

$$K_d = \frac{[C]_{sed}}{[C]_{aq}} \qquad \text{Eqn. 2}$$

Column experiments – Retardation factors

A retardation factor is the ratio of the average linear velocity of groundwater to the velocity of the contaminant. Therefore, a conservative tracer should have a retardation factor of 1.0, but a contaminant that transports more slowly through a system than the tracer will have a retardation factor greater than 1.0. The retardation factor is estimated based on the mean residence time τ (Eqn. 3) and can be expressed in terms of the aqueous volume V (Eqn. 4). The final retardation factor is calculated by dividing the aqueous volume, V_{aqu}, by the pore volume, V_{pore}, of the column. The pore volume was estimated for each column based on the difference in the dry, packed column mass and the wet column mass.

$$\tau = \frac{\int tC(t)dt}{\int C(t)dt} \quad \text{Eqn. 3}$$

$$V_{aqu} = \frac{\int VC(t)dV}{\int C(t)dV} - \frac{V_{spike}}{2} \quad \text{Eqn. 4}$$

D References

Simpkins, L. (2011). The Influence of Natural Organic Matter on Plutonium Sorption to Gibbsite. Masters of Science, Clemson University.